Pathological angiogenesis and endothelial dysfunction in Graft-versus-Host Disease after allogeneic hematopoietic stem cell transplantation

Inaugural-Dissertation
to obtain the academic degree
Doctor rerum naturalium (Dr. rer. nat.)

submitted to the Department of Biology, Chemistry, Pharmacy
of Freie Universität Berlin

by

Lydia Maximiliane Verlaat

2023

The present thesis was prepared from July 2018 until October 2022 at the Medical Department of Hematology, Oncology and Tumor Immunology, Charité University Medicine under the supervision of Prof. Dr. Olaf Penack.

First Reviewer: Prof. Dr. Olaf Penack

Second Reviewer: Prof. Dr. Silke Rickert - Sperling

Date of defense: 23.09.2024

Declaration of authorship

I hereby declare that I alone am responsible for the content of my doctoral dissertation and that I have only used the sources or references cited in the dissertation.

Berlin, 14.10.2023

Lydia Verlaat

Zusammenfassung

In den vergangenen Jahrzehnten wurden auf dem Gebiet der allogenen hämatopoetischen Stammzelltransplantation (allo-HSCT) beträchtliche Fortschritte erzielt, so dass dieses Verfahren für eine wachsende Zahl von Patienten, die an malignen hämatologischen oder autoimmunen Erkrankungen leiden, eine kurative Behandlung darstellt. Trotz zahlreicher Verbesserungen ist die Rate der Komplikationen nach allo-HSCT immer noch hoch: Mehr als die Hälfte der transplantierten Patienten entwickelt eine Graft-versus-Host Disease (GvHD), welche mit einer Gesamtmortalität von bis zu 40 % die wichtigste Folgeerkrankung nach allo-HSCT darstellt. Die GvHD kann akut (aGvHD) oder chronisch (cGvHD) als systemisch entzündliche Reaktion auftreten, die verschiedene Organe und Gewebe befällt. Die chronische Entzündung führt dabei zu Fibrose und zieht eine schwere Morbidität der cGvHD-Patienten nach sich. Gängige therapeutische Ansätze zielen darauf ab, alloreaktive T-Zellen, die inflammatorischen Mediatoren der GvHD, zu unterdrücken. Der Einsatz von immunsuppressiven Steroiden geht jedoch mit GVHD-assoziierten Komplikationen wie Behandlungstoxizität, Tumorrezidiven oder tödlichen Infektionen einher. Daher besteht ein dringender Bedarf an alternativen Therapien, welche die GvHD wirksam verhindern und abschwächen, ohne die notwendigen Immunreaktionen zu eliminieren.

Jüngste Studien schlagen das Endothel als neues Ziel für Behandlungsansätze bei GvHD vor. Während die Angiogenese, also die Bildung neuer Blutgefäße, ursächlich für die Entzündungsreaktionen in der frühen GvHD ist, kommt es durch die anhaltende Inflammation in späteren GvHD-Stadien zur Endothelschädigung. Aufgrund des Mangels an geeigneten Mausmodellen ist die Beteiligung des Endothels insbesondere an der cGvHD-Pathologie nur unzureichend charakterisiert, weshalb anti-angiogene Therapien und neue endotheliale Therapieziele nur begrenzt zur Verfügung stehen. Ziel dieser Arbeit ist es, die Mechanismen, die zur endothelialen GvHD führen, zu ergründen und potenzielle Zielstrukturen für die Behandlung der GvHD zu identifizieren.

Im ersten Teil dieser Studie wurden Stoffwechselgene untersucht, die während der pathologischen Angiogenese differentiell reguliert sind. Durch genetische Deletion mittels CRISPR/Cas9 wurden die Enzyme Enolase 3 und Glukose-6-Phosphat-Dehydrogenase (G6pdx) identifiziert, welche an der endothelialen Regulation unter allogenen Bedingungen beteiligt sind. Sie konnten durch spezifische pharmakologische Inhibitoren *in vitro* erfolgreich beeinflusst werden. Die Therapie mit dem G6pdx-Inhibitor Polydatin führte zur

Abschwächung der Entzündung in Pfotenödem-Assays sowie einer Verbesserung der GvHD-Morbidität und der Normalisierung der Gefäßintegrität *in vivo*.

Der zweite Teil des Projekts befasst sich mit dem Endothel während der cGvHD. Es wurden zwei neue murine und ein humanisiertes cGvHD-Mausmodell etabliert, die den klinischen Merkmalen der cGvHD in Patienten ähneln. Bei allen Modellen wurde eine verlangsamte Rekonstitution von Zellen des hämatopoetischen Systems festgestellt, gefolgt von einer massiven Infiltration von T- und B-Zellen und einer schweren Sklerose/Fibrose in Geweben der cGvHD-Zielorgane. Bei der Bestimmung des Endothelzustands während der späten cGvHD wurde eine ausgeprägte vaskuläre Schädigung und Dysfunktion festgestellt: Neben dem Verlust von endothelialem CD31 und VE-Cadherin und dem Anstieg von von-Willebrand-Faktor war die endotheliale Integrität durch den Verlust des Tight-Junction-Proteins Zonula occludens protein-1 und des Perizytenmarkers Neuron-glial antigen 2 gestört. Außerdem fanden sich während cGvHD zirkulierende Endothelzellen und endotheliale Progenitorzellen. Analyse von endothelialem *alpha*-smooth muscle actin und Fibroblast-specific protein-1 zeigte eine deutliche endotheliale Fibrose. So konnte erstmals eine Umwandlung von Endothelzellen in einen mesenchymalen Zelltyp (Endothelial-to-mesenchymal transition) nachgewiesen werden, ein Prozess, der bisher nicht im Zusammenhang mit GvHD beschrieben wurde. Die auftretende EndoMT konnte durch Anwendung von Pirfenidone *in vivo* erfolgreich verhindert werden, wodurch sich ebenfalls die Anzahl der CD31+ Blutgefäße normalisierte. Darüber hinaus wurde eine Gruppe von fünf neuen, endothel-relevanten Biomarkern (Endostatin, Connective tissue growth factor, Endoglin, Follistatin, Endocan) vorgeschlagen, welche im Blutserum von cGvHD-Patienten erhöht waren und welche für die Prognose und Diagnose von cGvHD in der Klinik von Nutzen sein könnten.

Diese Studie trägt dazu bei, den Zusammenhang zwischen dem Endothel und der Pathologie der GvHD zu verstehen. Sie identifiziert potenzielle therapeutische Ziele zur Verbesserung der GvHD, welche zur Normalisierung der gestörten Gefäßfunktion und zur Verhinderung von Endothelfibrose führen können, ohne dabei die Anti-Tumor-Reaktion nach allo-HSCT zu beeinträchtigen.

Abstract

During past decades, considerable progress has been made in the field of allogeneic hematopoietic stem cell transplantation (allo-HSCT), enabling the procedure as a curative treatment to an increasing number of patients suffering from hematopoietic malignancies or autoimmune diseases. Despite numerous improvements of allo-HSCT, the rates of post-treatment complications are still high: more than half of the transplanted patients develop Graft-versus-Host Disease (GvHD), with an overall mortality up to 40%, making GvHD the major treatment sequelae after allo-HSCT. GvHD can occur acute (aGvHD) or chronic (cGvHD) as a systemic inflammatory disease, affecting various organs and tissues. Chronic inflammation subsequently leads to fibrosis and severe morbidity in cGvHD patients. Common therapeutic approaches aim to suppress alloreactive T cells, the inflammatory mediators of GvHD, but the use of immunosuppressive steroids is accompanied by GVHD-associated complications, as treatment toxicity, tumor relapse or fatal infections. Therefore, an urgent need for alternative therapies exists, which effectively prevent and attenuate GvHD without eliminating the necessary immune responses.

Recent studies proposed the endothelium as a novel target for treatment approaches of GvHD. While angiogenesis, the formation of new blood vessels, is a cause of inflammation during early GvHD, the endothelium is damaged from the persisting inflammation at later GvHD stages. Due to the lack of suitable mouse models, the endothelial participation especially in the cGvHD pathology is inadequately characterized, resulting in limited anti-angiogenic therapies and novel therapeutic endothelial targets. This thesis intends to elicit the mechanisms leading to endothelial GvHD and identify such potential target structures for GvHD treatment.

In the first part of this study, we examined metabolic genes that are differentially regulated during pathologic angiogenesis. By genetic deletion with CRISPR/Cas9, the enzymes Enolase 3 and Glucose-6-phosphate dehydrogenase (G6pdx) were identified to participate in the endothelial regulation under allogeneic conditions and were successfully intervened by specific pharmacologic inhibitors *in vitro*. Therapy using the G6pdx-inhibitor Polydatin resulted in attenuated inflammation in footpad swelling assays, ameliorated the GvHD morbidity and normalized the vascular integrity *in vivo*.

The second part of the project deals with the endothelium during cGvHD. Two novel murine and one humanized mouse model of cGvHD were established, which closely resemble the

clinical features of cGvHD in patients. Characterizing these models, a decelerated immune and hematopoietic cell reconstitution was found, followed by a massive infiltration of T and B cells and severe tissue sclerosis/ fibrosis in GvHD target organs. Determining the endothelial condition during late cGvHD, a prominent vascular damage and dysfunction was found: Next to a loss of endothelial CD31 and VE-Cadherin and an increase of von-Willebrand factor, the endothelial integrity was disturbed by the loss of tight junction protein Zonula occludens protein-1 and pericyte marker Neuron-glial antigen 2. Additionally there was occurrence of circulating endothelial cells and endothelial progenitor cells in cGvHD. Severe endothelial fibrosis by analysis of *alpha*-smooth muscle actin and Fibroblast-specific protein-1 was quantified. Hence for the first time, a transformation of endothelial towards a mesenchymal cell type (Endothelial-to-mesenchymal transition) was detected, a process which has not been described in the context of GvHD before. This transition was successfully prevented by administration of Pirfenidone, which normalized the CD31+ vessel quantity and ameliorated the endothelial fibrosis *in vivo*. Furthermore, a panel of five novel endothelium-related biomarkers (Endostatin, Connective tissue growth factor, Endoglin, Follistatin, Endocan), which were increased in blood serum of cGvHD patients, was proposed and might be beneficial for prognosis and diagnosis of cGvHD in the clinic.

This study helps to provide knowledge about the connection between the endothelium and the GvHD pathology. It identified potential therapeutic targets to ameliorate GvHD without interfering the anti-tumor response after allo-HSCT, normalizing the disturbed vascular function and prevent endothelial fibrosis.

Table of contents

Abbreviations

6-AN	6-Aminonicotinamide
αSMA	*alpha*-smooth muscle actin
Acsm3	Acyl-CoA Synthetase Medium Chain Family Member 3
ADAMTS13	A disintegrin and metalloproteinase with a thrombospondin type 1 motif, member 13
aGvHD	acute Graft-versus-Host Disease
ALK5	Activin-receptor-like kinase 5
allo	allogeneic
Ang-2	Angiopoietin-2
Ang4	Angiogenin-4
APC	Antigen presenting cell
auto	autologous
BM	Bone marrow
BMC	Bone marrow cell
BMT	Bone marrow transplants
Casp3	Caspase-3
CD	Cluster of differentiation
CEC	Circulationg endothelial cell
CEP	Circulationg endothelial progenitor
cGvHD	chronic Graft-versus-Host Disease
CMV	Cytomegalovirus
CTGF	Connective tissue growth factor
CTL	Cytotoxic T lymphocyte
CXCL	C-X-C motif ligand
DAMPs	Damage-associated molecular patterns
DC	Dendritic cell
EBMT	European Society for Blood and Marrow Transplantation
EC	Endothelial cell
ECM	Extracellular matrix
EndoMT	Endothelial-to-mesenchymal transition
ENG	Endoglin (CD105)
Eno3	Enolase 3; *ß*-Enolase
ET1	Endothelin-1
ES	Endostatin
ESAM	Endothelial cell-selective adhesion molecule
ESM1	Endothelial cell specific molecule-1; Endocan
FN	Fibronectin
FSP-1	Fibroblast-specific protein-1
FST	Follistatin
G6pdx	Glucose-6-phosphate dehydrogenase, X-linked
G-CSF	Granulocyte colony-stimulating factor
GvHD	Graft-versus-Host Disease
GvT	Graft-versus-Tumor

HA	Histocompatibility antigens
HLA	Human leukocyte antigens
HSC	Hematopoietic stem cell
HSCT	Hematopoietic stem cell transplantation
ICAM1	Intercellular adhesion molecule 1 (CD54)
IFN-α	Interferon-*alpha*
IL	Interleukin
LPS	Lipopolysaccharide
MCAM	Melanoma cell adhesion molecule (CD146)
MCEC	Murine cardiac endothelial cell
MHC	major histocompatibility complex
MuMEC	Murine microsvascular endothelial cell
NG2	Neuron-glial antigen 2
NIH	National Institute of Health
NK	Natural killer (cell)
NRM	Non-relapse related mortality
PAMPs	Pathogen-associated molecular patterns
PB	Peripheral blood
PDGF-α	Platelet-derived growth factor-*alpha*
PDGFR-ß	Platelet-derived growth factor receptor-*beta*
PECAM	Platelet endothelial cell adhesion molecule (CD31)
RA	Rheumatoid Arthritis
TBI	Total body irradiation
TGF-ß	Transforming growth factor-β
Tie2	TEK receptor tyrosine kinase 2
TMNK1	immortalized human liver sinusoidal EC line
TNF-α	Tumor-necrosis-factor-*alpha*
s	soluble
SLE	Systemic lupus erythematosus
SSc	Systemic Sclerosis
syn	syngeneic
VCAM1	cell-adhesion molecule 1 (CD106)
VECad	Vascular endothelial-cadherin
VEGF	Vascular endothelial growth factor
vWF	von-Willebrand factor
ZO-1	Zonula occludens protein-1

1. Introduction

1.1. Allogeneic Hematopoietic Stem Cell Transplantation

Allogeneic hematopoietic stem cell transplantation (allo-HSCT) is an established therapeutic procedure for treatment of underlying malign and non-malign hematologic diseases. In general, the term describes the transfer of multipotent hematopoietic stem and progenitor cells from a donor to a recipient, aiming to replace the recipient's immunological repertoire and restore normal hematopoiesis [1].

Historically, HSCT has developed from clinical observations of nuclear bomb survivors at Hiroshima and Nagasaki, who showed severe myelosuppressive symptoms after high-dose radiation [2]. In the early 1950s, experimental efforts, including the transfer of bone marrow cells (BMCs) into irradiated animal models, were conducted to reverse radiation caused bone marrow injury [3, 4]. 1957, Thomas et al. were the first to infuse acute leukemia patients with bone marrow transplants (BMT), albeit the survival quote was poor due to disease relapse and graft rejection [5]. Continuous research shed light on the immunologic backgrounds of BMT failures, determining the major histocompatibility complex (MHC) and the human leukocyte antigens (HLA) as major features for effective engraftment [6–8] and pioneering the first successful clinical BMTs to cure anemic and immunodeficient patients in the 1960s and 70s [9–11]. Thomas et al. also realized first BMT approaches with cells of allogeneic origin in acute leukemia patients [12].

HSCs are characterized by their source, based on the relationship between donor and recipient: while autologous (auto) HSCs are obtained from the recipient's tissue itself, syngeneic (syn) cells come from an identical twin. Allo-HSCs originate from a related or non-related, genetically non-identical donor. Until today, allo-HSCT has become a standard therapy in the treatment of severe hematologic disorders and diseases, thus contributing to the emerging field of stem cell therapy, cancer immunotherapy and personalized medicine.

1.1.1. Numbers, Trends & Indications of allo-HSCT

Considering published numbers from the European Society for Blood and Marrow Transplantation (EBMT) as well as the U.S.-based Center for International Blood and Marrow Transplant Research® (CIBMTR®), nearly 50,000 allo-HSCTs are performed worldwide every year [13, 14]. In 2020, allo-HSCT was the second most performed type of transplantation after auto-HSCT with increasing numbers since 1990 (Figure 1A). With

upcoming of the SARS-CoV-2 pandemic the amount of total allo-HSCTs slightly decreased by 5.1% [13], but the nearly unvaried high proportion of performed HSCTs at this time period still emphasizes its importance as a life-saving treatment option. Especially Germany, Scandinavia and other west-European countries show leading transplantation rates (Figure 1B).

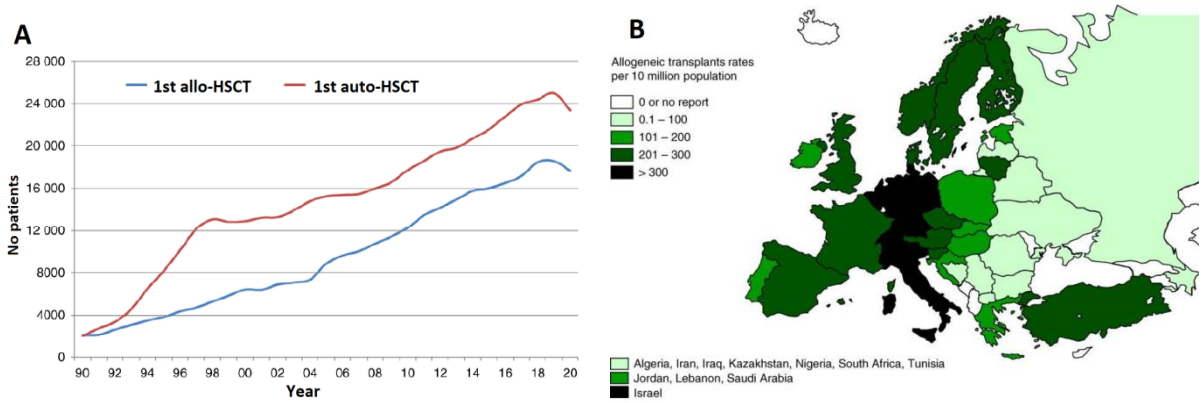

Figure 1: A: Absolute number of patients receiving a 1st HSCT until 2020 in Europe. Adapted from [13]. **B: Allo-HSCT rates per 10 million population and absolute numbers in Europe 2018.** Adapted from [15].

While in the past HSCTs remained reserved for patients with inherited immunodeficiency disorders and anemias to repopulate their missing or defective HSC niche, nowadays a much wider indication spectrum for allo-HSCT has developed. One great advantage of an allo-setting is a donor-graft free of malign cells, which additionally contains immunoreactive lymphocytes, capable of combating against foreign antigens (and for example cancer cells) in the recipient, thus mediating a so called 'Graft-versus-Tumor' (GvT) effect [16, 17]. For a multitude of cancer patients, combination of myeloablative irradiation/ chemotherapy followed by allo-HSCT can eradicate a variety of malign diseases and declines the risk of disease relapse [18].

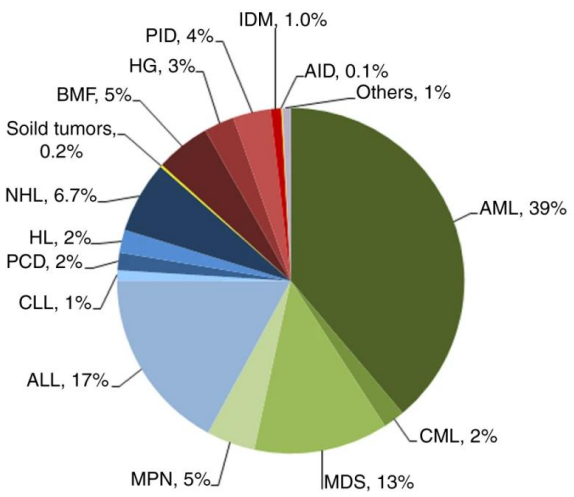

AML	Acute myeloid leukemia
CML	Chronic myeloid leukemia
MDS	Myeloproliferative disorders
MPN	Myeloproliferative neoplasms
ALL	Acute lymphoblastic leukemia
CLL	Chronic lymphocytic leukemia
PCD	Plasma cell disorders
HL	Hodgkin lymphoma
NHL	Non Hodgkin lymphoma
BMF	Bone marrow failure
HG	Hemoglobinopathies
PID	Primary immune disorders
IDM	Inherited disorders of metabolism
AID	Auto immune disorders

Figure 2: Relative proportion of allo-HSCT in Europe 2020. From [13].

The EBMT annual report 2020 summarizes the different indications for allo-HSCT (Figure 2), with the main proportion applying to acute myeloid leukemia (39%) followed by acute lymphoblastic leukemia (17%) and myelodysplastic syndromes (13%). Within the non-malignant diseases, major indications for allo-HSCT were bone marrow failures like severe aplastic anemias, and primary immune disorders or inherited immune disorders of metabolism, for example sickle cell disease or thalassemia.

The fact that constantly growing allo-HSCT numbers and an expanding range of indications can be observed is caused by advances in the selection of donors, well-orchestrated conditioning regimens and aligned supportive care. Use of allo-HSCT to cure hematologic malignancies was restricted to younger patients with stem cells coming exclusively from HLA-identical siblings until the 1990s. The establishment of large registries recording voluntary unrelated bone marrow donors permitted access to allo-HSCTs for a wider margin of recipients [19]. Furthermore, better treatment outcomes and reduction of transplant-associated complications could be achieved, when allo-HSCT was administered in early disease stages rather than in late progressive phases as a ‘last rescue’ attempt [20, 21]. Not least, the introduction of non-myeloablative conditioning regimens, with reduced-intensity irradiation and recipient-adapted chemotherapy, contributed to a reduced regimen-related morbidity and mortality [22]. All these developments made allo-HSCT more and more available for elderly, medically infirm patients, where the greatest incidence of malignant hematologic diseases can be seen.

1.1.2. Technical aspects: principle and procedure of allo-HSCT

The decision for a cellular immune therapy is always made in compliance with an individual benefit-risk-assessment. The long-term advantages of an allo-HSCT as curative treatment must surpass the enhanced risk for complications and toxicity, occurring especially short time after the therapy. Customized factors as medical condition, age, comorbidity, underlying indication and donor availability have to be considered for every patient.

1.1.2.1. Donor selection

Selection of a suitable donor for each recipient is based on the MHC-/ HLA-system. The MHC complex describes a gene-rich locus on chromosome 6 in humans, while the murine pendant ‘histocompatibility-2‘ (H2) is located on chromosome 17 [23, 24]. The human MHC

constitutes a number of HLA-genes, which are classified into 3 groups: MHC class I, II and III. Those MHC-molecules are expressed on the surface of cells crucial for the recognition of non-self antigens. Their essential function is to bind and display foreign antigens to cells of the adaptive immune system, thus regulating immune responses. The human MHC class I region is composed of HLA-A, -B, and –C genes, while MHC II harbours the genes HLA-DP, -DQ and DR (Figure 3). MHC I peptides can be found on all nucleated cells and present intracellular antigens exclusively to CD8+ T lymphocytes, MHC II receptors are primarily expressed on antigen-presenting immune cells, showing peptide-antigens to CD4+ T cells [25, 26]. MHC class III encodes different immune modulating proteins, such as complement components, several inflammatory cytokines or heat shock proteins.

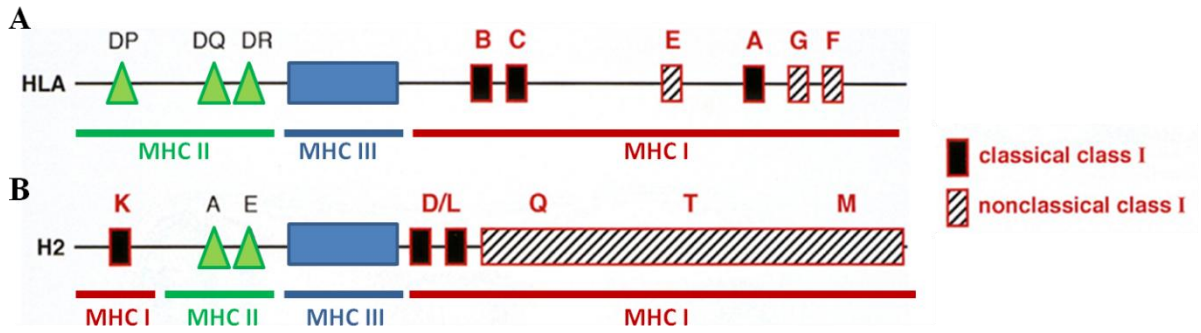

Figure 3: Simplified schema of the regions coding for MHC-genes in A: human (HLA) and B: mouse (H2). Adapted from [27, 28].

MHC alleles are inherited in a mendelian fashion as single sets - so called haplotypes - from each parent, resulting in HLA pairing [29]. To the present day more than 35,000 HLA alleles have been documented (HLA-Database, Release 3.49; 2022-07) [30], so basically each person's HLA type can be seen as an almost unique fingerprint. In this context, matching of donors and recipients regarding their HLA compatibility occurs after simplified criteria for the five classical MHC I and II loci (HLA-A, -B, -C, -DRB1 and -DQB1) in first place [31]. A HLA-match is important to minimize graft rejection, disease relapse, transplant-related mortality and overall Graft-versus-Host Disease (GvHD) [32, 33], which is still one of the most severe complications after allo-HSCT [34] and discussed in detail in the following chapters.

A fully HLA-matched sibling or unrelated donor represents the preferred source with the least expected complications after allo-HSCT [35, 36, 35], followed by a partially HLA-matched family member (first-degree relatives, haploidentical in at least one set of genes) [37, 38] or a partially HLA-matched unrelated donor [39]. Latter can be recruited by a voluntary donor registry [36].

1.1.2.2. Stem cell acquisition

Over time, the term ‘BMT’ has been substituted by ‘HSCT’, considering the fact, that transplanted cells can be of different anatomic origin than bone marrow (BM), including peripheral blood (PB) or umbilical cord blood [29]. Up to 20 mL/kg BM-HSCs are aspirated with a large-bore needle under epidural or general anesthesia from the posterior (or anterior) iliac crest until a sufficient cell number is achieved. For transplantation, an amount between 1×10^8 - 2×10^8 total nucleated cells per kg is considered adequate [40, 41]. Since HSC collection from PB is easier to conduct, less invasive and bears a decreased risk for complications and side effects, it has recently become the standard choice for HSC acquisition. Because the relative low proportion of HSCs in the PB, donors get administered with hematopoietic growth factors prior to apheresis, usually granulocyte colony-stimulating factor (G-CSF), which mobilizes HSCs into the PB circulation [42]. After leukapheresis, erythrocytes are removed and the HSCs are infused immediately or cryo-conserved until use [42, 43]. Although naive umbilical cord stem cells can be transplanted without stringent HLA matching and harbour a lower risk for GvHD development, this type of transplantation does not provide a reasonable alternative, because stem cell yields from neonates are not adequate to treat adults and those cells cannot be used in auto-transplantation setups to treat genetic disorders or malignancies in the same individual with the same genetic constitution or underlying premalignant condition [44].

1.1.2.3. Recipient conditioning

Before HSC infusion, recipients receive disease-specific conditioning regimens, mostly combining radiation and chemotherapy [45]. Preceding conditioning is performed to meet the following requirements: 1) Induction of an adequate immunosuppression in the recipient to prevent graft rejection, 2) eradication of malign cells to reinforce the anti-leukemic effect and 3) to create a ‘marrow niche’ for transplanted HSCs. Conditioning can be classified after its intensity: myeloablative, non-myeloablative or reduced-intensity conditioning. Most common, a combination of cyclophosphamide and total body irradiation (TBI) with doses between 800-1400 cGy are used for complete myeloablation [46]. A standardized non-myeloablative conditioning embraces administration of the chemotherapeutics cyclophosphamide and busulfan without TBI [47, 48].

1.1.3. Complications

Allo-HSCT has emerged to the therapy of choice for a variety of hematologic, congenital and neoplastic disorders. Although positive treatment outcomes have significantly improved due to refined HLA typing, conditioning regimens and supportive care, non-relapse related mortality (NRM) and long-term morbidity still form major obstacles after HSCT, with NRM rates reaching up to 49% [49]. Different transplantation-related toxicities [50–52], graft failure and rejection [53], infections [54] and the occurrence of GvHD are the most common post-transplant related causes for morbidity and NRM. Because of its high impact on this thesis, GvHD is specifically elaborated in the continuing chapter 1.2.

Graft failure can result either from incomplete hematopoietic recovery, loss of bone marrow function after initial reconstitution or reappearance of host cells attacking the graft. It may be evoked by several factors, such as inadequate conditioning or stem cell dose, HLA-mismatches, administered immunosuppressive drugs or infections, especially with Cytomegalovirus (CMV) [55, 56]. In general, recipients are exposed to a higher risk of viral, fungal or bacterial infections because of the strong immunosuppressive medication given post-transplantation to prevent graft rejection or to mitigate GvHD [57]. Besides the mentioned CMV infections, frequently seen pathogens in allo-HSCT patients include e.g. species of *Streptococcus*, Herpes simplex-, Epstein-Barr- and Varizella-Zoster-Virus as well as pathogenic *Candida* and *Aspergillus* species [58].

As conditioning- and transplant- related complications, organ toxicities especially in the liver or urinary system are frequently described [59–61]. The veno-occlusive disease (VOD)/ sinusoidal obstruction syndrome (SOS) is caused by endothelial damage in hepatic sinusoids. It is one of the most common liver complications occurring after allo-HSCT and causes high NRM rates [51, 62].

Deficiencies in the humoral and cellular immune system seem to partially arise from an immunosuppressive anti-GvHD therapy and appear generally prolonged in GvHD patients [63]. In some cases, super-infections or treatment-related toxicities occur in parallel to the onset of GvHD [64], making a clinical differentiation difficult and shifting GvHD into the main focus as the major allo-HSCT related complication.

1.2. Graft-versus-Host Disease

Unless significant improvement in the past 20 years, GvHD remains still one of the major treatment sequelae of allo-HSCT, contributing substantially to high morbidity and mortality in transplanted patients [65]. GvHD describes a systemic, immunologically mediated response caused by donor stem cells in the recipient's tissue and can be divided into an acute (aGvHD) and a chronic form (cGvHD), which are both clinically complex phenomena.
Historically, GvHD was first mentioned in 1966 by Billingham and colleagues, who described it as immunologic reaction called 'Runt disease', characterized by nausea and rash after BMT [66]. Billingham et al. postulated three general requirements for the evolution of GvHD, which are still applicable until present day: I) the donor graft harbours competent immune cells, II) the recipient's immune system is unable to eliminate transplanted reactive cells and III) the recipient expresses tissue antigens, which are recognized as 'foreign' and lead to stimulation of donor immune cells. Today, GvHD still has an overall incidence between 30% -50% after allo-HSCT and a mortality rate up to 40% [67, 68].

1.2.1. Acute GvHD

Most frequently, symptoms of classical aGvHD occur within the first 100 days after transplantation but the inception of persistent, recurrent or late onset aGvHD can start at any time after allo-HSCT. Diagnosis of acute or chronic GvHD is confirmed by application of several manifestation-criteria, defined by the National Institute of Health [69]. Mainly, aGvHD affects the principal target organs skin, liver and colon with diverse clinical manifestations, which are further described in Table 1. Less common, ocular involvement (dry eye syndrome, conjunctivitis) as well as participation of the kidneys (nephritis), lungs (interstitial pneumonitis) or the hematopoietic system (thymic atrophy, thrombocytopenia) has been described [70–72]. aGvHD symptoms are graded in 4 stages (I-IV) according their severity, ranging from mild to life-threatening [73]. To verify the diagnosis, histological examinations of biopsies, especially from skin and gastrointestinal tract, are mostly conducted in parallel.

Table 1: Clinical Manifestations of aGvHD. Adapted from [74].

Organ	Clinical manifestation
Skin	Erythematous maculopapular rash, often initially involving palms and soles. May progress to involve the entire body surface; pruritic and/or painful. In severe cases: bullae, leading to desquamation.
Liver	Cholestasis w/o frank jaundice. Cholestatic enzymes comparatively more deranged than transaminases.
Gastrointestinal tract	*Upper*: Anorexia, nausea, vomiting *Lower*: Diarrhea (green and watery); severe case: diarrhea contains fresh blood and mucosa & abdominal cramps and paralytic ileus

The development of aGvHD can be divided into three main phases, which are schematically illustrated in Figure 4:

1) Initially, the first phase is characterized by tissue damage in the host due to the underlying disease and its treatment as well as the conditioning regimen prior to transplantation. The injured epithelial tissue augments the expression of cell adhesion molecules, releases chemokines as well as pro-inflammatory cytokines, e.g. tumor necrosis factor alpha (TNF-α), interleukin-1 (IL-1) and lipopolysaccharides (LPS), originating especially from the intestinal tract. All these factors lead to amplified activation of antigen presenting cells (APCs) in the host [75].

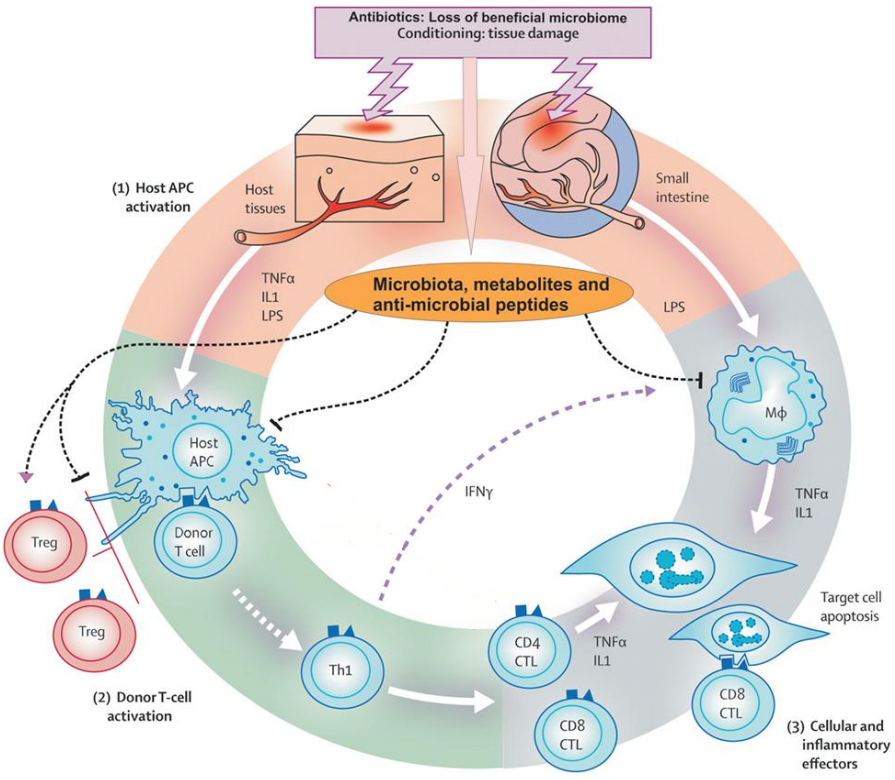

Figure 4: Pathophysiology of acute GvHD. Adapted from [76].

2) Secondly, host APCs directly display host alloantigens, which can be recognized by donor lymphocytes in the graft and stimulate donor T cell activation. Alternatively, donor T cells can also be activated by indirect presentation of alloantigens through donor APCs [77]. While $CD4^+$ T cells recognize the disparity of MHC II (HLA-DR, -DQ, and -DP), $CD8^+$ T cells react to MHC I mismatches (HLA-A, -B, and -C) [78]. Although the strength of the immune reaction increases with elevated HLA-disparity, also HLA-matched transplantations can be causative to GvHD, owing to minor HLA mismatches [79]. Host regulatory T cells (Treg) are able to dampen the inflammatory reaction by secreting anti-inflammatory cytokines, e.g. IL-10 and by suppressing alloreactive T cell priming. Though, normal Treg function is mostly impaired due to prior conditioning or immunosuppressive medication in the host [80].
3) In the last phase, target organs are damaged by inflammatory cytokines and cells of the innate and adaptive immune system. The previously antigen-primed donor T cells differentiate into Th1 and Th17 effector lymphocytes, which can subsequently activate cytotoxic T lymphocytes (CTL) and natural killer (NK) cells, all mediating tissue damage. The inflammatory reaction is systemically enhanced by effector T cells, promoting CTL reactions by production of pro-inflammatory cytokines, which act together with the LPS from the gastrointestinal tract and further stimulate monocytes and macrophages to secrete special inflammatory mediators. This leads to a propagation of a ‘cytokine storm’ and apoptosis, causing profound tissue damage [78].

1.2.2. Chronic GvHD

cGvHD occurs in up to 70% of transplanted patients. The disease, which profoundly impairs recipients life-quality, is the major cause for late NRM, accompanied with 25% of deaths after allo- HSCT [81]. Its overall incidence is even increasing recently, because of the rising age of patients, unrelated-donor- and MHC-mismatched-transplantations as well as the use of reduced intensity conditioning regimens [82]. Other major risk factors include prior aGvHD, PB-HSCs as stem cell source, the type of underlying malignancy or female-donor to male-recipient transplantations [83]. The onset of cGvHD is fluent, beginning approximately 3 months up to 2 years or even later after transplantation [84]. cGvHD mainly simulates characteristics of autoimmune diseases with features of impaired immune tolerance mechanisms, like the involvement of auto- and alloreactive donor-derived T and B cells, the participation of alloantigens and mechanisms of chronic inflammation with subsequent fibrosis [85].

Similar to aGvHD, cGvHD can involve the classical target organs skin, liver and the gastrointenstinal tract. In addition, a variety of other organ systems, as lung, mouth, joints and fasciae, muscles, eyes, the hematopoietic system or mucosal tissues, e.g. in the oesophagus or genital system may be affected [84]. The most frequently described manifestations are listed in Table 2. Because of the heterogeneous symptoms, diagnosis of cGvHD can be difficult and is made after a clinical disease model established by National Institute of Health (NIH) consensus criteria [69, 84]. The severity of cGvHD is assessed by grading the involvement of single organs to a summarized overall cGvHD-Score, ranging from a "mild" to "moderate" to "severe" disease stadium.

Table 2: Clinical Manifestations of cGvHD. Symptoms are grouped after "diagnostic" (sufficient for cGvHD diagnosis) and "distinctive" (frequently seen, but not sufficient alone for diagnosis) criteria. Adapted from [84].

Organ	Clinical manifestation
Skin	*diagnostic:* Poikiloderma, Lichen planus-like / Sclerotic / Morphea-like/ Lichen sclerosus-like features, Erythema, Macropalpular rash *distinctive:* Depigmentation, Papulosquamous lesions
Liver	*diagnostic*: Total bilirubin, alkaline phosphatase > 2 × upper limit of normal alanine aminotransferase> 2× upper limit of normal
Gastroint.tract	*diagnostic:* Esophageal web, Strictures or stenosis in the upper to mid third of the esophagus, Anorexia, Nausea, Vomiting, Diarrhea, Weight loss
Lung	*diagnostic:* Bronchiolitis obliterans diagnosed with lung biopsy, Bronchiolitis obliterans syndrome (BOS) *distinctive:* Air trapping and bronchiectasis on chest CT
Muscles, Fascia, Joints	*diagnostic:* Fasciitis, Joint stiffness or contractures secondary to fasciitis or sclerosis *distinctive*: Myositis or polymyositis
Mouth	*diagnostic:* Lichen planus-like changes, Gingivitis, Mucositis, Erythema, Pain *distinctive:* Xerostomia, Mucoceles, Mucosal atrophy, Ulcers, Pseudomembranes
Genitalia	*diagnostic:* Lichen planus-like / Lichen sclerosus-like features, Vaginal scarring or clitoral/labial agglutination, Phimosis or urethral scarring or stenosis *distinctive:* Erosions, Fissures, Ulcers
Eyes	*distinctive:* New onset dry, gritty, or painful eyes, Cicatricial conjunctivitis, Keratoconjunctivitis sicca, Confluent areas of punctate keratopathy
Nails, Scalp & Body Hair	*distinctive:* Dystrophy, Longitudinal ridging, splitting or brittle features, Onycholysis, Pterygium unguis, Nail loss, New onset of scarring or non-

scarring scalp alopecia, Loss of body hair, Scaling

The pathophysiological concept of cGvHD development is highly complex and can be described in three phases, of which the

1) first phase is characterized by initial tissue injury followed by early inflammation (Figure 5). Tissue is damaged by a variety of factors, i.e. conditioning regimens, cytotoxic therapy, infections and preceded aGvHD. Dying cells release several soluble pro-inflammatory mediators such as damage-associated molecular patterns (DAMPs, e.g. cytokines) and translocated pathogens and their products triggering pathogen-associated molecular patterns (PAMPs, e.g. lipopolysaccharide) into extracellular spaces. Sensing of these inflammatory mediators through different receptor signaling pathways causes rapid activation of innate immune cell subsets and an increased antigen presentation by monocytes, macrophages, neutrophils and dendritic cells (DC). DCs upregulate costimulatory molecules and different APCs secrete high levels of leukocyte-attractant cytokines such as TNF-α, interferon-alpha (IFN-α) and IL-1 in consequence of tissue damage [86]. Resultant, donor T cells are activated upon contact with DCs. T cells are recruited to the sites of inflammation via elevated levels of chemokines, as e.g. CXCL9/CXCL10 through the bloodstream, where they further augment the inflammatory reaction [87, 88].

Additionally, non-hematopoietic cells, as endothelial cells (EC) or fibroblasts, are damaged and activated to facilitate inflammation. As of great relevance for this thesis, the involvement of endothelium in GvHD pathology is further elucidated in chapters 1.4.1 and 1.4.2.

2) The second phase of cGvHD is composed of chronic inflammation and a dysregulated adaptive immunity. Alloreactive T- and B cells in the graft are primed by APCs. After recognition of presented antigens, these cells are differentiated and expanded into Th1, Th2 or Th17 cells [89] and autoantibody-producing germinal center B cells. In a healthy immune system immune-cell polarization is counterbalanced by multiple tolerogenic features. Most important, the thymus mediates tolerance by producing regulatory cell populations or by selecting and ‘outsourcing’ autoreactive T- and B cells. In cGvHD patients, functional tolerance is partly impaired or completely deficient due to thymic destruction through toxic conditioning, medical immunosuppressive prophylaxis and alloreactive T- and B cells. As a result, regulatory cell populations (Tregs, Bregs, NKregs) are decreased or missing and alloreactive CD4+ or CD8+ T cells, that have escaped thymic selection are released into the periphery, where they produce additional pro-inflammatory cytokines, as IL-17, IL-21 or IFN-γ [90, 91].

3) The third phase is characterized by an aberrant tissue repair and propagating chronic inflammation and fibrosis. Key players for the release of pro-fibrotic factors are activated macrophages, which induce the production of extracellular matrix (ECM) collagens in fibroblasts by secretion of platelet-derived growth factor α (PDGF-α) and transforming growth factor β (TGF-ß). [92] Acute lymphoid cell infiltration at the sites of tissue injury provoked by endothelial damage is followed by persistent immune activation due to a miscommunication between adaptive and innate immune system, which initiates the fibrotic cascade. Tissue architecture and organ function are continually destroyed by massive accumulation of ECM-components produced by activated myofibroblasts [93]. Chronic inflammation is sustained by IL-17–producing Th17 cells and pathogenic immunoglobulin deposition, evoked by over-activated plasma B cells, both contributing to persistent organ damage and fibrosis [90].

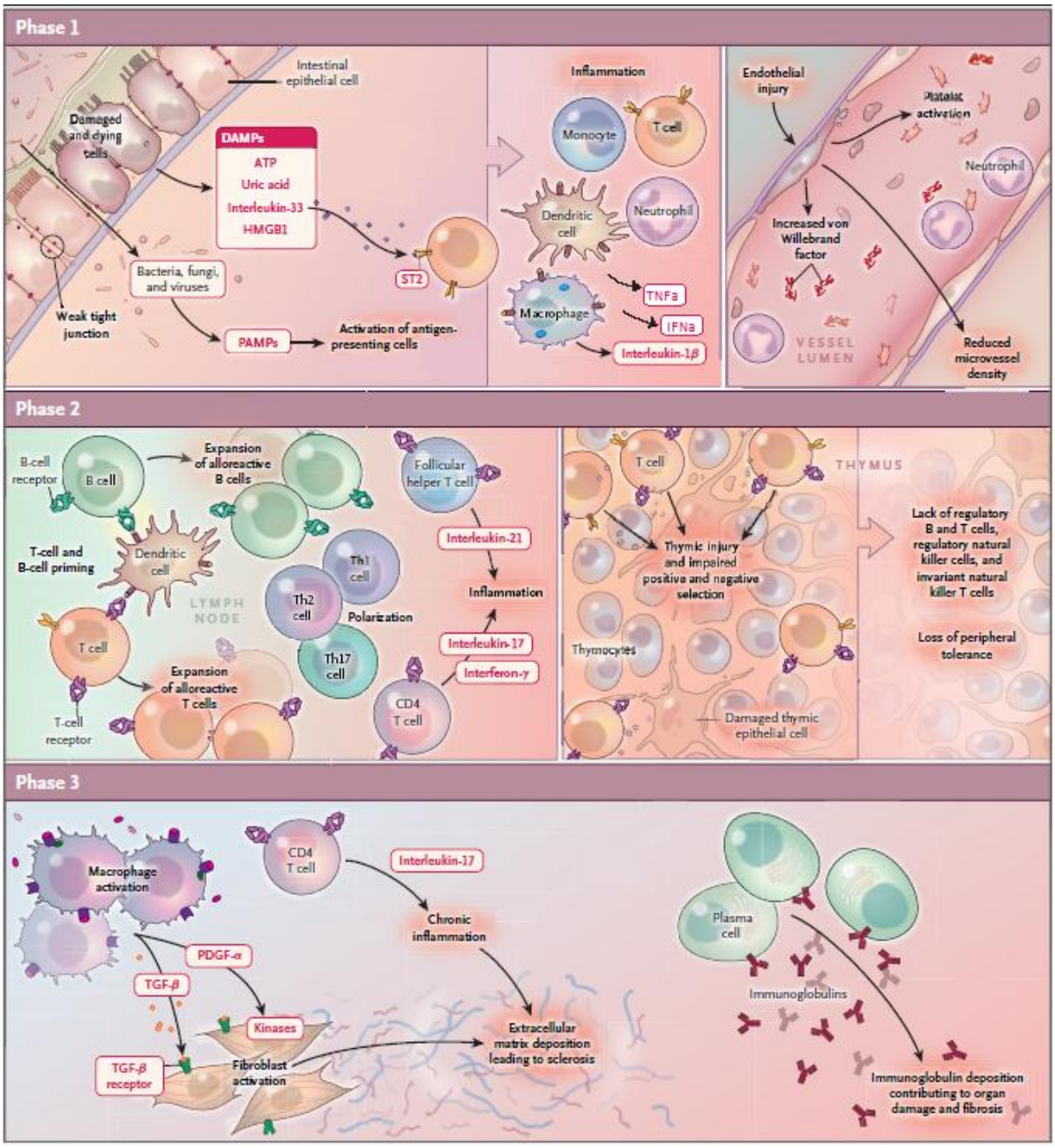

Figure 5: 3-phase model of the pathophysiology of cGvHD. From [94].

1.2.3. Mouse Models of GvHD

The establishment of animal models, especially mouse and canine models has been of central importance for the identification and the general understanding of GvHD pathophysiology as well as the preclinical testing of reliable treatment strategies for translation into humans. Historically, Korngold and Sprent made a substantial contribution to the elucidation of GvHD pathophysiology in 1970, when they first described the T cell dependence of GvHD [95]. A steady development of new preclinical mouse models proceeds until today. With help of

murine models, aGvHD as well as cGvHD phenotypic characteristics have been elucidated (Table 3), delineating the two forms of disease as distinct pathological entities.

Table 3: Phenotypic readouts of acute and chronic GvHD in mouse models. Adapted from [96].

Acute GvHD	Chronic GvHD
• High Mortality • Severe acute morbidity (weight loss, decreased activity) • Acute Inflammation, apoptosis and necrosis in target organs (Gastrointestinal tract, Liver, Skin) • Th1 response → Cytokines IL-2, IFN-γ, TNF-α, IL-1β • Immune Deficiency	• Long-term Survival • Chronic Morbidity • Chronic Inflammatory Changes and Fibrosis / Sclerosis (Skin, Lungs, Livers) • Th2 response → Cytokines IL-4, IL-10, TGF-ß • Autoantibody Production • Dysfunctional tolerance mechanisms

Of big advantage the genetically determined MHC variability between donors and recipients can be tightly controlled in murine models [97–99]. Current GvHD models can be categorized into major MHC (class I, class II or both) or minor histocompatibility antigen (HA) mismatch, which mainly determines if GvHD is induced by CD4+ or CD8+ T cells: CD4+ induction is not dependent from MHC II presentation on host tissue and antigen presentation is performed by either host or donor APCs [100, 101], while CD8+ provokes GvHD by MHC I recognition on target tissue and exclusively host APCs display antigens [100, 102]. For the majority of models, inbred mouse strain recipients are conditioned with TBI and subsequently transplanted with HSC grafts from BM, which is supplemented with T cells from donor mice [103]. Hence, the severity and onset of GvHD can be adjusted by adaption of radiation doses and T cell numbers [104]. The different available mouse models for both acute and chronic GvHD, relevant developments and limitations of murine models are covered below.

1.2.3.1. Mouse Models of aGvHD

Table 4 depicts a brief compendium of classical aGvHD mouse models. All models use myeloablative TBI and subsequent hematopoietic reconstitution is achieved through T cell depleted BMCs with additional donor lymphocytes. The most studied aGvHD model is the MHC mismatched transplantation of C57BL/6 [$H2K^b$] → BALB/c [$H2K^d$] or vice versa. It results in a systemic disease with high mortality. Korngold and Sprent developed the minor HA mismatched models B10.D2 [$H2K^d$] → DBA/2 [$H2K^d$] and B10.BR [$H2K^k$] → CBA [$H2K^k$]. The advantage of these models is the close relation to clinics, where major MHC mismatches are rarely performed. Parent-into-F1 models as C57BL/6 [$H2K^b$] → B6D2F1 [$H2K^{b/d}$] can be used with or without TBI, to study e.g. reduced intensity conditioning

regimens. A major advantage of the parent-into-F1 model is the elimination of the host-versus-graft rejection, which is a T cell dependent phenomenon occurring frequently when non-myeloablative conditioning is performed. Whole splenocytes can be infused into non-irradiated mice, resulting in mixed chimerism, while BMCs + T cells are transferred only into irradiated recipients.

Table 4: Commonly used aGvHD mouse models. Donor and recipient strains of aGvHD models, type of MHC mismatched antigens—MHC class I (I), MHC class II (II)—or minor HA mismatch, TBI (+chemotherapy conditioning) doses, T cell dependence of evoked GvHD (CD4 and/or CD8 driven) and GvHD Mortality (Major ≥50%, Minor = 10% to 50% mortality). Adapted from [103, 105].

Donor	Recipient	MHC mismatch	TBI Dose (cGy)	T cell dependence	Mortality	Reference
C57BL/6	B6D2F1	I, II, minor	1100-1500 or no TBI	CD4 (±CD8)	Major	[106, 107]
C57BL/6	BALB/c	I, II, minor	900	CD4 (±CD8)	Major	[108]
B10.D2	DBA/2	minor	1000	CD4	Major	[95, 109]
DBA/2	B10.D2	minor	1100	CD8	Minor	[95]
B10.BR	CBA	minor	1100	CD8	Major	[95, 110]
human PBMCs	NOD/SCID	I, II, minor	200-250 or no TBI	CD4	Major	[111, 112]

In the clinical setup, standardized conditioning for most malignancies involves the use of chemotherapy in allo-HSCT patients, whereas TBI is applied infrequently. To overcome this issue of absent transferability to the clinical situation, aGvHD models using cytotoxic conditioning recently came into focus. Riesner et al. established a minor HA mismatched aGvHD mouse model LP/J [$H2k^b$]→C57BL/6 [$H2k^b$] and Sadeghi et al. described a major MHC mismatched C57BL/6 [$H\text{-}2K^b$] → BALB/c [$H\text{-}2K^d$] model, both conditioned with busulfan and cyclophosphamide [113, 114].

Compared to mouse models, humans exploit an enormous TCR repertoire. To mimic this variability and to study and modify human GvHD *in vivo*, xenogeneic (humanized) models have been developed, where human PBMCs can be transplanted into immunodeficient mice strains. Nonobese diabetes (NOD)/severe combined immunodeficiency (SCID) mice lack functional T- and B lymphocytes, thus are susceptible for human immune cells, although engraftment numbers for human leukocytes did not provide satisfactory results [115]. From the genetic background of NOD/SCID other immune-competent mouse strains were generated for xenotransplantation. As one example, NOD/SCID gamma (NSG) mice are deficient in their IL2-receptor-function, resulting in a missing T-, B- and NK- cell repertoire and deficient

macrophage- and DC activity [116]. In xeno-HSCT experiments this model showed promising engraftment numbers and an aGvHD phenotype with human T-cell infiltration of mouse skin, liver, intestine and lungs [111].

1.2.3.2. Mouse Models of cGvHD

cGvHD is a highly heterogeneous disease with complex clinical manifestations in patients. Even if several mouse models were established (Table 5), which helped to understand the intricate cGvHD pathophysiology and facilitated interventional treatment strategies, there is still no individual mouse model reliably comprising the diverse pathological and immunological characteristics of cGvHD. So far, researchers may use more than one mouse model to study cGvHD depending on the scientific hypothesis, because most preclinical models show dominant manifestations in limited tissues or do not replicate a stable cGvHD phenotype [117].

cGvHD mouse models can be broadly categorized into sclerodermatous/pro-fibrotic models, autoantibody-mediated/ lupus-like models and a transgenic thymic dysfunction model, which was described by Sakoda et al [118]. Sclerodermatous models, as the B10.D2 [$H2K^d$] → BALB/c [$H2K^d$] or the LP/J [$H2K^b$] → C57BL/6 [$H2K^b$] are mismatched in minor HAs and exhibit fibrotic depositions in skin, lung or liver within 30 days after transplantation. The most studied autoantibody-mediated model is the parent-into-F1 DBA/2 [$H2K^d$] → B6D2F1 [$H2K^{b/d}$]. It resembles human cGvHD, as it shows lupus-like manifestations as nephritis, liver cirrhosis, salivary gland fibrosis and skin involvement. Due to a massive activation of recipient B cells, lymphadenopathy, splenomegaly and autoantibody production can be detected in this model. Some mouse models manage to mimic a mixed cGvHD phenotype: transplantation of DBA/2 [$H2K^d$] → BALB/c [$H2k^d$] results in autoantibody production combined with scleroderma, when recipients are sublethally irradiated. In C57BL/6 [$H2K^b$] → (C57BL/6 × BALB/c)F1 [$H2K^{b/d}$] transplantation, pro-inflammatory aGvHD is progressing to cGvHD. Since this overlapping transformation is common in patients, mouse models can help to identify mechanisms of the causal link between allo- and autoreactivity.

Table 5: Commonly used cGvHD mouse models. Donor and recipient strains of cGvHD models, type of MHC mismatched antigens—MHC class I (I), MHC class II (II)—or minor HA mismatch, TBI (+chemotherapy conditioning) doses, T cell dependence of evoked GvHD (CD4 and/or CD8 driven) and GvHD Mortality (Major ≥50%, Minor = 10% to 50% mortality). Adapted from [103, 105].

Donor	Recipient	MHC mismatch	TBI Dose (cGy)	T cell de-pendence	Lethality	Reference
B10.D2	BALB/c	minor	600-900	CD4	Minor	[95, 119, 120]

LP/J	C57BL/6	minor	1100	CD4	Minor	[121]
DBA/2	B6D2F1	I, II, minor	no TBI	CD4	Minor	[122–124]
C57BL/6	(C57BL/6 × BALB/c)F1	I, II, minor	no TBI	CD4	Minor	[125]
DBA/2	BALB/c	minor	650		Minor	[126]
BALB/c	(BALB/c × A)F1	I, II, minor	no TBI	CD4	Minor	[127, 128]

1.2.4. Treatment of GvHD

Prevention of GvHD is the most important approach in disease management after allo-HCT. Since aGvHD is described to be a mainly T cell driven disease, the majority of prophylactic treatments are directed to target T cell reactivity. Administration of calcineurin inhibitors as cyclosporine A or tacrolimus combined with cytostatics, e.g. methotrexate remains the standard prophylaxis after transplantation [129–131]. These drugs exert immunosuppressive features by blockade of T cell activation through IL-2 inhibition, but the treatment includes a variety of significant side effects and toxicities [132]. By far the strongest risk factor for the development of cGvHD is the presence and severity of precedent aGvHD [133, 134], albeit specific attempts to prevent aGvHD by administration of varying calcineurin inhibitor – cytostatic combinations or immune-modulatory therapeutics i.e. thalidomide did not adequately decrease cGvHD rates [135].

Once established, moderate to severe forms of acute and chronic GvHD require continuous monitoring and appropriate treatment. First line therapy of both diseases still includes systemic or topical application of high-dose corticosteroids (mostly methylprednisolone) alone or together with calcineurin inhibitors [131, 132, 136]. Only 40% - 50% of patients show responses to first line therapy and complete disease eradication can only be achieved in less than 20% of these patients [132, 137–139]. Additionally, therapeutic success decreases in more established, severe GvHD forms. Non-responding patients may develop steroid-refractory GvHD, persistent aGvHD or transform into cGvHD, all be associated with poor prognosis, high morbidity and mortality [140]. According to the EBMT guidelines, there are still no standard treatment regimens for steroid-refractory patients, since data on existing therapeutics are mostly based on retrospective studies or small, single-armed phase II trials [141].

Until today, there is no consensus about second line aGvHD therapy, if first line therapies fail to show remedy [141]. A plethora of alternative choices have been tested, including anti-

thymocyte globulin or other monoclonal antibodies, with limited success [138, 142, 143]. High-dose cyclophosphamide can eliminate alloreactive donor T cells, but is has to be administered early after allo-HCT and can only be applied short-term, because of toxic side effects [144]. Second line therapy strategies for cGvHD patients vary between transplantation centers with erratic outcomes. Commonly used therapeutics include irutinib [145], the mammalian target of rapamycin (mTOR) inhibitor sirolimus and tacrolimus (both prohibiting proliferation and activation of T cells), the anti-B cell-antibody rituximab, the cytostatic pentostatin or the TGF-ß/PDGF-inhibitor imatinib [146–149].

Summarizing, complete GvHD eradication is rare and the greatest challenge remains the maximization of the GvT-effect with the simultaneous minimization of GvHD. Especially in cGvHD the therapy duration can last for months up to years, which is problematic when steroids are administered [68]. High-dose, long-term immunosuppression causes high mortality rates in anyway immune-compromised GvHD patients, mainly due to increased side effects, drug toxicities and augmented opportunistic infections [137, 141]. Furthermore, the high probability of graft failure or disease relapse resulting from suppression of the GvT-effect, should not be neglected [74, 150].

The urgent demand for alternative treatments and prevention strategies brings the endothelium into focus. It represents the first contact between transplanted donor HSCs and recipient's tissue. After allo-HSCT, related complications as the above mentioned VOD/SOS syndrome [51, 151], capillary leakage [152] or transplantation-associated-microangiopathy [153] are frequently described and suppose a pathologic participation of the endothelium. Besides, it is involved in early aGvHD progression [154] and is damaged or destroyed in later aGvHD stages [155, 156]. In steroid-refractory GvHD and in aGvHD, serum markers of endothelial stress and damage were found elevated [157, 158], proposing evidence for the endothelium being an important player in disease pathogenesis. It remains still unclear, how the endothelial function influences the development of acute and chronic GvHD and to which extend the vascular damage aggravates the GvHD severity. Therefore, the endothelium may represent an alternative target for prophylactic protection or therapeutic intervention of GvHD after allo-HSCT. Characterization of the endothelial function and its relevance in HSCT with focus on GvHD, especially the susceptibility to immune-mediated vascular injury and possible pharmacologic strategies to normalize endothelial dysfunction are the major questions of the present thesis and are covered in more detail in the following sections.

1.3. Physiology and pathology of the endothelium

The endothelium forms the inner lining of all blood and lymphatic vessels and represents, with all arteries, veins and capillaries, the biggest organ system in the human body. With an average weight of more than 1 kg and a spatial distributed size of more than 4000 m^2 it fulfills a multitude of physiologic functions and acts as a clinically relevant player in a variety of pathologic conditions [159].

1.3.1. Structure and function of healthy endothelium

In a blood vessel wall, endothelial cells (ECs) are anchored to the basal lamina and orientated along the vessel axis in a cell monolayer. The basal lamina and polarized ECs constitute the tunica intima, lining the entire circulatory system. This scaffold is covered by smooth muscle cells (SMCs) and pericytes (Figure 6). Those mural cells can be distinguished from ECs by expression of several exclusive markers, such as alpha-smooth muscle actin (αSMA), platelet-derived growth factor receptor-β (PDGFRβ) or neural/glial antigen-2 (NG2) [160].

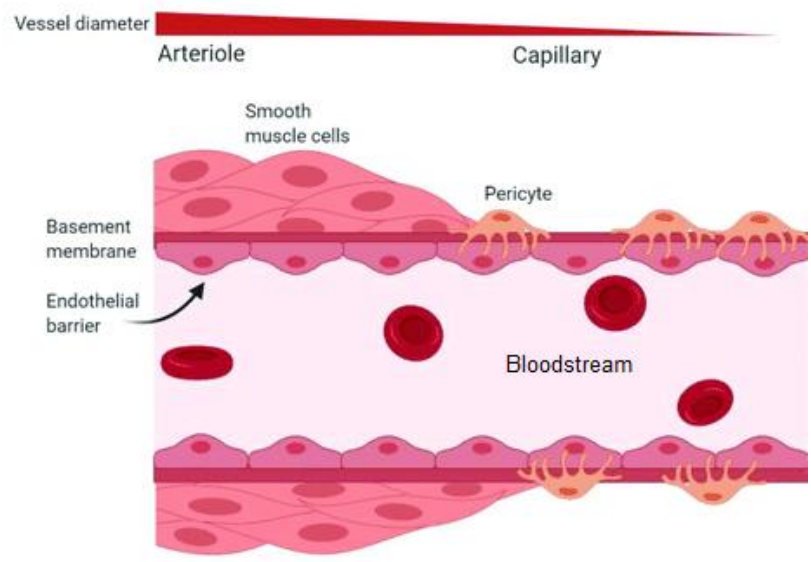

Figure 6: Schematic illustration of the endothelium/ vessel architecture. Modified after [161].

ECs exhibit a remarkable phenotypic heterogeneity in structure and function. Normally they display a flat, elongated, cobblestone-like form, while irregularly shaped cell morphologies have been described in different vascular beds [162]. As illustrated in Figure 7, endothelium can be continuous or discontinuous. To maintain integrity as a selective barrier, the continuous endothelial layer harbours intercellular junctions, which are impermeable for macromolecules. Tight junctions are promoted by different adherent proteins, such as claudins or occludin. Both are linked to the actin filament by the zonula occludens protein-1 (ZO-1). Transmembrane vascular endothelial-cadherin molecules (VECad) in adherens junctions link neighbouring ECs and are further coupled to actin or

vimentin filaments in the cytoskeleton. Apart from junctional regions, platelet endothelial cell adhesion molecule (PECAM; CD31), endothelial cell-selective adhesion molecule (ESAM) or melanoma cell adhesion molecule (MCAM; CD146) interconnect ECs [163, 164]. The fenestrated endothelium contains transendothelial pores and fenestrae (70 nm) and allows transport of smaller molecules, while the discontinuous endothelium harbours large gaps (up to 200 nm), which allows the permeation of cells [162].

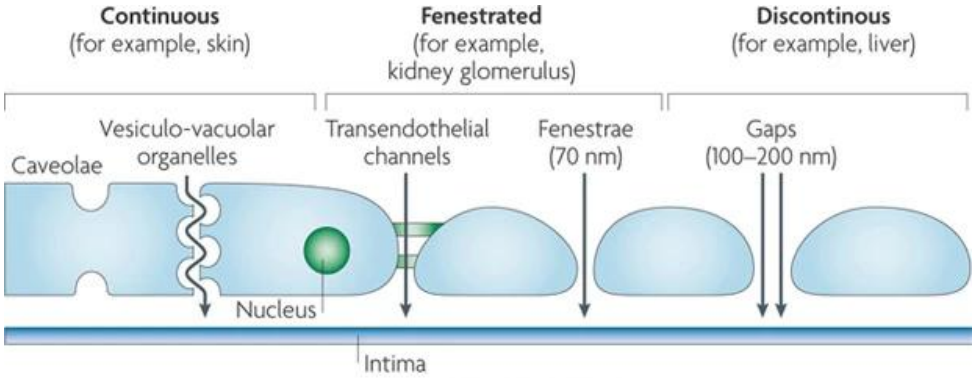

Figure 7: Heterogeneous architecture of the endothelial monolayer. Adapted from [165].

As described, the main function of EC monolayers is represented in its barrier function. ECs form a permselective membrane for soluble molecules, cells, gases and liquids between the blood and surrounding tissue, thus maintaining vasomotor tone (blood pressure) mainly by nitric oxygen (NO) synthesis and controlling hemostatic balance (coagulation). Moreover, the endothelium mediates leukocyte trafficking, the development of new blood vessels (angiogenesis & vasculogenesis) and takes part in antigen presentation and innate immunity [159].

1.3.2. Angiogenesis

There are two mechanisms of blood vessel development: 1) Vasculogenesis, in which ECs or hematopoietic precursors (angioblasts or hemangioblasts) differentiate from the embryonic mesoderm *in situ* and build an early vasculature and 2) Angiogenesis, where blood vessels proliferate, branch and sprout from existing ones to maturate and propagate the vascular system [166]. Angiogenesis is involved in growth, reproduction, wound repair or as response to certain stimuli as hypoxia or inflammation. Pathologic angiogenesis and insufficient vessel maintenance, which has to be considered individually from physiologic angiogenesis, is described to participate in numerous diseases [167], such as inflammatory responses, cancer [168], diabetes mellitus [169] and cardiovascular complications (stroke, myocardial infarction), ulcerative disorders and neurodegeneration, inflammatory disorders, pulmonary hypertension and blindness [170]. The role of pathologic angiogenesis in GvHD is further delineated in the following chapters 1.4.1 and 1.4.2.

Angiogenesis is a highly orchestrated, sequential process comprising vasodilation, degradation of the basement membrane, EC migration & chemotaxis, increasing vascular permeability and formation of new vessels. As a first step, hypoxia (NO) induced vasodilation increases vascular permeability. Hypoxic tissues release angiogenic factors, which terminate endothelial quiescence and activate surrounding ECs. ECM and the basal lamina are degraded by various proteinases in corroboration with Angiopoietin-2 (Ang-2), which acts as an antagonist to Tie2, a tyrosine-kinase receptor preventing vascular leakiness in non-angiogenic settings [171]. The degraded matrix drives the release of numerous angiogenic growth factors such as VEGF, fibroblast growth factor 2 (FGF-2), TGF-β and TNF-α. Hence key angiogenic growth factor VEGF binds to VEGF receptor 2 (VEGFR2) and ECs are specified into tip- and stalk cells. Tip cells harbour the highest VEGFR2 levels and guide the sprouting vessels towards chemoattractants, while the proliferative stalk cells elongate the growing tubes [172]. Concurrently, inhibitors of angiogenesis e.g. thrombospondin-1, arrestin, fibronectin (FN), endostatin (ES) are secreted from the dissolving matrix in order to switch off the angiogenic process [173]. Once assembled in vessels, ECs become dormant and maturation (‘arteriogenesis’) is finalized with superimposition of mural cells. In this last step, pericytes and SMCs are recruited to the newly built vessels by a multitude of chemoattractants and assembled to the nascent endothelium promoted by Ang1, Tie2 and others, such as TGF-ß1, TGF-βR2, endoglin (ENG; CD105) an endothelial TGF-β binding protein as well as Smad5, a downstream TGF-β signaling molecule [174].

1.3.3. Endothelial metabolism

ECs throughout the body are exposed to a myriad of microenvironmental conditions e.g. different growth factors, cytokines, chemokines as well as changing oxygen (O_2) and pH levels, temperature fluctuations, variable concentrations of blood glucose and nutrients and cell-contacts with cells from the blood stream, which can cause shear stress to the EC layer [162]. As these conditions may change rapidly, ECs have to react fast to coordinate their metabolism and adapt metabolic fluxes and biomass production to the prevalent ambient conditions. To meet these requirements, ECs are able to convert their cellular phenotype, protein or mRNA expression, proliferation, angiogenesis, apoptosis or the release of certain inflammatory mediators [159]. Exemplifying, ECs express an elevated need of nutrients and

energy levels during angiogenesis to implement cell migration, proliferation and biosynthesis of new compounds for cell division [175]. As angiogenesis mostly occurs in hypoxic tissue starved of nutrients, the EC metabolism needs to work independently from the surrounding tissue. Figure 8 gives an overview of the different metabolic pathways in healthy endothelium. Different to other cell types, which generate energy (adenosine triphosphate; ATP) primarily by oxidative phosphorylation under O_2 presence and only switch to glycolysis in anaerobic stages, ECs produce high amounts of ATP through aerobic glycolysis (so called 'Warburg effect'), with proangiogenic molecules e.g. VEGF enhancing the process [176]. Albeit the preferred use of glucose instead of O_2 from the blood appears inefficient for ATP production, it harbours some advantages: Glucose is the most profuse nutrient and the kinetics of glycolysis are fast, which can be beneficial for rapid energy transfer in EC sprouting. O_2 deprivation is only affecting EC behaviour when glucose is limited at the same time, increasing the tolerance towards hypoxia. This might be of importance when ECs sprout into hypoxic tissues upon angiogenesis. Additionally, metabolic intermediates from glycolysis (Glucose-6-phosphate) are branched from glycolysis into the pentose phosphate pathway (PPP) and diverted into intermediates for nucleotide biosynthesis (ribose-5-phosphate) [177, 178]. Another important metabolic pathway for endothelial cells involves the process of fatty acid oxidation (FAO). Fatty acids are imported via the transport protein carnitine palmitoyltransferase 1a (CPT1a) into mitochondria, where they were oxidated and enter deoxyribonucleotide (dNTP) production required for DNA synthesis during EC proliferation. Moreover, deletion of CPT1 causes sprouting defects *in vivo* and *in vitro,* indicating that FAO is regulating vessel sprouting [179].

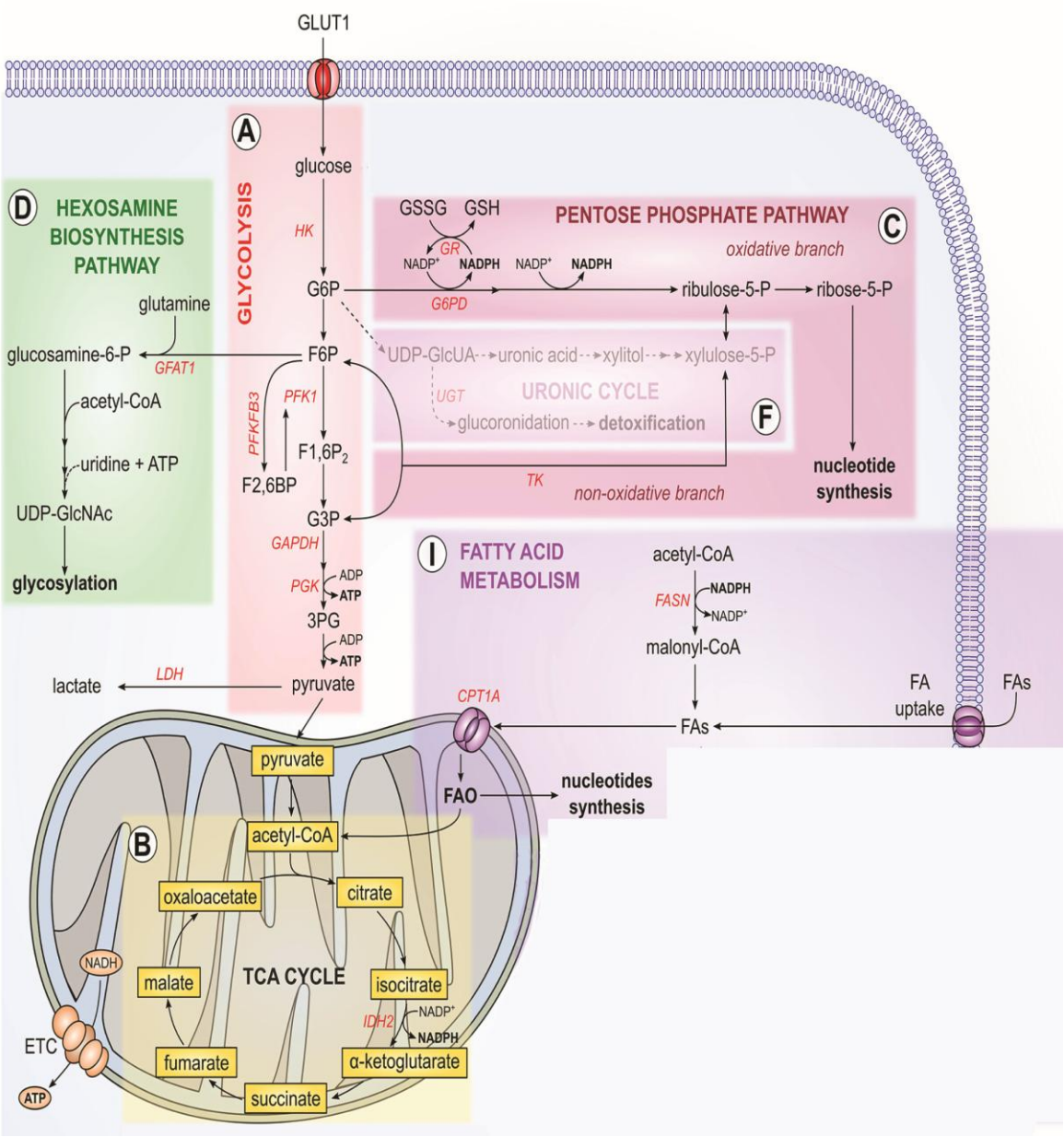

Figure 8: Schematic representation of the endothelial cell metabolism. Modified after [180].
A: glycolysis; **B:** tricarboxylic acid (TCA) cycle; **C:** pentose phosphate pathway; **D:** hexosamine biosynthesis pathway; **F:** uronic cycle; **I**: fatty acid metabolism.

A dysfunctional EC metabolism is described in various pathologic stages. Enhanced glycolysis rates are anticipated to be coherently responsible for vascular inflammation [181], cancer cell invasion [182] and neovascular ocular diseases [183]. Understanding EC metabolism promises to reveal new perspectives on disease mechanisms in the vascular system with therapeutic implications for disorders with aberrant vessel growth and function.

1.3.4. Endothelial activation & immune cell interactions

Endothelium is quiescent in non-inflammatory settings. Quiescence is defined by minimal or absent proliferation and migration, minimal or no vascular leakage and reduced expression of leukocyte adhesion molecules. Injured tissue cells release danger signals, which stimulate resident mast cells, monocytes, DCs or macrophages to secrete cytokines and pro-inflammatory mediators, thus activating the resting endothelium [184]. Endothelial type I response (stimulation) to acute inflammation occurs rapidly and is independent of gene expression, different to the more sustained type II response (activation). Following a signal cascade mediated through ligand binding to G-protein coupled receptors, type I response causes ECs to increase the blood flow and the plasma protein leakage into tissue, both supporting leukocytes to reach sites of inflammation. P-Selectin, an adherens junction protein normally stored in secretory vesicles known as Weibel-Palade bodies in resting ECs, is exocytosed to the cell surface and promotes binding and activation of neutrophils to the EC layer [185]. Type II response is evoked by inflammatory cytokines secreted from activated leukocytes, such as TNF-α or IL-1ß [186]. Cytokines activate endothelial transcription factor $NF\kappa_B$ through various signaling complexes, resulting in expression of newly synthesized genes and translation of pro-inflammatory proteins: E-selectin, intercellular adhesion molecule 1 (ICAM1; CD54) and vascular cell-adhesion molecule 1 (VCAM1, CD106) which foster leukocyte adhesion.

Since the endothelium is in direct contact with all cells entering the blood stream, it mediates targeted transmigration of leukocytes from the blood into the tissue, which comprises a multistep adhesion cascade (Figure 9). This process is mainly associated with inflammation, but is also involved in physiologic hemostasis, wound repair and thrombosis.

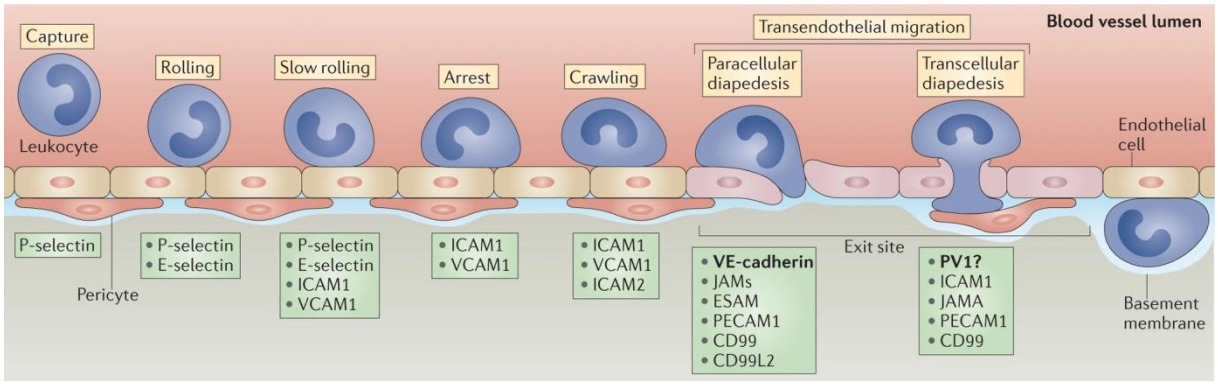

Figure 9: Multistep process of leukocyte transmigration through the endothelial barrier. Adapted from [187].

1) ‘Catch & Roll’: Following previously described endothelial activation, endothelial selectins (P- and E-selectin) are induced at the EC surface, promoting a transient adhesion of passing leukocytes from the blood stream. The blood flow pushes the loosely attached leukocytes forwards, ensuing a rolling of cells at the EC layer.

2) ‘Arrest & Crawl’: Chemoattractants and chemokines are released from the ECs and/or the infiltrating leukocytes triggering the activation of leukocyte integrins. ECs externalize receptors as ICAM1 or VCAM1 upon stimulus from pro-inflammatory cytokines, to which the leukocyte integrins lymphocyte function-associated antigen (LFA) and very late antigen 4 (VLA4) firmly bind. Leukocytes get arrested and ‘crawl’ on the luminal surface until a suitable transmigration site arises.

3) ‘Transendothelial migration/ diapedesis’: Migration through the vessel wall can occur transcellular or predominantly paracellular through junctions or between adjacent ECs. EC-cell contacts are loosened and tight junctions are opened by dissociation of VECad transmembrane receptors, mediated by ICAM1/VCAM1 binding and supported by soluble factors like vascular endothelial growth factor A (VEGFA) and histamine. Leukocytes are guided through the EC layer by binding of diapedesis receptors PECAM1, CD99 and others [187, 188].

Additionally, activated ECs do not only upregulate several leukocyte adhesion molecules on their surface, but also express MHC I and MHC II molecules [189, 190] and co-stimulatory peptides. ECs might participate as semi-professional APCs in antigen presentation to specialized T cells, which particularly persist in chronic inflammatory processes [191]. Human ECs share various T cell co-stimulatory surface proteins with professional APCs: lymphocyte function-associated antigen (LFA-3; CD58), CD40 or inducible T-cell co-stimulator (ICOS) which are involved in T cell memory functions. ECs are described to effectively stimulate memory and effector-memory T cells but fail to activate naive T cells, probably because of the absent expression of CD28-engaging co-stimulatory molecules [192].

1.3.5. Circulating endothelial progenitor cells (CEPs) and circulating endothelial cells (CECs)

Upon EC monolayer injury, a subset of BM-derived circulating endothelial progenitor cells (CEPs) might contribute to cell layer regeneration. CEPs only account to 1% of blood cells and are characterized by the HSC markers CD133 or CD34, as well as by VEGFR2, VECad

and von-Willebrand factor (vWF) when expanded *in vitro* [193, 194]. CEPs, which are stimulated by ischemia, have shown to exhibit prohibitive functions in atherosclerosis [195] and diminished numbers are associated with higher risk for cardiovascular disease [196]. In contrast, CEPs in presence of pro-inflammatory cytokines, may not differentiate into mature ECs, but develop characteristics of myeloid cells such as macrophages and DCs, thus contributing to endothelial pathology [197].

In consequence to persistent inflammation and concomitant endothelial activation, mature ECs can lose integrity, become senescent and detach from vessel walls [198]. Those circulating endothelial cells (CECs) can be identified through expression of classical EC- and apoptosis-markers in absence of HSC markers, e.g. CD31+, CD146+, CD133-, CD34-, CD45- [199, 200]. Elevated levels of CECs can be observed in atherosclerosis, as well as other inflammatory and autoimmune diseases, as rheumatoid arthritis (RA) [201] and systemic lupus erythematosus (SLE) [202].

1.3.6. Endothelial-to-mesenchymal transition (EndoMT)

During the pathogenesis of certain diseases, the transition of vascular ECs into mesenchymal cells has been described. This process, referred to as endothelial-to-mesenchymal-transition (EndoMT) has been implicated to contribute to vascular remodeling and disease progression of numerous malignant, vascular, inflammatory and fibrotic disorders [203]. It has been shown to stimulate angiogenesis and metastasis in cancer [204, 205], to promote vascular fibrosis and vascular loss in diabetes mellitus [206] and to stimulate fibrosis in fibrotic/sclerotic and inflammatory diseases e.g. systemic sclerosis-associated pulmonary [207], intestinal [208] and cardiac fibrosis [209], idiopathic pulmonary hypertension [210] or irradiation-induced rectal fibrosis [211], to list only a few.

During EndoMT, ECs lose their specific endothelial properties and progressively evolve into a mesenchymal phenotype that includes acquisition of cellular motility and invasive and contractile properties. The initiation is accompanied by the progressive reduction, emerging to a complete loss of EC-specific proteins including vWF, CD31/PECAM-1, and VECad [212]. Successively, mesenchymal and fibroblast markers such as αSMA, fibronectin (FN), N-cadherin, vimentin, fibroblast-specific protein-1 (FSP-1; also known as S100A4), fibroblast activating protein (FAP), and fibrillar collagens I and III are expressed (Figure 10).

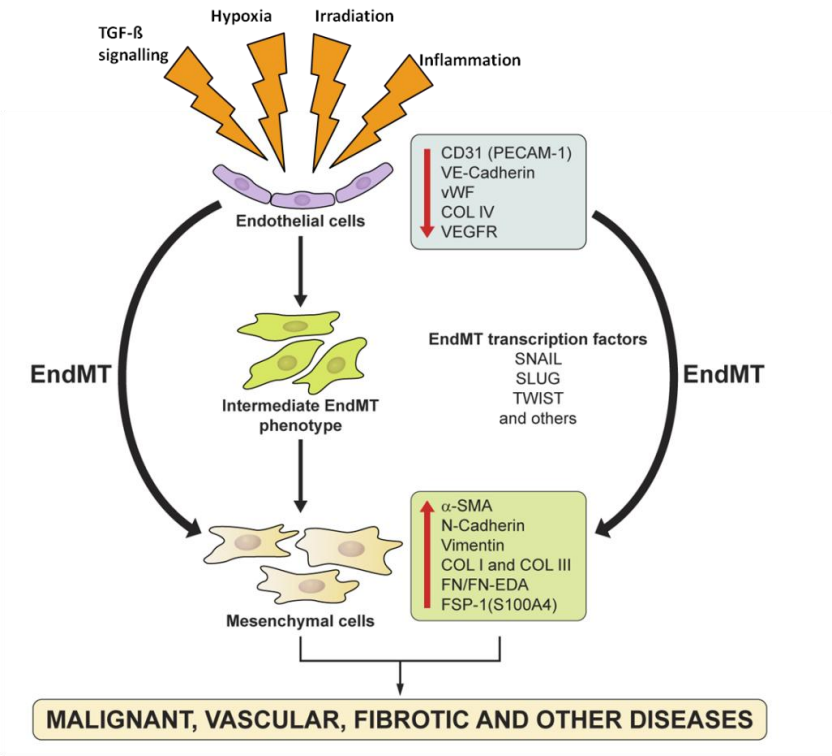

Figure 10: Phenotypic modifications of ECs during EndoMT. Upon transformation, ECs lose specific endothelial markers, activate EndoMT-triggering transcription factors and switch towards a mesenchymal cell-type by upregulating mesenchymal markers. Modified after [213].

Initiation of EndoMT can be triggered by certain stimuli: Oxidative stress, hypoxia, tissue damage resulting from irradiation or inflammation and shear stress, while the most potent inducer is known to be TGF-ß, especially isoform TGF-ß2 [214]. Early pioneering studies have proven that isolated mature ECs were able to express αSMA through a transdifferentiation under the influence of TGF-ß without cell division or proliferation *in vitro*. Also intermediate phenotypes (both EC and mesenchymal features) were detected and the transition was partially reversible following TGF-ß-free culture [215, 203].

TGF-ß signaling is a highly complex process and can occur via non-canonical pathways or via canonical Smad-dependend signaling (Figure 11), with focus on latter. Activated TGF-ß homodimers, secreted in large amounts from a variety of immune cells during inflammation (lymphocytes, DCs, macrophages, monocytes) and from fibroblasts during fibrotic/sclerotic diseases, bind to serine/threonine kinase transmembrane receptors in the first step of the signaling cascade. The most common TGF-ß receptors (TGF-ßR) are TGF-ßRI, also named activin-receptor-like kinase 5 (ALK5) and TGF-ßRII. Signaling can be transduced by fusion of a TGF-ßR2 homodimer with an ALK5 homodimer. Alternatively, ALK1 and ALK5 homodimers can pair for signal transduction. ENG functions as an accessory TGF-ß-binding receptor. Upon ligand binding, TGF-ßRII phosphorylates ALK5 on specific serine and threonine residues in the juxtamembrane region. Following, receptor-regulated Smads (Smad 2/3 for ALK5 and Smad 1/5 for ALK1) are recruited and phosphorylated by ALK5/ALK1

[212]. Together with the common mediator Smad4, R-Smad-complexes translocate into the nucleus, where they regulate the transcription of specific target genes with contribution of transcription factors SNAIL, SLUG and TWIST [216, 217]. Inhibitory Smads can prevent activation of R-Smads by competing ALK5 interaction [218, 212].

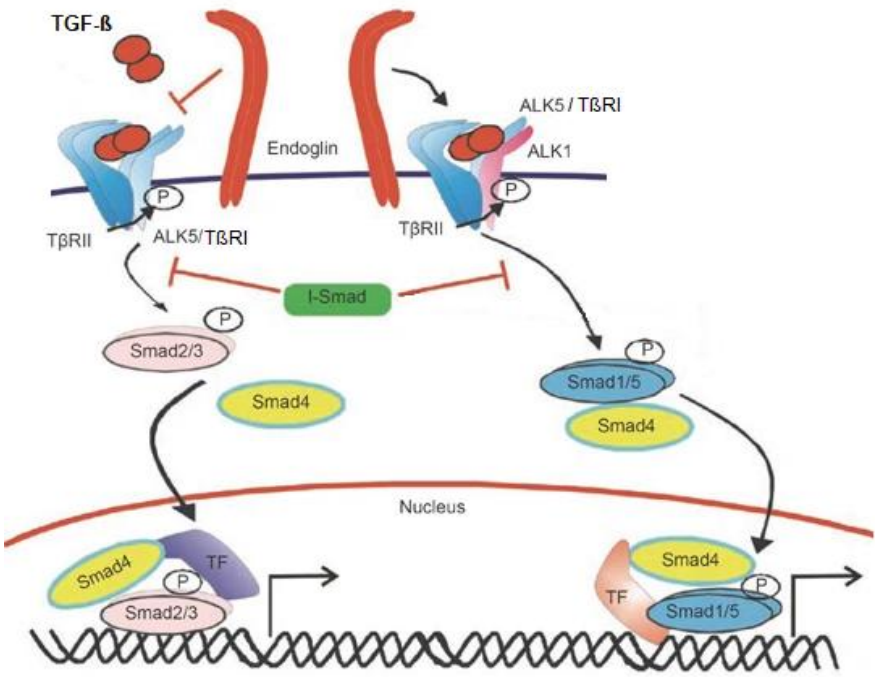

Figure 11: Canonical TGF-β pathways in EndoMT. P = phosphorylated, TF = transcription factor, TßR = TGF-ß receptor; ALK = activin-receptor-like kinase. Modified after [218].

EndoMT increases fibronectin deposition and accumulation of other fibroblast-related proteins. It enhances expression of ICAM and VCAM, thereby not only further promoting recruitment of circulating monocytes and leukocytes and augmenting chronically persisting inflammation, but also inducing the formation of new mesenchymal cells, which leads to the expansion of fibrotic lesions. Additionally, the endothelial metabolism was shown to be affected: TGF-ß induced EndoMT is accompanied by reduced fatty acid oxidation. In consequence, acetyl-CoA levels are diminished and acetylation and activation of inhibitory Smads is malfunctioning, resulting in augmented EndoMT and vessel thickening [219]. Therapeutic inhibition or prophylactic treatment for prevention of EndoMT might be a promising novel strategy to eradicate fibrotic and chronic inflammatory diseases with endothelial involvement.

1.4. Endothelial dysfunction after allo-HSCT

Failure of ECs to perform any of their basal functions adequately is termed as ‘endothelial dysfunction'. Commonly, this term describes the deficiency of ECs to produce and balance NO, thus maintaining vasoconstriction, and the malfunction to control coagulation and permeability or to quiesce leukocytes [185]. In a multitude of diseases as rheumatoid arthritis [220], early systemic lupus erythematosus [221], inflammatory colitis [222] or psoriasis [223], dysfunctional features concerning endothelial mechanisms play an important role in disease pathogenesis. For the understanding of this work, the following chapters will focus on endothelial dysfunction in the context of allo-HSCT and GvHD.

The host endothelium is preferentially the first contact for transplanted donor HSCs. Before, during and after allo-HSCT, ECs are consecutively challenged by toxicities of the conditioning regimen, by systemically administered therapeutic drugs or immunosuppressive prophylaxis and by inflammatory molecules released from damaged cells and tissues, donor leukocyte engraftment and alloreactive immune responses (Figure 12).
Studies showed that ECs directly respond to irradiation, lipopolysaccharides [224], cytokines as TNF-α [225] and cytotoxic lymphocytes as outcomes of early endothelial activation, inflammatory circumstances or alloreactions [226, 227]. Although interactions like endothelial activation and leukocyte transmigration of donor leukocytes with host ECs are tightly controlled, the precise process of endothelial involvement during allo-HSCT and GvHD development has not yet been fully defined. As previously described, vascular ECs might function as APCs and can present cognate antigens to alloreactive T cells, but might likewise also be susceptible to direct immune attacks resulting in endothelial damage.

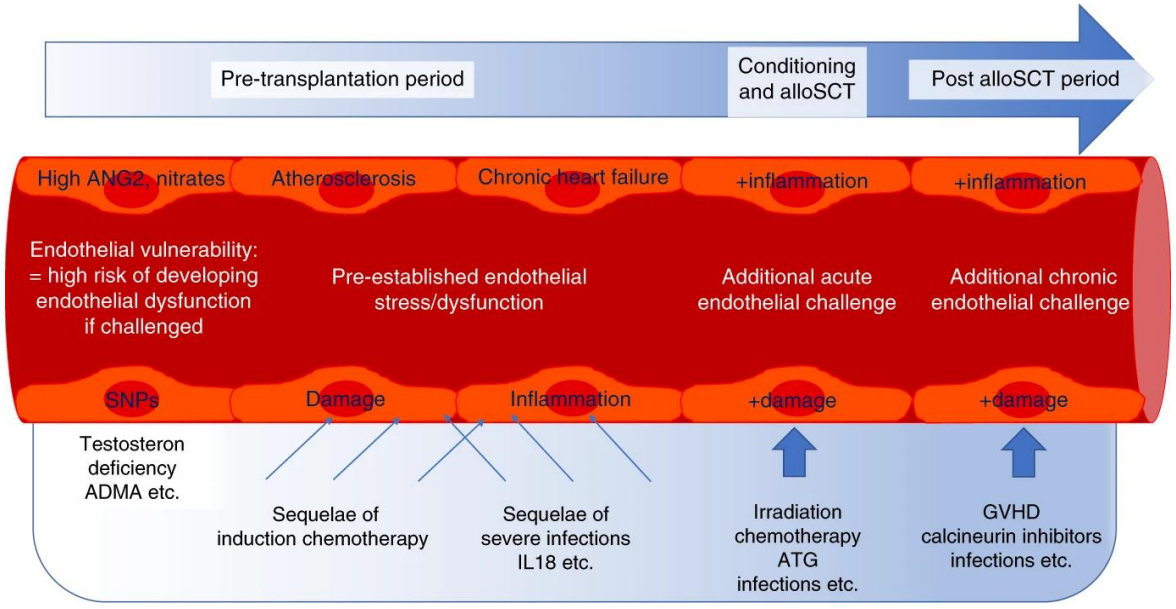

Figure 12: Endothelial challenges during allo-HSCT. Adapted from [228].

Multiple complications involving injury of recipient endothelium have been described to occur during different phases after transplantation. During allo-HSCT, recipients are prone to infections. Initially, they exhibit a reduced immune status due to prior chemical immunosuppression and conditioning, afterwards in consequence of immunosuppressive treatments for GvHD prophylaxis [54]. Additionally, the EC layer is damaged from irradiation or from leukocyte infiltration and the release of inflammatory cytokines, which terminates in raised vascular leakage and permeability and eases the invasion of pathogens.

Vascular leakiness is also delineated in the cytokine storm-provoked capillary leakage syndrome (CLS) and in engraftment syndrome [229, 230]. Both are associated with massive release of proinflammatory cytokines (IL-2, TNF-α, IFN-γ, IL-6) and systemic endothelial damage [230]. In CLS patients, VEGF levels were found to be increased, proving the pathologic relation to capillary injury [231].

Haploidentical transplantation with G-CSF-mobilized PBMCs is today a frequently performed and standardized allo-HSCT procedure, however with an elevated risk for cytokine release syndrome (CRS) [232], which can develop rapidly to a life-threatening complication and is still a great challenge for physicians. Severe cases are initially characterized by hypotension and high fever and can progress to an uncontrolled systemic inflammatory response with vasopressive circulatory shock, vascular leakage, disseminated intravascular coagulation, and multi-organ system failure [233]. The pathophysiology of CRS is still not fully understood, but the considerable numbers of vascular complications implicate an endothelial involvement in disease pathology. Its significance is further underlined by the high occurrence of CRS after the currently emerging chimeric antigen receptor (CAR) T cell therapies.

The most common developing SOS/VOD syndrome appears early after transplantation. It results from conditioning-related toxicity in liver sinusoids, developing to EC injury, subendothelial edema, red blood cell extravasation and fibrin deposits, escalating in subsequent thrombosis and fibrosis or even multi-organ failure [51, 151]. Several endothelial factors showed to be elevated in serum of SOS patients, e.g. P-Selectin, Ang2 or VCAM1 [234, 235].

The increasing use of calcineurin inhibitors as GvHD prophylaxis after allo-HSCT, which comprises EC-toxic side effects, is accompanied by higher rates of transplant associated microangiopathy (TAM). Specifically, TAM manifests as a multi-organ disease occurring after small vessel endothelial injury, leading to subsequent tissue damage with a high morbidity and mortality rate [236, 153]. Patients with TAM showed increased biomarker

levels for endothelial damage, such as vWF or thrombomodulin [237] and high levels of endothelial apoptosis [238].

1.4.1. Endothelium in acute GvHD

While clinical endothelial complications after allo-HSCT have been discovered for many years, the role of ECs in GvHD pathogenesis has recently moved into focus. *In vitro* studies showed initial conditioning-induced EC damage, which was aggravated by LPS-mediated inflammation and followed by allogeneic cytotoxic T-cell attacks, leading to EC apoptosis [239]. Penack et al. utilized murine models to demonstrate the occurrence of neovascularisation during GvHD after conditioning. An increased vessel density in skin, liver and colon facilitated the migration of donor leukocytes to GvHD target organs [240, 241]. From this perspective, Penack and Holtan published a model for EC involvement in GvHD pathogenesis (Figure 13): After conditioning caused EC damage, the recipients' innate immune system is activated by several soluble inflammatory mediators, such as cytokines, chemokines, DAMPs and PAMPs. Transplanted donor cells recognize recipient cognate antigens as foreign and respond in an alloreactive manner. Vasculature itself might be contributing to allo-antigen presentation and concomitantly be targeted by attacking allo-T cells. Combined activation of innate immune system and allo-T cells promote angiogenesis in early GvHD stages [242].

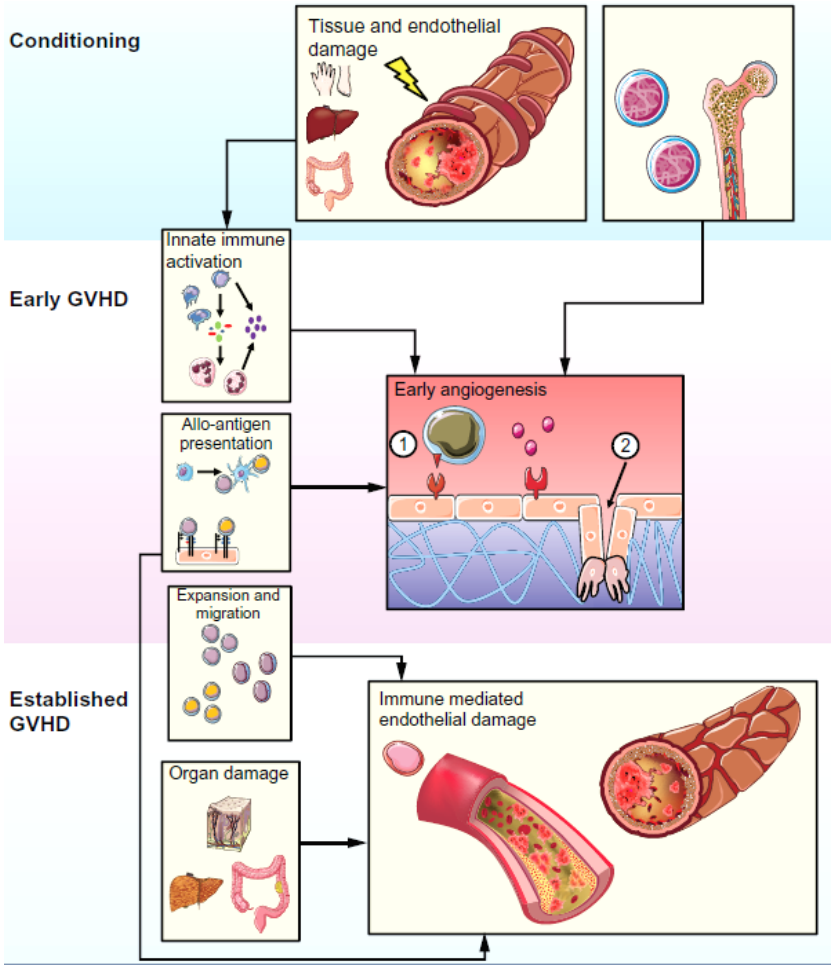

Figure 13: Model of endothelial damage during GVHD after allo-HSCT. Modified after [242].

The initial participation of angiogenesis in GvHD pathogenesis was confirmed by Riesner et al. by showing in aGvHD mouse models, the occurrence of angiogenesis at d+2 after transplantation in hepatic, intestinal and dermal tissues, while the earliest time point for leukocyte infiltration was detected at d+7. This process was limited on allo-transplantation, assuming that pathologic angiogenesis was the initial basis for facilitated leukocyte propagation in early aGvHD development. In line, significant metabolic and cytoskeleton changes were revealed by gene array and proteomic analyses in isolated ECs from aGvHD target organs in early aGVHD. Among others, specifically genes translating for enzymes in glycolysis, PPP, lipid metabolism, fatty-acid-oxidation or angiogenic function were found to be upregulated in early aGvHD, especially Acyl-CoA Synthetase Medium Chain Family Member 3 (*Acsm3*), Angiogenin-4 (*Ang4*), Enolase 3 (ß-Enolase; *Eno3*) and glucose-6-phosphate dehydrogenase, X-linked (*G6pdx*) [154]. As mentioned in chapter 1.3.3, glycolysis and PPP are the major pathways for energy generation and nucleotide-biosynthesis [177, 178].

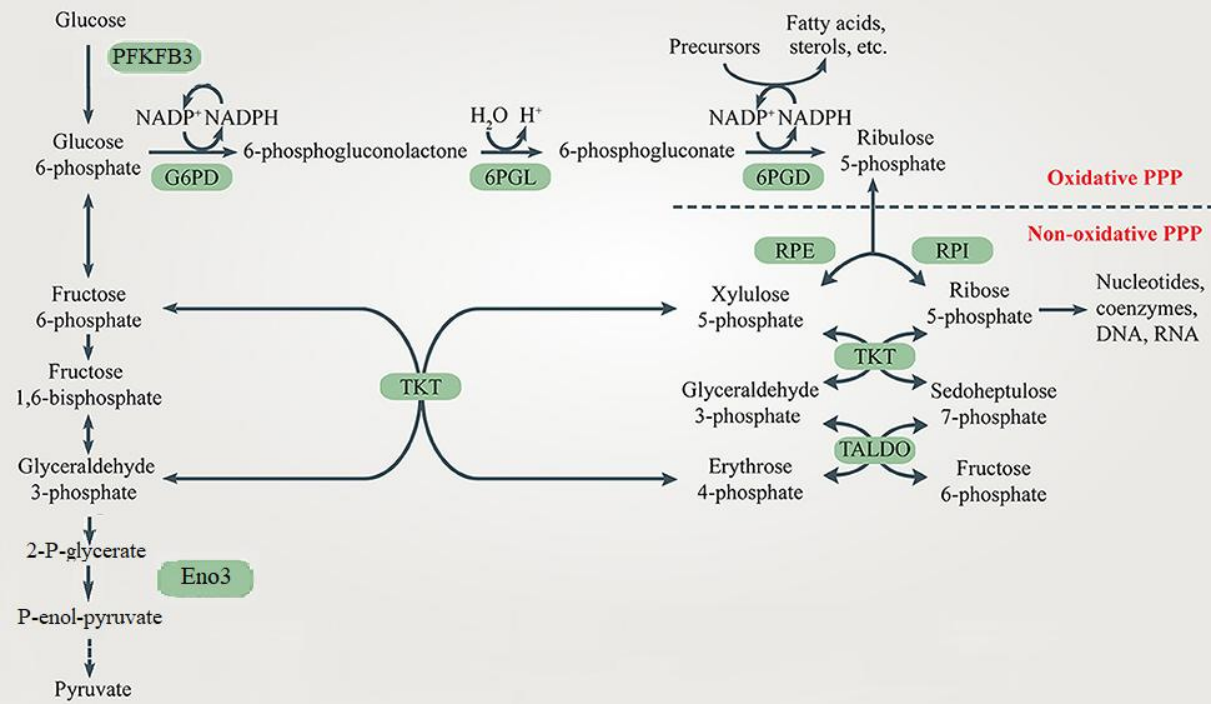

Figure 14: Glycolysis and Pentose-Phosphate-Pathway. Modified after [243]. Enzymes are depicted in green.

The essential enzyme G6pdx catalyses the rate-limiting conversion of 6-phosphogluconate into Ribulose-5phosphate in the PPP. Data from Riesner et al. support the theory of G6pdx as potential target to mitigate pathologic-angiogenesis, since enzyme levels were found to be higher in pathologic angiogenesis during aGvHD [154]. Studies showed that a reduction of EC viability and migration [244, 245] as well as decreased NO bioavailability and enhanced susceptibility to oxidative stress [246] emerged from blocking G6pdx. The involvement of G6pdx in angiogenesis can also be affected by manipulating the glycolytic pathway, thus interfering also with the PPP: Responsible for controlling the steady-state cytoplasmic levels of fructose-2,6-bisphosphate is the major regulator of glycolysis: the bifunctional 6-phosphofructo-2-kinase/fructose-2, 6-bisphosphatase 3 (PFKFB3). Inhibition of PFKFB3 resulted in accumulation of intermediate glucose-6phosphate (G-6-P), which is branched into the oxidative PPP, where it is further catalyzed to 6-phosphogluconolactone by G6pdx and led to decreased neovascularization in pathologic angiogenesis [176]. Silencing the enzymatic activity of G6pdx can be managed by genetic modification or by pharmacologic inhibition. Two pharmacologic inhibitors are Polydatin and 6-Aminonicotinamide (6-AN) [247, 248]. Polydatin is a natural resveratrol derivate found in *Polygonum cuspidatum*, peanuts, grapes, red wine, cocoa, and others. It has already been used for many years in traditional chinese medicine because of its positive anti-inflammatory, anti-oxidative, immunoregulatory and anti-fibrotic features [249] and was shown to prevent VEGF-induced angiogenesis [250] Synthetic 6-AN, a potent antimetabolite of nicotinamide, competitively binds and inhibits G6pdx. Endothelial lung injury caused by dysmorphic vasculogenesis and EC proliferation in neonatal mice was described to be attenuated by blocking the PPP with 6-AN, implicating an impact of G6pdx in pathologic vasculogenesis or angiogenesis [251].

Another relevant glycolysis protein found upregulated during pathologic angiogenesis in aGvHD was Eno3 [154], participating in the conversion of 2-phosphoglycerate to phosphoenolpyruvate (Figure 14). The involvement of Eno3, which is predominantly expressed in muscle tissues, in angiogenesis is previously unknown, while another member of the isoenzyme family, Eno1, was described to promote tumor angiogenesis under hypoxic conditions [252]. ENOblock, a therapeutic inhibitor, was found to inhibit enolase function, thereby preventing cancer cell metastasis [253] and mitigate diabetes type 2 symptoms [254].

Further proteins found upregulated during pathologic angiogenesis in aGvHD were Ang4 and Acsm3 [154]. In contrast to humans only possessing one *Ang* gene, mice express six different *Ang* paralogs with various functions [255], of which Ang4 exhibits angiogenic [256] as well

as antimicrobial functions, since it was first isolated from intestinal Paneth-cells as an anti-microbial peptide [257]. Acsm3, a mitochondrial synthetase enzyme, catalyzes the activation of fatty acids to produce Acyl-CoA, the first step in fatty acid metabolism. Its association in angiogenesis is unclear, while downregulation of Acsm3 is associated with cancer progression and metastasis [258].

Various clinical studies support the hypothesis of the endothelium as a major player in aGvHD pathogenesis, as several vascular biomarkers were shown to be increased in aGvHD patients. To list a few, vWF and VCAM1 levels in skin biopsies and ICAM1 levels in gastrointestinal tract biopsies were elevated at onset of aGvHD [259, 260]. Soluble ICAM1, E-Selectin, Ang2 [261, 262], thrombomodulin [158] and CECs [263] were found to be higher in aGvHD blood plasma and serum The findings of increased vessel density during aGvHD described by Penack et al. could also be confirmed in aGvHD patients by other research groups [264, 265]. Cordes et al. described increased apoptosis of ECs from intestinal biopsies of patients with severe aGvHD. These findings were manifested in murine aGvHD models, which exhibited microstructural endothelial damage and reduced endothelial pericyte coverage (αSMA), accompanied by loss of endothelial tight junction proteins (ZO-1+), which resulted in endothelial leakage in aGVHD target organs [155].

1.4.2. Endothelium in chronic GvHD

In contrast to aGvHD, studies of endothelial involvement in the cGvHD pathogenesis are rare. Shulman et al. described vascular complications as intimal arteritis similar to allograft vasculopathy and a reduced microvessel density in the skin of cGvHD patients in 1980 [266]. Since the last 40 years, new insights into the endothelial biology of cGVHD have been rarely provided. In sclerotic cGvHD, the progressive loss of dermal microvessels could be confirmed. This was accompanied by dense perivascular infiltration foci of cytotoxic T lymphocytes in human skin biopsies, correlated with high plasma vWF levels. Results suggested that allogeneic T cells react against ECs and caused endothelial injury, leading to the increased release of vWF from damaged ECs and vessel rarefraction in cGvHD [267]. Furthermore, soluble forms of VCAM1 and E-selectin could be measured in the blood of patients with severe cGvHD [261]. In a mouse model, endothelial injury and apoptosis preceded epithelial injury in the cGvHD target organs mouth and lungs, proposing a role of vessel loss and resulting tissue ischemia in organ fibrosis [268]. To date, no validated biomarkers, neither of epithelial nor of endothelial or cellular origin, have been established,

although several candidates, such as CXCL9 and CXCL10, have been nominated to be of potential value for prognosis or diagnosis of cGVHD [269, 270].

1.4.3. Endothelial biomarkers in allo-HSCT

Albeit endothelial dysfunction plays a major role in a multitude of disease pathologies, assays for diagnosis of endothelial-based complications are infrequently performed in clinical settings. Flow cytometry can be used to detect CECs [199] or CEPs [271], while soluble (s) mediators, which get shed from the EC layer into circulation upon inflammatory stages, can be measured as biomarkers by antigen-based immune-assays e.g. ELISA. Endothelial markers include factors involved in hemostasis (svWF), cell adhesion (sE- and sP-selectin, sICAM1, sVCAM1), vasomotor tone (endothelin-1; ET-1) and angiogenesis (VEGF, Ang1 and Ang2, sENG) [272]. Many studies report a correlation of single markers with the presence of certain diseases, e.g. ICAM-1 and VCAM-1 in rheumatoid arthritis [273], Ang-2 or VEGF in systemic sclerosis [274] or CD146 in uterine sarcoma [275] but most markers are not EC specific, thus are not suitable to consistently and reliably predict disease incidences, prognosis or therapy responses in varying patient populations [159].

Focusing on allo-HSCT, reliable biomarkers not only help to diagnose established transplant-related diseases as GvHD, but aid to function as prognostic tools for risk prediction of GvHD development and other HSCT-associated complications or assess the response to certain treatments. The ‘Endothelial Activation and Stress Index’ (EASIX) correlated with increased levels of endothelial homeostasis biomarkers such as CXCL8 and can be used to predict mortality in patients after allo-HSCT [276].

Unfortunately, validated prognostic or diagnostic biomarkers are rarely described especially for cGvHD. Since cGvHD closely resembles features of fibrotic autoimmune diseases, with both showing endothelial involvement and dysfunction, it might be interesting to analyse endothelial biomarkers with relevance in autoimmune disease also in cGvHD pathology. The following Table 6 portrays certain biomarkers, which already have been described to play a role in autoimmune-pathology or in allo-HSCT complications:

Table 6: Endothelial biomarkers in autoimmune disease. SLE = Systemic Lupus Erythematodes, RA = Rheumatoid arthritis; SSc = Systemic sclerosis, SS = Sjögrens syndrome

Marker	present in	Function	Reference
Fibronectin (FN)	SLE, RA, SSc, cutaneous GvHD	adhesion, tissue repair and endothelial cell migration	[277–280]
Endothelin-1 (ET1)	SLE, SSc, Atherosclerosis, intestinal GvHD	vasoconstriction	[281–284]
Endoglin (ENG)	aGvHD, Atherosclerosis, RA, SSc	angiogenesis, endothelial adhesion	[281, 285, 286]
Follistatin (FST)	aGvHD, RA, SLE, SS, SSc	vascularization, migration	[285, 287, 281]
Endostatin (ES)	SSc, Lung Fibrosis	inhibition of angiogenesis	[288, 289]
Connective tissue growth factor (CTGF)	RA, pulmonary & sclerodermatous GvHD	angiogenesis, fibrosis	[290–293]
Caspase-3 (Casp3)	SLE, SSc, renal fibrosis	activation and execution of apoptosis	[294–296]
Endocan (endothelial cell specific molecule-1; ESM1)	Atherosclerosis, aGvHD	angiogenesis, vascular remodeling	[297–299]

1.5. Objective of the present thesis

Despite considerable advances in understanding the pathophysiology of acute and chronic GvHD and extensive research in the field of new prophylaxis and treatment strategies, GvHD still remains one of the major hurdles in allo-HSCT patients, with a mortality rate still up to 40% [67]. Treatment response rates range from 30 - 50%, with even poorer outcomes in severe GvHD cases or when first line therapy fails [137]. Prophylaxis is the most important approach in disease management, followed by first line therapies, which both mainly aim to suppress alloreactive T cell responses by administration of immunosuppressive drugs. This immunosuppression features various side effects and toxicities, augments opportunistic infections and may repress the desired GVT effect. In cGVHD, the heterogeneous clinical manifestations, the incomplete understanding of the pathophysiology and the lack of reliable preclinical mouse models, result in a missing consensus about a satisfactory prophylaxis and

an absent adequate second line therapy. From that point, there is an urgent medical need for alternative therapeutic strategies in GvHD prevention and management.

Recently, the endothelium has emerged as a potential target for therapy. Several studies demonstrated an endothelial involvement in the pathogenesis of aGvHD [241, 226]. In particular, pathologic angiogenesis was described to precede leukocyte infiltration in aGvHD, proving it to be a cause rather than a consequence for inflammation. The detected pathologic angiogenesis was accompanied by differentially regulated genes and overexpressed proteins from various metabolic pathways in ECs [154], proposing new GvHD-initiating mechanisms.

Especially in cGvHD, little is known about the involvement of the endothelium in disease progression and pathology, what might be related to missing appropriate preclinical mouse models. Unpublished preliminary data of the Penack group indicate an association of endothelial dysfunction with cGvHD, which needs to be characterized in more detail to provide insights and guarantee better understanding of the endothelial participation.

The present study attempts to

1) acquire a better knowledge about the mechanisms leading to pathologic angiogenesis in the initiation of aGvHD. The previously revealed upregulated metabolic genes *Ang4*, *Acsm3*, *Eno3* and *G6pdx* and their related proteins are genetically deleted and their influence on the angiogenic function is analysed in allo-stimulated *in vitro* EC culture models. Angiogenesis-specific inhibitors against the identified potential targets are tested *in vitro* and *in vivo* with the underlying objective to find new therapeutic approaches for the inhibition of pathologic angiogenesis.

2) analyse and characterize the target structures and mechanisms of endothelial dysfunction during cGvHD. On that purpose, clinically relevant murine cGvHD models, which display high long-term morbidity but low mortality and resemble the diverse manifestations of cGvHD seen in patients, are established. Improved mouse models guarantee a more reliable translation of the experimental findings into the human setting of allo-HSCT. The project aims to examine endothelial dysfunction and damage during severe fibrotic cGvHD with the help of the established mouse models. Additionally, it intends to test novel pharmacologic endothelial-protective therapeutics, aspiring to prevent and protect the endothelium during inflammatory and fibrotic cGvHD. Beyond the murine studies, novel endothelium-related biomarkers are identified for prognosis and risk analysis in cGvHD patients.

This present thesis is directed to develop new translational treatment strategies out of the gained knowledge and data, with the objective to normalize endothelial function of allo-HSCT complications and to attenuate GvHD.

2. Material and Methods

2.1. Instruments and devices

Table 7: Routinely used instruments and devices, sorted alphabetically.

Device / Instrument	Manufacturer
BD FACS Aria II	Becton Dickinson, USA
BD FACS Canto II	Becton Dickinson, USA
Binocular Microscope S/N S 1486403	Motic, Japan
CFX96™ C1000 Touch™ Thermal Cycler Real-Time System	Bio-Rad Laboratories, USA
CO2 Cell Incubator Series CB	Binder GmbH, Germany
CryoStar™ NX70 cryostat	Thermo Fisher Scientific, USA
Halogen Lamp MXH-100	Motic, Canada
Heraeus Megafuge 1.0 R	Heraeus, Germany
Heraeus Pico 17 Centrifuge	Heraeus, Germany
IncuCyte S3 live-cell imaging system	Essen BioScience, UK
Irradiation device GSR D1	Gamma-Service Medical GmbH, Germany
Laboratory peristaltic pump PLP 380	Behr Labor-Technik, Germany
Microscissor Aesculap OC498R	Aesculap AG & CO, Germany
Mouse tail restrainer	Braintree Scientific, USA
Motic AE31 inverted microscope	Motic, Japan
Motic MXH-100, TRITC (EX AT540/25x, BS AT565DC, EM AT605/55m)	Motic, Canada
Moticam 3.0 Microscope Camera	Motic, Canada
Nanodrop 1000 spectrophotometer	PEQLAB, Germany
Neubauer Counting Chamber	Marienfeld Superior, Germany
Microdissection forceps	Fine Science tools, Germany
Microdissection scissors	Fine Science tools, Germany
Mini-PROTEAN® Tetra Handcast Systems for Western Blot	Bio Rad Laboratories Inc., USA
Inverted fluorescence microscope Zeiss Axio Observer 7	Carl Zeiss, Germany
Inverted fluorescence microscope Zeiss PALM MicroBeam	Carl Zeiss, Germany
Objective EC Plan-Neofluar 5x/0.16 M27	Carl Zeiss, Germany
Objective "Plan-Apochromat" 10x/0.45 M27	Carl Zeiss, Germany
Precision tweezers	Dumont Nr. 5, Switzerland
RT-PCR cycler C1000 Touch™ CFX96™	Bio-Rad Laboratories, California, United States
Tecan Infinite M Plex microplate reader	Tecan Group, Switzerland
Ultra turrax t25 basic	IKA®-Werke GmbH & CO. KG, Germany
Western Blot Power Blotter XL	Invitrogen, USA

2.2. Kits, reagents and consumables

Table 8: Routinely used kits and consumables, sorted alphabetically.

Kits	**Manufacturer**
DNA Maxi Kit	QIAGEN, Netherlands
Innuprep Gel extraction Kit	Analytik Jena, Germany
MTT Cell Proliferation Kit I	Roche, Switzerland
Nucleo Spin Plasmid Kit	Macherey-Nagel, Germany
Pan T cell isolation kit II	Miltenyi Biotec, Germany
Pierce™ Protein Quantification BCA-Kit	Thermo Fisher Scientific, USA
QuantiTect Reverse Transcription Kit	QIAGEN, Netherlands
RNeasy Mini Kit	QIAGEN, Netherlands
TaqMan™ Gene Expression Master Mix	Thermo Fisher Scientific, USA
TransIT-X2® Dynamic Delivery System	Mirus-Bio, USA
Reagents / Chemicals	**Manufacturer**
Accutase	Invitrogen, USA
Agarose, LE	Biozym Scientific GmbH, Germany
Bovine serum Albumin (BSA, Albumin Fraction V)	Carl Roth, Germany
β- mercaptoethanol >99%	Merck, Germany
Dimethylsulfoxid (DMSO)	Carl Roth, Germany
Dulbecco's Modified Eagle Medium (DMEM)	Gibco, USA
Dithiothreitol (DTT) ≥99,5%	VWR International, USA
Endothelial Growth Medium 2 (EGM2)	PromoCell, Germany
Ethanol 70%, denaturated	Carl Roth, Germany
Ethanol 99,9%	Carl Roth, Germany
Ethylendiamintetraacetat (0.5M EDTA)	VWR life science, USA
Fetal Calf Serum (FCS), Premium	PAN Biotech, Germany
Forene (100%, Isofluran)	Abbvie, USA
GlutaMAX™ cell culture supplement	Gibco, USA
HEPES buffer 1M for cell culture	Gibco, USA
4X Lämmli buffer	Bio-Rad, USA
Matrigel®	Corning, USA
Methanol >99%	Carl Roth, Germany
MuMEC medium	InSCREENeX, Germany
Opti-MEM™ I Reduced Serum Medium	Thermo Fisher Scientific, USA
Penicillin / Streptomycin 5.000 U/ml (Pen/Strep)	Gibco, USA
Phosphate Buffered Saline (DPBS 1x)	Gibco, USA
Polydatin >95%	Sigma-Aldrich, USA
Pork gelatine (Peptone)	Thermo Fisher Scientific, USA
RPMI 1640 Medium with L-Glutamine	Gibco, USA

Skim milk powder	Sigma-Aldrich, USA
sodium dodecylsulfate (SDS), ultra pure	Carl Roth, Germany
Sodium pyruvate 100 mM for cell culture	Gibco, USA
Tissue-Tek® O.C.T.™ cryo embedding medium	Sakura Finetek, Netherlands
Triton-X 100	Sigma-Aldrich, USA
2,5 % Trypsin	Gibco, USA
Tween® 20	Acros Organics, Belgium
Vybrant™ DiI cell labeling solution	Thermo Fisher Scientific, USA
Water, DEPC-treated, nuclease free	Fisher Bioreagents, USA
Consumables	**Manufacturer**
96-well plate, flat bottom, adherent	Sarstedt, USA
24-well plate, flat bottom, adherent	Sarstedt, USA
6-well plate, flat bottom, adherent	Sarstedt, USA
6 cm petri cell culture dish, adherent	Sarstedt, USA
20 G injection needle	B.Braun Melsungen AG, Germany
23 G injection needle	B.Braun Melsungen AG, Germany
40 µm cell strainer Nylon	Corning Incorporated, United States
70 µm cell strainer Nylon	Corning Incorporated, United States
100 µm cell strainer Nylon	Corning Incorporated, United States
15 ml Polypropylene tubes	Corning Incorporated, United States
50 ml Polypropylene tubes	Corning Incorporated, United States
Braun Injekt® Solo syringe (Luer) 1 ml	B.Braun Melsungen AG, Germany
Braun Injekt® Solo syringe (Luer) 5 ml	B.Braun Melsungen AG, Germany
Cryo conservation tube 2 mL	Greiner Bio-One, Austria
Cryomold cassettes (Standard & Intermediate)	Sakura Finetek, Netherlands

2.3. Mice

Female C57BL/6NCrl (B6) (H-2K^{b}), B6D2F1 (BDF) (H-2K$^{b/d}$) and BALB/c (H-2K^{d}) mice were purchased from Charles River Laboratories (Sulzfeld, Germany). Female immunodeficient NOD scid gamma (NSG) (NOD.Cg-Prkdc^{scid} Il2rg^{tm1Wjl}/SzJ) were bred and ordered from the group of Prof. Hans-Dieter Volk (Charité/BIH, Berlin, Germany). Recipient mice in all hematopoietic stem cell transplantation (HSCT) experiments and donor mice of acute GvHD (aGvHD) experiments were 8 to 10 weeks old. Donor mice in chronic GvHD (cGvHD) experiments aged at least 16 weeks before HSCT. All animals were housed in a 12-hour light-dark cycle under specified pathogen-free conditions in the Charité Animal Facility (Forschungseinrichtung für experimentelle Medizin) in open housing cages; NSG mice were housed in individually ventilated cages (IVC). All experiments were approved by the local

Ethics Committee for Animal Research (State Office of Health and Social Affairs, LaGeSo) and executed in compliance with the European Union guidelines.

2.4. Mouse models of GvHD

For GvHD experiments, different murine MHC-mismatch models were used, depending on their stem cell mobilization and -source and their haplotype combinations of donors and recipients (see Table 9).

Donor mice in cGvHD experiments underwent 5 injections with Granulocyte colony-stimulating factor (G-CSF) prior to HSCT to mobilize hematopoietic stem cells from the bone marrow (BM) into the spleen and the peripheral blood (PB) (see chapter 2.4.1).

All recipient mice received a total body irradiation (TBI) from a ^{137}Cs source on the day of SCT (day 0). B6 and BDF mice underwent a myeloablative conditioning, performed by half dose irradiation and followed by a second irradiation with a resting phase of at least 4 hours in between. NSG mice were conditioned with reduced intensity for non-myeloablative irradiation on day -1 before HSCT (see Table 9).

On day 0, bone marrow (BM) cells, splenic T cells or whole splenocytes were isolated from donor mice and injected intravenous (i.v.) into conditioned recipients (see chapters 2.4.2 and 2.4.4). NSG mice were injected i.v. with human peripheral blood mononuclear cells (PBMCs), isolated beforehand from buffy coats and stored frozen until injection (see chapter 2.4.3).

As control, syngeneic (syn) transplantation (e.g. BDF → BDF) was carried out by injection of splenocytes (in cGvHD) or BM cells only (in aGvHD), in the same dose as in allogeneic (allo) HSCT. In the humanized Xenograft model, control NSG mice received only TBI with no injection of human PBMCs.

Table 9: Mouse models of experimental acute and chronic GvHD. Listed are donor and recipient mouse strains, stem cell mobilization and conditioning regime as well as cell source and MHC mismatch type. B6 = C57BL/6N; BDF = B6D2F1, NSG = NOD scid gamma, PBMC = Peripheral Blood Mononuclear Cells, G-CSF = Granulocyte colony-stimulating factor, s.c. = subcutaneous, TBI = Total Body Irradiation; BM = Bone marrow.

GvHD model	Donor	Recipient	Donor stem cell mobilization	Conditioning	Cell numbers & source	Type of mismatch
acute	B6	BDF		TBI: 1100 Gray, split dose	1 x 10^7 BM cells 2 x 10^6 splenic T cells	haploidentical (H-2K^b) → (H-2K$^{b/d}$)
chronic	BALB/c	B6	day -4 to -1: G-CSF 10 mg/kg/day, s.c.	TBI: 1200 Gray, split dose	1 x 10^7 splenocytes	major mismatch (H-2K^d) → (H-2K^b)
chronic	B6	BDF	day -4 to -1: G-CSF 10 mg/kg/day, s.c.	TBI: 1100 Gray, split dose	5 x 10^7 splenocytes	haploidentical (H-2K^b) → (H-2K$^{b/d}$)
chronic	human PBMCs	NSG		TBI: 200 Gray, single dose	1x 10^6 human PBMCs	Xenograft (humanized)

2.4.1. Stem cell mobilization in donor mice of cGvHD

In cGvHD models, BALB/c → B6 and B6 → BDF donors received a daily s.c. injection of 10 mg/kg G-CSF (Filgrastim, 48 Mio. U.; Hexal, Germany) in 100 µl of sterile 5% glucose solution (Sigma-Aldrich, USA) for 5 consecutive days prior to transplantation to mobilize HSCs. Peripheral blood of each treated mouse was collected by facial vein or tail vein puncture before stem cell mobilization and on day 3 and 5 after G-CSF injection to determine the increase of CD45+ and Gr-1+ granulocyte fraction within whole PBMCs via flow cytometry on a BD FACS Canto II.

2.4.2. Cell isolation from bone marrow and spleen

Donor mice were sacrificed by cervical dislocation. Further processing was performed under sterile conditions. Mice were sterilized with 70% Ethanol and femur, tibia and spleen were dissected and collected on ice. Bones were opened and BM was flushed out with isolation buffer (PBS + 2% FCS + 1 mM EDTA) through a syringe with 23G needle. BM cells were separated by filtering through a 70 µm cell strainer. Next, erythrocytes were removed by ammonium-chloride-potassium (ACK) lysis buffer (150 mM NH_4Cl + 10 mM $KHCO_3$ + 0.1 mM Na_2EDTA). Lysis was stopped by adding isolation buffer, followed by second washing

with isolation buffer and passing cells over a 70 µm cell strainer. Cells were counted with a Neuberger counting chamber. The cell number was adjusted according to the required number for transplantation.

For splenocyte isolation, spleens of donor mice were meshed through a 40 µm cell strainer with a syringe plunger under continuous addition of isolation buffer. Following cell pelleting and ACK-lysis, the cell suspension was washed again with PBS and filtered through a second 40 µm cell strainer. Cells were counted with a Neubauer counting chamber and the cell number was adjusted according to the required number for transplantation.

For enrichment of splenic T cells, the Pan T cell isolation kit II from Miltenyi was used according to the manufacturer's instructions. The enriched suspension was analysed via flow cytometry for T cell purity using CD3, CD4 and CD8. The cell number used for transplantation was adjusted by taking the measured percentage of CD3+ cells into account.

2.4.3. Human PBMC isolation from buffy coats

To generate a human PBMC suspension for transplantation, cells were isolated from buffy coats from unknown donors provided by the German Red Cross (DRK) Berlin. Blood was flushed out of the blood collection bag with a 100 ml syringe. 35 ml buffy coat were slowly overlayed onto 15 ml Ficoll-Paque solution (GE Healthcare, USA) in 50 ml tubes to generate a gradient. After density gradient centrifugation (30 min at RT, 2000 rpm, without deceleration) the PBMC layer was transferred into a new 50 ml tube and filled with isolation buffer (PBS + 2% FCS + 1 mM EDTA). Cells were washed twice with PBS and pelleted (4°C, 10 min, 1500 rpm). The supernatant was discarded and each cell pellet was resuspended in 10-15 ml erythrocyte lysis buffer (ACK lysis buffer) and incubated on ice for 5 minutes. The reaction was stopped by adding isolation buffer and cells were washed twice (4°C, 10 min, 1500 rpm) $1x10^7$ PBMCs per Cryo-conservation tube were slowly frozen (Mr. Frosty, Thermo Fisher Scientific, USA) in 90% FCS + 10% DMSO and stored at -80°C until usage.

2.4.4. Transplantation

The required amount of splenocytes, huPBMCs or BM+T cells was resuspended in PBS in a total injection volume of 200 µl per mouse, respectively. Prior to injection, mice tails were warmed under an infrared lamp for a few minutes to increase the visibility of the veins. Mice were fixed in a tail vein restrainer and injected into the tail vein.

2.4.5. Engraftment & chimerism analysis

Successful engraftment of donor cells in recipients, chimerism grade and immune status of each mouse was assessed by flow cytometry. Around d+15 (aGvHD), d+20 (cGvHD) and d+30 (Xenograft) after HSCT, blood was sampled from recipient mice by facial vein or tail vein puncture. After erythrocyte lysis with ACK-buffer, cells were stained with different antibodies specific for donors and recipient's minor antigens as well as different immune cell subsets (see Table 10). Positive engraftment was defined as a minimum of 85% murine donor cells in the CD3+ fraction of the recipients' blood. For the Xenograft model, positive engraftment was defined by the presence of human CD3+ cells in peripheral blood at d+30 after HSCT and a minimum of 1% of human CD3+ cells or > 5% human CD45+ cells in the spleen of NSG mice upon the day of experiment abortion.

Table 10: Overview of antibodies used for engraftment & immune status analysis by flow cytometry. mu = murine, hu= human. FITC=Fluorescein-5-isothiocyanate, PE=Phycoerythrin, APC=Allophycocyanin, PerCP=Peridinin-chlorophyll- protein complex, Cy7=Cyanine7.

used in	Epitope	Fluorophor	Clone	Dilution	Manufacturer
B6, BDF	mu H2kb	PE	AF6-88.5	1:100	Biolegend, USA
	mu H2kd	FITC	SF1-1.1	1:50	BD Biosciences, USA
	mu CD3	APC	BM10-37	1:200	BD Biosciences, USA
	mu CD4	PE-Cy7	RM4-5	1:200	BD Biosciences, USA
	mu CD8	APC-Cy7	53-6.7	1:200	BD Biosciences, USA
	mu NK1.1	PerCP-Cy5.5	PK136	1:200	BD Biosciences, USA
	mu CD11b	APC-Cy7	M1/70	1:200	BD Biosciences, USA
	mu CD11c	PE	N418	1:100	Invitrogen, USA
	mu Gr1	PE-Cy7	RB6-8C5	1:200	Biolegend, USA
	mu CD80	APC	RB6-8C5	1:200	Biolegend, USA
	mu CD45	FITC	30-F11	1:50	Biolegend, USA
	mu B220	PerCP-Cy5.5	RA3-6B2	1:200	BD Biosciences, USA
NSG	hu CD3	APC	UCHT1	1:20	Biolegend, USA
	hu CD4	PerCP-Cy5.5	SK3	1:20	Biolegend, USA
	hu CD8	APC-Cy7	SK1	1:40	Biolegend, USA
	hu CD56	PE-Cy7	HDC56	1:20	Biolegend, USA
	hu CD19	FITC	SJ25C1	1:40	Biolegend, USA
	hu CD15	APC	HI98	1:50	Biolegend, USA
	hu CD14	PE	63D3	1:20	Biolegend, USA
	hu CD11b	PerCP-Cy5.5	ICRF44	1:40	Biolegend, USA
	hu CD45	PE-Cy7	2D1	1:20	Biolegend, USA
	mu CD45	FITC	30-F11	1:200	Biolegend, USA
	mu CD11b	APC-Cy7	M1/70	1:50	BD Biosciences, USA
	mu CD11c	PE	N418	1:100	Invitrogen, USA
	mu Gr-1	PE-Cy7	Gr1 RB6-8C5	1:200	Biolegend, USA
	mu CD80	APC	RB6-8C5	1:200	Biolegend, USA

2.4.6. GvHD monitoring

Recipient mice were individually scored once or twice a week from d+10 after transplantation for five clinical parameters (posture, activity, fur, skin, and weight loss) on a scale from 0 to 2 according to Cooke et al. [110]. cGvHD mice weight loss was scored according to the 'body condition score' described by Ullman-Cullere [300]. The total clinical GvHD Score was calculated by summation of the single parameters. Animals were sacrificed when exceeding a total score of >5 or a single score of >2 in aGvHD and a body condition score of BC1 in cGvHD. Survival was monitored daily.

2.4.7. Therapeutic treatment of GvHD

Transplanted animals in aGvHD and cGvHD experiments were treated with 100 mg/kg/day and 150 mg/kg/day Polydatin (Sigma-Aldrich, USA), respectively. A sterile stock solution of Polydatin was prepared in 100% DMSO and diluted freshly to the desired concentration with PBS in a 1:10 ratio on injection day. Each mouse was intraperitoneally (i.p.) administered with 100 µl Polydatin every second day, starting on day+7 after transplantation for aGvHD mice or on day +30 after transplantation for cGvHD mice for a maximum of 60 injections or until organ harvesting.
Polydatin was also tested in Paw Edema experiments. For that, 100 µl of 100 mg/kg/day Polydatin was i.p. injected for 5 consecutive days to C57BL6/N mice. On day 5, 1 hour after the last Polydatin injection, the Paw Edema experiment was performed as described in section 2.5.1. For HSCT- as well as for Paw Edema treatment experiments, the control group comprised mice which were injected with 10% DMSO in PBS solution (Vehicle).

Secondly, Pirfenidone was tested in the cGvHD mouse model. This treatment was performed by the group of Prof. MD Bruce R. Blazar (Department of Pediatrics, Division of Pediatric Blood and Marrow Transplantation & Cellular Therapy Program, University of Minnesota, USA) as published in [301]. Prof. Blazar was so friendly to support this thesis by sending cryo-conserved organs of Pirfenidone-treated cGvHD mice, which were further immunhistologically analysed according the protocols in chapter 2.6.2.

2.5. Analyses of GvHD mouse models

2.5.1. Analysis of inflammation: Paw edema (Footpad swelling)

To evaluate the inflammation in cGvHD mice and the impact of therapeutic treatments on inflammation, paw edema assays / footpad swelling assays were performed similar as described in [302]. One hour before footpad injection, mice subcutaneously received analgesic 0.03 mg/kg buprenorphine (Temgesic; Invidia, USA). For induction of footpad swelling, mice were injected with 30µl of 1% λ-Carrageenan (Sigma-Aldrich, USA) in 0.9% saline into one footpad. The other footpad was injected with 30 µl of 0.9% saline only and served as control. Footpad thickness of both paws was measured with a caliper each hour up to 4 hours after injection. At 4h mice were sacrificed by cervical dislocation and footpad biopsies were taken using a 6mm biopsy punch (Stiefel, Research Triangle Park, USA). Footpad biopsies and harvested spleens were weighted.

For footpad conservation, paws were incubated in 4% paraformaldehyde (Carl Roth, Germany) overnight, washed in PBS and transferred into 0.5 M EDTA, pH 8.0 for 72 hours. After washing with PBS, a solution of 20% sucrose + 2% polyvinylpyrrolidone (PVP; Sigma-Aldrich, USA) + H_2O was added for at least 48 hours. All steps were performed under continuous shaking at 4°C. A solution composed of 8% pork gelatine + 20% Sucrose + 2% PVP + H_2O was heated to 80°C, paws were embedded in the gelatine solution in cryomold cassettes and dried at room temperature until hardening. Gelatine blocks were stored at -80°C and cut for analysis to 7 µm sections with a cryostat.

2.5.2. Analysis of vessel permeability: Evans blue assay

To evaluate vessel permeability in mice, an Evans blue assay was performed. A 0.5% solution of Evans blue (Sigma-Aldrich, USA) diluted in PBS was injected i.v. 30 minutes before sacrificing by cervical dislocation and spleens, colons, livers, lungs and skin were harvested. Organs were weighed and directly transferred to an Eppendorf tube containing 500 µl formamide (Carl Roth, Germany). Next, organ samples were incubated on a shaker at 55°C for 24 hours to extract the albumin-bound Evans blue dye. After 24 hours, the Evans blue concentration in the supernatant was determined via absorbance measurement at 610 nm on a Tecan microplate reader. The vessel permeability was calculated from the amount of extravasated Evans blue per mg tissue.

2.5.3. Analysis of ocular cGvHD (Retina staining)

Eyes of cGvHD mice were carefully dissected under a binocular microscope. Using a microdissection spring scissor, the whole bulbus including the edge of the eyelids was removed from the orbital cavity and the optic nerve and snap frozen in liquid nitrogen. Immunocytochemical staining of the eye and the lid was performed in cooperation with Prof. Dr. Philipp Steven from the Division of Ophthalmology with focus on ocular GvHD at the University Hospital Cologne. Eyes were analysed for the markers CD31, CD4, ICAM and Lyve-1.

2.5.4. Tissue harvesting and conservation

At experiment finalization, mice were euthanized with Isofluran. Bodies were sterilized with 70% Ethanol and fur at the abdomen was completely removed with razor blades. A small piece of outer skin (epidermis & dermis) was dissected from the inner peritoneal skin and slowly frozen over liquid nitrogen in Tissue-Tek® cryo-embedding medium. The peritoneum was opened completely and the trachea was exposed. A 1:1 PBS-Tissue-Tek® mixture was injected into the trachea to fill the lungs. The colon was removed at the rectum and the caecum and cut longitudinal. After washing in PBS, the colon was coiled up. The colon as well as one of each lung and liver lobes were embedded in Tissue-Tek® in cryomold cassettes and frozen in -80°C pre-cooled methylbutan (Carl Roth, Germany). Pieces of colon, skin, lung and liver were additionally snap frozen in liquid nitrogen for RNA- and protein isolation.

2.5.5. Liver sinusoidal endothelial cell (LSEC) isolation

Animals were anesthetized with 100 mg/ml Ketavet (Pfizer, USA), 2% Rompun (Bayer Vital GmbH, Germany) and PBS in a 1:1:2 ratio until footpad reflexes were completely inhibited. The abdominal cavity was opened after sterilization with 70% ethanol and the portal vein of the liver was cannulated with an intravenous cannula (Introcan, B. Braun Melsungen, Germany). The liver was perfused with PBS at a flow rate of 5 ml/min, while the inferior vena cava was opened to release pressure, until the liver tissue was cleared from blood. The solution was switched to 0.5 mg/ml collagenase D (Roche Diagnostics, Switzerland) and 1 µl/ml DNase (Sigma-Aldrich, USA) in Krebs-Ringer Buffer (KRB; 154 mM NaCl + 5.6 mM KCl + 5.5 mM Glucose + 20.1 mM HEPES + 25 mM NaHCO3, pH 7.4). After flowthrough of 20 ml digestion buffer the liver was dissected and incubated in collagenase D solution at 37°C under continuous shaking for 5 to 10 minutes. Digested liver tissue was first passed over

a 100 µm and a second time over a 70µm cell strainer. The cell solution was low-centrifuged twice at 50g for 3 minutes. The pellet containing hepatocytes was discarded. After another centrifugation step at 600 g, 10 min, 4°C the cells were further enriched by density gradient centrifugation using OptiPrep Density Gradient solution (STEMCELL-Technologies, USA). The cell pellet was resuspended in 17,8% OptiPrep-Solution (in DMEM), overlayered by 8,2% OptiPrep-Solution, topped by 2 ml PBS + 0,5% BSA and centrifuged at 1400g, 30 min, 4°C without deceleration. The LSEC containing interphase was taken and further enriched via magnetic activated cell sorting (MACS) using CD31 microbeads (Miltenyi Biotec, Germany) according to the manufacturer's instructions. The purity of sorted cells was checked by flow cytometry staining against CD31, CD146 and CD3.
Isolated LSEC were pelleted and frozen immediately at -80°C for further RNA isolation, or stained and analysed via flow cytometry or cultured. For primary cell culture, cells were washed and resuspended in supplemented Endothelial Growth Medium (EGM2). LSEC were seeded into an adherent 96- or 24- well plate, which were pre-coated for 30 minutes at 37°C with 0.1% pork gelatine.

2.5.6. Lung Endothelial cell (MLEC) isolation

At experiment finalization, mice were sacrificed by cervical dislocation. The protocol for MLEC isolation was performed under sterile conditions, when MLECs were isolated for cell culture and under non-sterile conditions when cells were used for RNA isolation. Mouse abdominal cavity was opened, lungs were dissected carefully and stored temporarily in isolation buffer (DMEM + 20% FCS + Pen/Strep 1%) on ice. Lungs were put into a 6 cm Petri dish, minced with a dissection scissor (Fine Science Tools, Germany) and incubated 30 - 40 minutes at 37°C in digestion buffer (DMEM + 3mg/ml Collagenase I (PAN Biotech, USA)). The suspension was pulled up and down 5 times with a 20G needle and pulled over a 70 µm strainer to further separate the cells. Remaining, not fully digested tissue particles were mashed through the cell strainer with a syringe plunger and washed with isolation buffer. The solution was centrifuged at 1200 rpm, 8 minutes, 4°C and the cell pellet was lysed with ACK-lysis buffer to remove remaining erythrocytes. Cells were washed twice with MACS buffer (PBS + 0.5% BSA + 0.5% EDTA). MLEC fraction was further enriched via magnetic activated cell sorting (MACS) using CD31 microbeads (Miltenyi Biotec) according to the manufacturer's instructions. The purity of sorted cells was checked by flow cytometry staining against CD31, CD146 and CD3. Cells were further cultured as described under 2.10.1 or the cells were pelleted and frozen at -80°C for further analysis.

2.5.7. Murine serum marker Multiplex analysis & serum TGF-ß analysis

Blood from recipient GvHD mice was sampled by retro orbital bleeding into 1.5 ml tubes. Blood was left at room temperature for approximately 30 minutes to clot and then centrifuged at 1200 rpm, 10 min a 4°C to separate the serum fraction. The clear serum phase was transferred into a new tube and stored at -80°C until further analysis. Serum was analysed with the LEGENDplex™ Mouse Inflammation Kit (Biolegend, USA) according to the manufacturer's protocol. Readings of the multiplex assays were performed at the BD FACS Aria II.

Evaluation of the TGF-ß protein concentration in murine serum was examined by using the LEGENDplex™ Mouse TGF-β1 Capture Bead B3 (Biolegend) kit following the manufacturers instruction.

2.6. Histology

2.6.1. Masson's Trichrome Fibrosis Staining

Histopathologic and fibrotic grading of GvHD in murine tissue was performed after adapted Lerner criteria [303], as described with Cooke et al. [304] and Shulman et. al [305] in Masson's Trichrome stained cryosections. Colon, liver, lung and skin samples of GvHD mice were harvested as described under 2.5.4. Before staining, 7 µm tissue cryosections were cut with a cryostat. Masson's receptures and chemicals are summarized in Table 11. Cryosections were fixed for 30 minutes in 10% ROTI®Histofix, rinsed in distilled water and etched for 10 minutes in 60°C Bouin's Fixative solution. First, nuclei were stained black by addition of Weigert's Hematoxylin working solution for 7 minutes. Subsequently, cytoplasm, keratin, muscle fibers and erythrocytes were marked red by incubation for 5 minutes in Biebrich scarlet-acid fuchsin solution. The tissue was differentiated for 15 minutes in Phosphomolybdic-phosphotungstic acid solution before collagen fibers were labeled blue by staining with Aniline blue solution for 5 minutes. The fully stained cryosections were dehydrated in an alcoholic dilution series (95% and 100% Ethanol), fixed with Xylene (Merck, Germany) and mounted with Eukitt® Quick-hardening mounting medium (Sigma-Aldrich, USA).

Table 11: Masson's Trichrome Staining: Used chemicals in working solutions.

Working Solution	Chemicals	Manufacturer
ROTI®Histofix 10%	10% Formaldehyde (ready to use)	Carl Roth, Germany
Bouin's Fixative Solution	300 mL Saturated Picric Acid 100 mL Formaldehyde solution 37% 20 mL Glacial acetic acid >99%	Clin-Tech, UK Carl Roth, Germany Sigma-Aldrich, USA
Weigert's Hematoxylin Working Solution A	5g Hematoxylin 85% 500 mL Ethanol 95%	Acros Organics, USA Carl Roth, Germany
Weigert's Hematoxylin Working Solution B	5,8 g Iron III Chloride >97% 5 mL Hydrochloric Acid 37% 495 mL Milli Pure Water	Thermo Fisher Scientific, USA Carl Roth, Germany
Biebrich Scarlet-Acid-Fuchsin Solution	1g Ponceau Biebrich Scarlet 10 mL Acid Fuchsin 1% aqueous 1 mL Glacial acetic acid >99% 100 mL Milli Pure water	Sigma-Aldrich, USA Clin-Tech, UK Sigma-Aldrich, USA
Phosphomolybdic-Phosphotungstic- Acid Solution	5g Phosphotungstic Acid 5g Phosphomolybdic acid 200 mL Milli-Pure Water	Santa Cruz Biotech, USA Santa Cruz Biotech, USA
Aniline Blue Solution	2,5 g Aniline blue 2 mL Glacial acetic acid >99% 100 mL Milli Pure Water	Santa Cruz Biotech, USA Sigma-Aldrich, USA

For evaluation of histopathologic and fibrotic scores in GvHD, cryo-conserved samples from colon, liver and lung were processed as described in the previous chapter 2.5.4. The histoscore was composed of the parameters inflammation (score A) and fibrotic changes (score B). Inflammation was assessed by evaluation of extent of infiltrating immune cells (0-4), while fibrotic changes were based on the level of collagen incorporation (0 - 4) and resulting tissue damage, respective changes in epithelial and mucosal architecture (Table 12). Both single scores were summed up and the average histoscore was calculated. Histopathologic changes of skin in cGvHD were illustrated by measuring alterations in skin thickness, particularly by calculation of the ratio between epidermis/ dermis and muscularis.

Table 12: Parameters for the evaluation of histopathological fibrotic and inflammation scores.

Grade	Fibrosis/Inflammation	Area of infiltrated cells	Area of fibrotic tissue
0	none	0 %	0 %
1	mild	1 – 5%	1-10 %
2	moderate	5 – 10%	10 - 25 %
3	severe	10 – 25%	25 – 40 %
4	extremely severe	> 25%	> 40%

2.6.2. Histology – Immunofluorescence of tissue cryosections

7 µm cryosections were re-hydrated in PBS for 15 minutes and fixed in ice cold methanol (Carl Roth, Germany) for 15 minutes. Following, sections were incubated in blocking buffer (PBS + 3% BSA + 5% FCS) for 1 hour at room temperature. Primary antibodies were diluted in blocking buffer and applied to the sections overnight at 4°C. The following day, sections were washed three times with PBS, before secondary antibody mixes, also diluted in blocking buffer, were added and incubated for 2 hours at room temperature. Table 13 and Table 14 show all used primary and secondary antibodies with dilutions. Nuclei were stained with 2mg/ml 4',6-Diamidino-2-phenylindole (DAPI; Sigma-Aldrich, USA) before washed again three times and mounted with Fluoromount-G® (Southern Biotech, USA) for microscopy.

Table 13: Primary antibodies used for immunohistofluorescence stainings of GvHD tissue and in cell culture.

Epitope	Host	Reactivity	Clone	Dilution	Manufacturer
CD3	hamster	Mouse	145-2C11	1:200	BD Biosciences, USA
CD4	rabbit	Mouse, Human	polyclonal	1:200	bioss antibodies, USA
CD19	rat	Mouse	6D5	1:200	Biolegend, USA
CD31	hamster	Mouse, Human	2H8	1:300	Invitrogen, USA
Endomucin	goat	Mouse	polyclonal	1:200	Invitrogen, USA
Endomucin	rat	Mouse	V.7C7	1:200	Santa Cruz Biotech, USA
FSP-1	rabbit	Mouse, Human	polyclonal	1:300	Merck, Germany
NG-2	goat	Mouse, Human	polyclonal	1:200	Merck, Germany
vWF	rabbit	Mouse, Human	polyclonal	1:700	Novus Biologicals, USA
VE-Cad	goat	Mouse	polyclonal	1:100	R&D Systems, USA
ZO-1	rabbit	Mouse, Human	polyclonal	1:200	Invitrogen, USA

Table 14: Secondary antibodies used for immunohistofluorescence stainings of GvHD tissue and in cell culture arranged by fluorophore. AF=AlexaFluor, Cy3= Cyanine.

Host	Reactivity	Fluorophor	Dilution	Manufacturer
αSMA (Epitope)	Mouse	Cy3	1:300	Sigma-Aldrich, USA
goat	hamster		1:1000	Jackson Laboratories, USA
goat	rat		1:1000	Biolegend, USA
donkey	rabbit	AF488	1:1000	Invitrogen, USA
goat	hamster		1:1000	Invitrogen, USA
donkey	rat		1:500	Invitrogen, USA
donkey	rabbit	AF555	1:1000	Invitrogen, USA
donkey	goat	AF647	1:1000	Invitrogen, USA
donkey	rabbit		1:1000	Invitrogen, USA
rabbit	rat		1:1000	abcam, UK

2.6.2.1. Fluorescence imaging

For Fluorescence imaging two inverse fluorescence microscope systems were used, either Zeiss Axio Observer 7 with Colibri7 LED light source or on a Zeiss PALM MicroBeam with X-Cite® Xylis LED light source and Axiocam 305 color/ Axiocam 712 mono cameras. Systems were using the ZEN blue software Version 3.1.

2.6.2.2. Image Processing and Analysis

Following acquisition, whole slide images were assembled from stitched tiles. Subsequently, high resolution images were generated using shading correction and background subtraction with the default settings of the ZEN blue software V3.1 (Carl Zeiss, Germany). Images of single fluorescence channels were converted to grayscale and further processed in FIJI Version 1.52p [306]. The stained area was calculated with a predefined threshold in FIJI. Quantification of positive fluorescence signal was measured by the area fraction of total area. Co-localization of markers was analysed with the FIJI plugin 'JACoP' [307] or by predefining regions of interest through manual gating. Masson's Trichrome stainings were analysed with the 'color threshold' selection tool in FIJI, extracting the positive stained collagen signal.
Color merged images were generated as appropriate (brightness, contrast) for illustration purposes.

2.6.3. Immunofluorescence of cell culture

Cells for fluorescence analysis were plated and cultivated in adherent 24-well plates or on sterile glass dishes. Medium was removed, cells were washed with PBS and fixed in 4% paraformaldehyde (Carl Roth, Germany) for 20 minutes at 4°C. After washing, cells were permeabilized for intracellular staining with 0.1% Triton™ X-100 (Sigma-Aldrich, USA) for 10 minutes and subsequently incubated with blocking buffer (PBS + 5% FCS + 3% BSA) for 1 hour. Staining protocol was continued identically as in 2.6.2. and imaging and analysis was performed as described under 2.6.2.1 and 2.6.2.2.

2.6.4. Flow cytometry staining

Flow cytometry stainings were performed on isolated primary endothelial cells, blood cells and cell lines. Antibody mixes were prepared in MACS buffer (PBS + 0.5% BSA +1 mM EDTA). Antibodies used for engraftment and immune status examinations in GvHD mouse models are listed in Table 10. All other antibodies used in flow cytometry stainings are listed

in Table 15. Cells were resuspended in the antibody mixes and stained for 20 minutes at 4°C. An unstained cell control was included in every staining panel. After incubation, cells were washed twice with PBS and resuspended in MACS buffer. Cells were detected with a FACS CantoII with BD FACSDiva™ Software v8.0.2 and the data was analysed with FlowJo 10.6.1 Software (TreeStar Inc., Ashland, OR, USA).

Table 15: List of antibodies used in flow cytometry experiments arranged by fluorophore.

Epitope	Fluorophore	Clone	Dilution	Manufacturer
ALK5	PE	141231	1:100	R&D Systems, USA
CD34		HM34		Biolegend, USA
CD31		MEC 13.3		BD Biosciences, USA
αSMA	Cy3	1A4	1:100	Sigma-Aldrich, USA
CD133	PE-Cy7	315-2C11	1:200	Biolegend, USA
cKit		2B8		BD Biosciences, USA
Sca-1	FITC	E13-161.7	1:50	Biolegend, USA
PDGFRβ		PY857		BD Biosciences, USA
CD45		30-F11		Biolegend, USA
CD146		P1H12		BD Biosciences, USA
CD146	APC	ME-9F1	1:200	BD Biosciences, USA
VE-Cadherin		16B1		Invitrogen, USA
CD44	PerCP-Cy5.5	IM7	1:200	Biolegend, USA
CD45		30-F11		BD Biosciences, USA
CD86		GL-1		Biolegend, USA
CD105	APC-Cy7	390	1:200	Biolegend, USA
CD31		MEC 13.3		Biolegend, USA
DAPI (Hoechst)	BV		1:1000	Sigma-Aldrich, USA

2.7. Serum marker analysis in cGvHD patients

The collection of patient serum samples was approved by the ethics committee of the Charité University Medicine Berlin and was in accordance with the Declaration of Helsinki. Study participants were allo-HSCT patients transplanted between 2014 and 2019, who were routinely examined in the Clinics for Stem Cell Transplantation at Charité University Hospital Berlin (Table 16). Whole blood was collected in serum collection tubes (BD Vacutainer; BD Biosciences, USA) from patients with diagnosed cGvHD and compared to patients with the same sex, who did not develop GvHD post transplantation after written informed consent was obtained. Serum tubes were centrifuged at 1200 rpm, 10 min, 4°C and the separated blood serum phase was transferred into Eppendorf tubes and stored at -80°C until analysis. Different

serum markers (summarized in Table 17) were analysed by Enzyme Linked Immunosorbent Assay (ELISA) according to the particular manufacturer's protocol.

Table 16: Clinical data of cGvHD patients in serum analysis. Tx= transplantation (allo-HSCT), f=female, m=male, AML=Acute myeloid leukemia, MDS=Myelodysplastic syndromes, MPN=Myeloproliferative neoplasms, NHL=Non-Hodgkin lymphoma.

Patient No.	Date of Birth	Sex	Diagnosed with	Age at Tx	cGvHD Score
1	09.07.1948	f	NHL	71	moderate
2	01.02.1959	m	MDS	58	mild
3	25.08.1951	m	other	63	severe
4	11.09.1970	f	AML	44	severe
5	27.07.1968	m	MPN	49	mild
6	30.05.1975	f	AML	41	severe
7	26.04.1953	f	AML	62	mild
8	25.10.1978	m	MDS	37	severe
9	23.11.1954	m	MDS	60	severe

Table 17: ELISAs used for analysis of cGvHD patient serum markers.

Serum marker	Gene	Manufacturer
Fibronectin	FN1	Abcam, UK
Endoglin	ENG	R&D Systems, USA
Endothelin-1	EDN1	Invitrogen, USA
Follistatin	FST	Invitrogen, USA
Endostatin	COL18A1	Invitrogen, USA
Connective Tissue Growth Factor	CTGF	Abcam, UK
Caspase-3	CASP3	Invitrogen, USA
Endocan / Endothelial-cell-specific molecule 1	ESM1	Origene, USA

2.8. Molecular biological methods

2.8.1. RNA isolation & cDNA synthesis

For fold change expression analysis, RNA was extracted from ~ 30 mg tissue of HSCT recipient mice using an Ultra-Thurax homogenizer. RNA from organs, isolated primary endothelial cells or endothelial cell lines was further purified following the protocol of the RNeasy Mini Kit by QIAGEN. Concentration and purity of the eluted RNA was checked using the NanoDrop 1000 before cDNA synthesis.

cDNA was transcribed from 1 µg of RNA using the QuantiTect Reverse Transcription Kit (QIAGEN) according to the corresponding manual. cDNA was diluted to a final concentration of 12.5 ng/µl in nuclease-free water and stored at -20°C until use.

2.8.2. Quantitative real-time PCR (RT-qPCR)

Based on the TaqMan-probe-assay, quantitative real-time polymerase chain reaction (RT-qPCR) was conducted. Primers and probes were ordered as ready-to-use primer-probe-mixes linked with a 6-carboxyfluorescein (FAM) dye from Thermo Fisher Scientific (Table 18). The respective primer-probe-mix and 2µl of total cDNA was added to the TaqMan™ Gene Expression Master Mix and the RT-qPCR amplification reaction was carried out in a CFX96™ C1000 Touch™ Thermal Cycler Real-Time System with the following thermal cycling conditions: 1) 50 °C for 2 minutes, 2) 95 °C for 10 minutes, 3) 60 °C for 1 minute and 49 repeated cycles of steps 2 and 3.

Achieved data were evaluated with the comparative 2-ΔΔCT method [308]. The expression of the respective genes of interest was normalized to housekeeping genes glyceraldehyde 3-phosphate dehydrogenase (*Gapdh*) or ß-actin (*ß-act*) and the binary logarithmic expression fold change of allogeneic samples was compared to syngeneic controls.

Table 18: TaqMan primers used for quantitative polymerase chain reaction.

Gene	**a-SMA (Acta2)**
TaqMan Assay ID	Mm00725412_s1
Amplicon Length	95
	ß-Actin
TaqMan Assay ID	Mm00607939_S1
Amplicon Length	115
	CD31 (Pecam1)
TaqMan Assay ID	Mm01242584_m1
Amplicon Length	71
	FSP-1 (S100a4)
TaqMan Assay ID	Mm00803372_g1
Amplicon Length	87
	GAPDH
TaqMan Assay ID	Mm9999991515_g1
Amplicon Length	107
	SMAD2
TaqMan Assay ID	Mm00487530_m1
Amplicon Length	72

	SMAD3
TaqMan Assay ID	Mm01170760_m1
Amplicon Length	59
	Snail1
TaqMan Assay ID	Mm00441533_g1
Amplicon Length	79
	TGF-ß1
TaqMan Assay ID	Mm01178820_m1
Amplicon Length	59
	Tie-2 (Tek)
TaqMan Assay ID	Mm00443254_m1
Amplicon Length	93
	Twist
TaqMan Assay ID	Mm00442036_m1
Amplicon Length	113
	VE-Cadherin (Cdh5)
TaqMan Assay ID	Mm03053719_s1
Amplicon Length	154
	Vimentin
TaqMan Assay ID	Mm01333430_m1
Amplicon Length	62
	vWF
TaqMan Assay ID	Mm00550376_m1
Amplicon Length	63

2.8.3. Protein isolation

Tissue from harvested, snap frozen organs of HSCT mice was minced in liquid nitrogen with mortar and pestle until grinded to a fine powder. Following, RIPA-buffer (150mM sodium chloride (Sigma-Aldrich, USA) + 1% Triton X-100 + 0.5% sodium deoxycholate (Thermo Fisher Scientific, USA) + 0.1% sodium dodecylsulfate (SDS) + 50 mM Tris base (Carl Roth, Germany), pH 8.0) was supplemented with the protease inhibitors 1 mM/ml sodium fluoride (Sigma-Aldrich, USA), 10 µg/ml Leupeptin (Thermo Fisher Scientific, USA), 2 µg/ml Aprotinin (abcam, UK) and 0.1 mM phenylmethylsulfonyl fluoride (PMSF; Sigma-Aldrich, USA), and shaken with the homogenized tissue or with cell pellets from endothelial cell culture for 30 minutes at 4°C. The lysate was spun down at 1200 rpm for 20 minutes and the supernatant was removed for protein quantification. The purity and concentration of the isolated protein was determined with the Pierce™ BCA-Kit from Thermo Fisher Scientific according to the manufacturer´s protocol.

2.8.4. Western Blot

Western Blot was performed to confirm knockout of different genes in endothelial cell lines and to analyse the endothelial pathology in cGvHD mouse models. First, a gel composed of separation and aggregation layer for SDS-polyacrylamide gel electrophoresis (SDS-PAGE) was poured in the Mini-PROTEAN® Tetra Handcast System. The separation gel contained H_2O + 30% Acrylamide Mix (Bio-Rad, USA), 1.5 M Tris ph 8.8 (VWR International, USA), 10% SDS, 15% APS, 0.4% TEMED (all Thermo Fisher Scientific, USA) and polymerized at RT for at least 30 minutes. The aggregation gel with 0.5 M Tris ph 6.8 (VWR International, USA) was poured on top of the separation gel and polymerized for 30 minutes. Next, a total of 40 µg protein per sample was reduced and denatured with 4X Laemmli buffer + 10% β-mercaptoethanol + 5% DTT at 95°C for 5 minutes. Denatured protein samples and the 250 kDA PageRuler Plus Prestained Protein Ladder (Thermo Fisher Scientific, USA) were loaded onto the SDS-gel placed in the buffer tank filled with 1X SDS-PAGE running buffer (2.5 mM Tris base + 19 mM Glycine + 0.1% SDS + ddH_2O). SDS-PAGE was initially run for 10 minutes at 80V to collect proteins in the aggregation gel, then the voltage was increased to 120V for 90 minutes for protein separation. After SDS-PAGE separation, proteins were transferred to a Polyvinylidenfluoride (PVDF) membrane (Bio-Rad, USA) using a Power Blotter- Semi-dry Transfer System with the supplied Pierce™ 1-Step Transfer Buffer (Invitrogen, USA). The pre-programmed default settings, matching the size of the transferred protein, were adjusted. The membrane was activated with methanol before transfer. After blotting, the successful transfer of the proteins was validated by incubation of the membrane in 1X Ponceau solution (Sigma-Aldrich, USA) for 10 minutes. The membrane was washed twice in ddH_2O and blocked for 1 hour at RT on a shaker in either 5% Milk Powder or 5% BSA +0.1% Tween + PBS, depending on the required antibody specifications. Primary antibodies were diluted in blocking buffer and applied to the membrane overnight at 4°C. The membrane was washed with PBST (PBS + 0.1% Tween) 3 times for 5 minutes and the secondary antibodies were prepared in blocking buffer and incubated for 2 hours at RT. All antibodies used in Western Blot are listed in Table 19.

Table 19: Primary and secondary antibodies used in Western Blot. Ang4 =Angiogenin4, G6pd(X) = Glucose-6-phosphate-dehydrogenase (X-linked), GAPDH = Glycerinaldehyd-3-phosphat-Dehydrogenase, ENO3 =Enolase 3, HRP = Horse raddish peroxidase

primary antibodies					
Epitope	**Host**	**Reactivity**	**Clone**	**Dilution**	**Manufacturer**
ANG4	rabbit	Mouse	polyclonal	1:1000	Abcam, UK
G6PD(X)	rabbit	Human, Mouse	polyclonal	1:300	ORIgene
GAPDH	rabbit	Human, Mouse	polyclonal	1:2000	Sigma-Aldrich
ENO3	rabbit	Human, Mouse	EPR11366(B)	1:1000	Abcam, UK
Vinculin	rabbit	Human, Mouse	EPR8185	1:1000	Abcam, UK
secondary antibodies					
Conjugate	**Host**	**Reactivity**	**Clone**	**Dilution**	**Manufacturer**
HRP	mouse	rabbit	6B9G9	1:2000	Biolegend, USA

Ensuing another washing with PBST, ECL Prime Western Blot detection reagent (GE Healthcare, USA) was prepared according the manufacturer´s protocol and applied to the membrane. Detection of positive protein signal was executed on a ChemiDog MP imaging system with Image Lab 5.2.1 software (BioRad Laboratories Inc.). Membranes were UV-imaged in the "chemi sensitive" acquisition mode for a total of 300 sec exposure time, taking pictures every 60 sec or until clear signals were achieved. Protein quantification was evaluated with FIJI.

2.9. Generation of endothelial knockout (KO) cell lines

The CRISPR-Cas9 system was used to create genetic knockouts (KOs) of different metabolic genes in the murine cardiac endothelial cell (MCEC) line.

2.9.1. CRISPR-Cas9-sgRNA vector generation

To target the genetic regions of interest with the CRISPR-Cas9 system, two pairs of 20 nucleotides-long single guide RNAs (sgRNAs), flanking each site of the gene (left (1) and right (A) of gene), were designed per genetic locus, implementing the online CRISPR design tool "CRISPOR" [309]. The top hits were selected based on predictive scores: specificity, efficiency and off-target efficiency. sgRNA sequences are listed in Table 20.

Table 20: Forward (fwd) and reverse (rev) sgRNA sites for application with CRISPR-Cas9. Ang4 =Angiogenin4, G6pd(X) = Glucose-6-phosphate-dehydrogenase (X-linked), ENO3 =Enolase 3, PAM= Protospacer adjacent Motif

Target	PAM	sgRNA sequence 5´-3´ (fwd & rev)
ANG4	TGG	Fwd_1: CACCGTTTGTTGTTGGTCTTCGTGC
		Rev_1: AAACGCACGAAGACCAACAACAAAC
	TGG	Fwd_A: CACCGCGCTCCTGAGTGCGTACAAG
		Rev_A: AAACCTTGTACGCACTCAGGAGCGC
ENO3	GGG	Fwd_1: CACCGCATGCAAAAAATCTTCGCCC
		Rev_1: AAACGGGCGAAGATTTTTTGCATGC
	AGG	Fwd_A: CACCGAAGAAAGTTCCGTAATCCAA
		Rev_A: AAACTTGGATTACGGAACTTTCTTC
G6PDX	GGG	Fwd_1: CACCGCCTGAAGATACCTTCATTGT
		Rev_1: AAACACAATGAAGGTATCTTCAGGC
	AGG	Fwd_A: CACCGTGAGGGTTCACCCACTTGT
		Rev_A: AAACACAAGTGGGTGAACCCTCAC

The designed sgRNA oligonucleotides were produced by BioTeZ Berlin-Buch GmbH and needed to be integrated into a plasmid backbone. For that, the vector pSpCas9(BB)-2A-GFP (PX458) (Supplemental Figure 1) [310]was purchased from Addgene, USA, which contains the endonuclease Cas9 from *S.pyogenes*, a GFP cassette and a sgRNA scaffold. 10 µg of PX458 plasmid was digested with 30U of the restriction enzyme BbsI in NEB2.1^{TM} buffer (New England Biolabs, USA) for 2 hours at 37°C. Successful digest of the vector backbone was checked on a 1% agarose gel together with an uncut vector control. The linearized plasmid DNA was eluted from the gel using the Innuprep Gel extraction Kit. Concentration and purity of the eluted plasmid was measured with the NanoDrop 1000.

The sgRNA oligonucleotides were annealed for 15 min at 95°C using 10 µl 10X T4 DNA ligase buffer (New England Biolabs), 10µl of each fwd and rev 100 µM sgRNA oligonucleotides and 70 µl of ddH_2O. Reaction was cooled down at RT before ligation of the annealed oligonucleotides into linearized PX458 plasmid backbone was conducted. 100 ng cut PX458, 2 ng annealed oligonucleotides, 2 µl 10X T4 DNA ligase buffer and 400 U T4 ligase (New England Biolabs) were incubated at 17°C overnight.

2.9.2. CRISPR-Cas9-sgRNA vector transformation and multiplication

Up to 100 ng of ligated PX458-sgRNA plasmids were transformed each into NEB 10-beta competent *E. coli* (New England Biolabs) by following the NEB protocol for high efficiency transformation. Bacterial suspensions were plated onto LB-agar-plates (LB-medium: MP

biomedicals, Germany; agar-agar: Carl Roth, Germany) supplemented with 100 µg/ml Ampicillin (Amp) (Sigma-Aldrich, USA) for positive selection of successfully transformed bacterial colonies and grown overnight at 37°C in a bacterial incubator. The next day, single bacterial colonies were picked with a sterile pipette tip and spread onto a new retransformation LB-Amp-agar plate. Plates were incubated over night at 37°C. Each picked colony was also analysed in a PCR for the presence of the transformed vector. As positive control, PX458 plasmid was amplified with plasmid specific primer pairs Fwd_U6 and Rev_Cbh. PCR master mix, Primer sequences and thermal cycling conditions are summarized in Table 21.

Table 21: PCR master mix formulation, primer pairs and thermal cycling conditions used for transformation check - PCR

PCR master mix		**Manufacturer**
0,4 µl fwd primer (fwd sgRNA oligonucleotide for specific gene)		BioTeZ Berlin-Buch
0,4 µl rev primer (Rev_Cbh binding on PX458 backbone)		BioTeZ Berlin-Buch
2 µl Taq standard buffer		New England Biolabs
0,25 µl Taq Polymerase		New England Biolabs
0,5 µl dNTP Mix (10mM)		New England Biolabs
16,45 µl ddH_2O		New England Biolabs
Primer sequences		
Fwd_U6	TAA AAT GGA CTA TCA TAT GCT TAC C	
Rev_Cbh	GAA AGT CCC TAT TGG CGT TAC	
Thermal cycling conditions		
94°C	3 min	
94°C	45 sec	
55°C	45 sec	32 cycles
72°C	45 sec	
72°C	7 min	
4°C	∞	

The PCR product was analysed on a 1.5% agarose gel. Successfully transformed colonies showed a PCR band at approximately 390 bp size. Two of the positive colonies were further processed for sequencing by picking from the retransformation plate and inoculated over night at 37°C in 2 ml LB-Amp medium in a 15 ml bacterial culture tube (Greiner Bio-One, Germany). The next day, DNA was isolated with the Nucleo Spin Plasmid Kit according to the manufacturer's protocol. The DNA concentration was measured with a NanoDrop 1000 and 200 ng of total DNA was sequenced by Eurofins Genomics, Berlin with the Fwd_U6 primer. Sequences were aligned against the corresponding PX458 vector sequence and analysed with ApE version 1.0.55 [311].

Bacterial colonies with correctly transformed sgRNA-PX458 plasmid were inoculated in 200 ml LB-Amp-medium over night at 37°C and DNA was isolated with the DNA Maxi Kit following the manufacturer's instructions. Purity and integrity of the isolated DNA was checked with the NanoDrop 1000.

2.9.3. Transfection of CRISPR-Cas9-sgRNA vectors

The prepared sgRNA-PX458 plasmid DNA and PX458 plasmid DNA without sgRNAs (empty vector control) were transfected with the TransIT-X2® Dynamic Delivery System into MCEC. The principle of the CRISPR-Cas9 system for KO generation is illustrated in Figure 15. MCEC were seeded into 6 cm cell culture petri dishes and cultured until 80% confluence was reached. MCEC medium was changed to Opti-MEM™ I Reduced Serum Medium and the transfection was executed for 24 hours according to the manufacturer´s protocol, with a 1:2 ratio of µg DNA to µl transfection reagent.

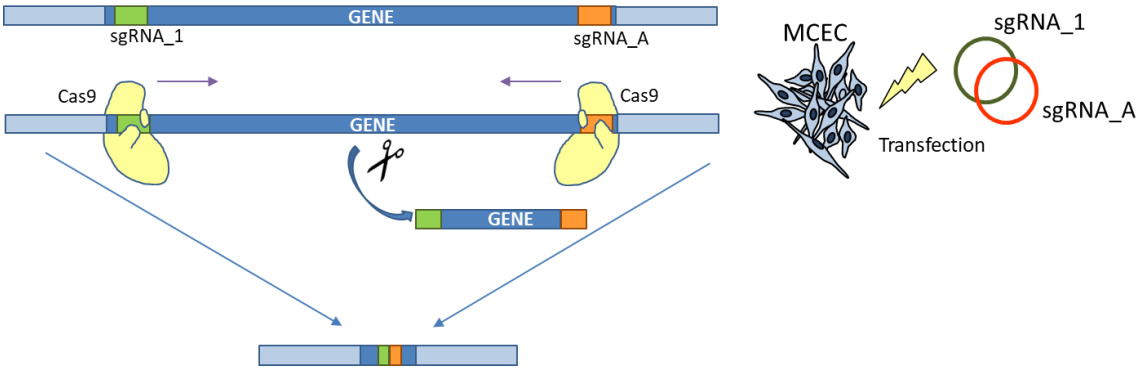

Figure 15: CRISPR-Cas9 working principle of genetic knockout generation. Two plasmids (sgRNA_1 and sgRNA_A) flanking both sites of the genetic target locus, are transfected at the same time. Cas9 is directed to the target sites to cut out the target completely. The flanking genomic sites are realigned together. sgRNA = single guide RNA, Cas9 = Caspase9, MCEC = Mouse cardiac endothelial cells.

2.9.4. Selection and analysis of Knockout cell lines

Selection of the positive transfectants was implemented by fluorescence activated cell sorting (FACS), performed at the FACS core facility of Charité Universitätsmedizin Berlin. Cells were detached from the culture dishes after 2 minutes incubation with Accutase and cell selection was performed at a BD FACS Aria II cell sorter. GFP- positive cells were selected and single cells were sorted into 0.1% gelatine coated 96-well plates filled with pre-conditioned MCEC medium. Single cell clones were incubated for up to two weeks until single cell colonies grew out to be passaged to 12-well plates for further analysis.

Knockout of target genes was confirmed by Western Blot (as described in chapter 2.8.4), PCR and Sanger sequencing. Two PCR primer pairs (Table 22) were designed per target gene, flanking the sgRNA sites upstream and downstream the gene (as illustrated in Figure 16). A successfully knocked out gene resulted in realigned flanking genomic DNA sites, so that the Fwd_1/ Rev_A primer pair combination amplified a fragment, which was visualized on a 1.5% agarose gel. The PCR product of this amplification was sent for sequencing to Eurofins Genomics, Berlin and analysed as described in 2.9.2.

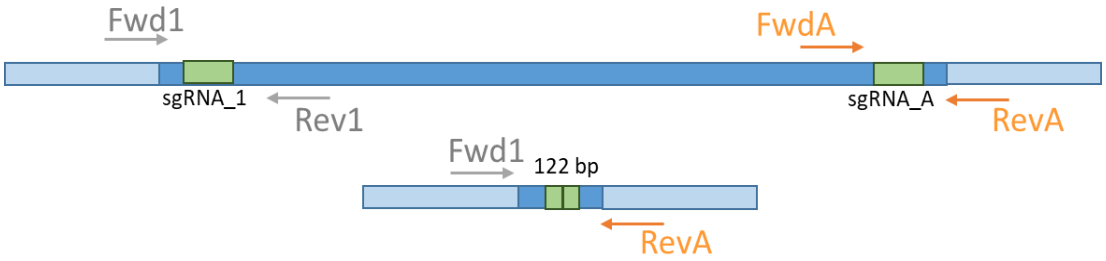

Figure 16: sgRNA PCR primer sites for detection of genetic Knockout. Fwd = forward, Rev = reverse, sgRNA = single guide RNA

Table 22: PCR master mix formulation, primer pairs and thermal cycling conditions used for knockout confirmation PCR. Fwd = forward, Rev = reverse

PCR master mix		**Manufacturer**
12,5 µl RedTaq Master Mix		Sigma Aldrich
0,3 µl 50 µM forward primer		BioTeZ
0,3 µl 50 µM reverse primer		BioTeZ
100 ng DNA		
Up to 25 µl ddH_2O		Thermo Fisher Scientific
Primer sequences		
Gene	**Sequence**	**basepair size**
ANG4	Fwd_1: CCACAGATGGCCCTGATGTT	436
	Rev_1: ATAGAGGAAGATGGCTGCGC	
	Fwd_A: TCTGGCCCATGACAGTGAAC	472
	Rev_A: TCCTCCAACTCTGGCTCAGA	
	Fwd_1 / Rev_A	326
G6PD(X)	Fwd_1: GTTGGCAAGGGAAAGCAAGG	451
	Rev_1: GGTGACCTGGCCAAGAAGAA	
	Fwd_A: TGGCAGCAGCATAGGACAAA	335
	Rev_A: AAGCAGGGCAGTGGGAATAC	
	Fwd_1 / Rev_A	460
ENO3	Fwd_1: GGGAGTGGTGTCATCTTGGG	355
	Rev_1: CCTGTGTTACCCTTGGCTGT	
	Fwd_A: TAGACCGTGGGGAGAGGAAG	267
	Rev_A: TTCCTGGCGAGCTTGTCATT	
	Fwd_1 / Rev_A	600

Thermal cycling conditions		
94°C	5 min	
94°C	45 sec	
55°C	45 sec	35 cycles
72°C	30 sec	
72°C	10 min	
4°C	∞	

2.10. Cell Culture

2.10.1. Endothelial cell culture

Different endothelial cell lines were used for *in vitro* studies of endothelial function and pathology during GvHD. Table 23 shows the endothelial cell lines which were used in cell culture assays. Cells were cultivated at 37°C under an atmosphere of 5% CO_2 in adherent T25 or T75 flasks until 85% confluence was reached. Cells were then passaged by removing the culture medium, washing with PBS, followed by detachment of MCEC and MuMEC with 1x Accutase or with 3x Trypsin for TMNK-1 for 2 -3 minutes at 37°C respectively. Detached cells were washed off twice with their respective medium, centrifuged and diluted in culture medium for seeding at approximately 30 to 40% confluence. Cells reaching passage 12 were discarded.

Primary endothelial cells isolated from mouse livers or lungs were cultured under the above described conditions in supplemented Endothelial Cell Growth Medium (EGM2) and passaged with 1x Accutase.

Table 23: Endothelial cell lines and required cell culture media used for *in vitro* studies. DMEM = Dulbecco's modified eagle medium; FCS = fetal calf serum, Pen/Strep = Penicillin/ Streptomycin

Cell line	Tissue origin	Distributor	Culture Medium
Mouse cardiac endothelial cells (MCEC) [312, 313]	heart	Cedarline, Canada	DMEM 5% FCS 1% Pen/Strep 1% GlutaMAX™
murine microvascular endothelial cells (MuMEC) [314]	skin	InSCREENeX GmbH, Germany	MuMEC medium 1% pen/strep
human-liver endothelial cells (TMNK-1) [315]	liver	tebu-bio GmbH, Germany	DMEM 10% FCS 1% Pen/Strep 1% GlutaMAX™

2.10.2. Stimulation of Endothelial-to-mesenchymal-transition with TGF-ß

Endothelial-to-mesenchymal transition was stimulated in MCECs and MuMECs *in vitro* by addition of H_2O_2 (30% w/w; Sigma-Aldrich, USA) and Transforming Growth Factor-ß (TGF-ß2; Miltenyi Biotec, Germany). $2x10^4$ MCECs and $1x10^4$ MuMECs per well were seeded in an adherent 24- well plate and cultivated overnight in their respective medium. Both EC lines were stimulated with 20 ng TGF-ß alone or together with 5 µM or 10 µM (for MCECs) and together with 10 µM or 20 µM H_2O_2 (for MuMECs). Medium was changed and supplemented freshly every day. After 96 hours, cells were detached with Accutase, centrifuged and cell pellets were harvested and frozen at -80°C for further analysis.

2.10.3. Wound Healing (Migration) Assay

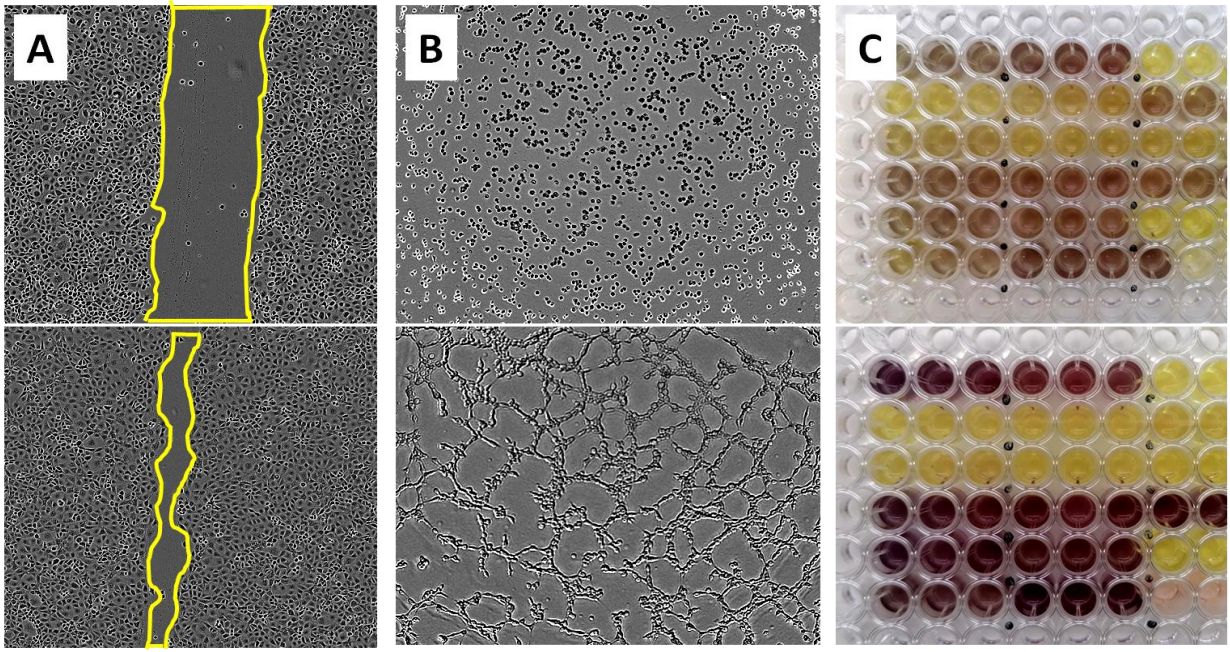

Figure 17: EC-Assays to determine endothelial function *in vitro*. A) Wound Healing Assay. A wound is applied to a confluent EC layer and wound closure is tracked over time, which resembles migration & proliferation capacities of ECs. B) Tubeformation assay. ECs are seeded onto a gel-matrix and tube-like structures are analysed for various parameters, e.g. tube-length, meshing or branching of tubes, relating to angiogenic properties of ECs. C) MTT-Assay. ECs are cultured and administered with yellow-coloured MTT-reagent, which is reduced to a purple metabolite by ECs. Colour change is measured by optical densitometry and calculated to assess viability and metabolic activity of ECs.

For assessing the migration of EC lines, the wound healing (scratch) assay was performed (Figure 17A). $7x10^4$ ECs per well were seeded into an adherent 24- well plate in 1 ml cell culture medium and cultured overnight. After 24 hours the cell layer was wounded with a

small pipette tip in a cross-shaped pattern, the medium was removed, the plate was washed once with PBS and fresh cell culture medium was added. If an allogeneic stimulus and/ or inhibitors were applied, T cells and/ or inhibitors were prepared and added as described in 2.10.5.1 and/ or 2.10.5.2. Plates were placed in the IncuCyte S3 live-cell imaging system and scanned in an interval of 3 hours for a total of 15 hours, using the 4X microscope objective. 5 pictures per well were taken in phase contrast (or red laser channel, if ECs were stained with dye in presence of T cells – see 2.10.5.1). The open wound area was manually gated and calculated with FIJI Version 1.52p. The wound closure (resembles migration) in % was calculated by normalization of the wound area at the different time points to the wound area at 0 hours.

2.10.4. MTT (cell proliferation) Assay

MTT assays, as first described by Mosmann et al. [316], were conducted to examine the viability and proliferation of ECs (Figure 17C). $3x10^3$ ECs per well were seeded into adherent 96- well plates and cultivated overnight. If a serum stimulus and/ or inhibitors were added, serum and/ or inhibitors were prepared and added as described in 2.10.5.1 and/ or 2.10.5.2 at four hours after EC seeding. The MTT assay protocol was executed following the manufacturer's instructions from the Cell Proliferation Kit I and the proliferation was determined after 24, 48 and 72 hours incubation by 570 nm colorimetric measurement at the Tecan Infinite M Plex microplate reader.

2.10.5. Tubeformation (Angiogenesis) Assay

To evaluate the angiogenic potential of ECs, tubeformation assays were performed (Figure 17B). A flat bottom 96- well plate was coated with 40 µl of liquid Matrigel® and incubated at 37°C until gel-solidification. $3x10^4$ MCECs and MuMECs per well were seeded in EGM2-medium. For TMNK-1, $2.3x10^4$ per well were seeded in MCEC medium. If an allogeneic stimulus and/ or inhibitors were applied, T cells and/ or inhibitors were prepared and added 30 minutes after EC seeding as described in 2.10.5.1 and/ or 2.10.5.2. Plates were placed in the IncuCyte S3 live-cell imaging system and scanned in an interval of 30 minutes for a total of 5 hours, using the 4X microscope objective. One picture per well was taken in phase contrast (or red laser channel, if ECs were stained with dye in presence of T cells – see 2.10.5.1). Blurred structures of the images were cropped and images were analysed with the FIJI 'angio analyzer' plugin [317], calculating 20 tube formation parameters (Supplemental Table 1) to

assess the tube-formation capacity. Tube formation parameters were normalized to the analysed area for comparison.

2.10.5.1. Allogeneic stimulation *in vitro*

All assays evaluating endothelial cell function described in the previous chapters were performed with and without mimicking an allogeneic stimulus *in vitro.* On that purpose, allo - GvHD conditions were simulated by adding splenic T cells or serum of C57Bl6/N ($H2k^b$) and BALB/c ($H2k^d$) mice to endothelial cell culture. Splenic T cells were isolated as described under 2.4.2. $6x10^6$ T cells were plated onto coated anti-CD3/CD28 well plates and cultivated in MLR medium (RPMI 1640 + 10% FCS + 1% Pen/Strep + 1% GlutaMAX™ + 1% HEPES + 1% sodium pyruvate) containing 4 ng/ml recombinant mouse IL-2 (Thermo Fisher Scientific, USA) for 2 days. Cells were washed off the plates with PBS, counted and added in a 1:10 ratio (endothelial cells:T cells) to wound healing assays and 1:5 ratio in tubeformation assays, including a proliferation factor of 1.4 for T cell numbers. When assays were performed using T cell stimuli, ECs were stained with 5 µl/ml Vybrant™ DiI cell labeling solution 24 hours prior to assay performance to guarantee distinction of different cell types.

Serum was harvested from C57Bl6/N ($H2k^b$) and BALB/c mice as described in chapter 2.5.7 and used in MTT assays in a concentration of 5%.

2.10.5.2. Pharmacologic inhibition *in vitro*

In the previously described endothelial cell assays, three different pharmacological inhibitors were tested. Inhibitors and administered concentrations are summarized in Table 24. An inhibitor - stock solution was made in 100% DMSO, which was further diluted with the respective cell culture medium, so the total DMSO concentration was never exceeding 1%.

Table 24: Inhibitor concentrations in µM used for endothelial cell assays *in vitro.*

Assay	ENOblock (AP-III-a4)	6-Aminonicontinamide (6-AN)	Polydatin
Wound Healing Assay	5, 10	500, 1000	500, 1000
MTT Assay	1, 5, 10	50, 100, 250, 500, 1000	300, 500, 1000
Tubeformation Assay	5, 10	500, 1000	500, 1000
Manufacturer	Selleckchem, USA	Sigma-Aldrich, USA	Sigma-Aldrich, USA
Target	Enolase	G6PD(X)	G6PD(X)

2.11. Statistics

Statistical significance of survival was calculated with the Mantel-Cox log-rank test, after analysis with the Kaplan-Meier estimate. Scratch, tube formation and MTT assays were analysed using a two-way ANOVA followed by Bonferroni's multiple comparisons tests and each biological repeat in the in vitro assays consisted of 3 averaged technical replicates. Serum levels of cGvHD patients were compared using the Mann-Whitney-Test. All other data was analysed using unpaired students t-tests. Values are presented as mean ± SEM (standard error of the mean). A p-value ≤ 0.05 was considered as statistically significant. All statistical analyses and visualizations were performed using GraphPad Prism software (GraphPad software Inc, USA).

3. Results

3.1. Pathological angiogenesis in acute GVHD

The following chapter covers experimental results for understanding the mechanisms leading to pathologic angiogenesis during acute GvHD (aGvHD). It elicits, in how far the deletion of metabolic genes influences the endothelial function in an allogeneic (allo) setting and describes a possible therapeutic approach for aGvHD using specific angiogenesis-inhibitors against the identified potential targets.

3.1.1. Generation of genetic knockouts of endothelial *Eno3, G6pdx, Ang4* and *Acsm3*

In previous gene and protein arrays, several targets were identified, which show an upregulation during pathologic angiogenesis and may contribute to initiation of GvHD after allo-HSCT. To analyse the function of these genes on endothelial behaviour and to gain fundamental knowledge about the mechanisms involved in angiogenesis, we created genetic knockouts of four genes in a murine endothelial cell (EC) line. On that purpose, we transfected MCECs with self-designed sgRNA- and Cas9-GFP-plasmids to generate complete CRISPR/Cas9-mediated excisions of the selected target genes *Eno3* (glycolytic enzyme), *G6pdx* (PPP enzyme), *Acsm3* (FAO enzyme) and *Ang4* (ribonuclease, angiogenesis). GFP-positive transfectants were single cell sorted (Figure 18) and further cultivated until clones were proliferated to reach cell numbers sufficient for analysis. Transfection efficiencies varied between the genes and ranged from 5.3-5.7% (*Eno3*), 3.6–5.2% (*G6pdx*), 2.6–4.0% (*Ang4*) to 2.0–2.5% (*Acsm3*). Sorting efficiency also varied from 12.6–21.5% (*Eno3*), 5.7–7.2% (*G6pdx*), 5.6 – 9% (*Ang4*) to 19.7-21.0% (*Acsm3*).

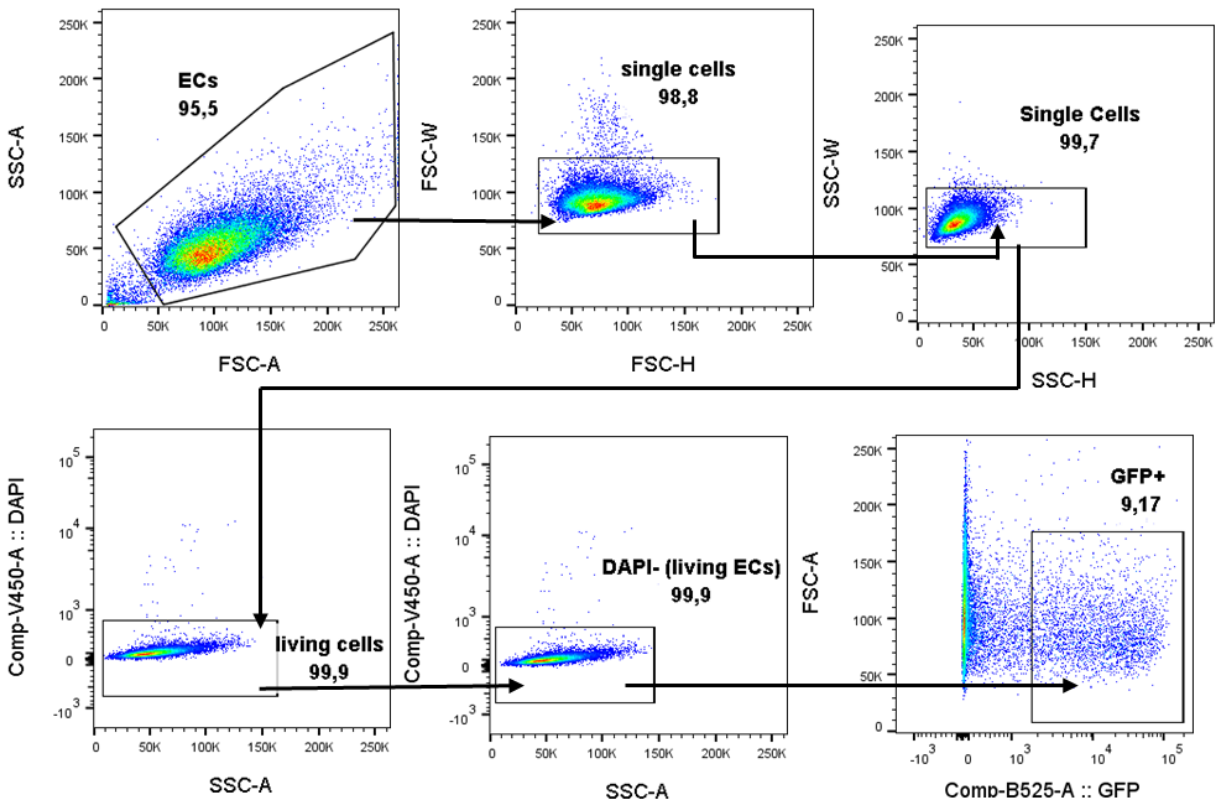

Figure 18: FACS-gating strategy for single cell sort of transfected MCECs. ECs were transfected with the appropriate sgRNA-plasmid for CRISPR/Cas9-mediated genetic KO and stained with DAPI immediately before FACS-sort. ECs were gated in FSC/SSC, cell duplets were removed by gating FSC/SSC- height and -width and living cells were determined as DAPI-negative fraction. Medium and high GFP+ cells were selected as positive transfectants and single cell sorted for further culture.

CRISPR/Cas9-created genetic modifications were confirmed on DNA- and protein levels. As Figure 19 shows, we could no longer detect protein fragments in the Knockout (KO) cell lines for none of the four target genes in Western Blot, while wildtype (WT), Mock and empty Cas9-vector (EV) transfected MCECs, which served as internal controls, showed appropriate protein bands. A first PCR was utilized, using two primer pairs flanking the sgRNA binding sites upstream (F_1/R_1) and downstream (F_A/R_A) of the genetic target region. With exception of *Ang4*, no PCR products were detected in the KO-cells, indicating a loss of the genetic target region between the sgRNA sites (middle row). To validate the results, a 'surrounding PCR' was designed, with a primer pair (F_1/R_A) flanking the complete genetic target region. This PCR only amplifies a fragment if the gene was excised completely between the sgRNA sites and the adjacent genomic sites were re-aligned together. DNA fragments were only amplified in the KO-cell lines, but not in the WT MCECs, confirming a successful gene excision (bottom row).

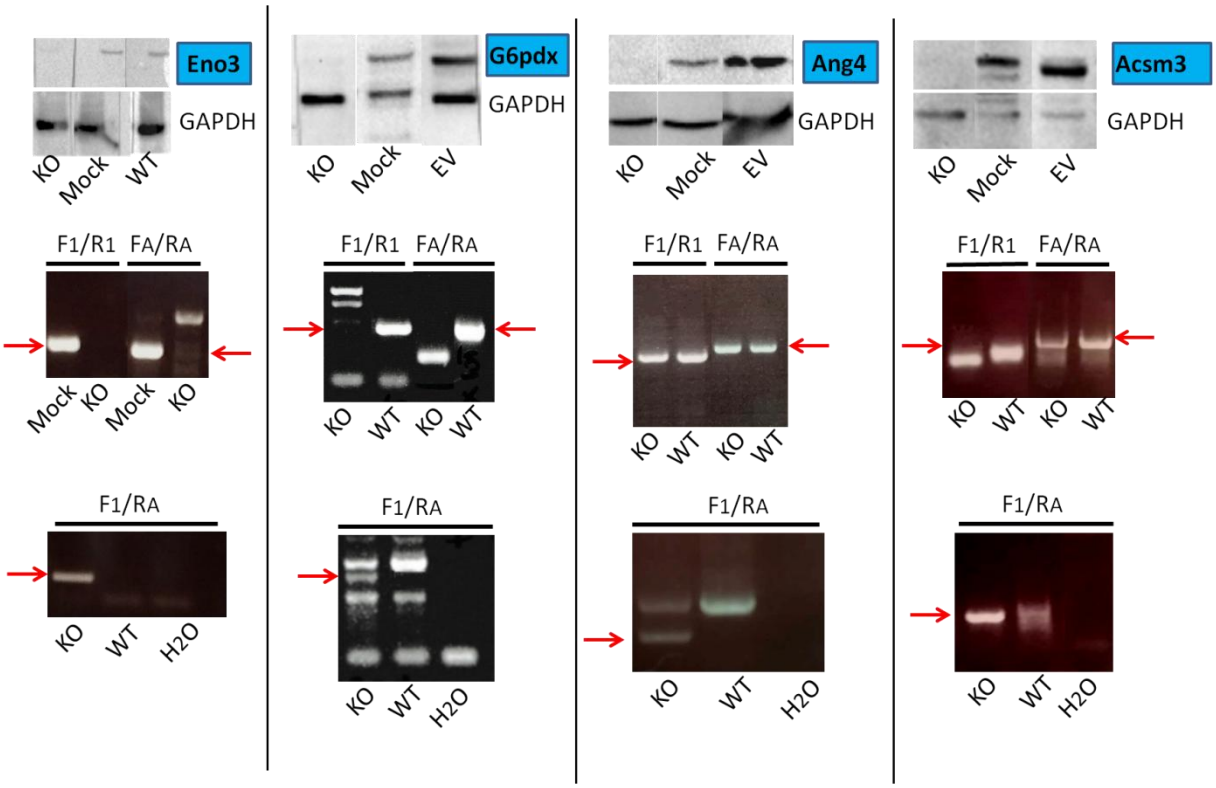

Figure 19: Validation of *Eno3*-, *G6pdx*-, *Ang4*- and *Acsm3*- KO in MCEC clones by Western Blot and PCR. Upper: CRISPR/Cas9-mediated genetic deletions of target genes resulted in loss of *Eno3*-, *G6pdx*-, *Ang4*- and *Acsm3*- protein synthesis in KO-MCECs, while protein was detected in WT-, EV- or Mock-controls in Western Blots. Housekeeping gene/protein *GAPDH* served as internal control. Middle: PCR-primers F_1/R_1 and F_A/R_A flanking the sgRNA sites of the genomic target regions. KO-MCECs (with exception of *Ang4*) in contrast to WT or Mock controls did not show DNA fragments, indicating genomic alterations around sgRNA sites. Bottom: Exclusively KO-MCEC lines but not WT controls showed a band in the surrounding PCR (F_1/R_A), confirming complete excision of the genetic target region between flanking sgRNA sites. KO=Knockout, WT=Wildtype, EV=Empty Vector, F/R=Forward/Reverse, H2O=Water Control.

In sequencing, we observed insertions or deletions of single or multiple nucleotides, inverted re-alignment of excised fragments and partial or whole excision of the genetic target region, Latter, together with a positive result in the surrounding-PCR and an absent protein detection in Western Blot were defined as successful knockouts. Clones showing minor genetic modifications however with detectable protein synthesis in Western Blot were taken as 'Mock' controls. In summary, for all candidate genes endothelial KO cell lines were successfully generated with corresponding control cells.

3.1.2. Endothelial function of genetic deletions of *Eno3, G6pdx, Ang4* and *Acsm3 in vitro*

To estimate the influence of the genetic deletions on EC behaviour, the four confirmed KO-cell lines of *Eno3*-, *G6pdx*-, *Ang4*- and *Acsm3* were tested *in vitro* in EC- functional assays. Parameters as viability, proliferation and metabolic activity of KO-MCECs were tested in the MTT-assay. Migration was analysed utilizing the Scratch/wound migration-assay and the angiogenic potential of the KO-MCECs was assessed by measuring the ability to build tube-like structures in a tube formation assay. In addition, KO-MCECs were co-cultured *in vitro* with freshly activated murine splenic T cells or murine blood serum to mimic an allogeneic activation of ECs found in allo-HSCT and to test functional EC-properties in this regard.

Genetic deletion of *Eno3* in MCECs exhibited significantly impaired endothelial functions exclusively under allo-stimulated conditions. Decreased migration and proliferation was detected only in T cell stimulated *Eno3*-KO-ECs compared to control cell lines empty vector (EV) and Mock (Figure 20A), particular 9 to 12 hours after wounding (Figure 20B). Angiogenesis was visibly impaired specifically in T cell stimulated *Eno3*-KO-cells: 11 of 20 angiogenesis-parameters in the tubeformation assay indicated significant changes in the endothelial tubeformation behaviour, which could not be detected in controls or under non-stimulated conditions (in excerpt Figure 20C and Supplemental Figure 2) . Interestingly, the T cell stimulation was rather prominent by addition of C57BL/6 T cells and only minorly pronounced when adding BALB/c T cells. In addition, only *Eno3*-KO-cells showed a significantly reduced viability exclusively under stimulation with C57BL/6 serum after 48 and 72 hrs culture (Figure 20D).

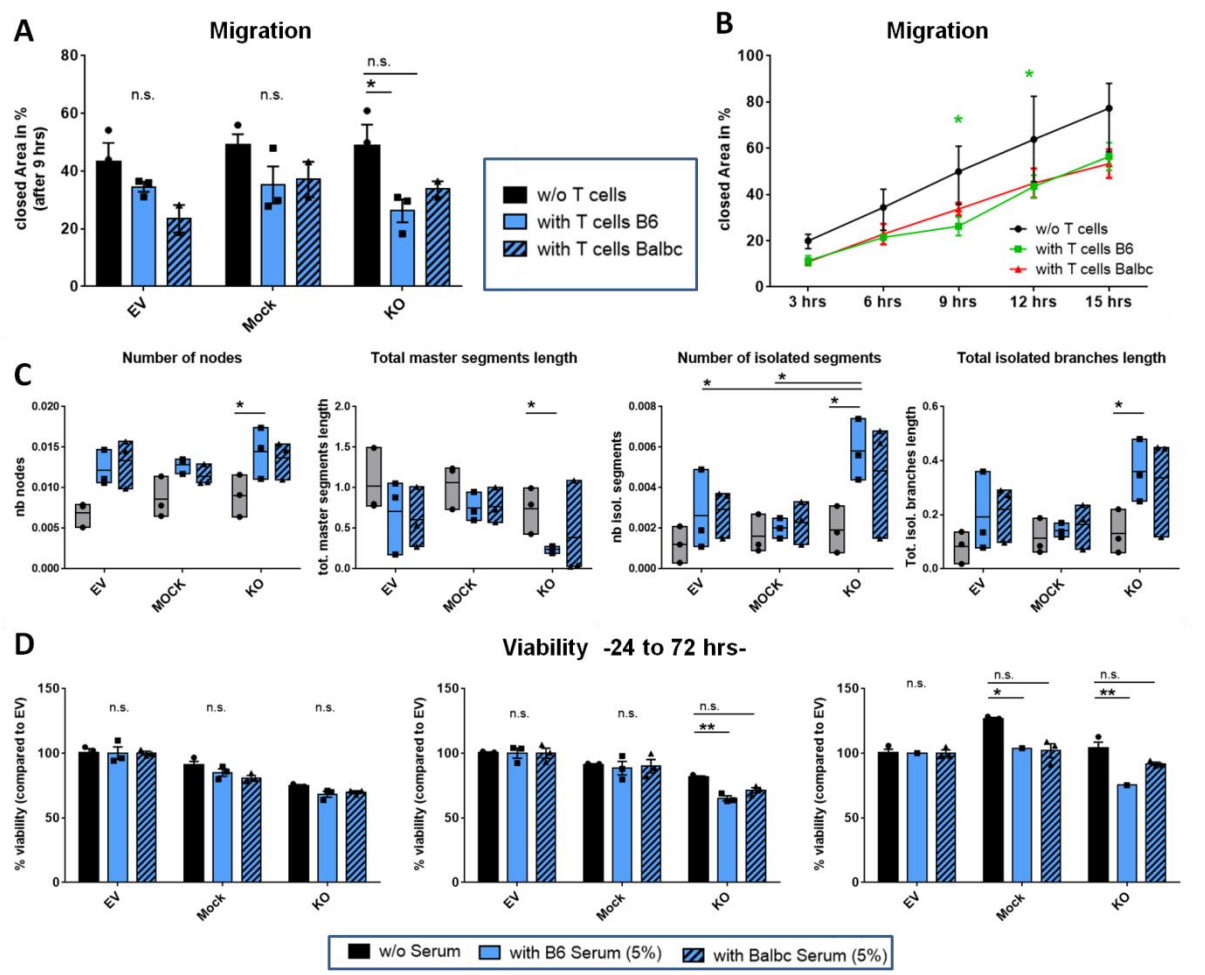

Figure 20: Endothelial behaviour of *Eno3*-KO in *in vitro* assays. (A) Wound healing assay at 9 hrs and **(B)** *Eno3*-KO growth over 15 hrs in wound migration assay and **(C)** Representative graphs from tubeformation assay under stimulated (+ mouse T cells) and non-stimulated conditions. **(D)** MTT assay over 72 hrs under stimulated (+5% mouse serum) and non-stimulated conditions. EV=empty vector, KO=knockout. Data pooled from 3 independent experiments. Error bars indicate mean ± SEM, *P<0.05, **P<0.01, ***P<0.001, n.s. not significant by one-way ANOVA/Turkey's multiple comparisons test (MTT) or by two-way ANOVA/Holm-Side's multiple comparisons test (Wound Healing) or by multiple unpaired students t-test with Holm-Sidak correction for α=0.05 (Tubeformation).

Under stimulated conditions, deletion of *G6pdx* in MCECs eventuated in significantly diminished migration (Figure 21A) pronounced 9 to 15 hours after wounding (Figure 21B). Angiogenesis was significantly impaired in the *G6pdx*-KO-cells under T cell stimulation, whereas control cells did not react. The *G6pdx*-KO showed altered tubeformation features in 12 of 20 tested parameters, particularly effecting junctioning, segmentation and meshing processes (in excerpt Figure 21C, D and Supplemental figure 3). Both origin of T cells (C57BL/6 or BALB/c) for allo-stimulation exhibited similar responding rates in the assays. Viability and metabolic activity of serum-stimulated *G6pdx*-KO was strongly decreased after 72 hrs culture in MTT-assay (Figure 21E).

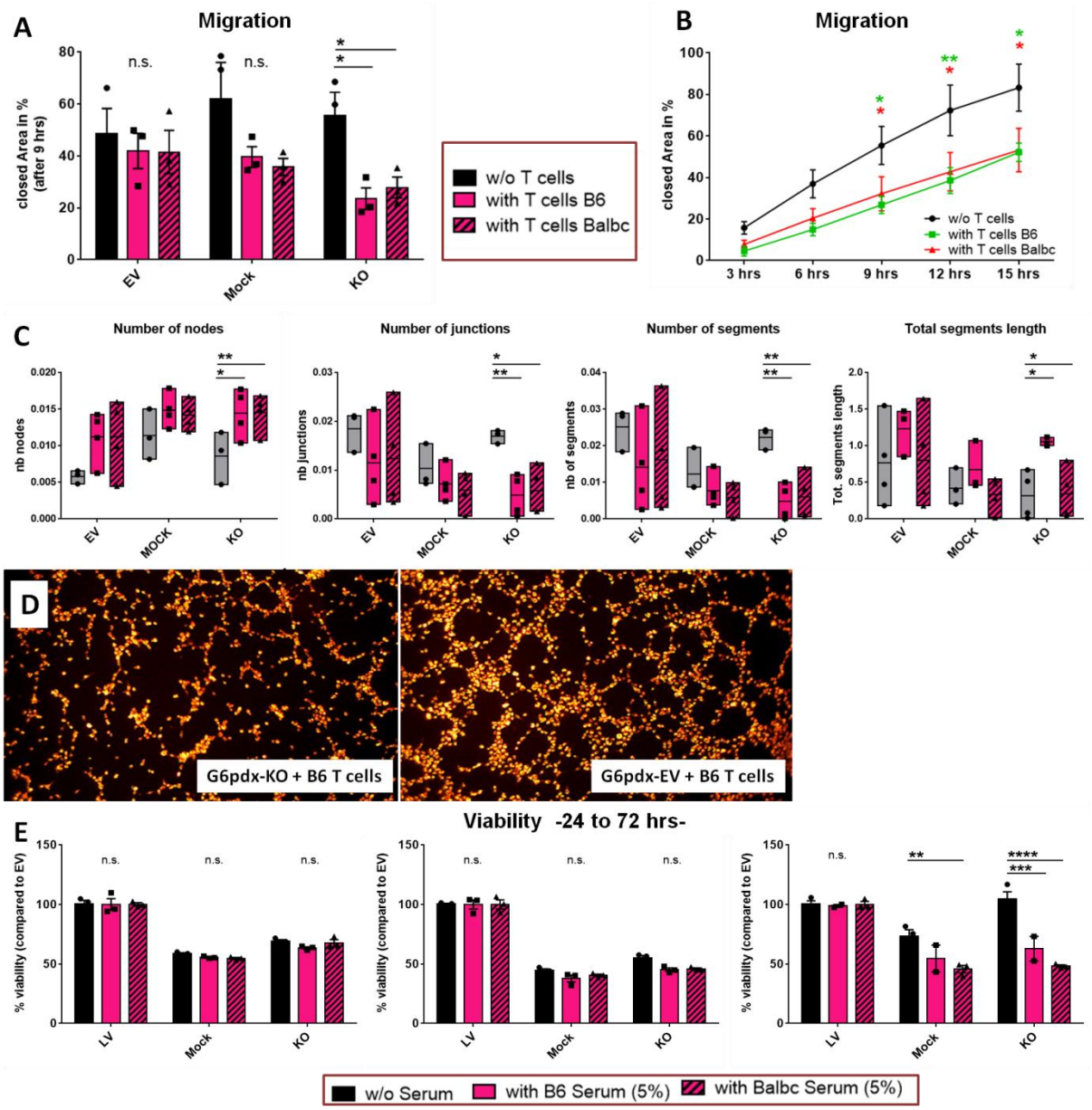

Figure 21: Endothelial behaviour of *G6pdx*-KO in *in vitro* assays. (A) Wound healing assay at 9 hrs and **(B)** *G6pdx*-KO growth over 15 hrs in wound migration assay. **(C)** Representative graphs and **(D)** representative fluorescence images (20x, Vybrant DiI-stain) from tubeformation assay under stimulated (+ mouse T cells) and non-stimulated conditions. **(E)** MTT assay over 72 hrs under stimulated (+5% mouse serum) and non-stimulated conditions. EV=empty vector, KO=knockout. Data pooled from 3 independent experiments. Error bars indicate mean ± SEM, *P<0.05, **P<0.01, ***P<0.001, n.s. not significant by one-way ANOVA/Turkey's multiple comparisons test (MTT) or by two-way ANOVA/Holm-Side's multiple comparisons test (Wound Healing) or by multiple unpaired students t-test with Holm-Sidak correction for α=0.05 (Tubeformation).

Genetic deletion of *Ang4* in ECs did not affect endothelial behaviour in the performed assays. Neither stimulated, nor non-stimulated *Ang4*-KO showed significant influence on endothelial migration and proliferation (Figure 22A,B) as well as on viability and metabolic activity

(Figure 22D). In tubeformation assay, only the 'mean mesh size' was detected to be altered in C57BL/6 T cell-stimulated *Ang4*-KO, however this applied also for control *Ang4*-EV-cells, while all other tubeformation parameters were not affected (Figure 22C).

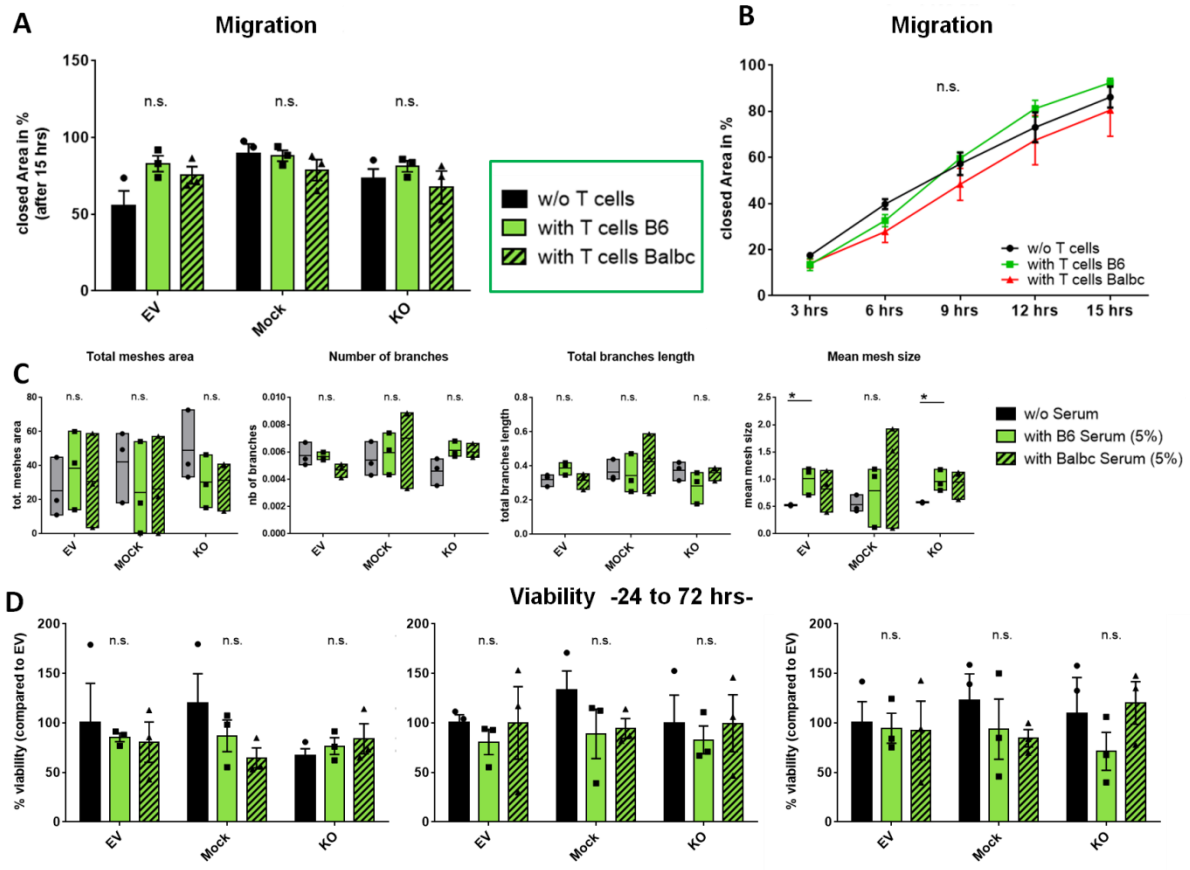

Figure 22: Endothelial behaviour of *Ang4*-KO in *in vitro* assays. (A) Wound healing assay at 15 hrs and **(B)** *Ang4*-KO growth over 15 hrs in wound migration assay .**(C)** Representative graphs from tubeformation assay under stimulated (+ mouse T cells) and non-stimulated conditions. **(D)** MTT assay over 72 hrs under stimulated (+5% mouse serum) and non-stimulated conditions. EV=empty vector, KO=knockout. Data pooled from 3 independent experiments. Error bars indicate mean ± SEM, *P<0.05, **P<0.01, ***P<0.001, n.s. not significant by one-way ANOVA/Turkey's multiple comparisons test (MTT) or by two-way ANOVA/Holm-Side's multiple comparisons test (Wound Healing) or by multiple unpaired students t-test with Holm-Sidak correction for α=0.05 (Tubeformation).

Acsm3 deletion seemed to only have minor impact on the endothelial phenotype. Migration and proliferation of MCECs was not influenced by deletion of *Acsm3* under non stimulated or stimulated conditions (Figure 23A, B). In tubeformation assays, T cell stimulated *Acsm3*-KO showed significantly modified angiogenic features only in 3 out of 20 analysed tubeformation-parameters (Figure 23C), while the rest of parameters seemed to be influenced

in tendency. Viability of the T cell stimulated *Acsm3*-KO was detected to be increased compared to controls after 48 hrs and 72 hrs (Figure 23D).

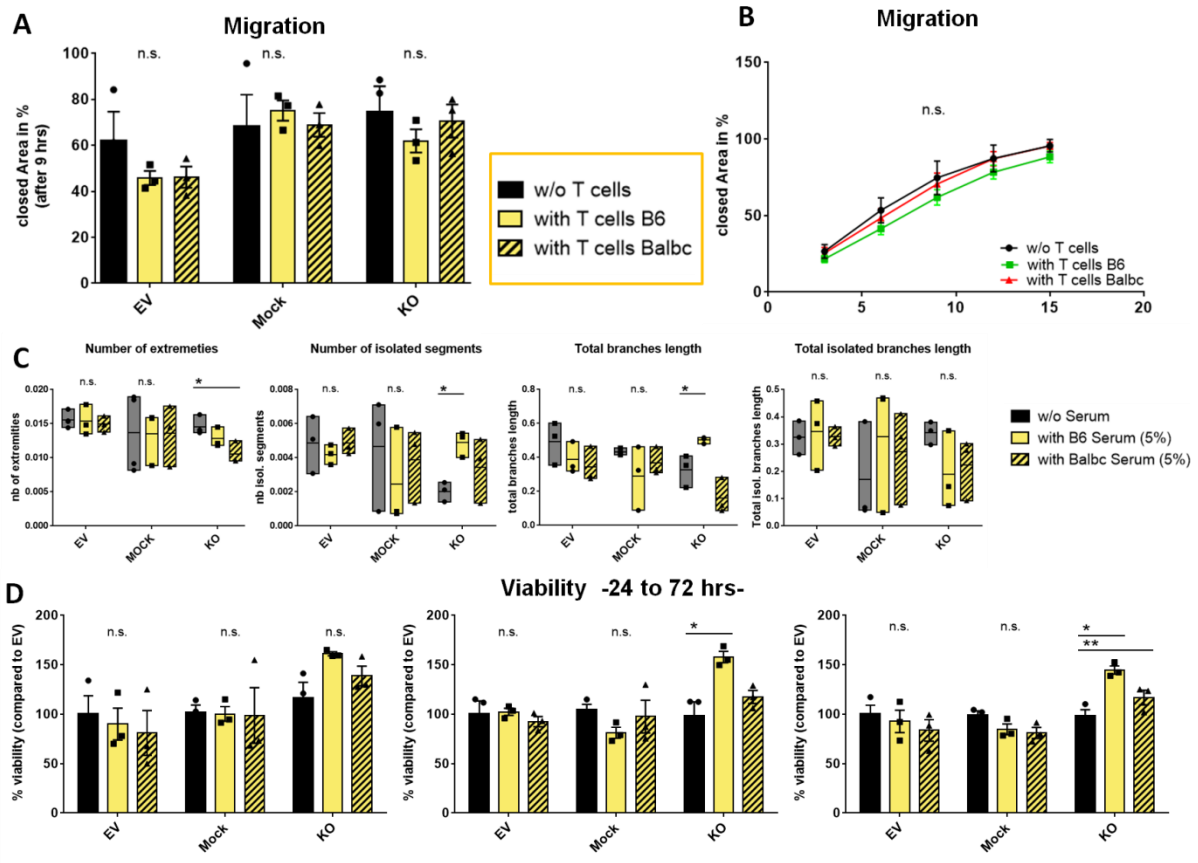

Figure 23: Endothelial behaviour of *Acsm3*-KO in *in vitro* assays. (A) Wound healing assay at 15 hrs and **(B)** *Acsm3*-KO growth over 15 hrs in wound migration assay. **(C)** Representative graphs from tubeformation assay under stimulated (+ mouse T cells) and non-stimulated conditions. **(D)** MTT assay over 72 hrs under stimulated (+5% mouse serum) and non-stimulated conditions. EV=empty vector, KO=knockout. Data pooled from 3 independent experiments. Error bars indicate mean ± SEM, *P<0.05, **P<0.01, ***P<0.001, n.s. not significant by one-way ANOVA/Turkey's multiple comparisons test (MTT) or by two-way ANOVA/Holm-Side's multiple comparisons test (Wound Healing) or by multiple unpaired students t-test with Holm-Sidak correction for α=0.05 (Tubeformation).

To summarize, the *Ang4*-KO did not show alterations in the endothelial behaviour. The genetic deletion of *Eno3*, *G6pdx* and *Acsm3* resulted in a significantly altered endothelial phenotype (angiogenesis, migration and viability and metabolism) especially under mimicked allo-stimulated conditions, making it suitable candidates for further analysis of GvHD-involvement and pathologic angiogenesis and nominating them as appropriate targets for pharmacologic interventions.

3.1.3. Endothelial function of pharmacologic inhibition of *Eno3, G6pdx, Ang4* and *Acsm3 in vitro*

To substantiate our results and test the therapeutic potential of the three targets, the effect of specific chemical inhibitors on endothelial function was tested in three different EC lines: ENOblock and Methylglyoxal (Eno3-Inhibitors), 6-Aminonicotinamide (6-AN) and Polydatin (G6pdx-Inhibitors) as well as the Acsm3-Inhibitor 4-Methylsalicylic acid (4-MSA) were initially administered to MCECs (murine cardiac ECs), MuMECs (murine microvascular ECs), and TMNK-1 (immortalized human liver sinusoidal EC line) in variable concentrations. In dose finding studies, toxicity and influence of the inhibitors on the endothelial metabolic activity was measured in MTT-assays (Figure 24 and Supplemental Figure 4).

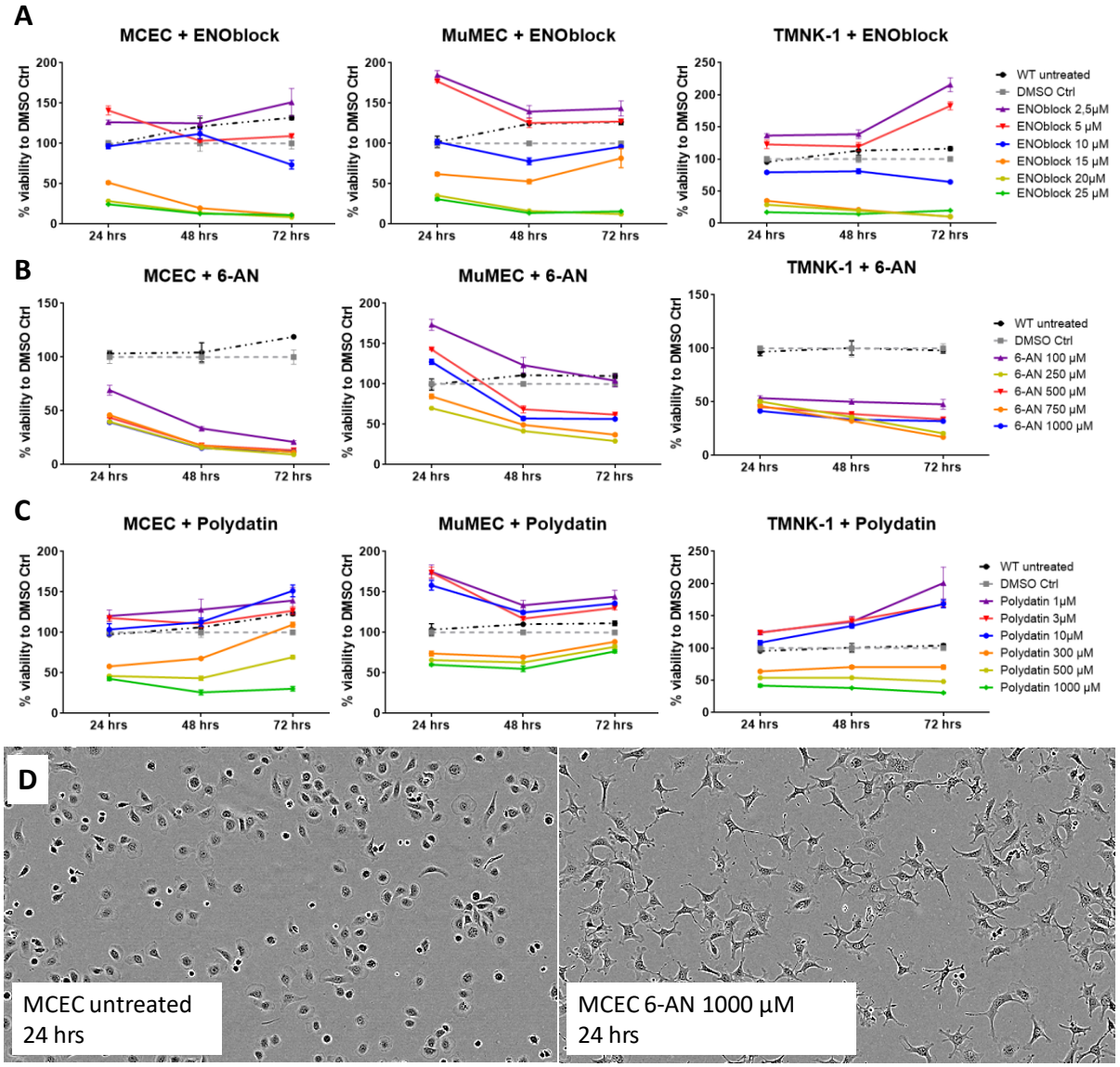

Figure 24: Influence of pharmacologic inhibitors on endothelial viability and metabolic activity in MTT-assays over 72 hrs. (A) Inhibition of Eno3 in MCEC, MuMEC and TMNK-1 by ENOblock.

Figure 24 (B) Inhibition of G6pdx in MCEC, MuMEC and TMNK-1 by 6-AN. **(C)** Inhibition of G6pdx in MCEC, MuMEC and TMNK-1 by Polydatin. **(D)** Representative images of morphology of MCECs treated for 24 hrs with or without 6-AN (magnification 10x). WT=Wild type, 6-AN=6-Aminonicontinamide, MCEC= Murine cardiac endothelial cells, MuMEC=murine microvascular endothelial cells, TMNK-1= immortalized human liver sinusoidal EC line. Data pooled from 2 independent experiments with 3 replicates per inhibitor-concentration. Error bars indicate mean ± SEM.

In contrast to the DMSO and WT control, ENOblock showed sufficient metabolic inhibition in all three EC lines at concentrations of 5 to 10 µM with low toxicity to ECs, while lower concentrations had no effect on the cells viability and higher concentrations resulted in increased cell death (Figure 24A). EC lines treated with 6-AN in high concentrations > 250 µM to 1000µM exhibited a reduced metabolic activity with increasing time with minor signs of cell death (Figure 24B), but a visibly altered cellular morphology (Figure 24D). Polydatin administration in concentrations above 300 µM did not display any signs of toxicity and cell death, but managed to decrease the endothelial metabolic activity in all three tested cell lines compared to untreated controls (Figure 24C). Methylglyoxal showed very heterogeneous results in MCECs, MuMECs and TMNK-1. While low concentrations of 10 µM were not sufficient to influence MCEC viability, higher concentrations resulted in immediate cell death. MuMECs and TMNK-1 showed diminished cellular activity at 300 µM - 400 µM (Supplemental Figure 4), but optical density measurements were inconsistent due to elevated turbidity occurring when solving higher doses of the yellow-coloured Methylglyoxal, which optically interfered with the MTT-reagent. 4-MSA was soluble in DMSO, but immediately precipitated when added to aqueous cell cultures allowing no valid analysis. Therefore, both inhibitors were excluded from further experiments.

The influence of ENOblock, 6-AN and Polydatin on the migration, proliferation and angiogenesis was further analysed in wound healing- and tubeformation assays in MCECs, MuMECs and TMNK-1 in a supervised master thesis project. Again, all assays were performed under non-stimulated and T cell stimulated conditions to mimic allogeneic conditions. Therapeutic inhibition of Eno3 by ENOblock exhibited only minor effects on endothelial function. Migration and proliferation were not affected in any of the cell lines. 5 µM ENOblock reduced angiogenic potential in T cell stimulated TMNK-1 in tubeformation assays. Therapeutic inhibition of G6pdx by Polydatin and 6-AN showed a significant effect on the endothelial function. Both compounds significantly decreased the EC metabolic

activity and proliferation of all three cell lines under non-stimulated and T-cell stimulated conditions in a concentration-dependent manner, ranging from 250 µM to 1000 µM. Wound closure was decelerated by 1000 µM Polydatin and delayed by >500 µM 6-AN under T-cell-stimulated conditions. At a concentration of 500 µM, both inhibitors were able to inhibit angiogenic functions in stimulated TMNK-1 (data not shown; data collected by Christiane Leß and published at FU Berlin as master thesis: Investigation and treatment of side effects after cellular immunotherapies. Dec 2021).

As the previously described results showed a significant influence of the genetic as well as pharmacologic deactivation of G6pdx on endothelial behaviour under simulated allo-HSCT settings, G6pdx-therapeutic targeting could be promising in attenuating pathologic angiogenesis and aGvHD.

3.1.4. Analysis of the therapeutic potential of G6pdx *in vivo*

To elaborate on the concept of G6pdx being a suitable candidate for therapeutic targeting of the endothelial function, *in vivo* studies were conducted using the G6pdx inhibitor Polydatin as prophylaxis in the paw edema mouse model of inflammation and early angiogenesis as well as therapeutic intervention in an aGvHD mouse model. Polydatin was chosen over 6-AN, because it showed no cellular toxicities in our former studies *in vitro* and was already tested without considerable side effects in experiments *in vivo*, in contrast to 6-AN, which was proven to harbour (neuro)toxicities in mouse studies [318, 319].

In two independent experiments, the positive impact of Polydatin-treatment in the inflammation-induced paw-edema model was elicited. Therapeutic inhibition of G6pdx significantly attenuated footpad swelling in Polydatin-treated mice compared to the control group up to 4 hrs after edema-induction (Figure 25A) indicating less inflammation. The spleen weight (normalized to body weight) of Polydatin-treated mice was decremented in comparison to controls, indicating less immune cell trafficking into the spleens due to lesser immune cell infiltration into paws in those animals (Figure 25B).

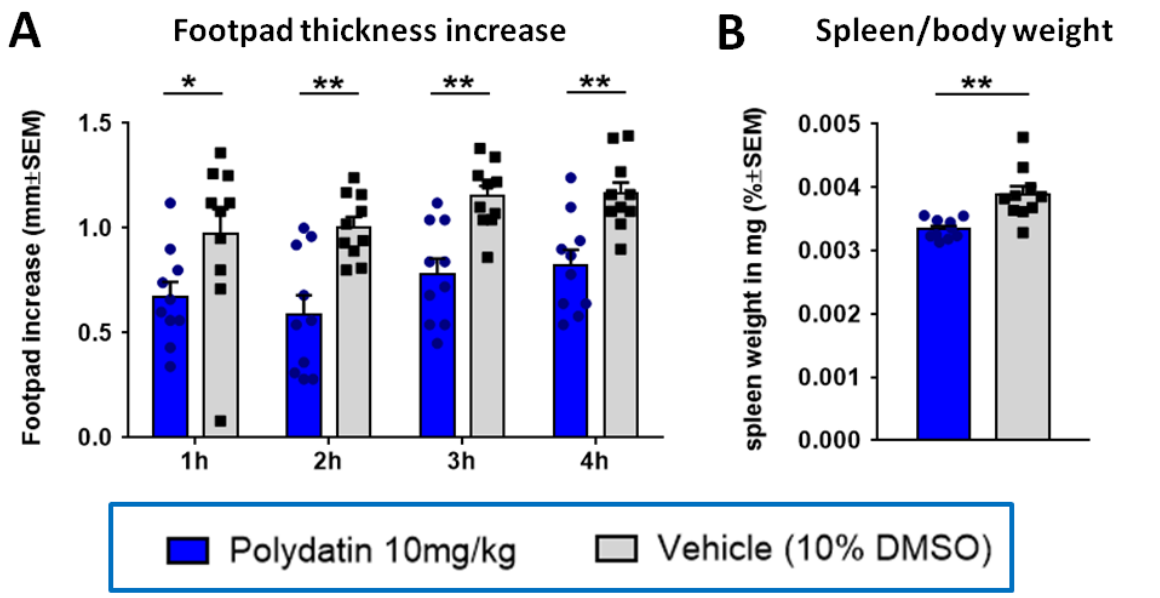

Figure 25: Influence of the G6pdx-inhibitor Polydatin on the paw edema mouse model of inflammation. C57BL/6 mice were i.p. injected daily with 100 mg/kg Polydatin or Vehicle (10% DMSO in PBS; control group) for 5 days. **(A)** Footpad swelling was measured up to 4 hrs after carrageenan injection. **(B)** Spleen weight normalized to individual body weight of each mouse 4 hrs after carrageenan injection. n=10 per group. Data pooled from two independent experiments. Error bars indicate mean+SEM. *P<0.05, **P<0.01 by unpaired students t-test with α=0.05.

In acute GvHD, Polydatin administration to allo-HSCT mice resulted in significantly improved GvHD morbidity (comprised of weight change and GvHD Score) and unchanged GvHD mortality (Figure 26A). In line, histological analysis of GvHD revealed less target organ GvHD in Polydatin-treated aGvHD mice compared to vehicle-treated mice in colon, liver and skin indicated by significantly reduced GvHD histoscores (Figure 26C). GvHD-typical T cell infiltration by CD3+ T cells was significantly reduced in the skin, and in tendency also in liver and colon of Polydatin-treated mice (Figure 26B;D). During aGvHD, an initial pathological angiogenesis and a damaged and dysfunctional endothelium was characterized by the Penack group [154, 155, 242]. As described in the previous chapter, the endothelial functions of allo-stimulated ECs can be impaired by Polydatin administration *in vitro*. To evaluate the effectiveness of Polydatin as an endothelial protector *in vivo*, the density of Endomucin-stained vessels was quantified (Figure 26B). In Polydatin-treated HSCT-animals, we measured a decreased vessel density in the liver and in tendency also in colon, while in skin the Endomucin signal was higher compared to vehicle-treated mice, indicating a normalization of dysfunctional vessel growth.

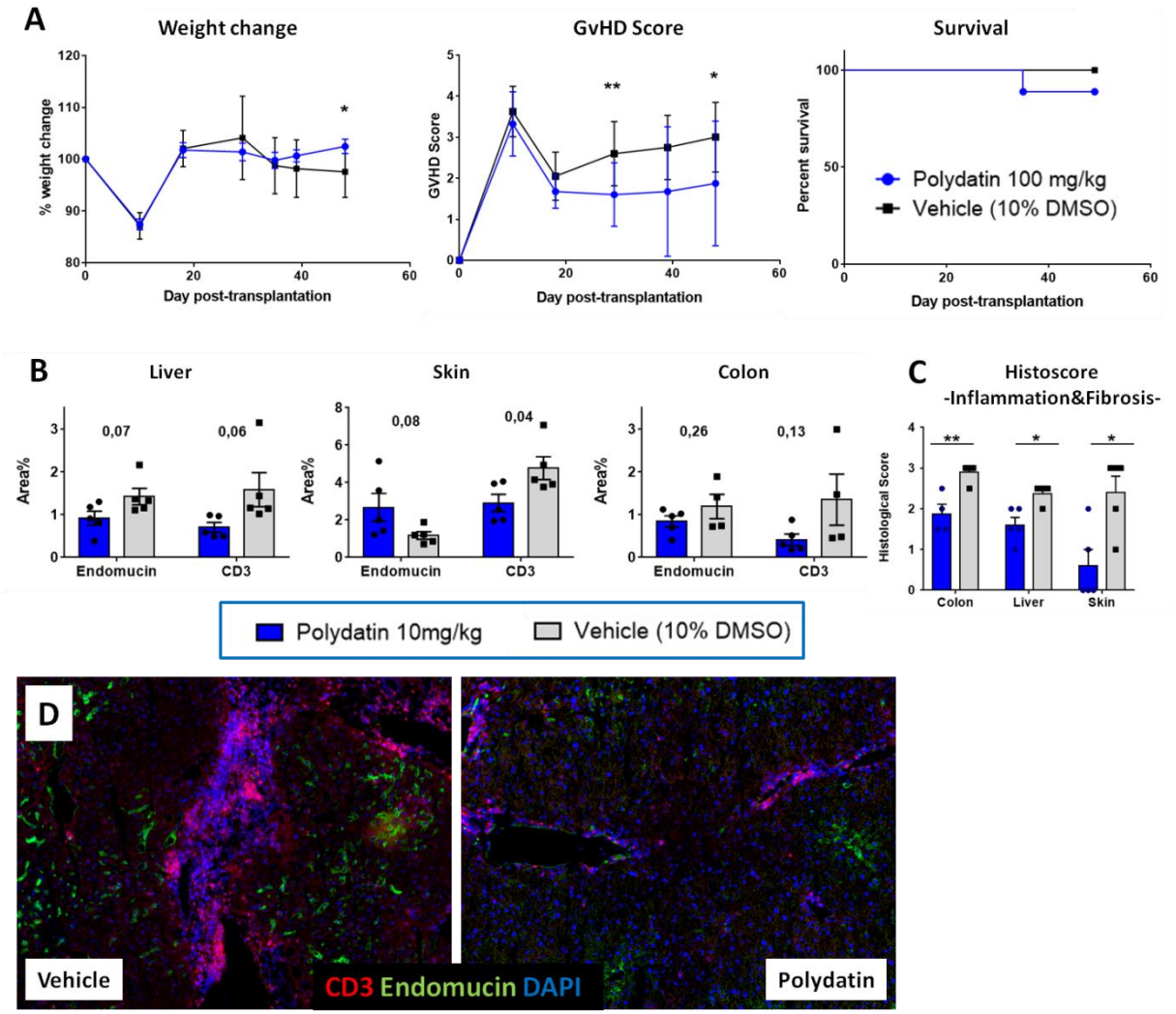

Figure 26: Influence of the G6pdx-inhibitor Polydatin on murine aGvHD. aGvHD radiation-based mouse model B6→ BDF. Mice were injected i.p. with 100 mg/kg/day Polydatin or with vehicle (10% DMSO in PBS, control group) starting d+7 after allo-HSCT, every second day until finalization on d+49. **(A)** Morbidity and mortality of Polydatin vs. vehicle-treated aGvHD mice composed of weight change, GvHD score and survival. n=10 per group. **(B)** Quantification of Endomucin and CD3 in liver, skin and colon from Polydatin vs. vehicle-treated aGvHD mice, determined by immunohistofluorescence. n=5 per group. p-values are indicated for each comparison in the graphs. **(C)** Histological Score (tissue leukocyte infiltration and tissue damage) of colon, liver and skin from Polydatin vs. vehicle-treated aGvHD mice. n=5 per group. Data from one representative experiment out of 2 performed experiments. Error bars indicate mean±SEM. *P<0.05, **P<0.01 by Holm-Sidak method, with alpha = 0.05. **(D)** Representative fluorescence images of aGvHD liver of Polydatin- vs. vehicle-treated mice. Endomucin+ vasculature (green), CD3+ T cells (red), Nuclei (DAPI; blue). Magnification 20x.

The influence of Polydatin was also tested in the chronic GvHD C57BL/6 → B6D2F1 mouse model where Polydatin was administered starting from day 35 after transplantation, when the acute phase deteriorated into established cGvHD. In contrast to acute GvHD, the treatment did neither improve the weight loss nor ameliorated the disease progression of cGvHD. In

fact, survival rates were even decreased and cGvHD scores slightly elevated in Polydatin-treated allo-HSCT recipients. Control Polydatin-treated syn-HSCT recipients exhibited similar weight change, cGvHD scores and survival compared to vehicle-treated syn-HSCT recipients excluding Polydatin-related mortality and side effects (Figure 27).

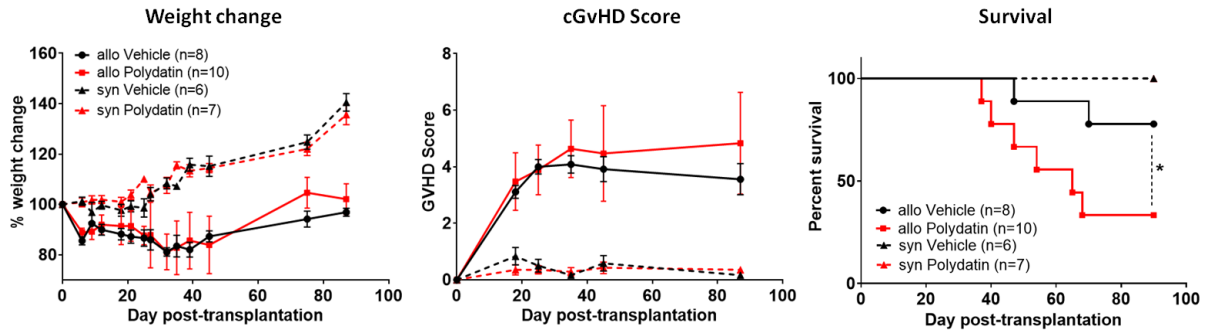

Figure 27: Influence of the G6pdx-inhibitor Polydatin on cGvHD. cGvHD radiation- and G-CSF based mouse model B6→ BDF. Mice were treated by i.p. injections with 150 mg/kg/day Polydatin or with Vehicle (10% DMSO in PBS, control group) starting d+35 after allo-HSCT, every second day until finalization on d+90. Morbidity of Polydatin vs. vehicle-treated cGvHD mice (solid lines) or syn-controls (dotted lines) composed of weight change, GvHD score and survival. Data pooled from two representative experiments. Error bars indicate mean±SEM. *P<0.05 by Log-rank (Mantel-Cox) test.

Summarizing, the candidate genes *Acsm3*, *Eno3* and *G6pdx*, which were found upregulated in initial pathologic angiogenesis during early aGvHD *in vivo*, were confirmed to participate in the endothelial regulation under allo-stimulated conditions by genetic deletion *in vitro* and can be targeted by specific pharmacologic inhibitors. Therapeutic inhibition of G6pdx using Polydatin exhibited promising effects on pathologic endothelial functions *in vitro*, exerted prophylactic influence on the early inflammation in footpad swelling assays and ameliorated the morbidity in aGvHD by decreasing T cell infiltration and stabilizing the vascular integrity *in vivo*. It was not able to improve the morbidity and mortality when administered in later stages of already established cGvHD.

3.2. Endothelial dysfunction in chronic GVHD

The following chapter delineates experimental results aiming to characterize target structures and mechanisms of endothelial dysfunction during cGvHD. It covers the establishment of improved cGvHD mouse models and describes the endothelial damage and dysfunction during severe fibrotic cGvHD in those models. Furthermore, it assesses the benefit of pharmacologic endothelial-protective therapeutics against cGvHD in mice and identifies endothelium-related biomarkers for prognosis and risk analysis in cGvHD patients.

3.2.1. Establishment of cGvHD mouse models

Lack of suitable murine cGvHD models, which display the heterogeneous clinical features of the disease, limit the understanding of cGvHD disease mechanisms and research for treatment options. To gain deeper insights, especially with focus on endothelial involvement in the pathophysiology of cGvHD, three novel mouse models (Figure 28A) were established.

In the first murine model, representing a MHC major mismatched combination, BALB/c donors were injected with human recombinant G-CSF. HSCs were mobilized into the circulatory system and secondary lymphatic organs and whole splenocytes were transplanted into lethally irradiated C57BL/6 recipients (Figure 28A;upper). An alternative murine haploidentical parent-into-F1-generation model utilizes a G-CSF-mobilized C57BL/6-donor to B6D2F1-recipient combination, with equally irradiated recipients (Figure 28A;middle). For murine syn-transplantation, donors equal recipient strains. Third, the humanized Xenograft model allows transplantation of human PBMCs into sublethally irradiated NSG-recipients (Figure 28A;bottom). All established cGvHD models run for 125 days after transplantation and were initially characterized on their resulting cGvHD phenotype and immune cell reconstitution by frequently performed GvHD scoring and periodically repeated blood analysis. Subsequently, endothelial damage and dysfunction mechanisms during cGvHD were examined in various *in vivo* and *ex vivo* approaches (Figure 28B).

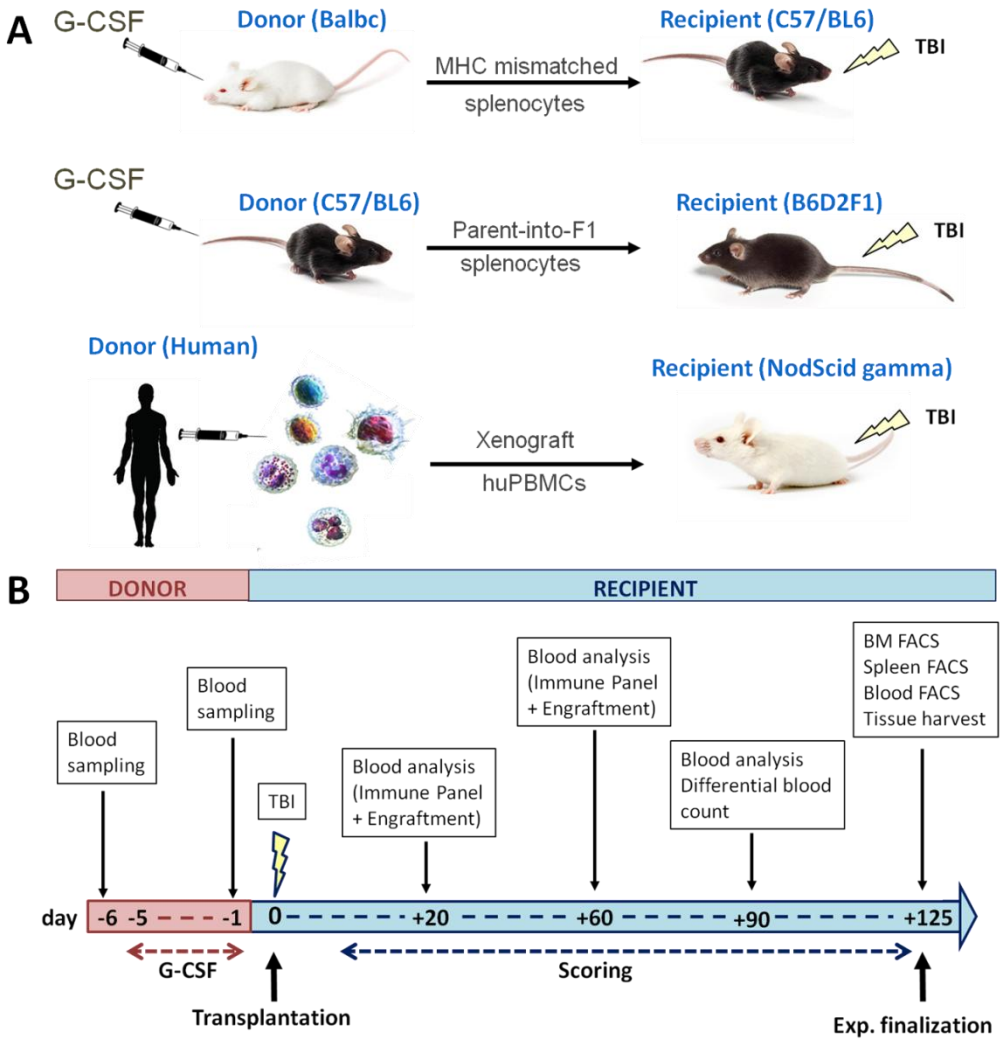

Figure 28: (A) Schematic illustration of novel established murine models of cGvHD. (A;upper) MHC-mismatched model: Stem cells of BALB/c-donors are mobilized with G-SCF and whole splenocytes are transplanted into lethally total body irradiated C57BL/6 recipients. **(A;middle)** Haploidentical parent-into-F1 model: Stem cells of C57BL/6-donors are mobilized with G-SCF and whole splenocytes are transplanted into lethally total body irradiated B6D2F1-recipients. **(A;bottom)** Xenograft (humanized) model: Isolated human PBMCs are transplanted into non-myeloablative total body irradiated, immunocompetent NSG mice. **(B) Overview on the experimental setup of cGvHD *in vivo* experiments.** Murine donors were HSC-mobilized with G-CSF for 5 days. Blood was sampled and cell-frequencies were compared before and after mobilization. Recipients were irradiated and transplanted (d0). Blood was sampled periodically to track immune cell reconstitution and HSC-engraftment. At d+90, a differential blood count was performed. The experiment was terminated at d+125 and tissue was harvested for further examination. G-CSF=Granulocyte-Colony Stimulating Factor; MHC=Major Histocompatibility Complex; TBI=total body irradiation; FACS=Fluorescence activated cell sorting.

3.2.1.1. Murine models of cGVHD

Mobilization of Hematopoietic Stem cells

Before splenocyte transfer, allogeneic C57BL/6- and BALB/c-donors and syngeneic C57BL/6- and B6D2F1-donors were treated with G-CSF to recruit cells from the BM to circulating peripheral blood and spleen. Flow cytometry highlighted a visible increase of myeloid cells, which were determined by staining of CD45+Gr1+ after 5 days of injection (Figure 29A). Nonetheless, there was a time- and strain-dependence of HSC-recruitment: CD45+Gr1+ cells were recruited more efficiently in BALB/c mice compared to BDF and C57BL/6 mice, which showed slowest rise in cell frequency after 5 days of G-CSF treatment. While CD45+Gr1+ cell frequencies were more than doubled in BALB/c mice already at day 3 of G-CSF injection, BDF mice recruited cells in a linear manner, reaching maximum numbers around day 5. C56/BL6 showed only slightly elevated CD45+Gr1 cell numbers at day 3 and reached a peak not before day 5 (Figure 29B). After 5 days of 10µg G-CSF recruitment, 33.22% CD45+Sca1+cKit+ HSCs accounted of all spleen PBMCs in G-CSF treated mice, while untreated wild type mice harboured only 8,76% of the same population (Figure 29C). Cell frequencies (Figure 29D) as well as absolute cell counts (Figure 29E) of CD45+Gr1 positive cells and unstained myeloids were significantly increased after 5 day G-CSF treatment in all three mouse strains.

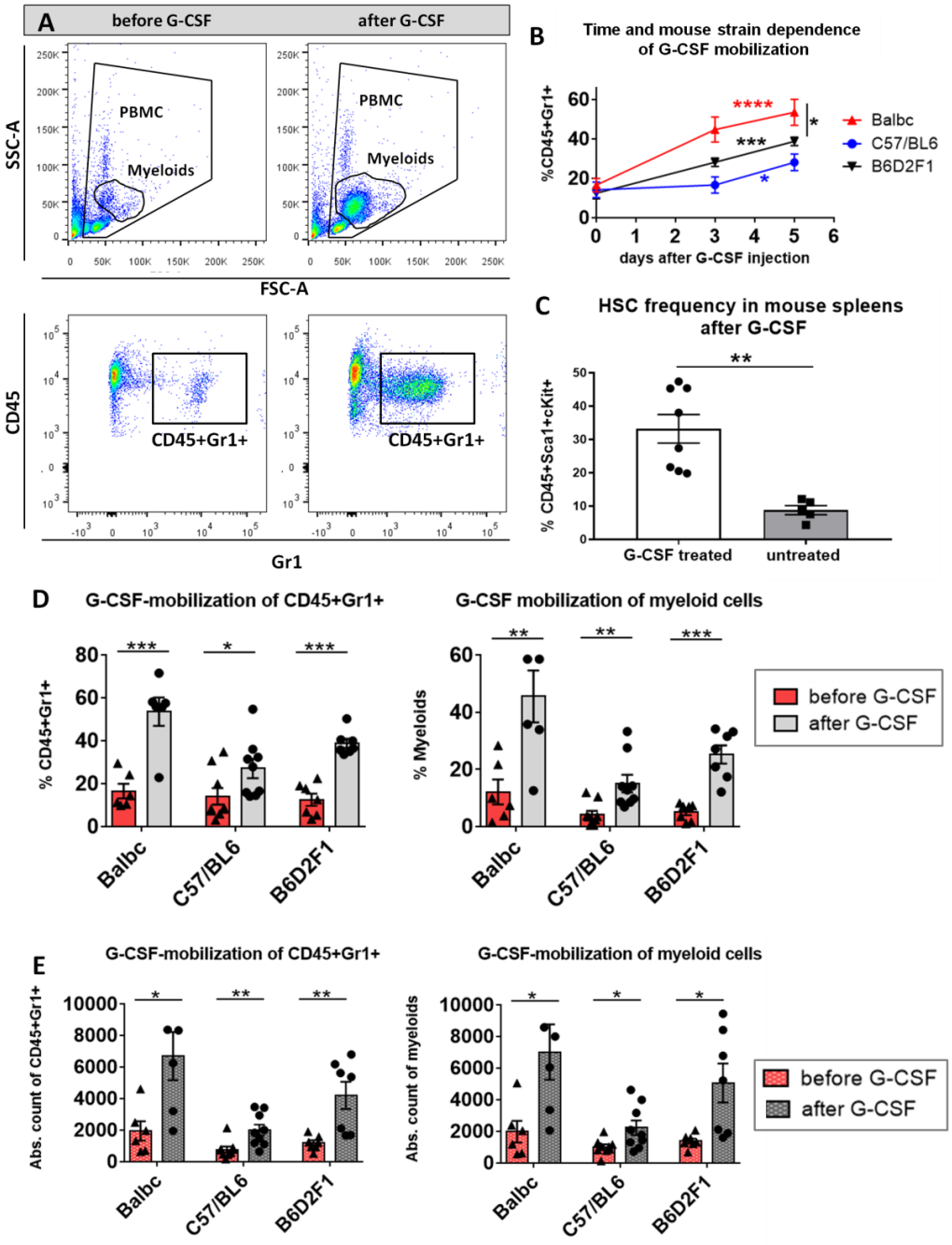

Figure 29: Myeloid cell-mobilization by G-CSF in peripheral blood of BALB/c, C57BL/6 and B6D2F1 mice. (A) FACS gating strategy of unstained myeloid cells in FSC/SSC and of stained CD45+Gr1+ cells. Example of a visible increase in myeloids and CD45+Gr1+ cells after 5 consecutive days 10 µg G-CSF injection in a BDF-mouse. **(B)** Temporal rise of % CD45+Gr1+ cells in the peripheral blood of different mouse strains from day 0 to 5 of G-CSF injection. **(C)** Frequency of CD45+Sca1+cKit+ HSCs in the spleen of untreated vs. G-CSF treated mice. Cell frequencies were determined from isolated FACS-stained whole spleen PBMCs with or without 10 µg G-CSF treatment for 5 days. Pooled BDF: n=3, BALB/c: n=2 and C57BL/6: n=3. Error bars indicate mean±SEM. **(D)** Significant increase in % CD45+Gr1+ and % myeloids and **(E)** in the absolute cell count of CD45+Gr1+ and myeloids in the peripheral blood of different mouse strains before and after 5 day G-CSF treatment. BALB/c: n=6, BDF: n=7, C57BL/6: n=9. Data pooled from three independent experiments. Error bars indicate mean+SEM. *P<0.05, **P<0.01, ***P<0.001 by Holm-Sidak test (B&C) and unpaired students t-test with α=0.05 (D).

Concluding, a 5-day administration of G-CSF successfully resulted in sufficient mobilization of HSCs into the splenic compartment, which can subsequently serve as HSC source for transplantation of the established cGvHD models. Adequate engraftment of the so gained splenocytes was verified in the G-CSF-dependent models.

Titration of the transplanted cell dose

Aiming to develop a stable cGvHD phenotype in the murine models, variable numbers of splenocytes were transplanted into irradiated recipients, which were frequently scored with onset of first GvHD signs and transplant-engraftment was determined around day +20 as depicted in Figure 28B. Criteria for a successful transplantation with GvHD signs were defined the following: (1) development of moderate weight loss (<20%), (2) a moderate average GvHD score of 2 - 4 out of 6 maximum scoring points, (3) low mortality rates and (4) detection of >85% donor cells and <15% of recipient cells in the peripheral blood of recipients around day +20 after transplantation (engraftment). In the model C57BL/6→BDF the highest cell dose of $5x10^7$ splenocytes fulfilled all criteria, showing a moderate GvHD score, 100% survival, reduced weight change compared to syn-controls or lower transplanted cell doses (Figure 30A) and 99.8% $H2k^b$-positive CD3+ donor cells engrafted in blood. Lower cell doses of $1x10^7$ and $5x10^6$ were disqualified for further experiments as only 3 out of 5 and 1 out of 5 recipients showed >85% $H2k^b$+CD3+ engraftment, and mixed chimerism was detected in two and one mice, respectively. In the second murine model BALB/c→C57BL/6 (Figure 30B), a cell number of $2x10^7$ splenocytes was excluded for further experiments because of acute mortality and morbidity. While both lower cell doses showed moderate weight change and GvHD scores, with low mortality rates, the $1x10^7$ dose was preferable as 95,5% $H2k^d$+CD3+ cells of BALB/c origin were detected in 100% C57BL/6-recipients compared to poorer engraftment with 82% $H2k^d$+CD3+ cells in $5x10^6$ dose. For further analysis of the murine cGvHD and characterization of the endothelium during cGvHD progression, the BDF model was utilized, for reasons of stable HSC recruitment by G-CSF, more reliable engraftment of HSCs in donors, lower dropout rates resulting from decreased mortality and lately a phenotype, which more closely resembles the clinic features of cGvHD than the C57BL/6-model.

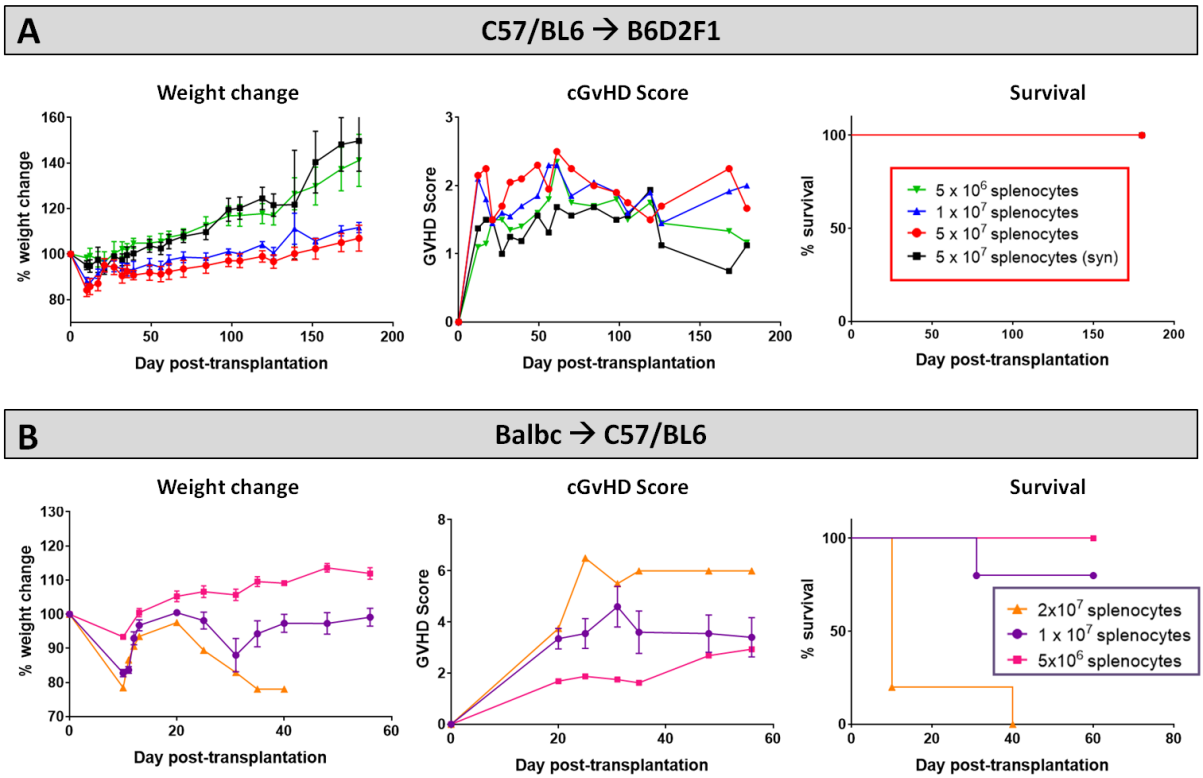

Figure 30: Cell dose titration for establishment of cGvHD in mouse models. (A) C57BL/6 → BDF model running for 180 days. Three different cell doses ($1x10^6$, $1x10^7$ and $5x10^7$) were transplanted in allo-HSCT and one as syn-control. Clinical GvHD was estimated by weight change (left), GvHD score (middle) and survival (right). **(B)** BALB/c →C57BL/6 model running for 60 days. Three different cell doses ($5x10^6$, $1x10^7$ and $2x10^7$) were transplanted in an allo-HSCT. Clinical GvHD was estimated by weight change (left), GvHD score (middle) and survival (right). Animals were regularly scored for five clinical parameters (weight loss, posture, activity, fur and skin) on a scale from 0 to 2. Clinical GvHD score was summarized of all five parameters. Error bars show mean±SEM. n=5 per group.

Clinical and histological manifestations of murine cGvHD

After cell dose evaluation, recipients were transplanted with $5x10^7$ allogeneic or syngeneic splenocytes and the developing cGvHD symptoms were monitored over 125 days, before tissues were harvested and histological and genetic analysis on the disease manifestations were conducted. Allo-transplanted cGvHD mice showed a significantly reduced weight gain and greater morbidity in contrast to the syn-transplanted mice, while the overall survival was not varying between syn- and allo-HSCT. GvHD developed around day +20 in an acute form with high scores (~4.5) and progressed from day +60 with moderate scores of ~3 as robustly manifested cGvHD (Figure 31A). As depicted in Figure 31B, cGvHD mice (upper row) evinced diverse clinical cGvHD symptoms around day +120, which were not detected in syn-controls (bottom row) including a hunched, kyphotic posture with impaired movement and stilt walk (posture and activity score), a ruffled, erected fur and loss of whiskers and alopecia

(fur score), and erythema with scaling, small lesions, especially of hairless areas as mouth, ears or tail, depigmentation of tail-skin (skin score) as well as blepharitis and dry, opaque eye lenses.

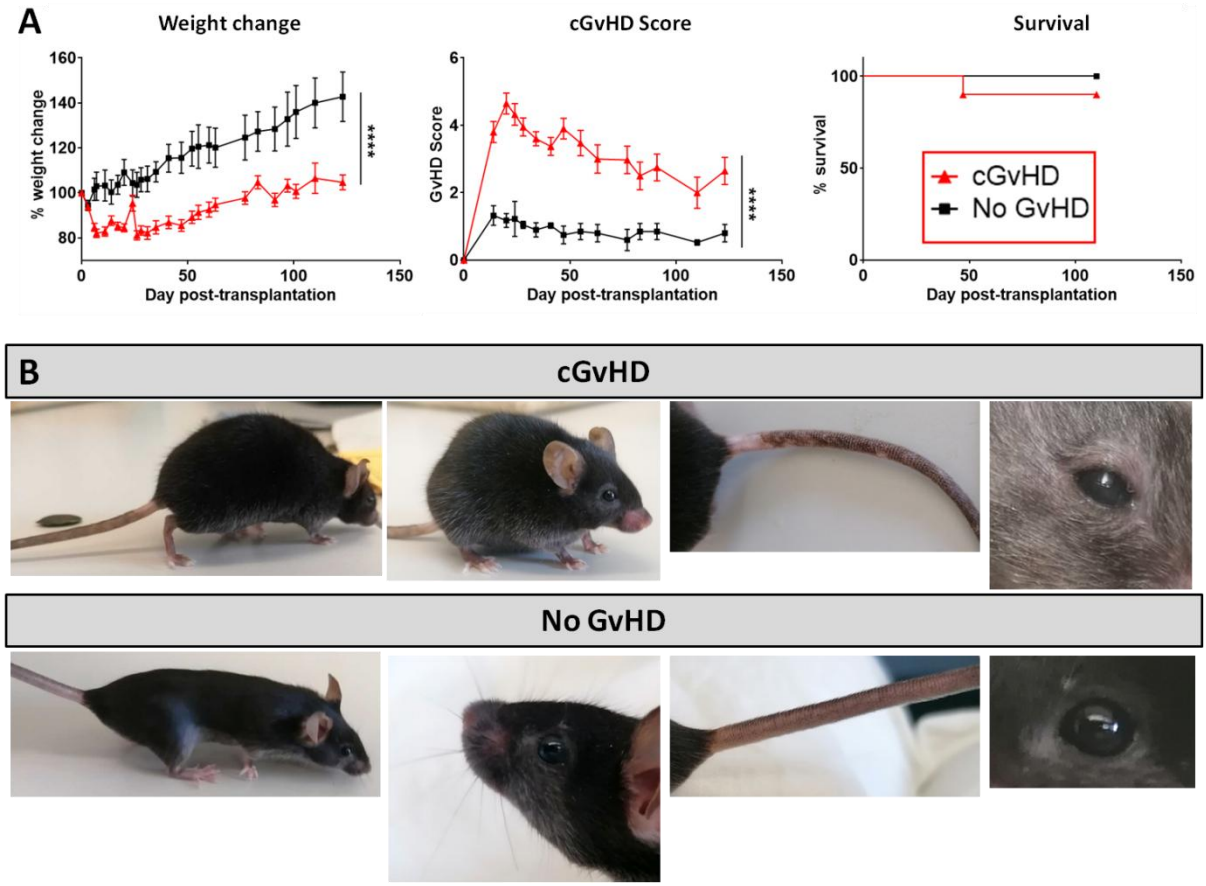

Figure 31: cGvHD morbidity and mortality over 125 days in C57BL/6 → BDF. (A) Clinical cGvHD was estimated by frequently assessing weight change (left), GvHD score (middle) and survival (right). Animals were regularly scored for five clinical parameters (weight loss, posture, activity, fur and skin) on a scale from 0 to 2. Clinical GvHD score was summarized of all five parameters. Error bars show mean±SEM. n=10 per group. Representative data from one out of four experiments. ****P<0.0001 by unpaired students *t*-test. Survival was tested by Mantel-Cox-log-rank test. **(B)** Frequently observed clinical manifestations of cGvHD in BDF-recipients (upper): Kyphosis, ruffled fur, alopecia, skin-depigmentation and blepharitis were seen in allo-transplanted animals, while syn-mice did not show any cGvHD-symptoms (bottom).

The cGvHD organ manifestation in the C57BL/6→BDF model was assessed by analysis of Masson's Trichrome staining to quantify fibrosis, immune cell infiltration and overall epithelial damage in cGvHD target organs. Histoscores of organ fibrosis and tissue inflammation (Figure 32A) of liver and lungs were considerably higher in allo- compared to syn-transplanted mice. cGvHD livers (Figure 32B) appeared pale, with intrahepatic bleedings and necrotic areas, emerging as cirrhotic changes, which were not detected in no-GvHD animals. The skin thickness of the dermis related to the underlying muscularis was elevated in

cGvHD animals compared to controls (Figure 32C) implicating a sclerotic skin thickening. Spleens of cGvHD mice (Figure 32D) were marked of sclerotic tissue loss and necrotic foci and were notably smaller in size than spleens of syn-mice due to cellular apoptosis.

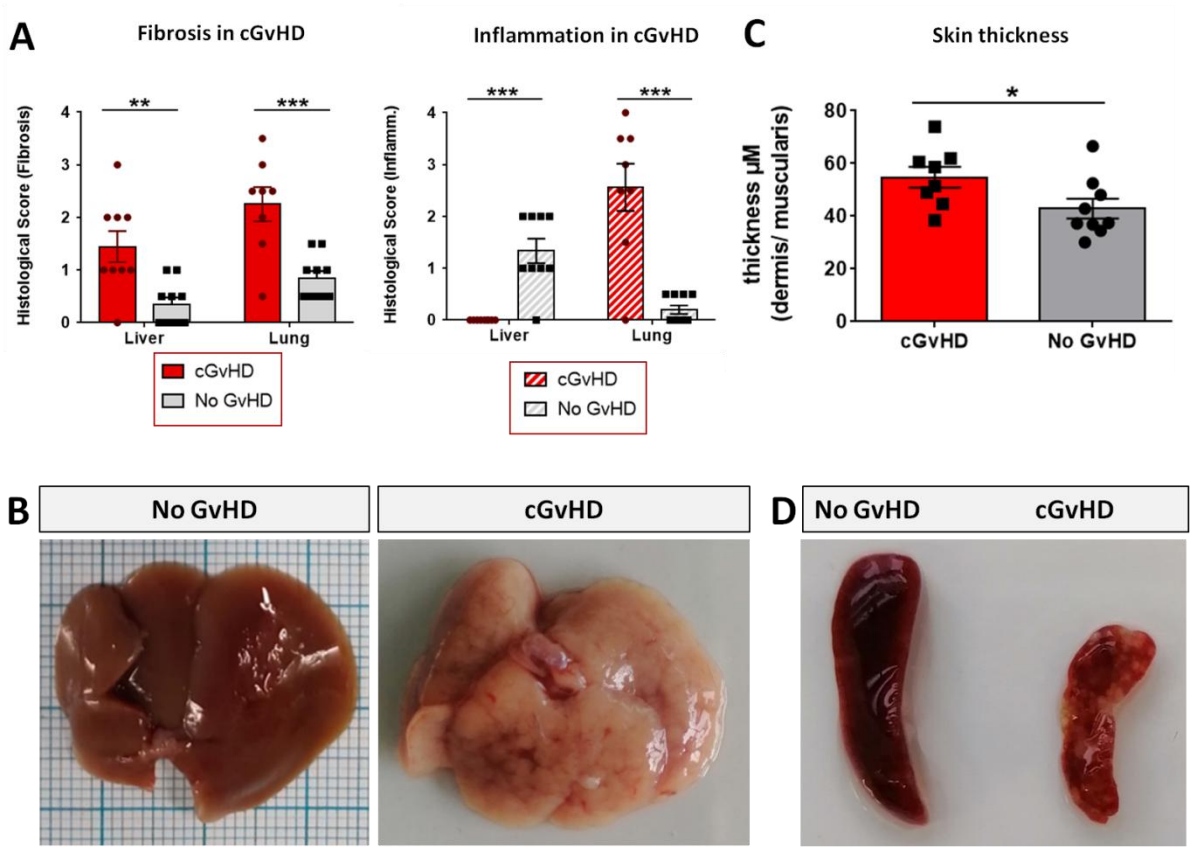

Figure 32: Clinical organ manifestations of cGvHD in C57BL/6→BDF at day +125 after allo-HSCT. (A) Histological quantification of fibrosis and inflammation in liver and lung of each individual mouse, based on histoscoring ranging from 0=no to 4= severe fibrosis/inflammation. Error bars show mean±SEM. n=9 (cGvHD); n=10 (No GvHD). Representative data from one out of four experiments. *P<0.05, **P<0.01, ***P<0.001by unpaired students *t*-test. **(B)** Livers of cGvHD vs. no-GvHD mouse at d+125 after transplantation with visible cirrhotic changes in cGvHD. **(C)** Skin thickness was increased in cGvHD vs. no-GvHD. Thickness was estimated by measurement of dermis-muscularis-ratio in Masson's Trichrome stainings. Error bars show mean±SEM. n=8 (cGvHD); n=9 (No GvHD). Representative data from one out of four experiments. *P<0.05 by unpaired students *t*-test. **(D)** Spleen of cGvHD vs. no-GvHD mouse at d+125 after transplantation with visible sclerotic and apoptotic changes in cGvHD.

Histology of cGvHD lungs showed massive immune cell infiltration around intrapulmonary bronchi (IPB) and pulmonary veins (PV). Infiltrates were surrounded by heavy collagen depositions, lining especially veins and small arteries, while syn-controls showed only minor collagen fibers around PV. The endothelial lining of large PV in cGvHD appeared superimposed by a visible blue collagen layer (yellow arrows), suggesting an Endothelial-to-mesenchymal transition (EndoMT) process in cGvHD mice (Figure 33A). While livers of

syn-transplanted mice showed normal hepatic architecture without significant collagen emplacement, cGvHD manifested in marked portal vein inflammation, interspersed with fibrotic tissue. Fibrosis and inflammatory infiltrates were also detected around bile ducts and hepatic arteries. In perihepatic areas, superficial tissue exhibited remarkable hepatic steatosis (Figure 33B). Cutaneous cGvHD occurred in allo-HSCT, with thickening, perivascular inflammation and sclerosis of the dermis. Single animals also exhibited vacuolization due to collagen degradation in dermal layers or showed epidermal desquamation (Figure 33C).

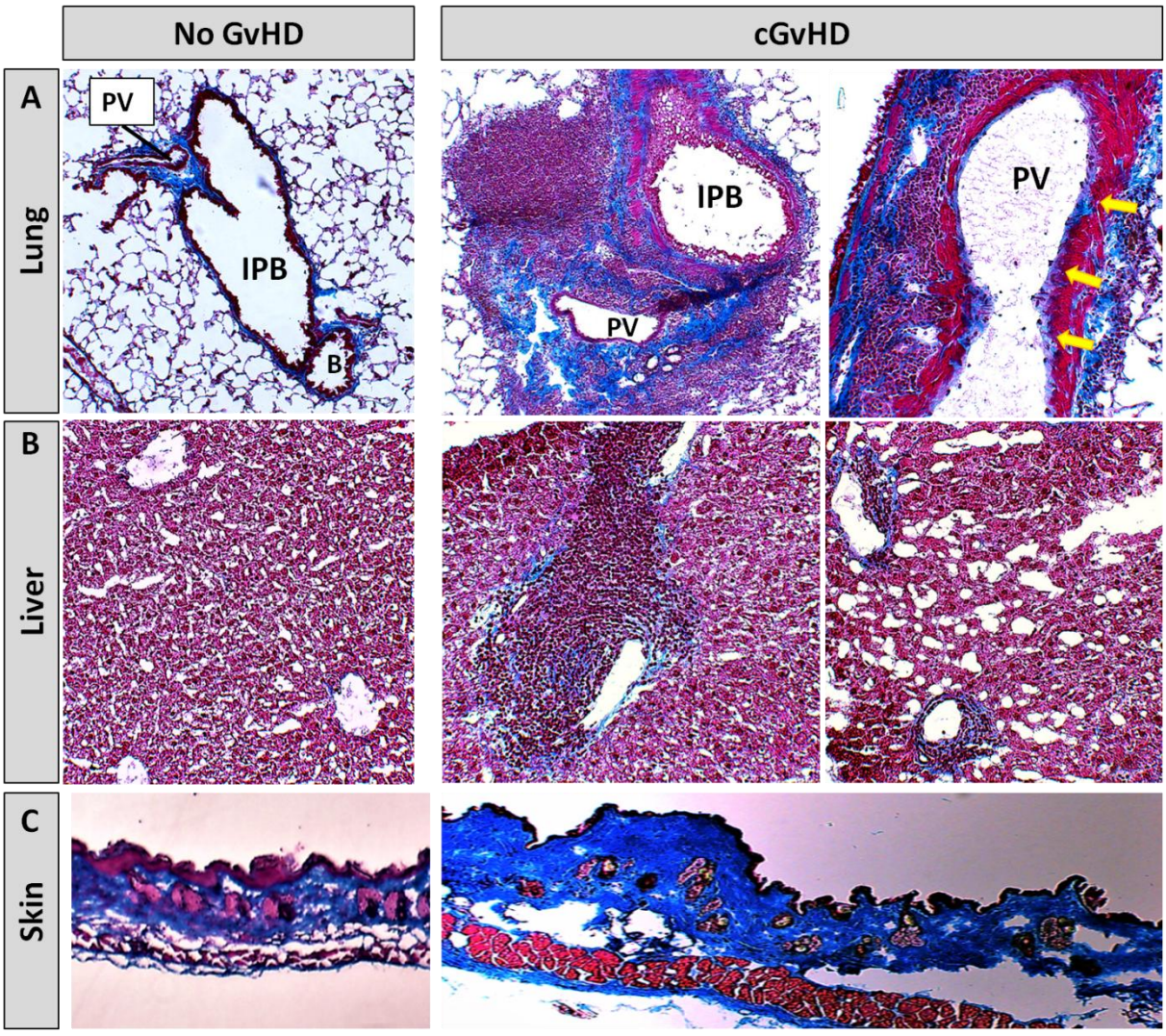

Figure 33: Histological characterization of murine cGvHD. Masson's Trichrome fibrosis staining in cGvHD target organs **(A)** lung, **(B)** liver and **(C)** skin of syn- and allo-transplanted BDF-recipients. Blue = collagen fibers (fibrosis), red= cytoplasm, keratin, muscle fibers and erythrocytes, dark red/ black = nuclei, infiltrating immune cells. 20x magnification. PV= Pulmonary vein, IPB=Intrapulmonary bronchus, B=Bronchiolus.

Tissue inflammation in cGvHD target organs lung, liver, colon, skin and eyes was characterized by dense B220+ B cell and CD3+ T cell infiltrates near CD31+ Endomucin+ blood vessels (Figure 36A). Systemic inflammation in cGvHD showed higher levels of pro-inflammatory cytokines CXCL9 and CXCL10 in serum during disease, exclusively in cGvHD-mice (Figure 34B). Both cytokines are also frequently observed to be elevated in clinical cGvHD in patients. Other pro-inflammatory cytokines e.g. IFN-α, TNF-α or IL-6 were sparsely increased in cGvHD, however where found only in low concentrations.

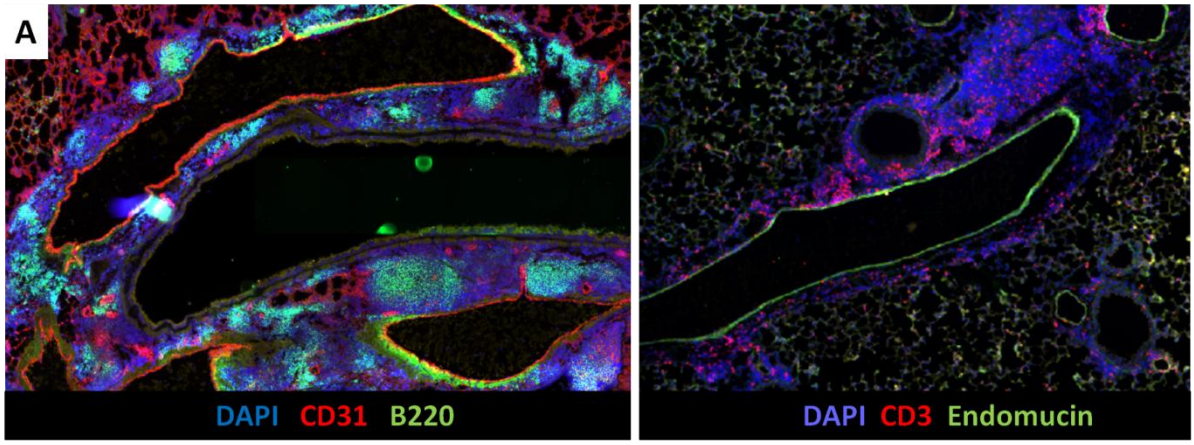

B

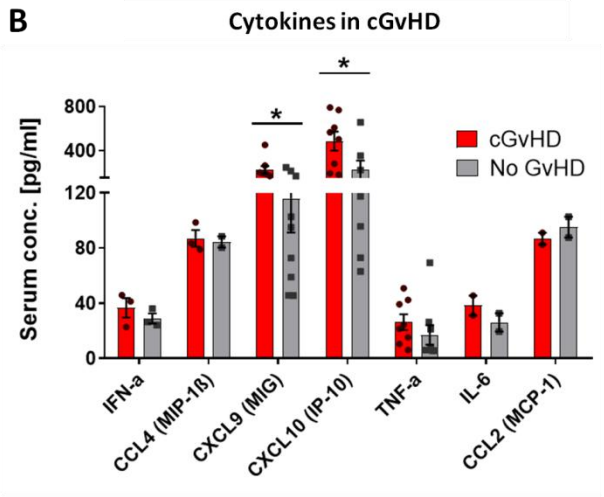

Marker	cGvHD			No GvHD		
	Mean	SD	n	Mean	SD	n
IFN-a	36,60	12,22	3	28,91	6,33	3
CCL4	86,99	10,24	3	84,34	5,73	2
CXCL9	222,48	98,20	8	115,81	73,99	9
CXCL10	485,32	244,86	8	225,16	215,80	7
TNF-a	26,26	16,21	8	17,00	21,10	9
IL-6	38,35	10,11	2	26,07	9,40	2
CCL2	86,71	6,05	2	95,09	10,70	2

Figure 34: (A) Representative Staining of tissue inflammation in lungs from C57BL/6 → BDF during established cGvHD. Representative immunohistofluorescence images of cGvHD lungs at day +125 showed massive immune cell infiltrates (indicated by DAPI staining, blue) around (CD31+ (left, red) or Endomucin+ (right, green) blood vessels with dense foci of B220+ B cells (left, green) and CD3+ T cells (right, red). Magnification 20x. **(B) Systemic inflammation characterized by cytokine levels in serum of cGvHD vs. no-GvHD in C57BL/6→ BDF model at day+87 after transplantation.** Table shows mean+SD for each analysed marker. Graph illustrates cytokine serum concentration in pg/mL. Error bars show mean±SEM. Representative data from one experiment. *P<0.05, by unpaired students *t*-test.

Immune cell reconstitution after allo-HSCT

After transplantation, donor syn- or allo-HSCs engrafted in myeloablative irradiated recipients and the reconstitution of various immune cell subsets was tracked in murine cGvHD (Figure 35). With the onset of aGvHD around d+20, progressing to cGvHD around d+60, reconstitution of CD3+ and CD4+ T cell subsets was significantly decelerated in cGvHD animals, while especially CD8+ cytotoxic T lymphocytes were massively expanded. Reappearance of B cells in cGvHD was delayed until day+125, when B cell numbers in cGvHD mice exceeded numbers in no-GvHD controls. There was no major difference in the myeloid or lymphoid DC subsets detectable between allo- and syn transplanted recipients. At d+20 and d+60, CD11b+CD11c- myeloid and mature NK cells were elevated in cGvHD, but cell numbers intensively dropped until d+125, reaching lower levels than the control mice. While eosinophil frequencies remained unchanged until d+125, when levels exceeded in cGvHD mice over control levels, the neutrophil count dropped at d+125 in cGvHD animals compared to no-cGvHD mice. We detected a higher proportion of Gr1+ $^{diminished/high}$ and vice versa less Gr1+ ^{low} monocytes and macrophages in cGvHD mice than in controls at GvHD onset but no difference in later established cGvHD.

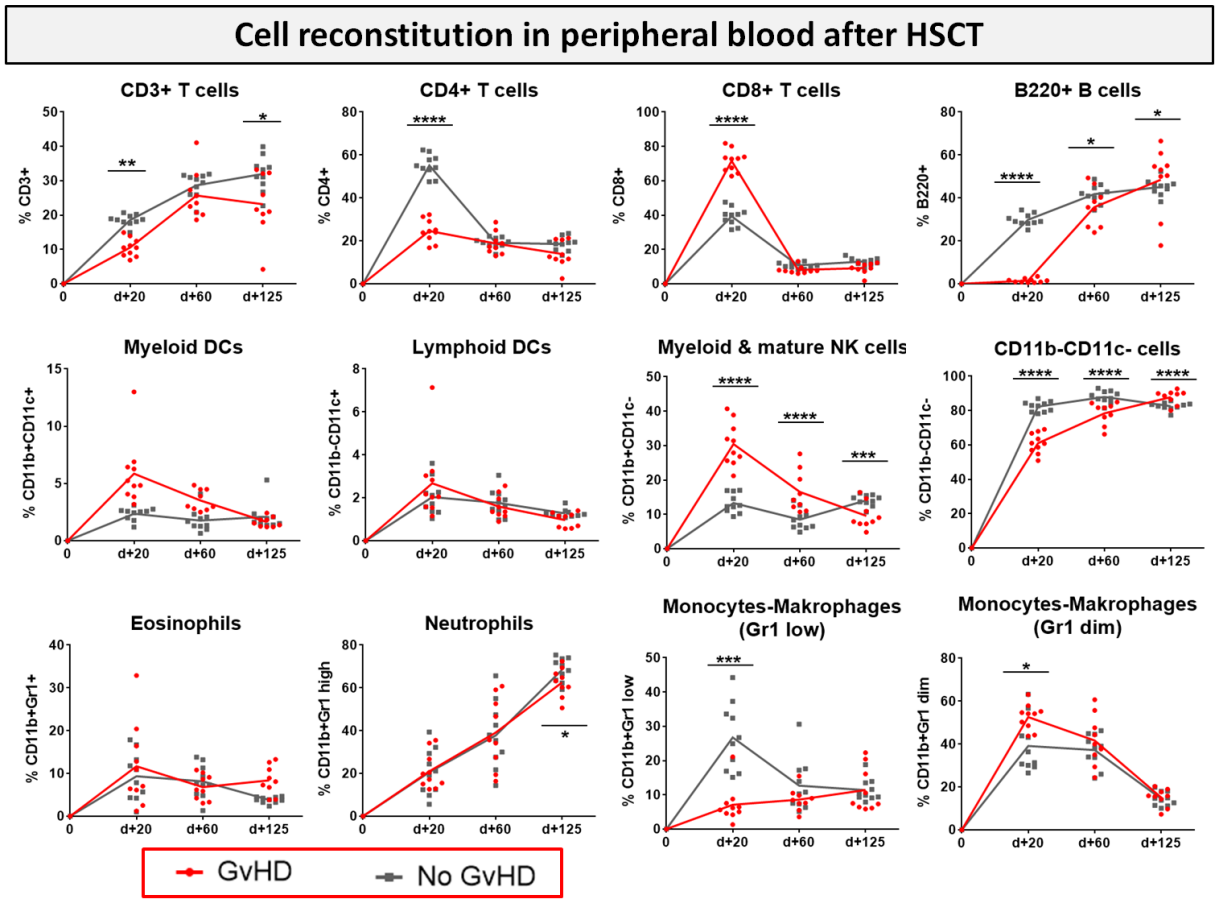

Figure 35: Immune cell reconstitution in peripheral blood of BDF-recipients over 125 days after allo- vs. syn HSCT. Tail vein blood was collected at three time points, PB cells were isolated, stained with the respective FACS-antibodies and samples were analysed with flow cytometry. DCs= dendritic cells; NK= natural killer cells; dim= diminished. n=9 (cGvHD); n=10 (No GvHD). Representative data from one out of four experiments. *P<0.05, **P<0.01, ***P<0.001, ****P<0.0001 by unpaired students *t*-test.

The immune cell reconstitution was also estimated in various lymphatic niches. Immune cell subsets were analysed in PB, BM and spleens during cGvHD (Figure 36). CD3+, CD4+ and CD8+ T cell subsets were decreased in the PB, but increased in spleens of cGvHD mice. cGvHD spleens were also associated with massive B cell loads, which were lower in controls. Observing the presence of different APC subsets, such as myeloid and lymphoid DCs, their frequency was decreased in cGvHD spleens, but not in the PB or BM. While the PB of cGvHD animals harboured less myeloid and mature NK cells at d+125, the opposite was detected for the subset of non-myeloids and lymphoid cells in the PB. As already previously described, eosinophiles were higher in cGvHD than in controls in the PB, but not in the spleen or BM. Completing the results of lower neutrophil counts at d+125 in the PB, we measured considerably higher frequencies in spleens of cGvHD animals, were also higher levels of

Gr1^{low} monocytes and macrophages were observed. Interestingly, immune cell levels in the BM were generally low and no differences in cell numbers were measured between cGvHD and controls, encouraging the hypothesis that mature immune cells were hosted mainly in secondary lymphatic organs.

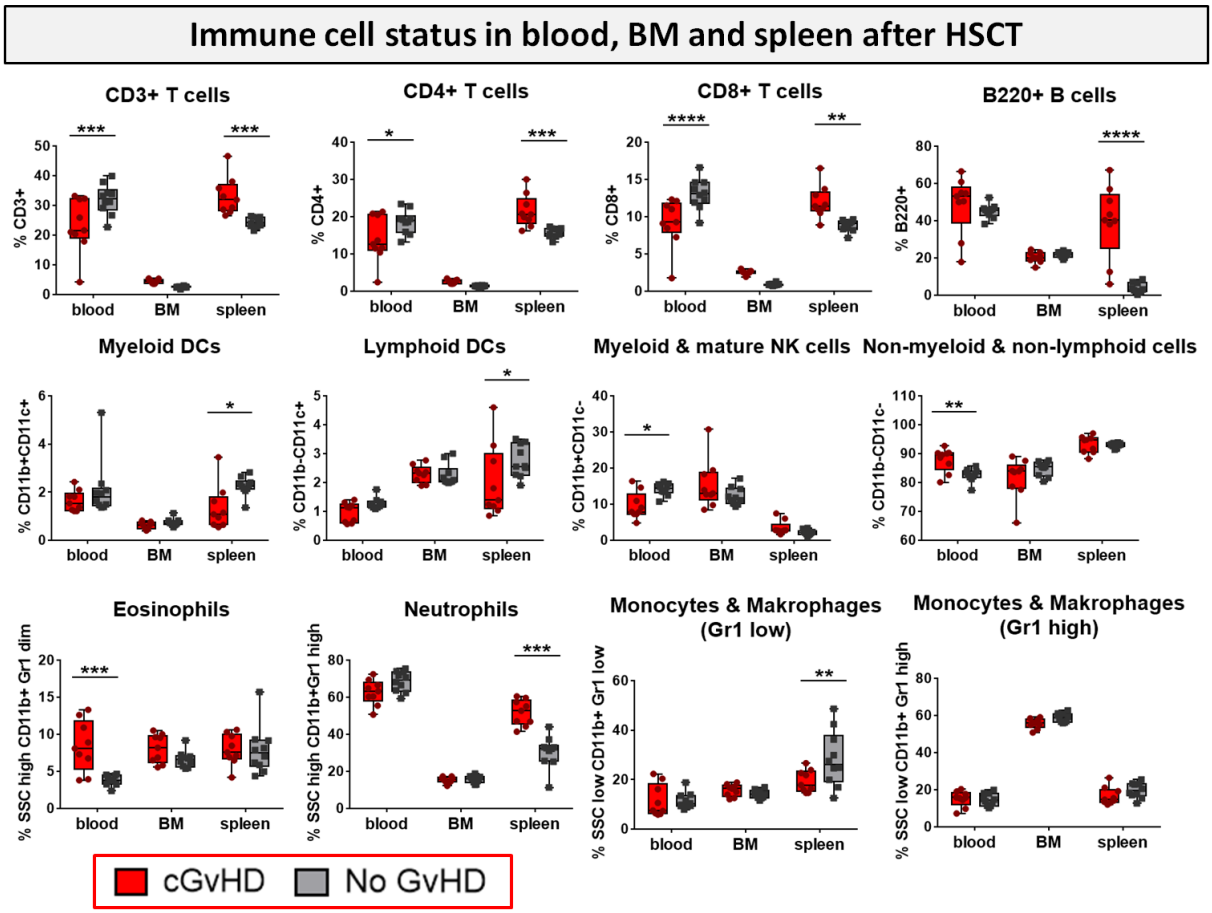

Figure 36: Immune cell status in peripheral blood, bone marrow and spleen of BDF-recipients at day +125 after allo- vs. syn HSCT. Blood was collected retrooribitally upon finalization. Spleens were harvested and BM flushed from tibia and femur. Immune cells were isolated, stained with the respective FACS-antibodies and samples were analysed with flow cytometry DCs= dendritic cells; NK= natural killer cells; dim= diminished. n=9 (cGvHD); n=10 (No GvHD). Representative data from one out of four experiments. *P<0.05, **P<0.01, ***P<0.001, ****P<0.0001 by unpaired students *t*-test.

The progression of the activation status of single populations was analysed by estimation of the expression of costimulatory receptor CD80+ in the PB from d+20 to d+125 (Figure 37A) and in BM and spleens at day+125 after HSCT (Figure 37B). Mice with cGvHD harboured significantly more activated myeloid (CD11b+CD11c+) and lymphoid (CD11b-CD11c+) DCs and myeloid NK cells (CD11b+CD11c-) in blood than control mice especially at GvHD onset. Activation levels of DCs dropped until day +125 but still stayed markedly elevated in

allo-HSCT. Since no differences in cellular activation in BM and spleen were revealed, we assumed the recipients circulatory, respectively the vascular system to represent the major activation site in cGvHD pathophysiology.

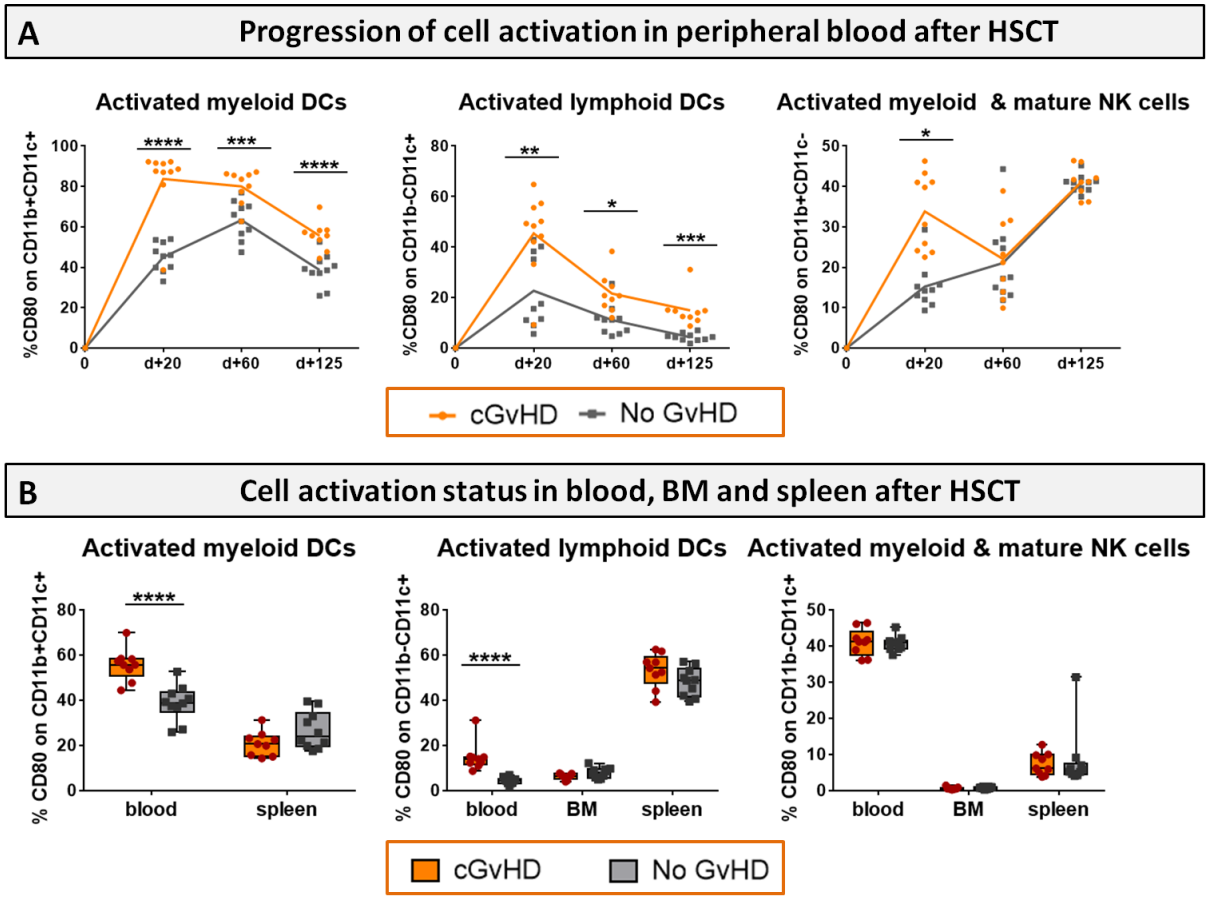

Figure 37: Activation status (CD80+) of DCs and NK cells in cGvHD in C57BL/6→BDF. (A) CD80+ expression on immune cell subsets in the PB over 125 days and **(B)** in PB, BM and spleen at d+125 after syn- and allo-HSCT. Blood was collected by tail vein bleeding or retrooribitally upon finalization. Spleens were harvested and BM flushed from tibia and femur. Immune cells were isolated, stained with the respective FACS-antibodies and samples were analysed with flow cytometry DCs= dendritic cells; NK= natural killer cells. n=9 (cGvHD); n=10 (No GvHD).Error bars represent mean±SEM. Representative data from one out of four experiments. *P<0.05, **P<0.01, ***P<0.001, ****P<0.0001 by unpaired students *t*-test.

In cGvHD, differential blood count analyses revealed remarkably decreased erythrocytes, hemoglobin and hematocrit , while mean corpuscular volume and –hemoglobin were elevated, clinically presenting as macrocytic anemia (Figure 38; Supplemental Figure 5). As of nucleated cells, only monocytes were detected to be diminished in cGvHD, which corresponds to the results from the flow cytometry analyses in PB.

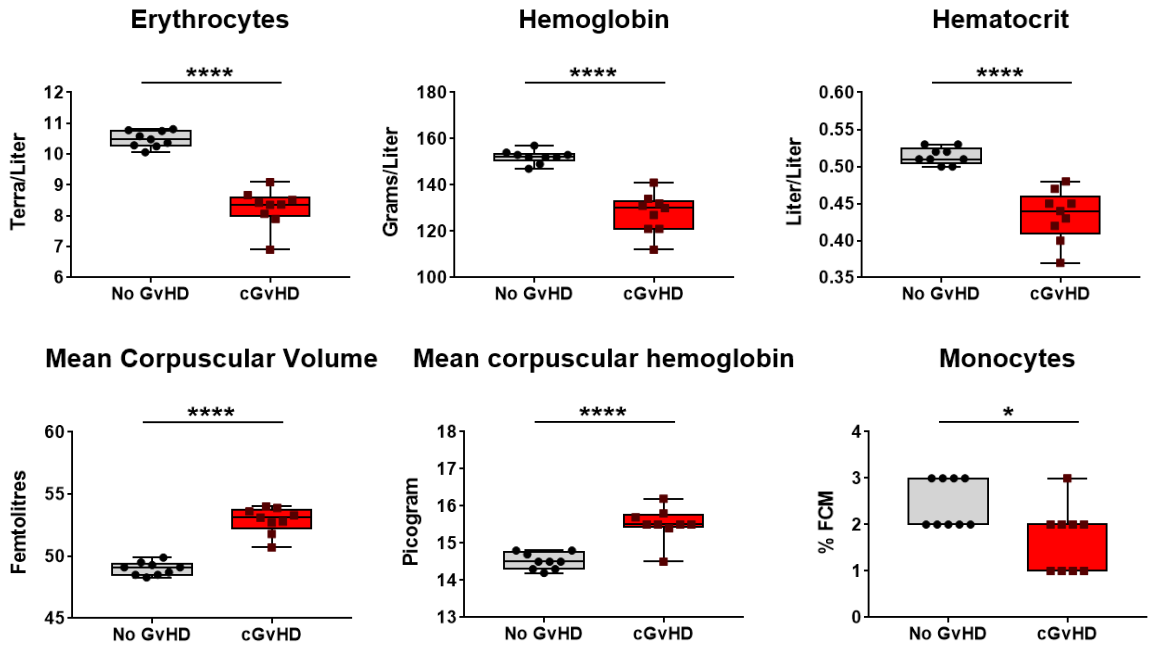

Figure 38: Recovery of red blood cells and related factors in cGvHD at d+90 after transplantation in C57BL/6→BDF. Blood was sampled from mice and differential blood count was performed by Synlab, Berlin. Data pooled from 2 independent experiments. n=9. Error bars represent mean±SEM. *P<0.05, **P<0.01, ***P<0.001, ****P<0.0001 by unpaired students *t*-test.

To resume, we observed a temporal and spatial variance in the reconstitution of different cell subsets after transplantation in the cGvHD recipients. In the PB, cGvHD mice exhibited a massively decelerated reconstitution of T helper subsets, while in contrast cytotoxic T cells as well as NK cells were visibly increased at GvHD onset, but cell frequencies of T cell subsets dropped in late cGvHD. The reappearance of B cells was delayed in cGvHD until d+125. In contrast, T as well as B cell subsets were found massively increased in spleens in established cGvHD. There was a higher proportion of Gr1+ $^{diminished/high}$ monocytes and macrophages detected at cGvHD onset, but not in late cGvHD. At late established cGvHD, frequencies of neutrophils lowered in the PB, but increased in spleens in cGvHD. Generally low immune cells frequencies in the BM indicated that the immune cell reconstitution proceeds in major in the periphery. cGvHD mice showed markedly more activated APCs in the PB. Lately, the erythropoietic reconstitution was decelerated, presenting in a macrocytic anemia in diseased recipients.

3.2.1.2. Humanized model of cGVHD

Titration of transplanted cell dose

Similar to the murine cGvHD-models, variable numbers of huPBMCs of different donors were transplanted into sublethally irradiated, immunocompetent NSG mice and developing cGvHD was assessed by surveillance of weight change, GvHD score and survival. Criteria for a successful transplantation with GvHD signs were defined the following: (1) development of moderate weight loss (<20%), (2) a moderate average GvHD score of 2 - 4 out of 6 maximum scoring points, (3) low mortality rates and (4) detection of > 0.5% huPBMCs in the PB of recipients around day +30 after transplantation (engraftment) and of >5% huPBMCs in the spleen at the end of the experiment. Three different donor sources (donor A,B,C) with transplanted cell doses ranging from $5x10^5$ to $5x10^6$ were tested for their dependency of developing cGvHD in NSG mice (Figure 39): the highest transplanted cell dose ($5x10^6$) resulted in high mortality and high morbidity independent from donor origin, with no significant weight loss at least in mice transplanted with huPBMCs from donor C origin. Nearly no differences in weight change, GvHD scores and in survival were observed among the lower transplanted cell numbers ($1x10^6$, $5x10^5$ and $1x10^5$) of donor A, indicating that it requires a minimum threshold cell number for cGvHD development. The dose of $1x10^6$ transplanted huPBMCs revealed the biggest variance between donors: while mice transplanted with cells from donor A developed the mildest cGvHD with a low average score of <2, 100% survival and no weight loss, cells from donor B caused rapid weight loss, high cGvHD morbidity and 100% mortality before day 60. NSG-recipients transplanted with $1x10^6$ huPBMCs from donor C developed moderate cGvHD scores of ~3 and moderate survival rates, designating this condition as most appropriate for further experiments. Donor-related cGvHD severity did not cohere with the transplanted T cell numbers, as donor A with mildest cGvHD comprised a high frequency of 52.8% CD3+ T cells of whole huPBMCs, while donor B and C with more pronounced cGvHD showed 42.0% and 31.3% CD3+ T cells, respectively.

Engraftment analyses revealed that huCD3+ T cell persistence in the PB is independent from the transplanted huPBMC dose: 12 of 13 NSG-recipients (92,3%) with the highest infused huPBMC number of $5x10^6$ cells per animal were found to have successfully engrafted with an average huCD3+ T cell frequency of 29.15±8.81 in the PB, while at $1x10^6$-transferred cells, only 20 out of 27 recipients (74.0%) harboured a minimum of >0.5 huCD3+ T cells, with an

average frequency of 14,2±2,48 % huCD3+ in successfully engrafted recipients. The lowest transplanted huPBMC dose of $5x10^5$ resulted in full engraftment of 8 out of 9 (88.9%) and a mean percentage of 22.05±0.97 % huCD3+ cells in the PB of NSG-recipients. As cell dose titration revealed, there existed a natural variance between the tested donors, when transplanting their PBMCs into mice, resulting in diverse engraftment rates and variable cGvHD outcomes. With the objective of a better comparability between the analysis, this variability was minimized by the exclusive use of $1x10^6$ cells from donor C in following experiments because this specific cell dose-donor combination equaled the clinical signs of human cGvHD the most.

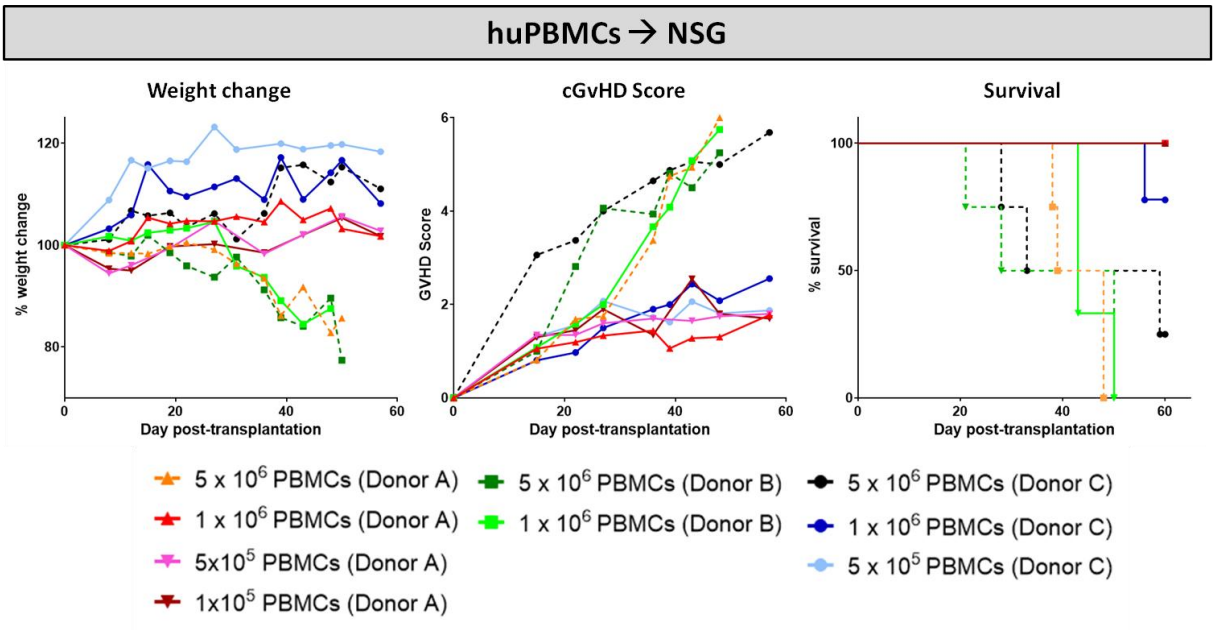

Figure 39: HuPBMC dose titration from three different donors for establishment of cGvHD in NSG-recipients over 60 days. Four different cell doses ($5x10^6$, $1x10^6$, $5x10^5$ and $1x10^5$) from three different donors were transplanted into sublethally irradiated NSG mice. Clinical GvHD was estimated by weight change (left), GvHD score (middle) and survival (right). Animals were regularly scored for five clinical parameters (weight loss, posture, activity, fur and skin) on a scale from 0 to 2. Clinical GvHD score was summarized of all five parameters. A high variance in weight change and GvHD scores was observed not only between the cell doses, but among donors. Dotted lines indicate highest cell doses.

Clinical and histological manifestations of humanized cGvHD

Transplanted mice exhibit steadily increasing cGvHD with scores to a maximum of ~4.5 and a higher transplant-related mortality compared to controls, emerging from day +50 and stabilizing around day+70, while weight loss was not frequently recorded in cGvHD (Figure 40A). Liver and lungs of cGvHD mice showed significantly augmented fibrosis and

inflammation, while severe inflammation in lung was detected intermingled with detection in a few control mice. This indicated that lung immune cell infiltration might at least be partly induced by irradiation and is further aggravated by cGvHD (Figure 40B). The epidermis is distinctly thickened in animals receiving $1x10^6$ huPBMCs, compared to controls (Figure 40C). Transplanted NSG-recipients experienced classic cGvHD symptoms as kyphosis, reduced activity, sporadic alopecia, severe skin scaling and dryness as well as opacity of the eye lenses and blepharitis (Figure 40D).

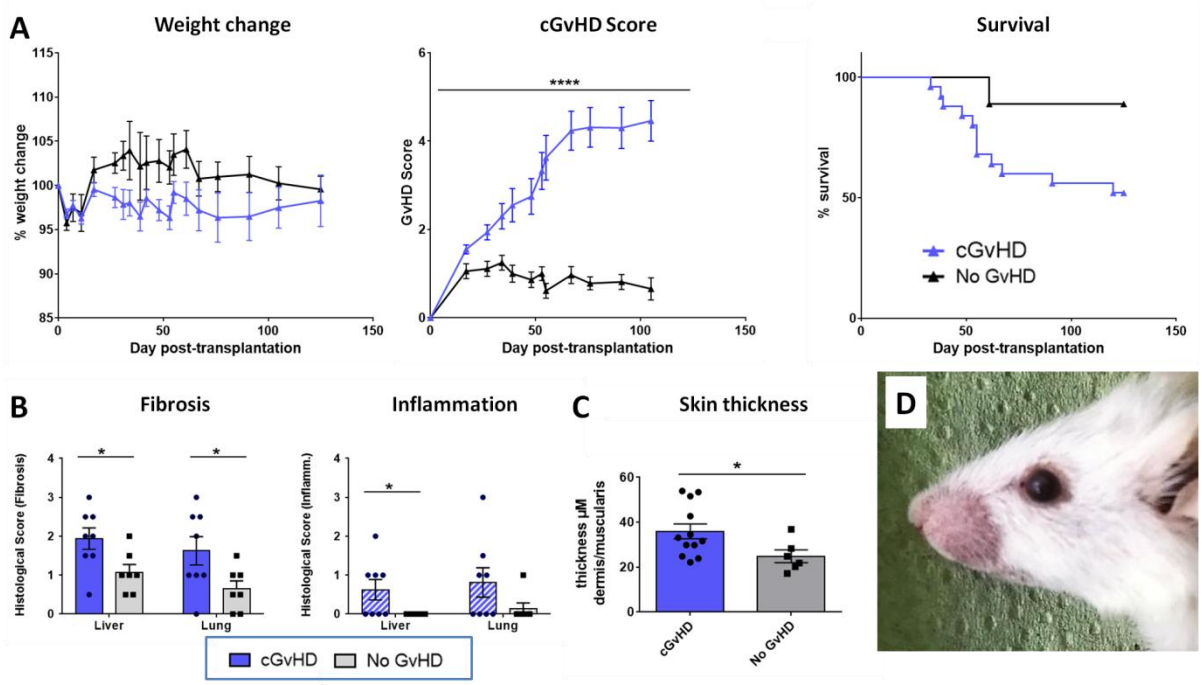

Figure 40: Clinical organ manifestations of cGvHD in huPBMCs→ NSG at day +125 after allo-HSCT. For cGvHD, NSG mice were irradiated and xeno-transplanted with $1x10^6$ human PBMCs from donor C. No-GvHD mice were only irradiated, without transplantation. **(A)** Clinical cGvHD was estimated by frequently assessing weight change (left), GvHD score (middle) and survival (right). Animals were regularly scored for five clinical parameters (weight loss, posture, activity, fur and skin) on a scale from 0 to 2. Clinical GvHD score was summarized of all five parameters. Error bars show mean±SEM. n=20 (cGvHD), n=8 (No-GvHD). Representative data from one out of two experiments. ****P<0.0001 by unpaired students *t*-test. Survival was tested by Mantel-Cox-log-rank test. **(B)** Histological quantification of fibrosis and inflammation in liver and lung, based on histoscoring ranging from 0= no to 4= severe fibrosis/inflammation. Error bars show mean±SEM. n=8 (cGvHD); n=7 (No-GvHD). Representative data from one out of two experiments. *P<0.05, **P<0.01, ***P<0.001by unpaired students *t*-test. **(C)** Skin thickness was increased in cGvHD vs. No-GvHD. Thickness was estimated by measurement of dermis-muscularis-ratio in Masson's Trichrome stainings. **(D)** Exemplary photo of eye-involvement in cGvHD pathology. Eyes showed signs of blepharitis and dryness and opacification of lenses**.** Error bars show mean±SEM. n=12 (cGvHD); n=6 (No-GvHD). Pooled data from three independent experiments. *P<0.05 by unpaired students *t*-test.

Histological characterization revealed clinical features of gastrointestinal involvement in cGvHD mice, such as mucosa inflammation with mild crypt and gland apoptosis, similar to the human cGvHD pathology (Figure 41A). Hepatic cGvHD mainly appeared as moderate fibrotic fiber incorporations around vessels, veins and bile ducts (Figure 41B), with minor signs of immune cell infiltrates surrounding only bigger vascular tissues. Lungs of syn-transplanted mice showed mild fibrosis around pulmonary veins and arteries without significant inflammation signs. cGvHD animals depicted altered lung parenchyma, damaged by dense infiltration-foci interspersed by fibrotic fiber-networks mainly around pulmonary veins and bigger bronchioles (Figure 40C).

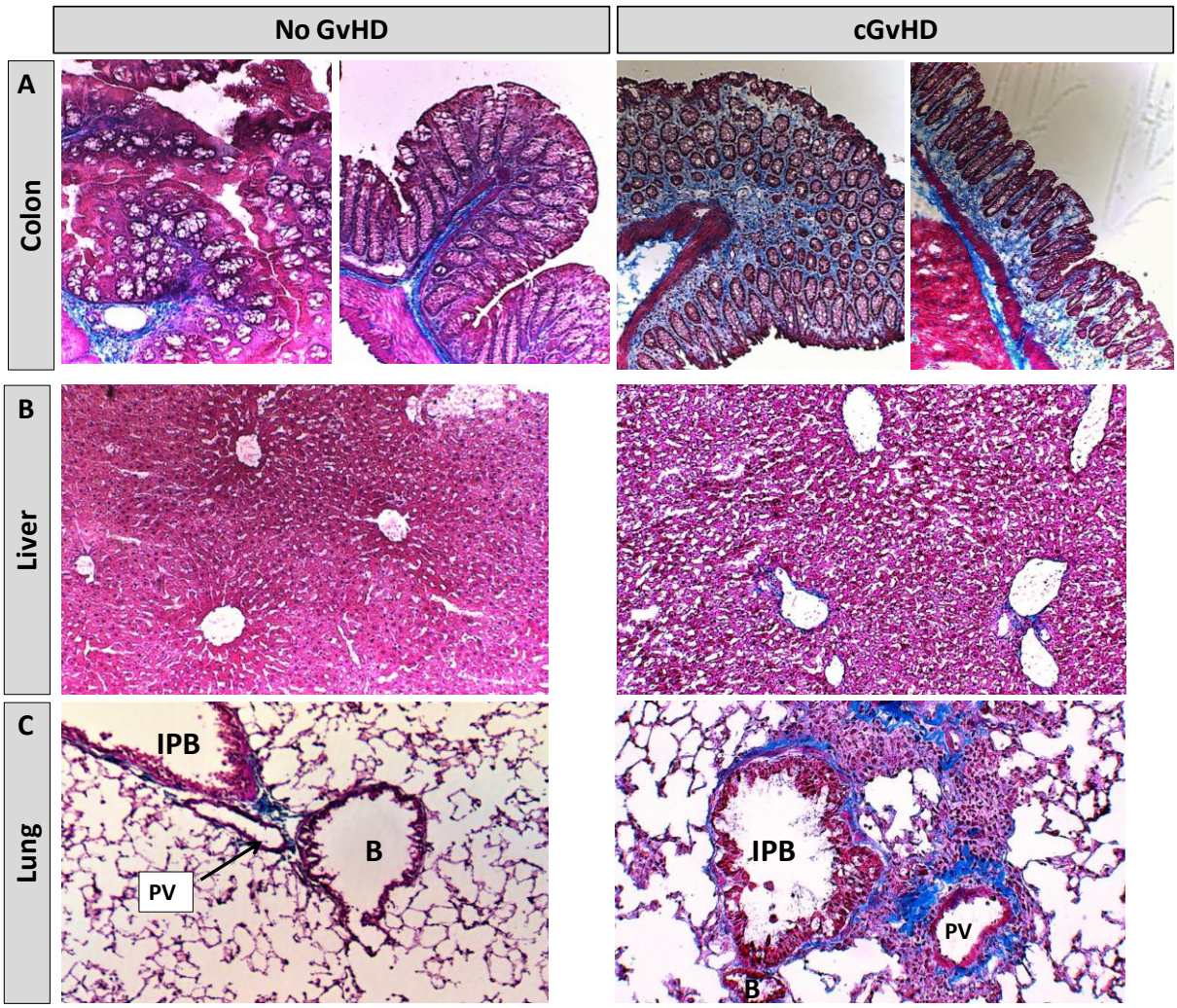

Figure 41: Histological characterization of cGvHD. Masson's Trichrome fibrosis staining in cGvHD target organs **(A)** colon, **(B)** liver and **(C)** lung of xeno-transplanted and only irradiated, but not-transplanted NSG-recipients. Blue = collagen fibers (fibrosis), red= cytoplasm, keratin, muscle fibers and erythrocytes, dark red/ black = nuclei, infiltrating immune cells. 20x magnification. PV= Pulmonary vein, IPB=Intrapulmonary bronchus, B=Bronchiolus.

Immune cell reconstitution after allo-HSCT

As expected, human cell proportions, especially of CD45+ leukocytes and CD3+ and CD8+ T cell subsets, steadily decreased over the examined time, while the frequency of CD4+ T cells remained stable and from day +60 (with cGvHD onset) even slightly expanded (Figure 42A, upper row), indicating a huCD4+-dependent cGvHD-pathophysiology. Around day +60, also the frequency of murine CD45+ leukocytes was elevated in cGvHD, introducing the hypothesis that human T cells can be stimulated by murine tissue and vice versa activate murine immune cells or damage murine tissue in a cross-reactive manner. A remarkably decelerated reconstitution of murine Gr1+ myeloid-derived cells and CD11b-/CD11c+ lymphoid DCs was measured around day +30, but normalized to syn-HSCT levels at later stages (Figure 42A, bottom row).To discern the issue, in which lymphatic organs the transplanted huPBMCs and murine donor-cells home PB, BM and spleen were analyzed at day+125. While huCD4+ T cells and huCD45+ leukocytes were mostly detected to circulate in the periphery and the spleen, but not the BM, huCD8+ T cells were predominantly found to reside in spleens and in small numbers in BM and PB. The majority of murine CD45+ leukocytes were found to home in the BM, indicating complete HSC-reconstitution and cell-recurrence after irradiation at day+125 (Figure 42B, upper row). Murine CD11b+ and Gr1+ myeloid-derived cells were measured with similar higher numbers to prevail in the BM and in the PB circulatory system, while both subsets appeared in spleens to a limited extent (Figure 42B; bottom row).

Considerable differences of cellular reconstitution among allo and syn-HSCT recipients were revealed in murine DCs of distinct origin: while the frequency of myeloid DCs was higher, lymphoid DCs were diminished in spleens of cGvHD-mice (Figure 42B, bottom row).

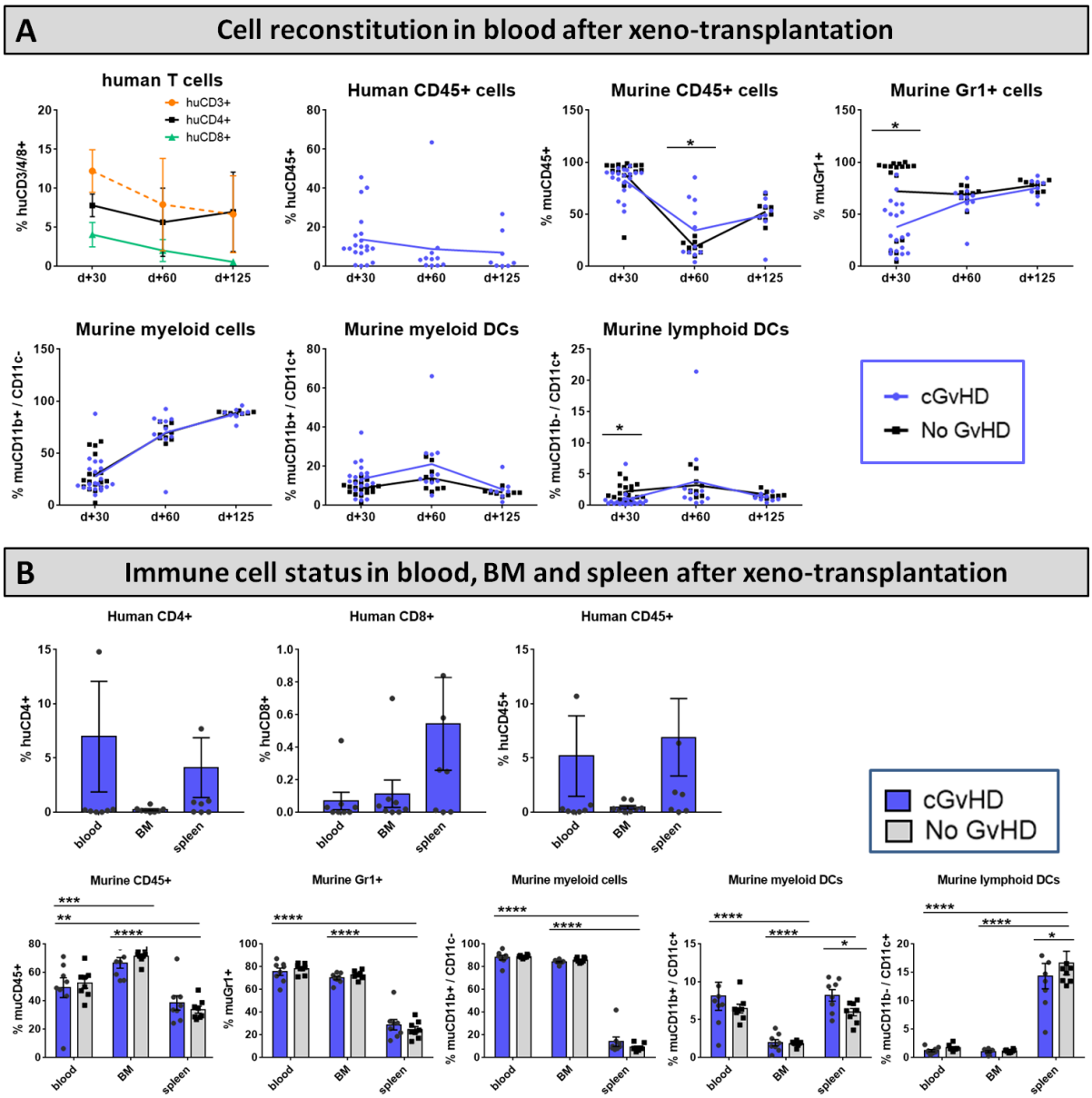

Figure 42: Immune cell reconstitution in (A) peripheral blood of NSG-recipients over 125 days and (B) in PB, BM and spleen at day+125 after xeno-HSCT. (A) Tail vein blood was collected at three time points, PB cells were isolated, stained with the respective FACS-antibodies and samples were analysed with flow cytometry. DCs= dendritic cells. **(B)** Blood was collected retrooribitally upon finalization. Spleens were harvested and BM flushed from tibia and femur. Immune cells were isolated, stained with the respective FACS-antibodies and samples were analysed with flow cytometry DCs= dendritic cells. n=8 per group. Error bars show mean±SEM. Representative data from one out of two experiments. *P<0.05, **P<0.01, ***P<0.001, ****P<0.0001 by unpaired students *t*-test.

Monitoring the erythropoietic recovery after xeno-HSCT, the differential blood count performed at d+90 displayed a significantly increased frequency of murine lymphocytes in cGvHD (Figure 43), indicating the transferred huPBMCs to effect a 'tissue-crossing' lymphocyte reaction in mice. Murine leukocytes, thrombocytes and neutrophils were

decreased in tendency in cGvHD compared to controls, while other erythropoiesis-related factors were not affected (Figure 43; Supplemental Figure 6).

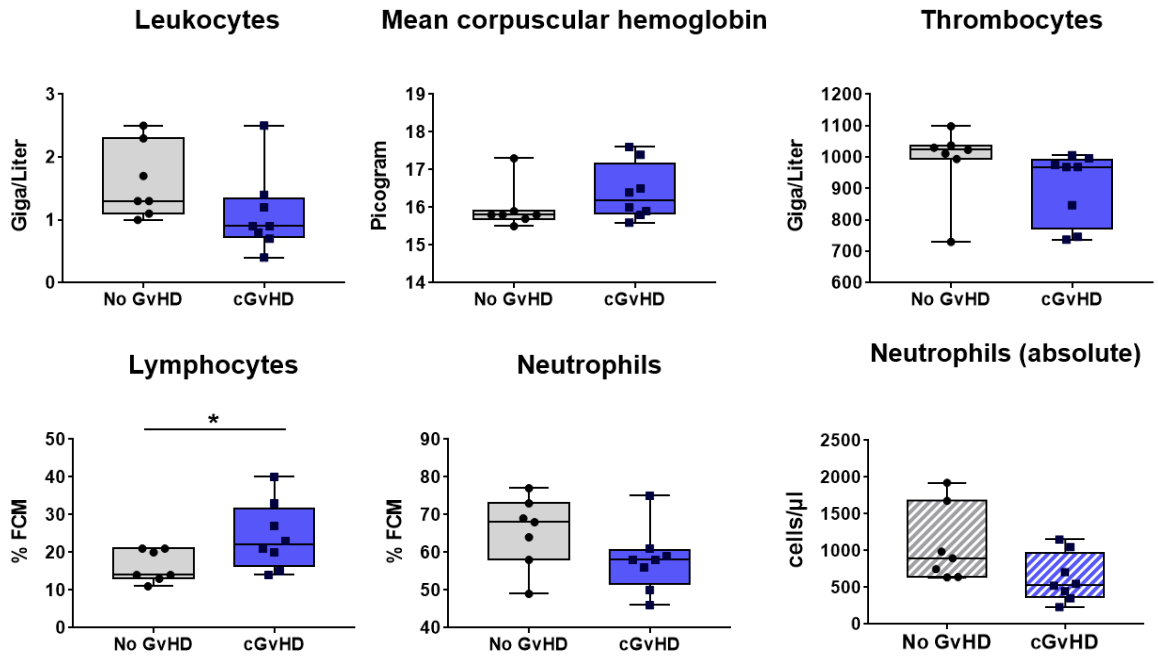

Figure 43: Recovery of red blood cells and related factors in cGvHD at d+90 after xeno-HSCT in huPBMC→NSG. Blood was sampled from mice and differential blood count was performed by Synlab, Berlin. Error bars show mean±SEM. Representative data from one out of two experiments. n=8 per group. *P<0.05, **P<0.01, ***P<0.001, ****P<0.0001 by unpaired students *t*-test.

3.2.2. Endothelial function and endothelial damage in cGvHD

Histological scoring revealed severe tissue damage, including fibrotic and inflammatory manifestations in cGvHD target organs of the previously described novel cGvHD mouse models. To evaluate the contribution of the endothelium to the cGvHD progression and to specifically examine the endothelial dysfunction and damage, the cGvHD target organs lung, liver, skin, colon, aorta and eye of the murine (B6D2F1) and humanized (NSG) cGvHD mouse models were analysed for different endothelial and fibroblastic markers.

The following graph depicts all significant differences, which were found in the analysis of single fluorescence markers, showing endothelial damage and dysfunction in cGvHD target organs of the murine B6D2F1- (Figure 44A and C) or the humanized NSG-mouse model (Figure 44B). All quantifications of organs not shown here can be accessed in Supplemental Figure 8A&B. At first, the vascular integrity and the vessel density was shown in the analysed tissue region by quantification of endothelial CD31 and VECad. Analysis pointed to a

significant reduction of the CD31+ vessel density in aorta, skin, liver and colon during established murine cGvHD. Expression of VECad showed similar expression patterns in aorta, skin and colon, but not in liver. On the contrary, we found increased pulmonary CD31+ and VECad expression in cGvHD mice compared to no-GvHD mice, indicating an angiogenic or vascular remodeling in cGvHD lungs. Following, vWF levels, reflecting endothelial damage and dysfunction, were elevated in cutaneous, hepatic and aortic tissues of cGvHD mice. The occurrence of endothelial damage and dysfunction in cGvHD was confirmed in the alternative humanized GvHD model. Upon examination of single markers (Figure 44B) , the target organs colon, liver and lung showed a diminished total CD31 expression in tissue, but no altered expression of the second vascular marker VECad. Total tissue vWF was significantly elevated in colon, but not in liver or lung of cGvHD.

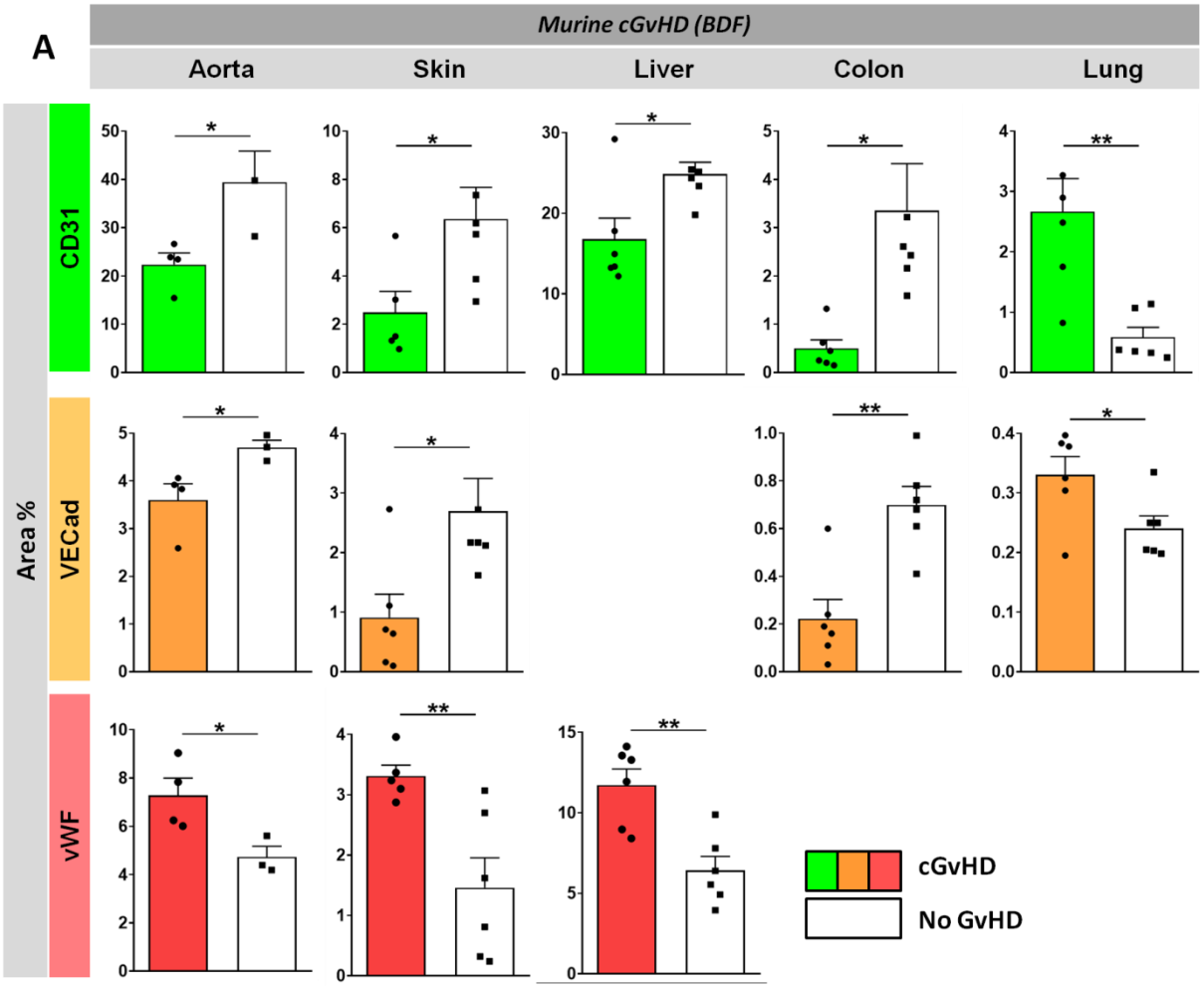

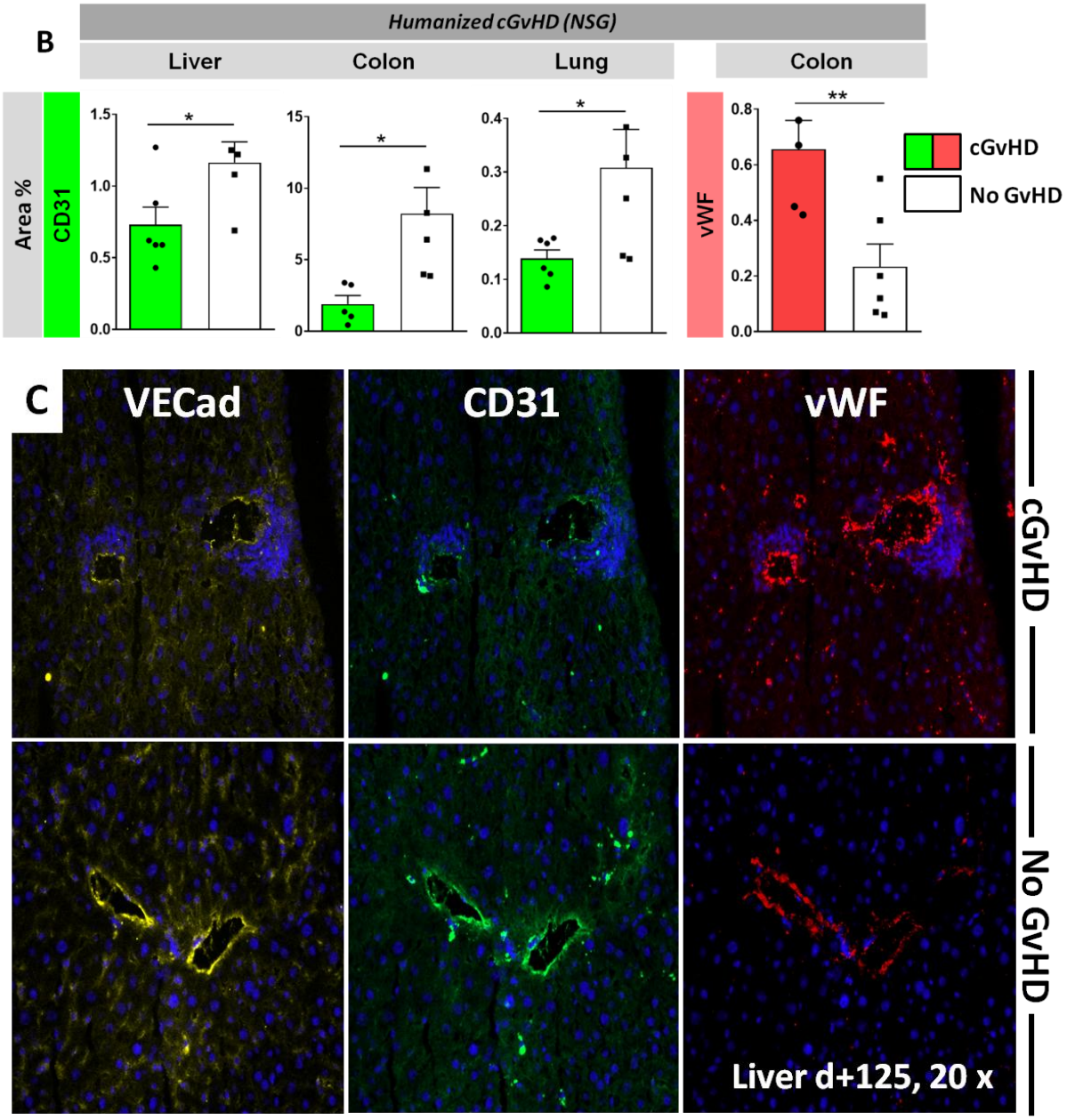

Figure 44: Single marker analysis of endothelial damage and dysfunction in murine cGvHD. Expression of endothelial CD31, VECad and vWF in total tissue from cGvHD target organs determined by immunohistofluorescence at day +125 after transplantation **(A)** in B6D2F1-recipients and **(B)** in NSG-recipients. Representative data from one out of two experiments. n=6 per group. *P<0.05, **P<0.01, ***P<0.001, ****P<0.0001 by unpaired students *t*-test. Error bars indicate mean +SEM. **(C)** Representative immunohistofluorescence image shows loss of VECad and CD31 as well as increased vWF expression in liver vasculature of cGvHD vs. control mice.

The endothelial dysfunction in cGvHD was further characterized by colocalization of single endothelial markers specifically at CD31+ blood vasculature sites in the murine B6D2F1- (Figure 45A) or the humanized NSG-mouse model (Figure 45B). All quantifications of organs not shown here can be accessed in Supplemental Figure 9A&B. In B6D2F1-recipients (Figure 45A), VECad+/CD31+ positive pulmonary vessels were found increased in cGvHD mice, while expression of double positive vessels in other organs was equal in syn- and allo-transplanted animals. vWF+/CD31+ levels were lower in lungs of cGvHD mice than in no-GvHD mice, while their expression was higher vice versa in liver and aorta, indicating endothelial damage in these cGvHD organs. To specify the endothelial dysfunction, tight junction protein ZO-1 and pericyte marker NG2, giving evidence of vascular integrity, e.g. leakiness when co-localized with CD31, were examined. The level of endothelium-related ZO-1 surrounding blood vessels was significantly reduced in all of the examined organs in cGvHD compared to no-GvHD controls, associated with a dysfunctional barrier function and increased endothelial permeability. The loss of ZO-1 in particular around vascular structures in the liver as well as the overall-tissue loss in skin and colon was microscopically visualized in Figure 46A-C. The expression of mural NG2 at blood vessels was significantly decreased only in cGvHD livers (Figure 45A and Figure 46 A). Moreover, the fibroblastic/ mesenchymal markers αSMA and FSP-1 were measured alone in whole-tissue or in interrelation with CD31 as both co-localizations indicating vascular fibrosis. Single marker evaluation in whole tissue revealed that αSMA was found increased in skin and liver, but was diminished in colon of cGvHD animals, while The FSP-1 expression was significantly higher in lung, skin and liver of cGvHD mice, but did not show a difference to the FSP-1 level in colon and aorta of controls (Supplemental Figure 8A). Co-localized αSMA+/CD31+ expression did not differ significantly between the two groups (Supplemental Figure 9A), but we found a marked enhancement in FSP-1+/CD31+ cells in cGvHD liver and colon and a tendencial rise in the other organs (Figure 45A).

Lately, Figure 45B confirms the vascular alterations, which were detected during murine cGvHD by colocalization of endothelial and endothelium-related markers, in NSG-recipients during humanized cGvHD. An increase of VECad+/CD31+ positive vessels was shown in colon of transplanted mice, conversely to the CD31+ vessel loss. The vasculature in liver and colon exhibited a significant rise of vWF, indicating endothelial damage in cGvHD. The expression of ZO-1 in pulmonary and intestinal endothelium was decreased, which is associated with impaired tight junction functionality, thus reduced endothelial integrity and

permeability. Single marker quantification demonstrated higher αSMA levels in whole-tissue of all three analysed organs, while FSP-1 was drastically increased only in colon of cGvHD mice (Supplemental Figure 8B).The expression of co-localized αSMA in CD31+ endothelium was strongly increased in lung and also in liver and colon of cGvHD mice. FSP-1+/CD31+ vessels were found to be expanded in all three target organs in cGvHD compared to controls, pointing towards a strong vascular fibrosis (Figure 46B).

The prominent endothelial damage in cGvHD, including a loss of vessels and endothelial tight junctions as well as an increased endothelial fibrosis, which was detected predominantly in liver and in colon of NSG-recipients, was connected to the amount of human CD4+ T cells infiltrating organ parenchyma in these target organs (Figure 46D). As expected, the T cell load was highest in liver with 1.29%, followed by 0.6% in colon and 0.17% in lung, thus correlated with the grade of endothelial dysfunction found in the respective organs.

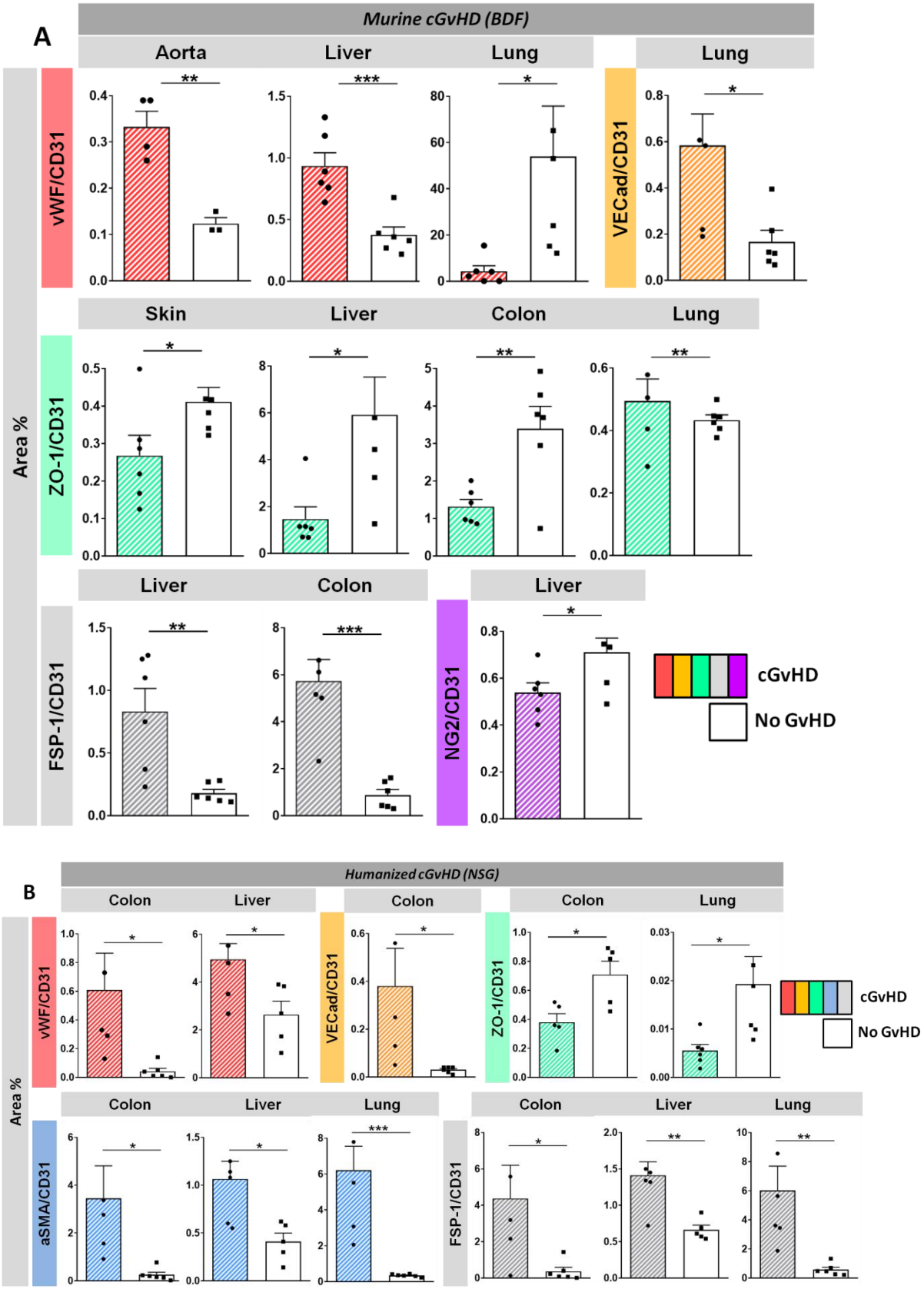

Figure 45: Colocalization analysis of endothelial damage and dysfunction in cGvHD. Expression of VECad, vWF, αSMA , FSP-1, ZO-1 and NG2 co-localized with CD31+ vessels in cGvHD target organs of **(A)** B6D2F1-recipients and **(B)** NSG-recipients. Representative data from one out of two experiments. n=6 per group. *P<0.05, **P<0.01, ***P<0.001, ****P<0.0001 by unpaired students *t*-test. Error bars indicate mean +SEM.

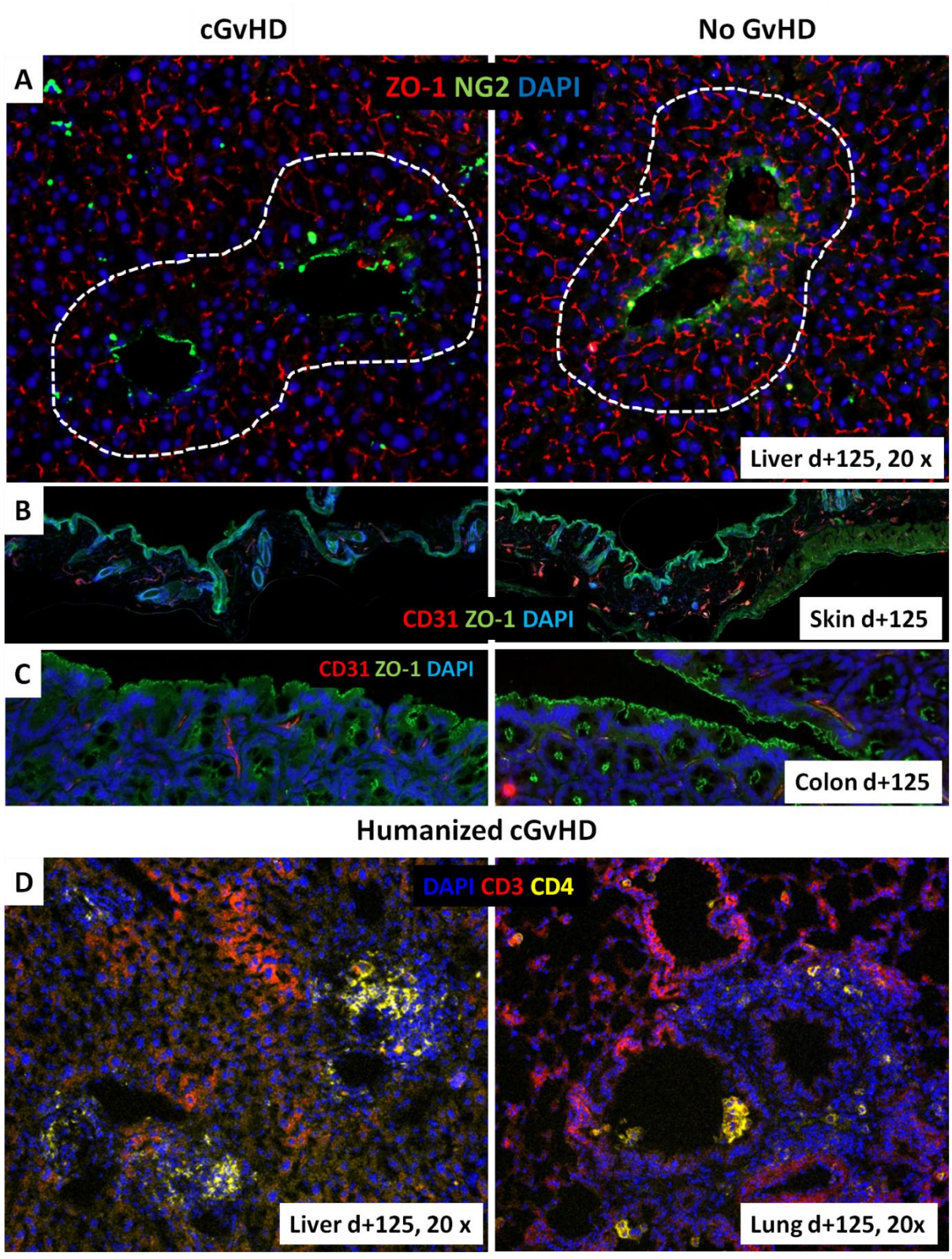

Figure 46: Endothelial integrity and damage and human immune cell infiltration in liver, skin, colon and lung biopsies of cGvHD mice. Representative immunohistofluorescence images show **(A)** loss of ZO-1 and NG2 around blood vessels in liver, **(B)** loss of CD31 microvessels in skin and **(C)** loss of ZO-1 tight junctions in colon of cGvHD vs. No-GvHD mice (BDF-mouse model). **(D)** Representative immunohistofluorescence image shows an increased amount of human CD4- and CD3-positive infiltrating immune cells in liver and lung parenchyma of cGvHD mice (NSG-mouse model).

FACS quantifications with isolated hepatic and pulmonary ECs showed, that the endothelial immunophenotype varied to a different extend in liver and lung and between cGvHD- and no-cGvHD mice. As Figure 47 shows, the subset of mature ECs (CD45+CD34-CD146+) was distinctly diminished in diseased lung, but not in liver. Remarkably, the fraction of HSCs (CD45+Sca1+cKit+CD34+) and of CD31+ or CD146+ positive EPCs (CD45+Sca1+cKit+CD31+/CD146+) was measured to be elevated in cGvHD, proposing EPCs playing a role in cGvHD pathology and might be a relevant disease predictor. In liver but not in lung, the subset of multipotent CD146+ MSCs (CD45-CD34-CD146+), which can differentiate to ECs but also give rise to fibroblastic cell subsets, was increased in cGvHD mice. ECs from both organs displayed a considerably decreased expression of TGF-ß receptor ALK5 as well as of PDGFRβ, implying a disturbed regulation in TGF-ß signaling. Data indicate that ECs not only display immunophenotypic changes during cGvHD, but that the occurrence of certain EC subsets also varies between different target organs.

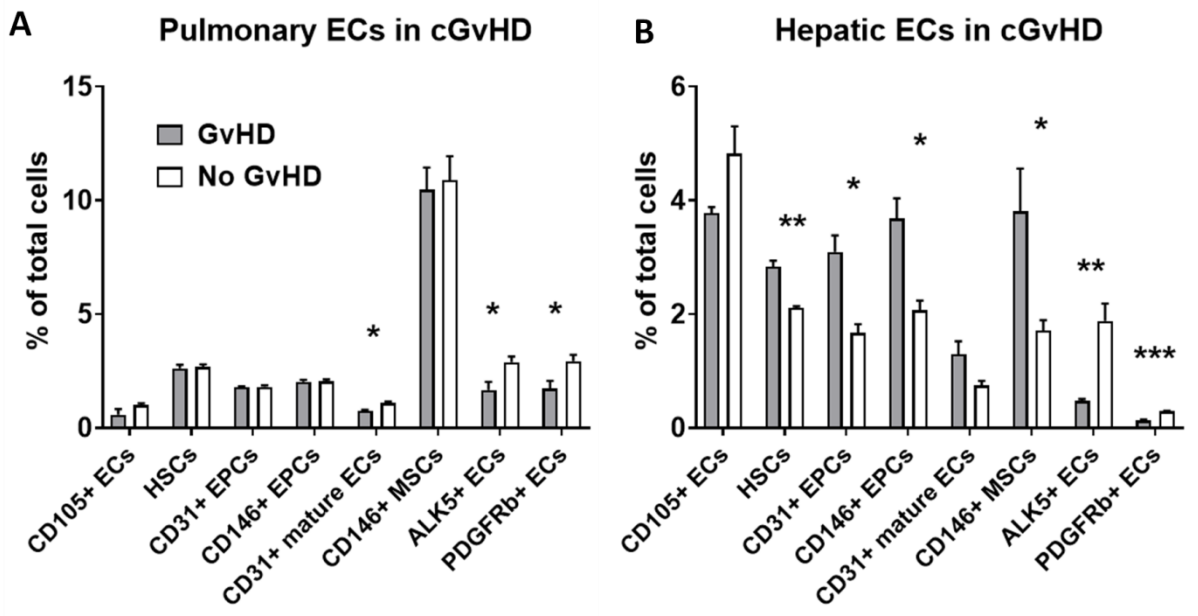

Figure 47: Immunophenotyping of (A) pulmonary and (B) hepatic EC subsets in cGvHD B6D2F1 model at day+125 after transplantation. ECs from liver and lung of cGvHD mice were isolated by CD31+ MACS separation, stained with flow antibodies and analysed with FACS. Data from one representative experiment. Error bars indicate mean +SEM. n=3 per group. *P<0.05, **P<0.01, ***P<0.001 by unpaired students *t*-test.

Since symptomatic disease manifestations were also detected in the eyes of cGvHD mice during cGvHD scoring, the involvement of ocular endothelium and related inflammation in the cGvHD B6D2F1 model was characterized in a preliminary study (Supplemental Figure 7). Endothelial (CD31) and lymphatic (Lyve-1) vessels in cornea and eyelids of the examined

mice did not show changed levels, neither altered ICAM-1 levels were found. cGvHD recipients presented with higher frequencies of CD4+ as well as CD8+ T cell infiltrates in cornea, retina and eyelids.

The endothelial leakiness was investigated in Evans blue assays as well as the inflammatory potential in Paw Edema assays. NSG mice suffering from cGvHD did not demonstrate higher vascular leakiness compared to control mice (Figure 48A). On the contrary, cGvHD diseased NSG mice exhibited significantly increased footpad swelling, thus increased inflammatory reactions, 3 to 4 hours after carrageenan injection than controls (Figure 48B). The average spleen weight normalized to each mouse's individual body weight was significantly higher in cGvHD than in syn-transplanted recipients (Figure 48C), indicating an elevated influx of inflammatory immune cells into splenic compartments.

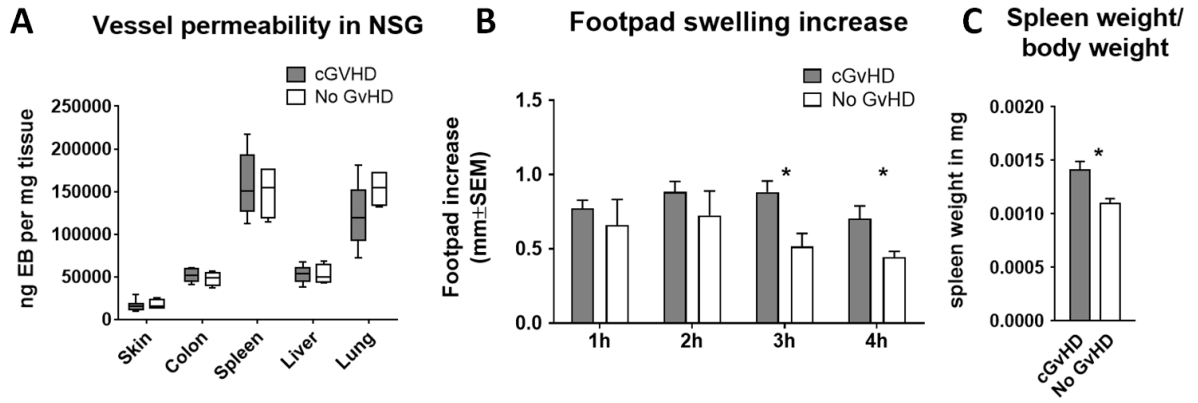

Figure 48: ex vivo analysis of cGvHD in huPBMC → NSG at day+125. (A) Vessel permeability determined by Evans Blue Assay and **(B)** footpad swelling over 4 hrs as an indicator of inflammation analysed in Paw Edema assay. **(C)** Spleen weight related to body weight at 4hrs after carrageen injection in Paw Edema assay. cGvHD n=6, No GvHD n=4. Data from one representative experiment. Error bars indicate mean+SEM. *P<0.05

Last, co-localized CD31/αSMA/FSP-1 was analysed. The triade of markers indicates the transition process of endothelial into mesenchymal cells (EndoMT). Significant EndoMT was detected in all cGvHD target organs of B6D2F1-recipients, with an increased expression predominantly in skin and liver and to a lesser extend also in lung and colon (Figure 49A), while in NSG-recipients differences in triple-co-localized CD31+/αSMA+/FSP-1+ signals were not detected between cGvHD and no-GvHD (Supplemental Figure 9). Representative images from immunohistofluorescence stainings impressively depicted superimposed FSP-1 and αSMA areas in large CD31+ pulmonary veins of cGvHD B6D2F1 mice (Figure 49B).

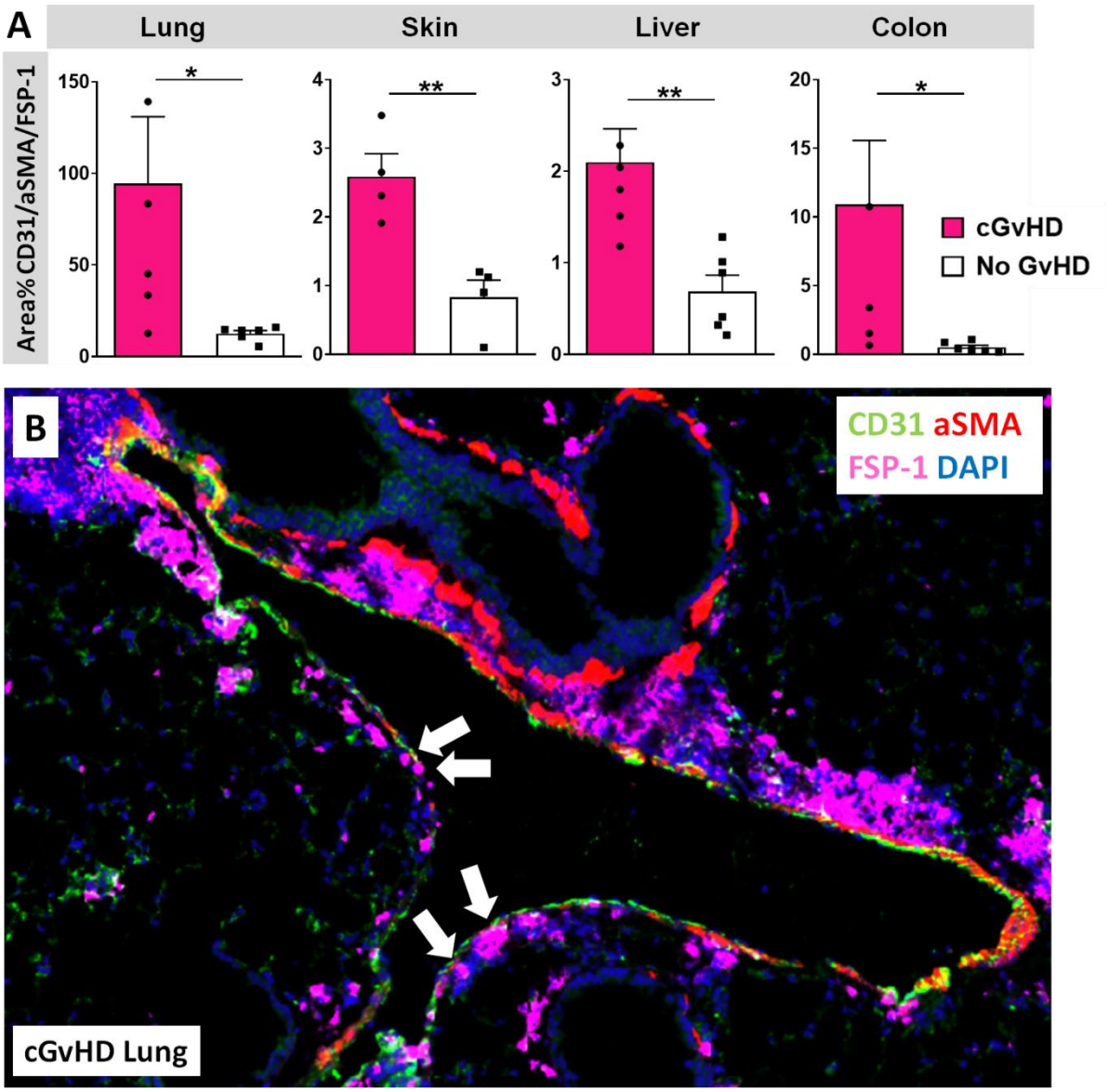

Figure 49: EndoMT in cGvHD. (A) Expression of co-localized CD31+/αSMA+/FSP-1+ in blood vessels of cGvHD target organs from B6D2F1-recipients as markers for EndoMT. Representative data from one out of two experiments. n=6 per group. *P<0.05, **P<0.01, ***P<0.001, ****P<0.0001 by unpaired students *t*-test. Error bars indicate mean +SEM. **(B)** Representative immunohistofluorescence image shows colocalization of CD31/αSMA/FSP-1 (EndoMT) in pulmonary vessels of cGvHD mice (B6D2F1) at day +125 after transplantation.

Taken together, the endothelium was multifariously damaged during severe cGvHD. Predominantly colon, liver and skin showed a loss of CD31+ and VECad+ vessels and an increase in soluble vWF. Tight junction protein ZO-1 was ubiquitously downregulated and NG2+ pericytes were concomitantly decreased in liver during cGvHD, altering endothelial permeability. Confirmative, a modified, more rapid influx of infiltrating immune cells in cGvHD mice was detected compared to no-GvHD mice in inflammation assays. cGvHD mice

displayed markedly more vascular fibrosis, characterized by elevated expression of αSMA or/and FSP-1 in CD31+ vessels. Results emphasize that EndoMT might be a mechanistic cause to the endothelial damage and dysfunction in cGvHD with relevance to the disease progression and was further investigated in the following section.

3.2.3. EndoMT in cGvHD

Addressing the question, to which extend endothelial cells are prone to EndoMT and how the transition process influences endothelial function in cGvHD, further *in vitro* and *ex vivo* experiments were conducted.

It was examined by FACS analysis to which extend TGF-ß stimulated MCECs and MuMECs were prone to EndoMT *in vitro.* After 4 day culture with TGF-ß, possible changes in mesenchymal markers CD105, CD44 or αSMA were compared to the expression of endothelial markers such as CD31, CD146 or VEGFR. As Figure 50A depicts, MCECs did not express CD31, but CD146 was slightly upregulated upon TGF-ß stimulation, while VEGFR expression seemed unaffected. The proportion of VEGFR+ as well as CD146+ MCECs, which were also positive for CD44 or for CD105 was significantly higher in TGF-ß stimulated cells. The expression of the VEGFR+αSMA+ population was marginally increased by TGF-ß stimulation. In MuMECs (Figure 50B), a marked rise in CD146 expression as well as an increase in CD31 was observed upon TGF-ß stimulation. In these ECs, CD44 and CD105 showed elevated expression levels. αSMA, similar to the results in MCECs, was only slightly increased in stimulated cells. Data indicate, that a conversion from endothelium towards a mesenchymal cell type involves not only classical EndoMT markers as αSMA, but also other adhesional and accessory markers e.g. CD44 and CD105.

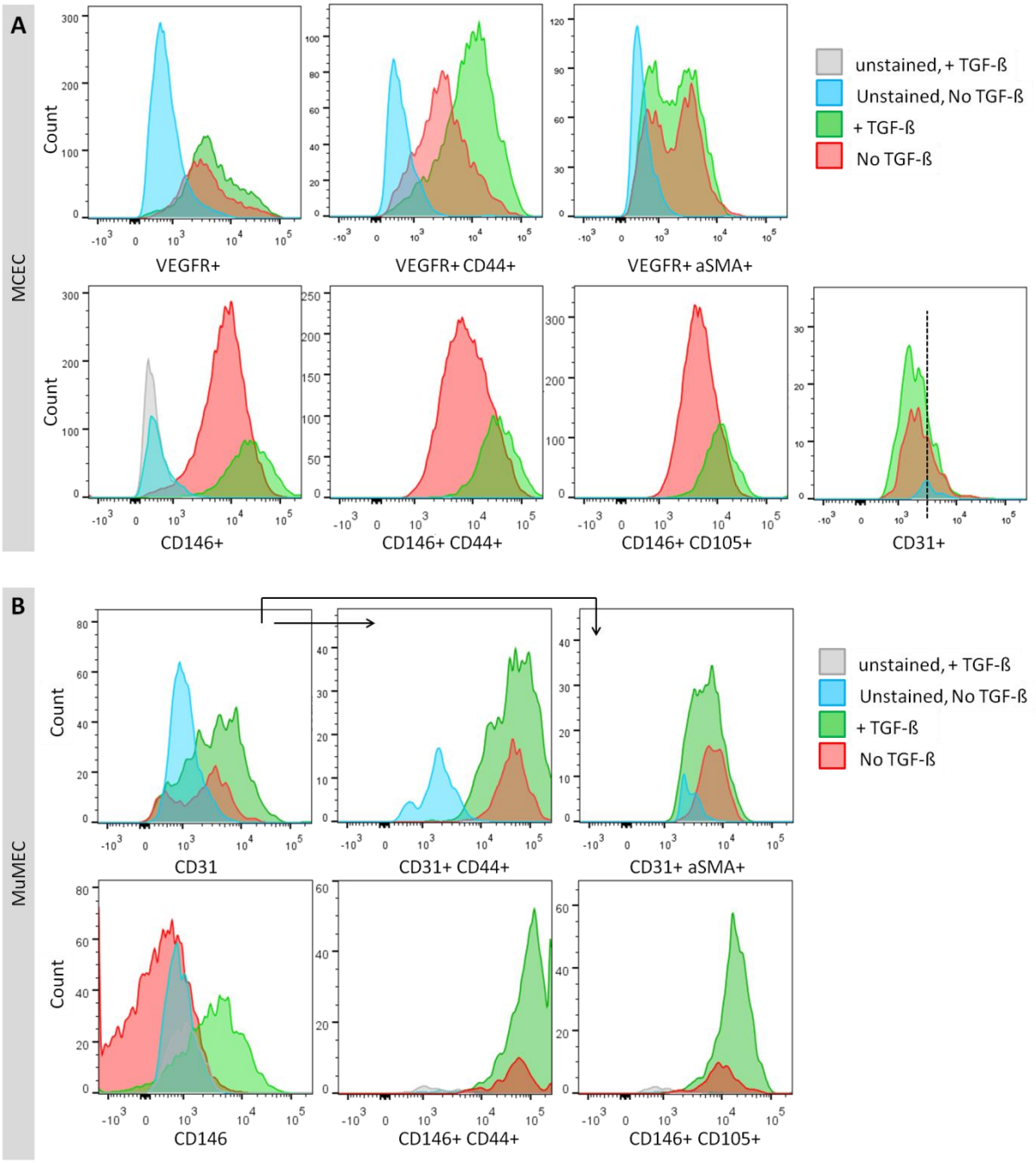

Figure 50: FACS analysis of endothelial and mesenchymal markers in TGF-ß stimulated MCEC (A) and MuMEC (B). Representative histograms from two independent experiments.

Following, the endothelial cell lines MCEC and MuMEC, which were stimulated with the EndoMT-trigger TGF-ß and additional H_2O_2 to simulate an oxidative stress reaction and to accelerate the transition process, showed altered migrative, proliferative and angiogenic behaviour under EndoMT. In Wound healing assays, TGF-ß stimulated MCECs and MuMECs showed an elevated migration at 3 hours, but not in the later course of time after

wounding (Figure A). Stimulated MCECs showed an increased viability compared to non-stimulated MCECs at 24 hrs up to 48 hrs in MTT assays (Figure B), but viability of EndoMT-transformed MCECs conversely diminished compared to non-stimulated cells at 72 hrs. Stimulated MuMECs were observed to exhibit a decreased viability after 72 hrs. In tubeformation assays (Figure C) the angiogenesis of TGF-ß stimulated cells was significantly impaired. Neither the EndoMT-transformed MCECs nor MuMECs showed a potential to form tubes at 4 hrs after seeding onto matrigel. 72 hrs after TGF-ß and H_2O_2 induction, a phenotypic conversion was detected especially in MuMECs (Figure D), which showed a transformation from an endothelium-specific cobblestone-like morphology into elongated, spindle-formed cells. In immunohistofluorescence stainings a visible increase of EndoMT markers (αSMA & FSP-1), but only minor reduction of CD31 signals was observed in TGF-ß treated MuMECs.

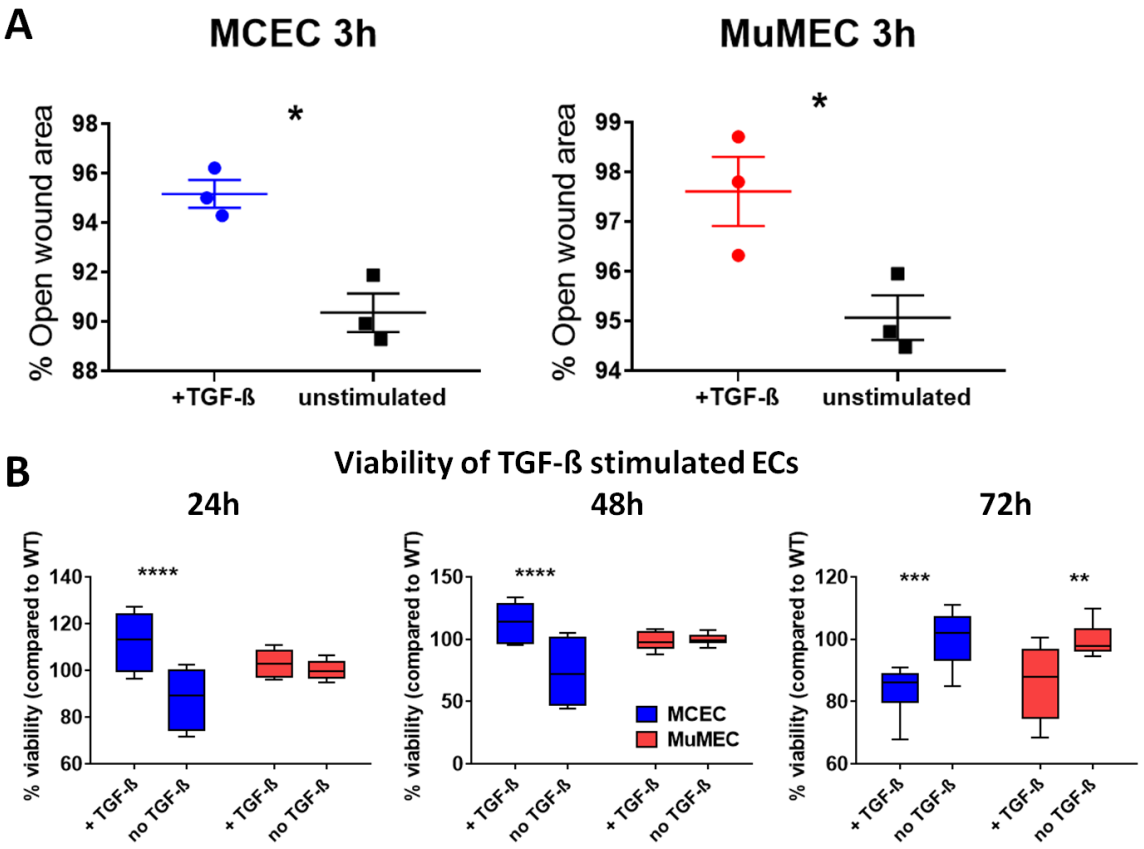

Figure 51: Functional characterization of *in vitro* stimulated EndoMT in MCEC and MuMEC. MCEC and MuMEC were stimulated with 10 ng TGF-ß + 5µM H_2O_2 (MCEC) or 20 ng TGF-ß + 10 µM H_2O_2 (MuMEC) for 72 hrs. **(A)** Wound healing Assay: Confluent cell layers were scratched and cell migration was tracked over 18 hours. **(B)** MTT Assay: Viability was assessed in TGF-ß stimulated vs. non-stimulated cells over 72 hours.

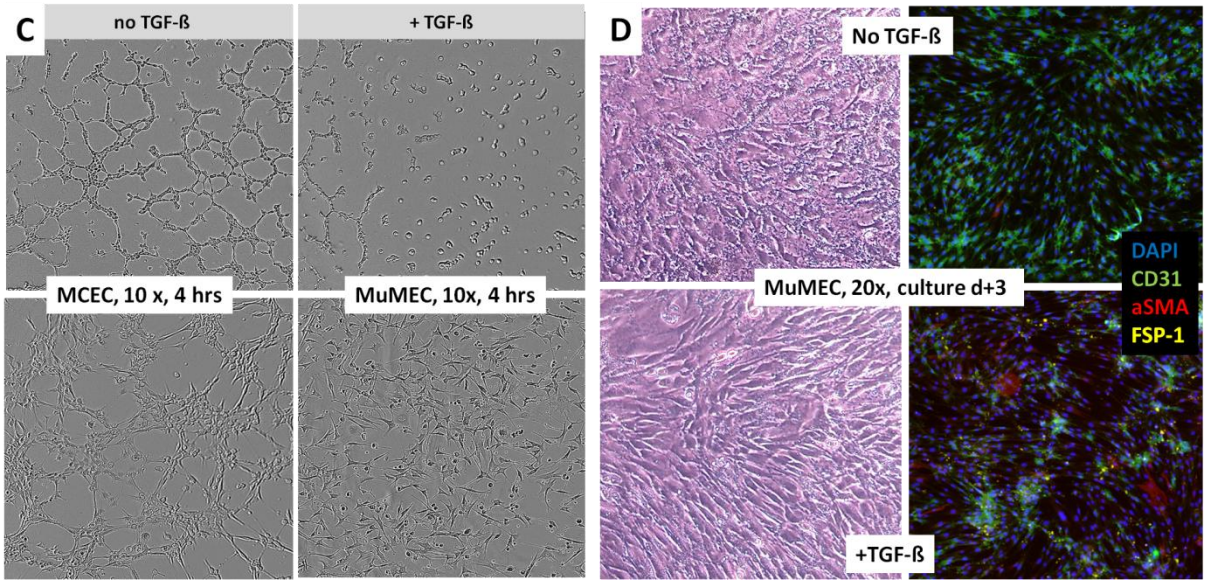

Figure 51 (contin.): Functional characterization of *in vitro* stimulated EndoMT in MCEC and MuMEC. MCEC and MuMEC were stimulated with 10 ng TGF-ß + 5µM H_2O_2 (MCEC) or 20 ng TGF-ß + 10 µM H_2O_2 (MuMEC) for 72 hrs. **(C)** TGF-ß stimulated vs. non-stimulated cells were seeded onto matrigel layer and tubeformation was measured after 4 hours. **(D)** Representative bright field (left) and fluorescence images (right) of 72 hrs TGF-ß stimulated (EndoMT) vs. non-stimulated MuMECs. Data pooled from 3 (MTT=2) independent experiments. Error bars indicate mean ± SEM, *P<0.05, **P<0.01,***P<0.001, **** P<0.0001 by two-way ANOVA/Holm-Side's multiple comparisons test (MTT) or by unpaired students t-test (Wound healing).

Attempting to transfer the results from the *in vitro* EndoMT experiments to an *in vivo* approach, a possible role for the EndoMT process in the cGvHD pathology was investigated in the previously established murine cGvHD mouse models. On that purpose it was first analysed by FACS, to which extend endothelial and mesenchymal markers were differentially expressed in isolated ECs from liver and lung of cGvHD vs. no-GvHD mice. In line with the immunohistological results a loss of endothelial CD31 in lung and liver, of CD146 in lung and of VEGFR+ ECS in liver was measured in C57BL/6 cGvHD (Figure 52). As expected, the expression of CD146+αSMA+ was higher in cGvHD than in control ECs. Conflicting, less CD146+CD105+ ECs were observed in cGvHD liver compared to controls. The loss of endothelial markers, such as CD31 and VEGFR during established cGvHD in liver ECs and the increased expression of mesenchymal markers as CD44 in liver and lung ECs were also confirmed in the B6D2F1 cGvHD model (Supplemental Figure 10).

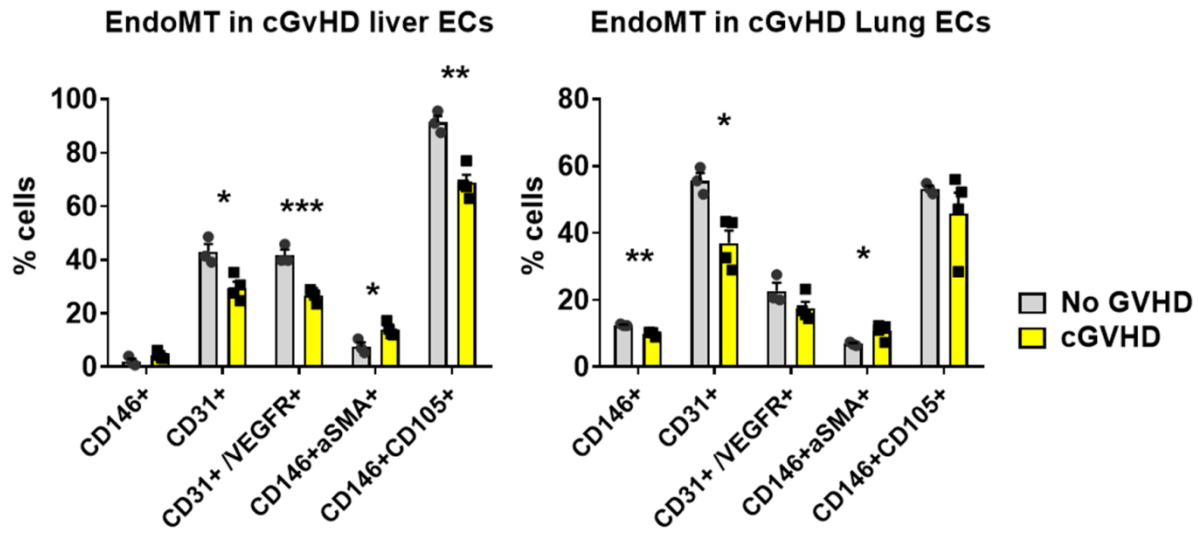

Figure 52: EndoMT markers in FACS analysis from isolated liver and lung ECs from BALB/c → C57BL/6 mice at day+90 after transplantation. No GvHD n=3; cGvHD n=4. Data from one representative experiment. Error bars indicate mean ± SEM, *P<0.05, **P<0.01, ***P<0.001 by unpaired students t-test.

RNA quantification of genes important for EndoMT processes confirmed EndoMT participation in cGvHD pathology, as seen by EndoMT stainings in cGvHD target organs. RNA levels of endothelial marker CD31 as well as VECad were significantly lower in isolated liver and lung ECs of cGvHD recipient mice compared to syn-controls (Figure 53, dark grey). Interestingly, the Tie-2 expression in liver was decreased, whereas in lung Tie-2 levels were contrastingly upregulated. Expression of the mesenchymal/ fibrotic markers (Figure 53, light grey) Vimentin and αSMA was increased in lung ECs, but both only increased in tendency in livers. FSP-1 exhibited a strong, nearly 3 fold changed rise in cGvHD liver and in tendency also in cGvHD lung. Quantifying expression levels of transcription factors (Figure 53, dashed), Snail showed lower levels in liver ECs of cGvHD than in control ECs. Transcription factor SMAD3 remained unvaried in both cGvHD and controls, while SMAD2 displayed opposing results. It was found downregulated in hepatic ECs and upregulated in pulmonary ECs of cGvHD mice. The loss of endothelial receptors as CD31 or VECad, the rise in fibrotic and mesenchymal markers Vimentin, αSMA and FSP-1 and the differential regulation of transcriptional factors as SNAIL or SMAD2 indicate, that an EndoMT is involved in endothelial damage, endothelial loss and fibrotic development in cGvHD. Since expression patterns vary between liver and lung, it could be hypothesized that different cGvHD target organs contribute differently to the EndoMT process.

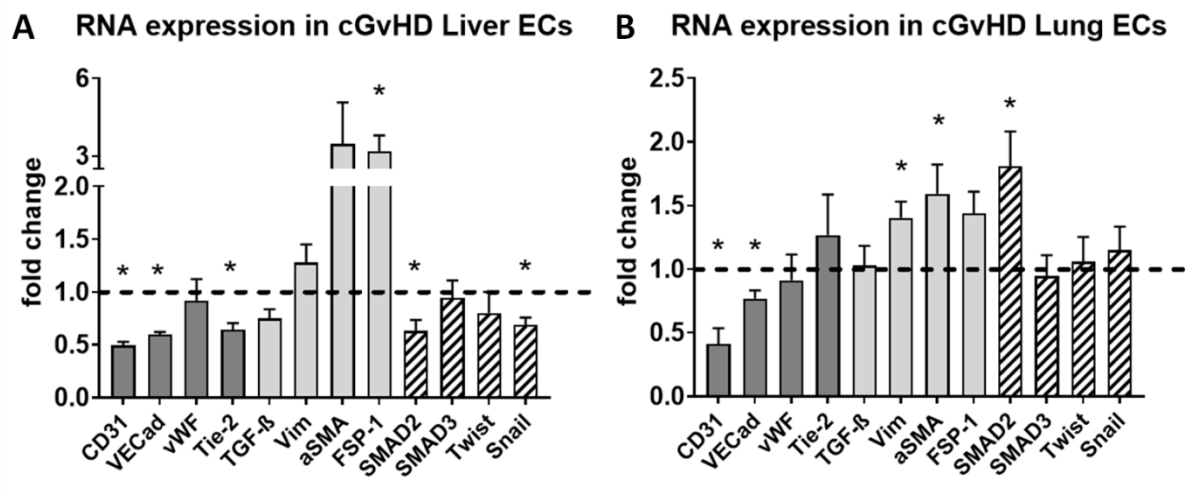

Figure 53: Gene expression analysis of endothelial (dark grey) and mesenchymal markers (light grey) and transcription factors (dashed) in (A) liver and (B) lung and of cGvHD B6D2F1 mice. Fold change expression of genes was measured by RT-qPCR analysis and normalized to ß-actin expression (1.0; dotted line). Data from one representative experiment. n=6 per group. Error bars indicate mean + SEM. *P ≤ 0.05 by unpaired Student's t-test.

To corroborate the hypothesis, whether ECs are more prone to acquire a multipotent stem-cell like phenotype during cGvHD, the isolated hepatic and pulmonary ECs from B6D2F1 and C57BL/6 cGvHD recipients were treated with TGF-ß for EndoMT conversion and cells were analysed by immunohistofluorescence and FACS for mesenchymal, stem- and progenitor cell markers as CD44 or CD133 after stimulation. E*x vivo* TGF-ß stimulation of liver and lung ECs from allo-transplanted recipient mice showed a higher vulnerability for mesenchymal transition during cGvHD than from syn-controls. After 72 hours, a visible loss of CD31+ signal and a switch towards CD31+αSMA+ cells could be detected microscopically in liver and with high intensity also in lung ECs (Figure 54A). In histological quantifications, the CD31 signal was marginally diminished, while the proportion of CD31+αSMA+, respectively CD31+FSP-1+ double positive cells was distinctly higher in the cGvHD hepatic ECs. After comparing initially seeded cell numbers with cell numbers following 72 hours stimulation, the amount of remaining living cells was nearly 4 fold higher in controls than in cGvHD (Figure 54B). Furthermore a rise in HSC markers was shown by FACS to occur in a higher frequency in TGF-ß stimulated hepatic and pulmonary ECs from cGvHD mice than from respective controls. After 72 hrs stimulation, a loss of CD31 and an approximately 3 fold higher CD44 expression was detected in cGvHD ECs than in controls in both investigated organs. CD133 was massively increased especially in C57BL/6 cGvHD lung endothelium (Figure 54C). A decrease of CD31 and a marked increase in CD44 and CD133 was also consistently shown in lung and liver of B6D2F1 recipients (Supplemental Figure 11).

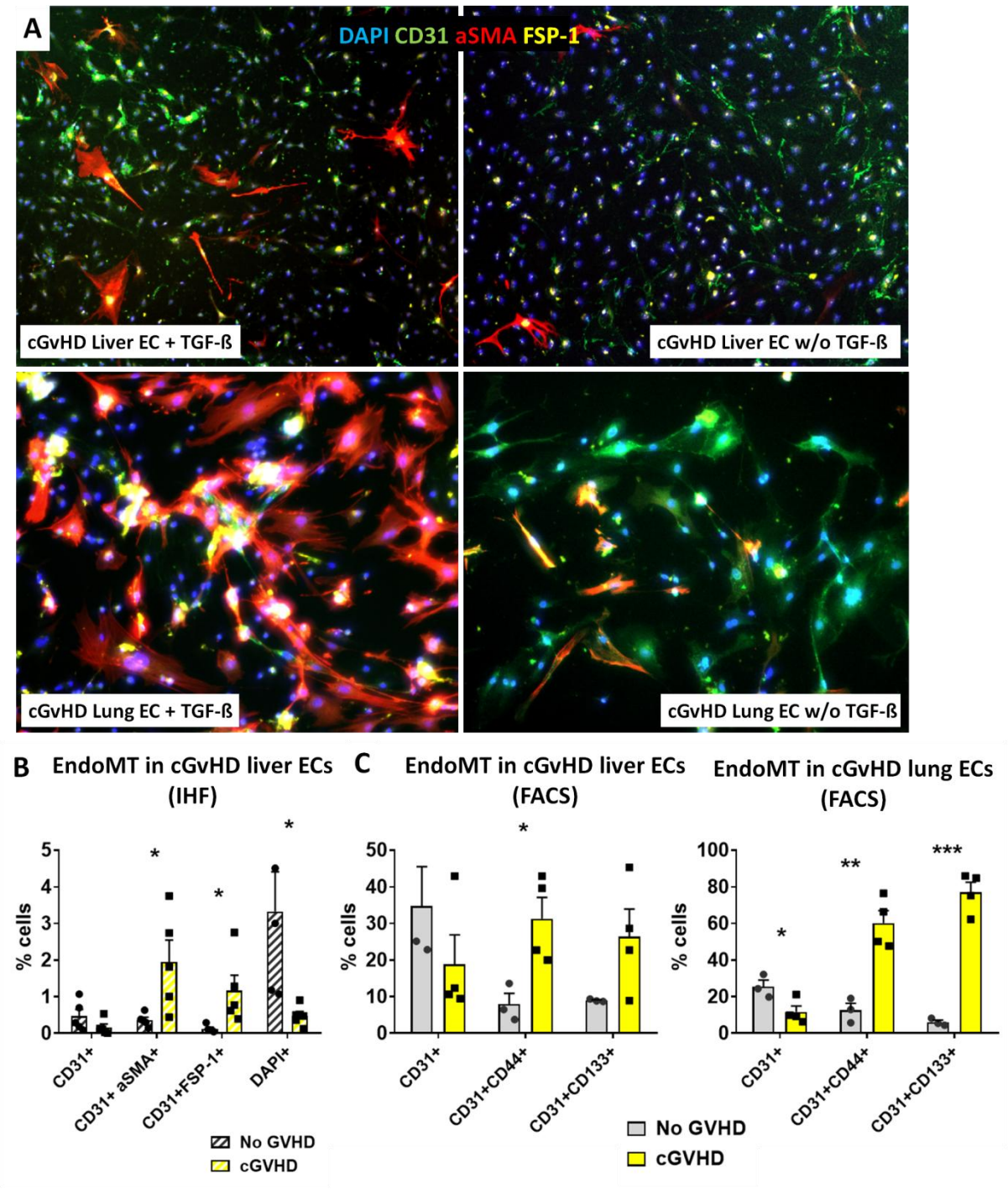

Figure 54: EndoMT in isolated lung and liver ECs from cGvHD recipients is triggered by TGF-ß stimulation. (A) Fluorescence image of 72 hrs TGF-ß treated (left) vs. non-treated (right) liver ECs from the same cGvHD B6D2F1 recipient at d+90 after transplantation. Objective 20x. Lung zoomed to 140%. **(B)** EndoMT markers in immunohistofluorescence analysis from TGF-ß stimulated liver ECs from BALB/c → C57BL/6 mice at day+90 after transplantation. **(C)** EndoMT markers in FACS analysis from TGF-ß stimulated liver and lung ECs from BALB/c → C57BL/6 at day+90 after transplantation. No GvHD n=3; cGvHD n=4. Data from one representative experiment. Error bars indicate mean ± SEM, *P<0.05, **P<0.01, ***P<0.001, ****P<0.0001 by unpaired students t-test.

Recapitulatory, isolated lung and liver ECs from allo-transplanted mice, which showed a dysfunctional phenotype, e.g. the loss of endothelial markers, e.g. CD31 or CD146, were more vulnerable for a TGF-ß triggered EndoMT conversion than respective cells from syn-recipients during severe, established cGvHD. Upon *ex vivo* stimulation, those ECs were characterized with an upregulation of mesenchymal markers such as αSMA or FSP-1 during cGvHD as well as an increased expression of stem cell markers e.g. CD44 or CD133, which are elevated on ECs a priori during cGvHD manifestation and seemed to occur additionally to EndoMT conversion.

3.2.4. Therapeutic treatment of endothelial dysfunction in cGVHD

With relevance for the clinical human setting, the therapeutic intervention targeting the endothelium with the anti-fibrotic agent Pirfenidone was successfully conducted to ameliorate EndoMT and endothelial dysfunction. A bone marrow transplantation model of C57BL/6 → B6D2F1 cGvHD (provided by Prof. MD Bruce R. Blazar and already described in [301]) was treated with Pirfenidone. The pharmacologic intervention already showed a positive effect on the cGvHD progression and morbidity in Prof. Blazars research group. In this project, the cGvHD target organs lung, colon, and liver of treated vs. non-treated mice were analysed with immunohistofluorescence to examine the effect of the treatment on the endothelial function.

Looking specifically at the vasculature (Figure 55), Pirfenidone exhibited remarkable decreases of endothelial vWF, αSMA and FSP-1 expression in the colon, where their expression levels in untreated cGvHD appeared higher. Upon Pirfenidone treatment, endothelial FSP-1 expression levels also showed a significant reduction compared to cGvHD in liver and in strong tendency in lung. Data indicate that Pirfenidone exerts endothelium-protective and anti-fibrotic features in cGvHD and is able to normalize the endothelial function especially in colon and to a lesser extend also in liver and lung Pirfenidone treatment normalized the CD31+ and VECad+ vessel loss, occurring in cGvHD, in all of the three examined organs (Supplemental Figure 12, upper row). Whole-tissue vWF levels, which were found increased in cGvHD colon and lung and indicate vascular damage, decreased to control level in Pirfenidone treated cGvHD mice. Especially the expression of the fibroblastic markers αSMA and FSP-1 in whole organ were drastically increased in cGvHD and adjusted to no-GvHD control niveau in Pirfenidone treated mice in colon, liver and (for FSP-1 in tendency) also in lung (Supplemental Figure 12).

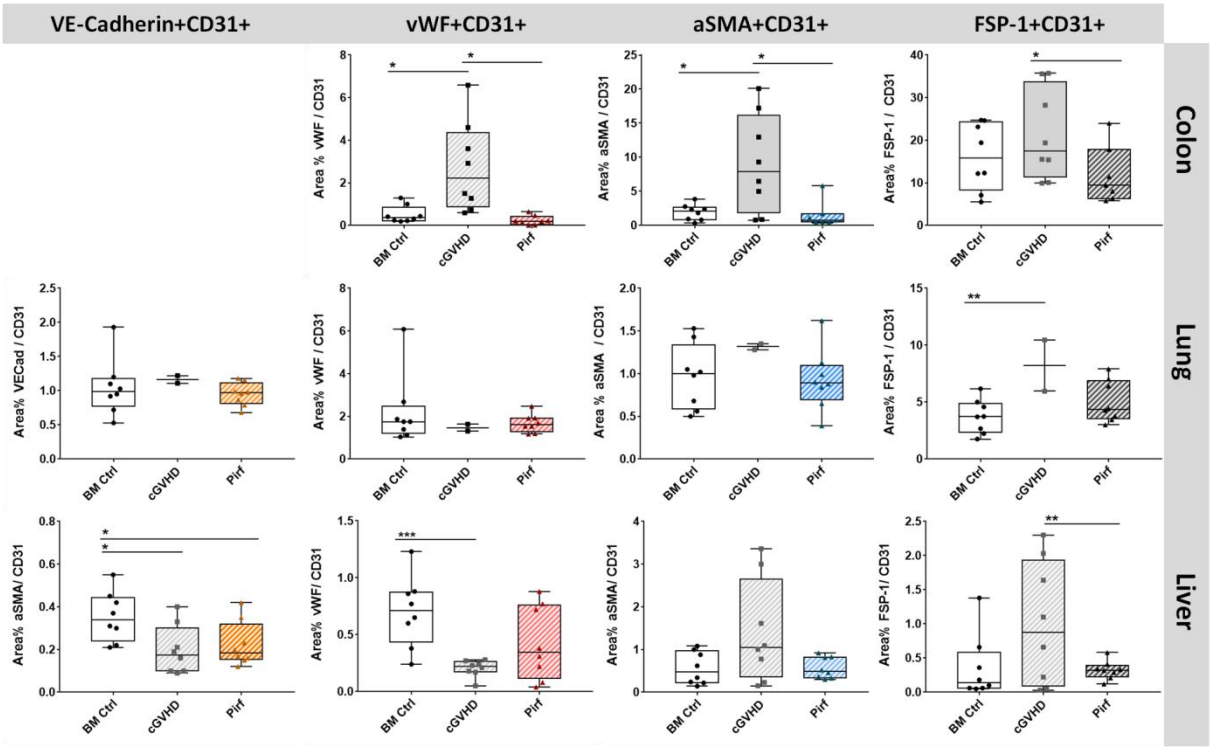

Figure 55: Expression of VECad, vWF, αSMA and FSP-1 co-localized with CD31+ vessels in C57BL/6 → B6D2F1 cGvHD target organs colon, lung and liver of Pirfenidone treated mice. n=8 per group, (except n=2 for cGvHD lung). *P<0.05, **P<0.01, ***P<0.001, ****P<0.0001 by unpaired students *t*-test. Error bars indicate mean +SEM. BM Ctrl = Bone marrow control (No GvHD); Pirf = Pirfenidone treated cGvHD.

We observed that Pirfenidone had the potential to normalize the endothelial dysfunction during murine cGvHD and was able to mitigate an endothelial vessel loss as well as fibrosis/ EndoMT in cGvHD target organs.

3.2.5. Endothelial serum biomarkers in human cGvHD

To transfer the previous results from murine and humanized cGvHD models into patients and to find novel biomarkers for prediction and diagnosis of cGvHD, eight markers with relevance in autoimmune diseases, which resemble cGvHD in their clinical manifestations, have been analysed in human blood serum, aiming to detect endothelial alterations. All markers (Endostatin, CTGF, Endoglin, Follistatin, Endocan, Caspase-3, Fibronectin and Endothelin-1) are involved in endothelial and/ or fibrotic pathology (Table 6). Additionally, TGF-ß1 levels were measured in human serum samples. Serum levels from cGvHD patients diagnosed after NIH criteria were combined to a control group of patients, who received an allo-HSCT without subsequent GvHD development.

Figure 56 demonstrates the TGF-ß1 concentration to be significantly increased in cGvHD patients (49.3 ± 17.74 pg/mL) compared to controls (29.5 ± 10.8 pg/mL), as well as the serum levels of Endostatin (99.46 ± 30.6 vs. 70.8 ± 13.8 ng/mL), CTGF (100.26 ± 26.6 vs. 61.53 ± 24,2 ng/mL), Endoglin (5.31 ± 0.8 vs. 4.41 ± 0.8 ng/mL), Follistatin (5.38 ± 2.9 vs. 2.96 ± 1.2 ng/mL) and Endocan (189.38 ± 127.3 vs. 89.23 ± 54.2 pg/mL). The Caspase-3 concentration in blood serum of cGvHD patients was tendentially higher than of controls (2.05 ± 1.0 vs. 1.35 ± 0.5 ng/mL). There was no difference in levels of Fibronectin (204.0 ± 90.3 vs. 212.1 ± 105.2 ng/mL) and Endothelin-1 (0.63 ± 0.4 vs. 1.46 ±2.1 pg/mL) between the two groups. To conclude, a change of the blood serum concentration of five different endothelial biomarkers was successfully verified in cGvHD patients and this marker combination could serve as a novel biomarker panel for diagnosis of cGvHD.

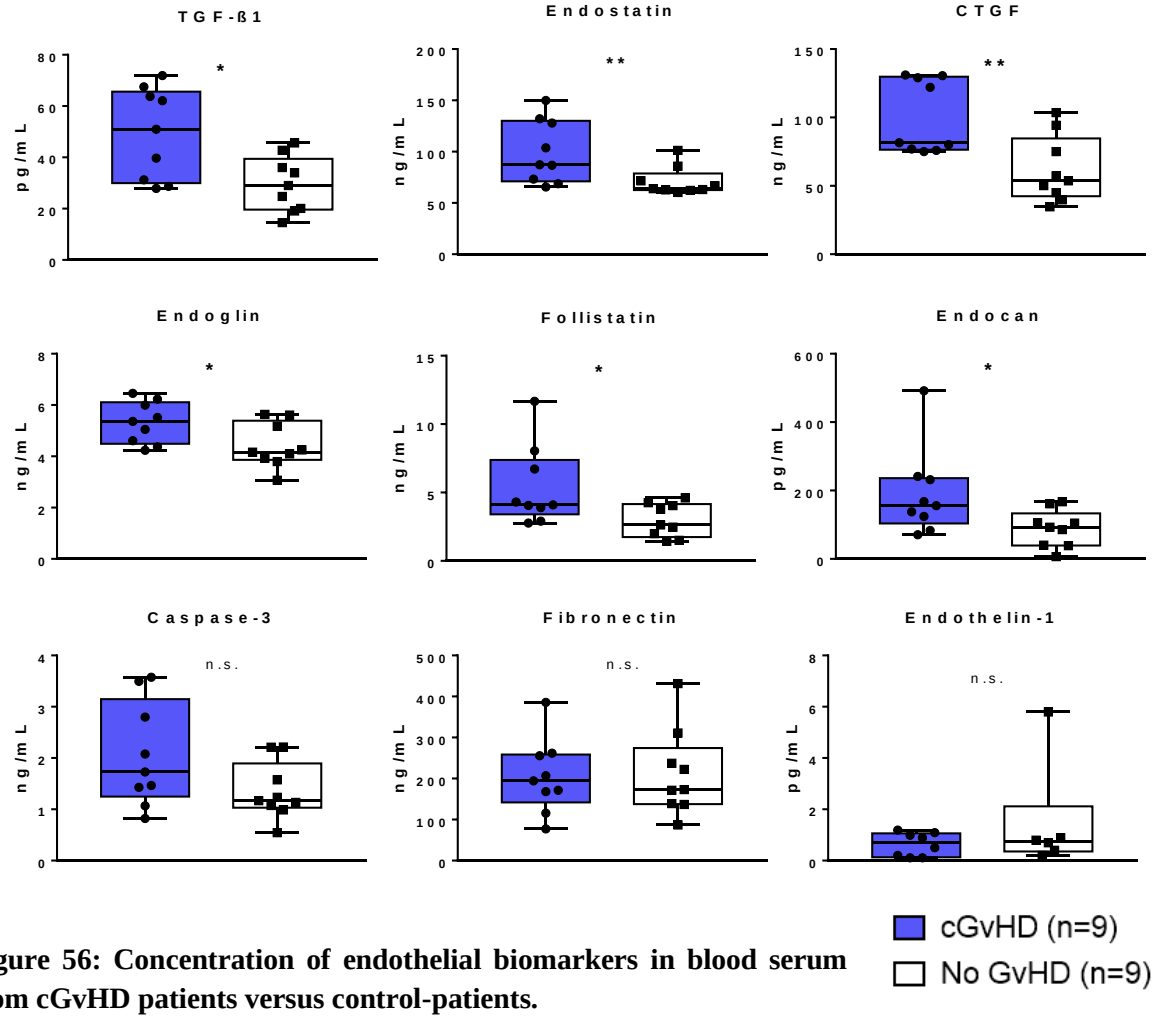

Figure 56: Concentration of endothelial biomarkers in blood serum from cGvHD patients versus control-patients.
Serum was purified from whole blood of diagnosed cGvHD patients and from allo-transplanted patients without clinical signs of GvHD. Serum samples were blinded, randomized and tested for their concentration in ELISAs for eight different endothelium-related biomarkers with relevance in autoimmune diseases. N=9 per group. Error bars indicate mean ± SD, significance was tested with Mann-Whitney-U-Test for unpaired samples. * p<0,05; ** p <0.01; n.s.= not significant.

4. Discussion

4.1. Investigation and the impact of novel targets of the pathological angiogenesis during the GvHD initiation phase

The first part of the present study aimed to investigate novel targets, which regulate the pathological angiogenesis in the initiation phase of cGvHD, thus might be potential treatment structures for cGvHD disease eradication and normalization of the endothelial function. Utilizing a CRISPR/Cas9-mediated approach, we created four endothelial cell lines with depletions of the candidate genes *Eno3* (glycolytic enzyme), *G6pdx* (PPP enzyme), *Acsm3* (FAO enzyme) and *Ang4* (ribonuclease in angiogenesis). The selected target genes were shown to be differentially regulated in ECs involved in pathological angiogenesis during the initial GvHD phase in previous studies [154]. In *in vitro* assays the migratory, proliferative and metabolic potential of the KO cell lines, respectively the influence of the genetic deletion on the endothelial function and angiogenesis was examined under stimulated conditions to mimic an allo-HSCT setting. We found impaired endothelial functions in the *Eno3*- and even more pronounced in the *G6pdx*-KO under allo-stimulated conditions.

Allo-HSCT is known to provoke oxidative stress [320], which in turn negatively contributes to the GvHD pathogenicity [321, 322]. G6pdx as the rate limiting enzyme of the PPP, is the critical determinant for maintaining sufficient cytoplasmic NADPH levels. NADPH is required by the cellular antioxidative machinery to reduce reactive oxidative species (ROS), meaning G6pdx-deficient cells are more susceptible to oxidative stress e.g. caused by an inflammatory insult [323]. Furthermore, *G6pdx* silencing was already shown to cause a decline in proliferation, migration, and tube formation of VEGF-stimulated aortic ECs, while adenovirally-induced *G6pdx* overexpression resulted in an increase of these EC functions.

Since elevated G6pdx levels contributed to heightened vascular proliferation and angiogenesis [244], it might promote and enhance pathologic angiogenesis in initial GvHD. As a possible explanation, G6pdx contributes to the synthesis of pro-angiogenic nitric oxygen (NO) species by providing NADPH as cofactor for the endothelial NO synthase (eNOS) [324]. Taken together, for interventional approaches in GvHD, it might be more beneficial to normalize *G6pdx* expression to physiologic levels and restore the antioxidative features of the enzyme than to completely inhibit its activity.

In healthy conditions, endothelial cells remain quiescent. A recently published study by Kalucka et al. demonstrated that FAO is indispensible for maintaining endothelial quiescence

by increasing NADPH regeneration, which is needed by NADPH-consuming vasculoprotective enzymes. *In vivo* inhibition of FAO elevated not only ROS levels, but also G6pdx in quiescent ECs, possibly attempting to cope the lower NADPH levels for prevention of EC dysfunction [325]. During the early phase of pathological angiogenesis in aGvHD, Riesner et al. arrayed several differentially regulated genes, which are also part of the FAO, among others Carnitine-Palmitoyltransferase II (*Cpt2*), intestinal fatty acid binding protein 2 (*Fabp2*) or *Acsm3* [154], whose KO did only result in minor impairments of endothelial viability and angiogenesis exclusively under C57BL/6 stimulation in the present project. Acsm3, a subunit of the CoenzymeA ligase, is involved in fatty acid uptake into the cell. Taken into account, that elevation of the FAO is a mechanism of ECs to maintain their function, upregulation of the enzyme during GvHD could rather have an endothelial-protective effect, but a genetic deletion of *Acsm3* is not sufficient to influence EC functions. It would be of special interest, if knocking down other genes from the FAO pathway also influence endothelial features during GvHD.

Currently, little is known about the relevance of *Eno3* in disease. The enzyme was discovered to be overexpressed in mutant lung cancer and genetic silencing of *Eno3* resulted in anticancer effects [326]. In metabolism, *Eno3* codes for ß-enolase and is one of three isoforms participating in the distal part of the glycolysis. Since the enzymatic conversion is reversible, enolases also catalyze the first step of gluconeogenesis during glucose-excess [327]. In high glucose-environments, ECs store glycogen synthesized from glucose as a critical energy backup and draw onto it in response to environmental changes, hypoxia or nutrient-deprivation [245]. Discher et al. proposed a regulatory effect of hypoxia on the ß-enolase activity [328]. An upregulation of enolase could be evoked by allo-HSCT-caused hypoxic conditions and the need for increased energy uptake to support vessel sprouting during pathological angiogenesis. We hypothesize, that *Eno3* promotes a switch towards an anaerobic metabolism upon hypoxic stress, hence exerting a protective but at the same time pro-angiogenic effect on ECs. This theory could be corroborated by the finding of Eno1 being upregulated in human pulmonary artery ECs during hypoxia induced pulmonary hypertension. Inhibition of Eno1 restored the hypoxia-induced endothelial dysfunction [329]. It would be of special interest, if targeting other enolase isoforms would likewise influence the endothelial function and alleviate the pathological angiogenesis in GvHD.

When targeting *Ang4*, deletion of this gene did not affect the EC behaviour. *Ang4*, a member of the ribonuclease family, is one of six angiogenins in mice and is exclusively expressed in

the gastrointestinal tract and the pancreas. It was described to harbour functions of an antimicrobial peptide in the intestinal system, therefore suggesting a participation in innate immunity [257]. The roll of *Ang4* in angiogenesis is not completely elucidated: a possible association in gut angiogenesis can be assumed, since an initial intestinal bacterial colonization causes angiogenesis in the mouse [330]. Crabtree et al. postulated a cell type specific angiogenic function of *Ang4*. While bovine corneal and brain ECs and mouse embryonic fibroblasts did not show alterations in proliferation assays, thoracic aortae sections started cellular sprouting after exposure to Ang4 [256]. The angiogenic features of *Ang4* were examined in ECs of cardiac origin, while Riesner et al. found the protein upregulated in the murine GI tract during GvHD, indicating that MCECs might not be the ideal cell line to investigate the proliferative and angiogenic properties during GvHD. To verify the influence of *Ang4* on ECs during pathological angiogenesis, the conducted experiments should be repeated using EC lines of intestinal origin e.g. human intestinal microvascular ECs [331].

In this study, *Eno3*-KO reduced the angiogenic capacities, the proliferation and the migration of the mutated ECs in particular under addition of T cells compared to BALB/c T cells. *G6pdx*-KO ECs displayed a markedly diminished migration, proliferation and a defective tube formation, regardless of the applied murine T cell strain. The idea of applying T cells or serum from two different mice strains as stimuli to mimic allo-conditions originated from the idea to present different haplotypes to the ECs. MCECs are of C57BL/6 background and display H2kb alloantigens. In theory, a stimulus from the same haplotypes could result in milder effects on the endothelial function than a major mismatched stimulus from BALB/c [H2kd] cells. Vice versa, we detected an even more impaired cellular function in C57BL/6-stimulated ECs, which indicates that not only the major haplotypes, but also minor antigens and, as of importance, the cell-cell contacts between ECs and leukocyte receptors may be mainly responsible for endothelial activation and resulting endothelial dysfunction during GvHD. It is common knowledge that leukocyte adhesion molecules are expressed on endothelium in pathological conditions, e.g. during aGvHD [259]. While ICAM-1 is constitutively expressed, E-Selectin, P-Selectin or VCAM-1 are transiently induced only upon stimulation, mainly by cytokines as TNF-α or IL-1. While TNF-α could be synthesized by the added T cells, the latter could be released from the activated endothelium itself [332]. It would be of interest, if a cell free stimulus using TNF-α and IL-1 alone or in combination has the same effects on the endothelial function as the utilized T cells and if E-Selectin or VCAM-1 can be induced by those cytokines during pathological angiogenesis *in vitro*.

4.2. EC metabolism as therapeutic target in GvHD

The progression of GvHD is known to be linked to concomitant metabolic changes in the alloreactive cell environment, affecting different pathways, such as glycolysis, FAO or the PPP. As an example, donor T cells undergo reprogramming towards a pro-glycolytic metabolism upon stimulation by mismatched recipient antigens after allo-HSCT [333]. So far, multiple approaches concentrate on the suppression of donor T cells or APCs, e.g. by the use of glycolytic inhibitors against immuno-metabolic targets for the treatment of GvHD [334]. First attempts seemed encouraging, but metabolic suppression of e.g. alloreactive T cells remains unspecific, since also GvHD-dampening regulatory cell types, e.g. Tregs, are hindered in their catabolism and anabolism and the perpetuation of the GvT-effect, which is maintained among others by regulatory and memory T cell subsets, is compromised [335]. An alternative to attenuate diseases, which are linked to pathological angiogenesis can be seen in targeting the endothelial metabolism [336]. The underlying idea is, that a transient shutdown of the endothelial metabolism will prohibit angiogenesis in sprouting ECs, which have a higher demand for energy and biomass generation [175], independent of the presence of angiogenic factors and without causing cellular damage by a complete metabolic suppression [336]. Reprogramming of endothelial catabolic and anabolic pathways could not only be promising in GvHD, but was also shown to be efficient in ocular neovascular diseases, pulmonary arterial hypertension or cancer [336]. As illustrating example, tumor ECs are characterized to be more glycolytic and express higher PFKFB3-levels in contrast to normal ECs. Blocking of PFKFB3 with low doses of a specific inhibitor or by genetic deletion of a single PFKFB3-allele normalized abnormal tumor vasculature, reduced metastasis and vascular inflammation and improved chemotherapy [181]. Lowering and normalizing dysregulated metabolic processes during GvHD could not only prevent abnormalities in the vasculature, but add a bona-fide therapeutic opportunity to other treatment options, e.g. chemo- or corticosteroid therapy. The pharmacologic intervention of the PPP enzyme G6pdx in GvHD *in vivo* will be discussed as possible metabolic target in the following chapter.

4.3. Pharmacologic intervention of G6pdx to ameliorate acute and chronic GvHD

Anticipating from the gained results in the KO-experiments, *Eno3* and *G6pdx* were nominated as suitable candidates for further research on their potential role as pharmacologic metabolic

targets in GvHD treatment. To prove, the effect of specific inhibitors against *Eno3* (ENOblock) and *G6pdx* (6-AN and Polydatin) on the endothelial function was tested not only in MCECs, but also in MuMECs and in TMNK-1. All of the three tested inhibitors carried out a reduction of the metabolic activity in all EC lines, but migration and proliferation were interrupted more reliable by G6pdx- than by Eno3-inhibition, which displayed results only in TMNK-1. In our assays, Polydatin and ENOblock were not toxic to cells, while 6-AN did show signs of cellular toxicity in higher concentrations >250µM and in a time-dependent manner. Adverse effects as weight loss, hunched posture or nausea combined with an increased lethality by 6-AN treatment were also detected in murine *in vivo* studies [337], disqualifying 6-AN as potential therapeutic substance. Polydatin was well tolerated *in vitro* and *in vivo* and did not show side effects. In a comprehensive review, Karami et al. summarized a magnitude of positive effects of Polydatin in health and disease: it was shown to operate as an anti-oxidant, to have anti-apoptotic, anti-fibrotic and anti-cancerogenous effects and to act protective to the cardiac/cardiovascular, gastrointestinal, hepatic, neurologic, vascular, renal and respiratory system [338].

By investigating the anti-inflammatory properties of Polydatin, the substance improved not only the inflammation-induced footpad edema but executed immuno-protective features in the aGvHD target organs colon, liver and skin, where we found less CD3+ immune cell infiltrates and less damaged tissue. Our findings go in line with a variety of Polydatin's immune-regulating properties, as the modulation of the expression of inflammatory cytokines and cell adhesion molecules, which have already been described: Xie et al. reported Polydatin to exert suppressive functions at ICAM-1, TGF-ß1 and directly block the expression of the pro-inflammatory cytokines TNF-α, IL-6 and IL-1β at mRNA-level [339]. Moreover, it alleviated an inflammatory damage in mice with ulcerative colitis [340] and blocked, respectively enhanced the proliferation of fibroblasts in a concentration-dependent fashion [249].

To our knowledge, Polydatin was not tested in allo-HSCT or in GvHD treatment or prophylaxis so far. Our data show, that Polydatin ameliorated the morbidity of established aGvHD in C57BL/6 recipients when administered early (d+7) after transplantation. The aGvHD-provoked mortality was not influenced by the treatment. In cGvHD, Polydatin treatment did neither affect the mortality nor the morbidity of diseased allo-recipients when delivered as cGvHD emerges from aGvHD, starting from d+35 after transplantation. These results indicate that Polydatin is a potent treatment against the development of aGvHD when administered before disease manifestation. It still needs to be elucidated if prophylactic

treatment is also able to improve cGvHD outcomes. In mice with induced systemic lupus erythematosus (SLE), a chronic progressive autoimmune disorder closely resembled to cGvHD, Polydatin treatment significantly attenuated disease activity by inhibiting the production of reactive oxygen species [341], which are also found to be causative of sclerodermatous modifications in cGvHD patients [342]. In consequence, Polydatin could likely be able to attenuate, if not prevent cGvHD when administered early in disease course, e.g. starting immediately after allo-HSCT.

Of particular importance to our study, Polydatin acted endothel-protective, as it normalized the Endomucin+ vessel density in aGvHD organs, while in comparison the vehicle treated animals showed a vessel loss. As literature demonstrates, many studies prove an influence of Polydatin on ECs: it was described to inhibit the ICAM-1 expression in LPS-stimulated ECs and to attenuate the adhesion of leukocytes and ECs [343]. In line, it inhibited the monocyte adhesion to TNF-α activated ECs and additionally suppressed the expression levels of ICAM-1 and VCAM-1 in ECs *in vitro* [344]. Hu et al. provided evidence of the anti-angiogenic properties of Polydatin, which inhibited the VEGF-induced formation of tubes in HUVECs by binding of VEGF, hence proposing Polydatin as a potential therapeutic agent for angiogenesis-related diseases [250]. To eradicate angiogenesis-related disease complications, anti-angiogenic therapy, among others treatment of different cancers with VEGF-neutralizing antibodies e.g. bevacizumab (Avastin) [345] or Sunitinib [346], has been approved for clinics. Unfortunately, anti-angiogenic VEGF therapy remains challenging because of the inconsistent response rates to variable malignancies, high toxicities, side effects or interactions with chemotherapy [345]. The question, how anti-angiogenic treatments can be improved, is still in doubt. Recently, combined administration of Polydatin was found to decrease the cardiotoxic adverse effects and enhance the anti-cancer effects of Sunitinib *in vitro* [346]. It would be of interest, if a combined treatment of Polydatin/Sunitinib could also mitigate the pathological angiogenesis in GvHD with additionally preventing from long-term treatment toxicity *in vivo*.

4.4. Limitations of EC cultures

Most *in vitro* assays of this study have been performed in MCECs. Advantages of EC lines over primary isolated ECs can be seen in the immortalization of cells, which don’t undergo senescence after a certain passage as well as the fact that experimental results obtained in EC lines can easily be reproduced, since they can be compared to each other, which does not

account for freshly isolated ECs because of their variable donor origin [347]. Above that, primary EC tend to lose specific endothelial characteristics and their responsiveness to treatments and stimuli with higher passages [348]. On the other hand, immortalization of cell lines comes in parallel with a non-physiologic, tumorigenic phenotype, which have to be considered e.g. when transferring experimental results from *in vitro* to *in vivo* approaches. Since the MCEC line is of cardiac origin and the heart does not belong to the classic GvHD target organs, we conducted our research also in different EC lines for refinement of the experimental approach: MuMECs are of murine skin microvessel origin and TMNK-1 is a human liver EC line [315]. All of the used EC lines were presented with specific adhesion molecules (CD31, CD146, ICAM-1, P-Selectin), thus showing the potential to interact with lymphocytes as well as the ability to form tubes and feature contact inhibition. For this project, we concentrated on the vascular endothelium, which has a high heterogeneity, since not only micro- and macrovascular ECs among themselves but also vascular ECs from different organs vary in their morphology, marker proteins or reactivity towards growth factors [348]. The use of different EC lines from varying tissues can help to evade this issue. Nonetheless, data from *in vitro* assays must be interpreted with caution, since ECs can undergo a phenotypic conversion resulting in a loss of specific proteins, when they are isolated from their native environmental niche [349]. As an example, the MCEC line showed an expression of the endothelial marker CD146, but a loss of membrane-bound CD31 in higher passages in our FACS analysis. It is elementary, that the integrity of cell lines is controlled on a regular basis in respect of the transferability to *in vivo* experiments. To a certain point the endothelial environment and the allo-HSCT conditions for mimicking GvHD were simulated *in vitro,* e.g. by 3-dimensional growing of ECs in a matrigel-matrix during tubeformation assay or by allo-stimulation with serum or T cells. Additionally, ECs could be grown in co-culture directly or in transwell-chambers with one or more accessory cell types, e.g. pericytes or fibroblasts, which are indispensible for vascular wall assembly. Furthermore, next to a direct EC- T cell contact, ECs could be provoked with pre-conditioned medium from immune cell suspensions, e.g. out of whole splenocytes, which were isolated from mice and supplement various growth factors, cytokines and other soluble factors into the medium. During all our assays, ECs were grown under static conditions. In the physiologic situation, ECs are exposed to continuous blood flow and shear forces, which could be simulated by cultivation of ECs in special flow chambers and resemble the *in vivo* hemodynamics [350]. Refinement of the EC culture conditions for studies on the pathological angiogenesis during GvHD can help to promote the reliability of *in vitro* gained data, until verified *in vivo.*

4.5. Advances and limitations of cGvHD mouse models

The following section, discussing advances, limitations and outlooks on the established murine cGvHD models was partly released as recent publication 'Novel pre-clinical mouse models for chronic Graft-versus-Host Disease' by Verlaat et al. in 'Frontiers Immunology' [351] and is also recited in the ensuing chapter, as not indicated differently.

The cGvHD pathology is extremely complex [94], thus still not fully understood. The establishment of different cGvHD mouse models has been of central importance for the general understanding of the cGvHD pathophysiology and the pre-clinical testing of reliable treatment strategies for translation into patients. Nonetheless, there is still no single mouse model reliably comprising the diverse pathological and immunological characteristics of cGvHD, because most pre-clinical models show dominant manifestations in limited tissues or do not replicate a stable cGvHD phenotype [117]. Examples of existing limitations are the mere sclerotic phenotype (without other typical features of human cGVHD) in some models, the short experimental duration of 30 to 60 days and the specific target organ tropism (e.g. lung or skin) in other models. Furthermore, nearly all models are transplanted with HSCs generated from BM instead of G-CSF mobilized PB-HSCs, making clinical translation to the human setting less reliable. For that reason, researchers may use more than one model to study cGvHD depending on the scientific hypothesis. The present study attempted to establish pre-clinically relevant murine cGvHD models, which display a high long-term morbidity combined with a low mortality and resemble the diverse manifestations of cGvHD found in patients. The murine parent-into F1 model C57BL/6 →B6D2F1 as well as the BALB/c→C57BL/6 use G-CSF-mobilized splenocytes as stem cell source, while the humanized model is constituted of transplantation of human PBMCs → NSG mice.

Most common, patients receive a stem cell infusion from a fully MHC-matched donor [35, 36], partially MHC-matched unrelated donor [39] or haploidentical donor (first-degree relatives, haploidentical in at least one set of genes) [37, 38]. The latter scenario, which is used increasingly in the last years, is simulated in our B6 [$H2k^{b}$]→ BDF [$H2k^{b/d}$] model that represents a parent-into F1-generation, thus haploidentical immunologic disparity. This setting may be advantageous and more clinically relevant compared to previously described fully MHC-mismatched models [103, 105].

One major improvement to other mouse models, which use the transfer of purified BM cells supplemented with T cells, is the G-CSF mobilization of B6- and BDF donor-HSCs, which

allowed us to perform HSCT of whole splenocytes. HSC recruitment from the BM into the PB applying G-CSF is also applied in clinical allo-HSCT [42]. However, several studies propose an increased risk of cGVHD development after G-CSF–mobilized allo-HSCT [352, 353], but the molecular basis for this hypothesis remains unsolved. According to our engraftment results from the FACS analysis in BDF mice, patients transplanted with G-CSF mobilized BM were found to harbour reduced CD4+ and increased CD8+ T cell numbers compared with non-primed BM, while the total CD3+ T cell count was unchanged in G-CSF primed patients and the platelet recovery was delayed [354]. Data indicate that the HSC engraftment after G-CSF mobilization works similar in mice and humans and that our mouse model might be applicable to study the molecular mechanisms of G-CSF stem cell recruitment for allo-HSCT.

In patients, the onset of cGvHD is fluent, beginning approximately 3 months up to 2 years or even later after transplantation [84]. Additionally, acute GvHD progresses to cGvHD in 70-80% of patients [355, 356]. Our B6→BDF mouse model showed acute GvHD around d+20 after allo-HSCT with spontaneous improvement afterwards. Later on, the animals developed typical cGVHD symptoms, which progressed until day+125, indicating a transformation of acute to cGVHD, as seen in many humans. Scores in the NSG model continuously increased until day+125 without an initial acute GvHD phase, but mortality rates stayed comparatively moderate. It is still not generally known, after which time cGvHD develops in mice, but the majority of published murine cGvHD models run less than 60 days, which might be too short-timed for a complete progression to robustly manifested cGvHD. The diagnosis of murine cGvHD is mainly defined by its clinical phenotype. At d+125, cGVHD mice of both of our models showed phenotypical as well as histological signs of cGvHD. Diseased NSG- and BDF recipients exhibited hunched posture, reduced activity, alopecia, skin scaling, erythema and ocular symptoms as dry and opaque lenses or blepharitis, all of which are frequently described to occur in cGvHD patients [85, 69, 84].

cGvHD simulates characteristics of autoimmune diseases with features of impaired immune tolerance mechanisms, like the involvement of auto- and alloreactive donor-derived T and B cells, the participation of alloantigens and mechanisms of chronic inflammation with subsequent fibrosis [85]. The disease mainly manifests in the target organs skin, liver, lung and the gastrointenstinal tract. In addition, a variety of other organ systems, as mouth, joints and fasciae, muscles, eyes, the hematopoietic system or mucosal tissues may be affected [84]. Our allo- as well as our xeno-HSCT model depicted severe fibrosis and inflammation in the lung, liver, colon and skin of cGvHD mice. In the Masson’s Trichrome Stainings, immune

cell infiltrates and fibrotic depositions as well as sclerosis were particularly found in cGvHD B6→ BDF recipients, where they were related to extensive tissue damage in the respective organ (e.g. epidermal thickening in the skin, hepatitis and steatosis in the liver and bronchiolitis obliterans in the lung and non-infectious colitis in the colon), with all mentioned symptoms contributing significantly to high morbidity and mortality rates after clinical allo-HSCT [357–361]. Our histopathological observations closely resembled the situation in patients, where fibrosis is mostly systemic, standing in contrast to the majority of published sclerotic mouse models, which mainly comprise a cutaneous pathology [103, 96]. It is reported that activated monocytes, macrophages as well as eosinophiles may mediate the induction of collagen production leading to systemic fibrosis [362, 92, 363]. Besides, pro-inflammatory neutrophils contribute to the process of chronic pulmonary fibrosis [364], a manifestation also seen in our cGvHD BDF mice. In existing sclerodermatous cGvHD models, mast cell and eosinophilic cell populations have been found increased in the skin [365] and liver [366] of transplanted mice. This theory is in line with our experimental findings in cGvHD from the BDF model, where CD11b+Gr1+ myeloid cells and macrophages were measured to be significantly elevated in the PB until day 60 after allo-HSCT and also showed signs of increased activation. Furthermore, eosinophiles in the PB and neutrophils in the spleen were shown to depict elevated levels in cGvHD. Since application of G-CSF in donors is known to mobilize especially CD11b+ myelomonocytic subsets, this could be an explanation for the high frequency of aforementioned monocytic and myeloid subsets and the augmented rates of fibrosis in our cGvHD mice. Effector T cells as inflammatory triggers and macrophages and monocytes as fibrotic mediators might be recruited by the presence of chemokines, such as CXCL9 and CXCL10, which were both validated as prognostic cGvHD biomarkers in humans [269, 270] and were shown to be significantly increased in cGvHD but not in controls of our BDF mouse model.

In flow cytometry experiments of cGvHD BDF recipients, we saw a decelerated B cell recovery early as d+20 after allo-HSCT during the acute GVHD phase, which is also observed in transplanted patients [367, 368]. During cGVHD at d+125 after HSCT, we detected massive T and B cell infiltrates in lungs and livers of cGvHD mice in flow cytometry as well as in histological immunofluorescence analyzes. It is known, that impaired B cell tolerance results in persistent activation and exaggerated proliferation of autoreactive and alloreactive B cells and contribute to the human cGvHD pathogenesis, both increasing auto- and alloantibody reactions in cGvHD patients [369, 370]. Still, it has to be further elucidated,

if the B cells in our BDF model are allo- or autoreactive, respectively determining the type of antibody reaction.

Furthermore, we found increased frequencies of CD3+, CD4+ and CD8+ T cells, B220+ B cells and neutrophils in the spleens of cGvHD mice, indicating that the observed splenic damage is evoked by inflammatory lymphocytes. While the induction of GvHD in the BDF mouse model was assumed to be mainly CD8+ driven, both CD4+ and CD8+ T cell subsets were not found to be significantly elevated in PB of cGvHD mice compared to controls at day+125, raising the concept of alternative factors to be responsible for cGvHD progression.

Moreover, we detected a diminished DC frequency in spleens of cGvHD BDF mice at day+125 after allo-HSCT. This resembles the clinical situation, since severe cGvHD is associated with impaired DC recovery and reduced circulating DC numbers, contributing to failing DC-mediated tolerance in allo-HSCT patients [371, 372].

Especially xenogeneic models were criticized to be highly artificial, because T cell reactivity by MHC molecules is restricted between species. Human antigen presenting cells are unable to process and present mouse MHC class II antigens to human donor T cells, making this model predominantly CD4+ T cell dependent [116]. Actually, our data showed primarily human CD4+ T cells to be proliferated and circulated in the PB of NSG recipients until day+125 after HSCT. Interestingly, also the proportion of murine CD45+ leukocytes at day+60 and the population of CD11b+CD11c+ myeloid DCs at day+125 was found increased in cGvHD, supporting the theory that there might be some crosstalk between murine cells, respectively tissue and human cells. Several studies indicate, that human cells can indeed recognize murine xeno-antigens in an MHC I and MHC II dependent manner and that the human CD28 T cell receptor is able to interact with its murine counterpart B7.2, facilitating co-stimulatory signals to donor T cells [112, 373, 374].

Moreover, general weaknesses occurring frequently in murine models are differences in the animal suppliers, age of mice, individual handling techniques or a homogenous microbial gut environment in mice when housed under specified, often pathogen-free conditions [375]. One risk factor for development of cGvHD is an increased age of both donor and recipient [82, 376]. To adapt to this situation, we used B6-donors aged more than 20 weeks and BDF and NSG-recipients aged at least 10 weeks. All mice were housed in open-housing cages and handled without tail fixation by tunnel or cupping techniques that might not only reduce

anxiety but can help to reduce stress-related weight changes, lethargy and other factors, which can adulterate GvHD scoring results [377].

A potential point to modify in the future is the type of conditioning. Transplanted patients are often administered with cytotoxic drugs as busulfan, cyclophosphamide or fludarabine as conditioning regime prior to allo-HSCT [48, 378]. To secure reliable engraftment, our BDF model received total body irradiation, which could be in future refined by applying chemotherapeutic conditioning with busulfan and cyclophosphamide, e.g. as already established for acute GvHD models [113].

Concluding, we were able to establish two improved cGvHD mouse models: an allogeneic, haploidentical B6→ BDF and a humanized PBMC→ NSG Xenograft model. Especially our well-characterized BDF model showed various clinical cGvHD manifestations as inflammation, fibrosis and an altered immunological reconstitution and could be utilized for future pre-clinical research on novel promising cGvHD treatment and prophylaxis strategies.

4.6. Mechanisms of endothelial damage and dysfunction during fibrotic cGvHD

Until today, sparsely is known about the endothelial pathophysiology during cGvHD and its participation in disease progression. A few studies give rise to the assumption, that there exists an endothelial form of cGvHD and that the vascular injury is substantially involved in worse overall prognoses. In 1980, Shulman et al. described “histologic (vascular) findings of uncertain etiology” and an “immunologically-mediated damage against endothelial cells” in cGvHD patients [266]. In 2003, Biedermann et al. identified a microvessel loss together with perivascular CD8 T cell infiltrates in the skin and found higher plasma concentrations of vWF of cGvHD patients [226]. Apart from that and in contrast to acute GvHD [228], the endothelial condition during cGvHD has been sparsely characterized. Most of the conducted studies showed a microvessel loss by staining of single vascular markers in single organs, but not on a systemic level. In the present project, we were able to characterize an endothelial form of cGvHD in different target organs by application of various endothelial markers alone or in colocalization analyses, which helped us to describe the profound endothelial damage occurring *in vivo* in murine cGvHD.

We found a decline in CD31+ and VECad+ vasculature in the murine cGvHD recipients, indicating a vessel loss in skin, liver, colon and aorta. Our results were corroborated in part in

the Xenograft mouse model, where a CD31+ vessel loss arose in colon and liver, while the VECad expression was not altered in any of the organs in cGvHD. vWF levels were elevated in skin, liver and aorta of BDF mice and in liver and colon of NSG recipients in cGvHD. The observations of a microvessel loss together with elevated vWF expressions go in line with the results from the Biedermann study [226]. The adherens-junction protein VECad is exclusively involved in leukocyte paracellular migration through the endothelial barrier [187]. Mice, which were genetically modified to display enhanced VECad-mediated adhesion showed an altered site-specific permeability due to a dysfunctional leukocyte extravasation and defective lymphocyte recruitment to inflamed tissue sites [379]. As a corollary, a loss of VECad in cGvHD liver, colon and skin terminates in dysfunctional barrier integrity, resulting in more severe inflammation, which can indeed be found in the cGvHD target organs. In cGvHD lung we detected massive immune cell infiltration despite increased VECad expression, which leads to the assumption that different mechanisms might be involved in pulmonary infiltration. Together with high VECad levels, we detected an increase in CD31 in the lung of BDF mice, but a decrease in vWF, which led us to the hypothesis, that the pulmonary endothelium, differently from the other organs, undergoes rather angiogenic or vascular remodeling than vascular injury in cGvHD. Both of the established cGvHD mouse models show severe pulmonary inflammation and infiltration, most akin to bronchiolitis obliterans, which is considered as the only pulmonary complication with diagnostic value for cGVHD [69]. Apart from the frequently emerging hepatic VOD, there was the more rare pulmonary VOD, a clinical form of pulmonary hypertension, described after allo-HSCT [380–382] and especially in association with cGvHD [383]. Pulmonary hypertension is caused by an increased vascular resistance, which is attributable to vascular remodeling due to EC hyperproliferation, disordered angiogenesis and a loss of small arterioles [384]. These pathologies might have led to a loss of small vessels in favour of angiogenesis in big veins and arteries, which were microscopically scanned in immunohistological stainings. As a result, more CD31+/VECad+ area was measured, although the total amount of vasculature did not increase, but was only transformed. It should be further characterized, if a form of pulmonary VOD/ hypertension appears frequently after allo-HSCT and in murine cGvHD.

To verify the impaired endothelial integrity in cGvHD, we additionally analysed the alternative tight junction protein ZO-1 and the pericyte marker NG2. In the BDF model, total tissue as well as endothelial ZO-1 expression was diminished in all investigated organs, in NSG mice lung and colon were especially affected. NG2 levels were lower only in liver. Loss of ZO-1 provided strong evidence of disrupted endothelial junctions and increased

permeability for leukocytes to enter epithelial tissue regions without the tightly controlled EC barrier function of targeted diapedesis. Cordes et al. delineated similar results in colon and liver in severe aGvHD at d+15 post-transplantation, [155], while Noth et al. described a loss of alternative tight junction protein occludin, but not of intestinal ZO-1 at d+6. Since both studies concentrated on the total tissue expression of the analysed tight junction markers, which are also expressed on epithelial and not exclusively at ECs, they rather show an increased total permeability of intestinal epithelium. Co-localizing CD31+ with ZO-1 helped us to prove a specifically impaired endothelial permeability in cGvHD for the first time. In an *ex vivo* Paw edema assay in cGvHD NSG recipients we detected an increased potential for tissue edema and inflammatory cell infiltration, which might be due to increased vascular leakiness. However, augmented leakiness could not be proved in an Evans Blue assay in the NSG model. For those studies we used a small number of samples, so the results stay only preliminary, thus should be interpreted with caution and repeated with a bigger sample size, respectively in the BDF model.

We speculate, that cGvHD is propagated through an increased EC barrier disturbance and that a normalization of the vascular permeability could help to ameliorate the cGvHD morbidity or treatment outcomes. With help of the murine BDF model, a functional characterization of the endothelial integrity, e.g. by implementing an Evans blue assay to evaluate vascular leakiness, should be performed. Furthermore a spatial quantification of the grade of endothelial permeability during the course of GvHD could be investigated.

Both of the established mouse models displayed significant fibrotic and sclerotic manifestations, hence it is not surprisingly that we found increased mesenchymal markers αSMA and FSP- in cGvHD. αSMA is a marker of vascular smooth muscle cells and pericytes [385] and is de-novo synthesized in activated fibroblasts participating in physiologic and pathologic tissue repair, providing them with a contractile phenotype [386]. Except from cardiac and aortic ECs [387], αSMA is not expressed on cells of endothelial origin under physiologic conditions. Same applies to FSP-1, which is a classical fibroblast marker and also found in inflammatory cells, but not on vascular cells, with exception in diseases [388]. As a highly interesting observation, we detected higher levels of CD31/FSP-1 double positive cells in liver and colon of our BDF model and in all analysed organs of the NSG model in cGvHD. Moreover, we found CD31/αSMA/FSP-1 triple positive ECs in all examined target organs in cGvHD, but not in controls. This finding encourages our assumption, that we first described the transitional process of ECs towards a mesenchymal phenotype, called EndoMT, to occur during cGvHD and that the transition participates in the endothelial dysfunction and the

cGvHD fibrotic progression. The phenomenon of EndoMT in cGvHD is further discussed in chapter 4.8.

Indeed, combining all the results from our immunohistofluorescence microscopy studies and recalling that the endothelium is no rigid compartment, there is steady cellular transformation and vascular remodeling. Concluding, there seems to be a vital necessity for the use of more than one endothelial marker and more than one mouse model to describe the vascular state in the cGvHD pathology on a systemic level. Since the endothelium is very heterogenic, tissue-specific endothelial adaptations to stress, e.g. inflammation, fibrosis or hypoxia, can explain why endothelial damage occurs locally [162], even if EC dysfunction in cGvHD is systemic. Applying a set of different markers in the two mouse models, we were able to describe a loss of endothelial microvessels, an increased endothelial damage with a decreased endothelial integrity and a substantial abundance of EndoMT during murine cGvHD. Nevertheless, the results should be confirmed within other experimental approaches, e.g. by analysis of the already tested markers on protein- and mRNA-level, utilizing Western Blots and RT-qPCR of isolated ECs from cGvHD organs.

Phenotypic heterogeneity is a hallmark of the endothelium since ECs, during physiological angiogenesis and during pathological processes, undergo steady alterations. In cGvHD and in general post-HSCT, not only mature ECs are prone to endothelial damage, but also EPC and CEC subsets are frequently described [263]. To complement the characterization of an endothelial form of cGvHD, we further analysed the various endothelial immunophenotypes spotted after allo-HSCT with FACS. In isolated ECs from liver and lung of cGvHD recipients, we measured markedly less CD45+CD34-CD146+ mature ECs in lung. This finding coincides with the microvessel loss we found in cGvHD lung and liver in the immunohistological analysis.

We detected a higher frequency of HSCs and EPCs in cGvHD. The former is unsurprising, since GvHD affects the hematopoietic reconstitution and has been associated with a failure of donor HSCs to functionally engraft in the recipient, leading to hematopoietic dysfunction [389]. The latter origin from a subset of hematopoietic progenitor cells with the feature to differentiate into proangiogenic cells, which home to sites of endothelial damage to regenerate and repair the normal vessel integrity [390]. Evidently, those proangiogenic EPCs are recruited from the BM by angiogenic factors and contribute to vascular health by incorporation into the vessel wall during various pathologic conditions [391, 392]. It is not fully clear, which factors are needed to differentiate from HSCs into EPCs, but Wara et al. reported that among others TGF-ß1, which we found increased in serum of cGvHD patients

but not in controls, mediated a conversion of myeloid progenitors into EPCs under ischemic conditions [393]. These specific cells express classical stem cell markers such as CD34, CD133, Sca-1, c-Kit as well as traditional endothelial markers, such as CD31, VEGF or CD146 [394]. It remains controversial whether EPCs are protective or detrimental to the cGvHD progression. During aGvHD, a recently published report described reduced clinical and pathological scores as well as improved survival and less immune cell infiltration in a mouse model treated with EPC infusions [395]. In humans, opposing results are published: Two studies measured decreased EPC counts in aGvHD patients in the blood and BM [396, 397], while another study found increased EPC levels in aGvHD [398]. However, since the definition of the EPC phenotype is inconsistent and there is no consensus on how to isolate and categorize cell types, different studies apply different surface markers for the EPC categorization, which makes it difficult to directly compare results from single studies. It is possible that EPCs are recruited to the sites of vascular injury early after transplant, but only until a certain severity of damage. Since hematopoiesis is impaired during GvHD, EPC numbers might stay lower and are not sufficient to repair endothelial damage resulting from chronic inflammation and persistent endothelial activation. Hence, it has to be further investigated, if the evolvement of EPCs during acute and chronic GvHD is a temporally regulated process and if certain GvHD grades/ scores can be correlated to the EPC count. Nevertheless, this cell type represents an easily detectable biomarker in the blood of GvHD patients, thus could be helpful for diagnosis, prevention or monitoring of treatment responses to cGvHD.

In ECs TGF-ß signaling is implemented via two distinct receptors: ALK 5, which represses the proliferation and migration of ECs and ALK1, which stimulates the two [399]. Both receptors work oppositely inhibitory to one another and act in concert with Endoglin (CD105). Overexpression of Endoglin inhibited ALK5 signaling and promoted proliferation induced by ALK-1, whereas absent Endoglin expression resulted in growth arrest because of increased ALK5 activity [400]. During cGvHD, we found reduced expression of ALK5 in cGvHD liver and lung ECs of BDF recipients compared to syn-controls and higher endoglin levels is serum of cGvHD patients. Higher endoglin levels together with an reduced ALK5 expression, which might be provoked as a preventive reaction to the high endoglin levels, should lead to dysbalanced TGF-ß signaling. Since TGF-ß signaling plays a vital role in EC activation and proliferation, in inflammation as well as in fibrosis [399], serum endoglin levels and the expression of ALK1 on ECs from cGvHD mice could provide insights in the perturbed TGF-ß pathway and might release potential therapeutic targets.

Directing the development and maintenance of the vasculature, ECs secrete 5 distinct platelet-derived growth factors to recruit PDGF receptor-expressing pericytes and vascular smooth muscle cells to stabilize the endothelial network [401]. Not surprisingly, the expression of PDGFRβ was decreased in CD146+ pericytes in cGvHD liver as well as in lung of BDF recipients, which implies a destabilized vessel network and increased vascular permeability in cGvHD. Elevated vascular leakiness and permeability heightens the risk for treatment failure and more severe inflammation, therefore the vascular integrity should be functionally qualified by Evan's blue or FITC-lectin-perfusion assays.

Up to a certain point, the data from our FACS results have to be interpreted with caution. As it is the most commonly recommended experimental protocol, we used enzymatic collagenase digestion to isolate ECs from the particular organs. Advantageous is the high yield and great purity of ECs after collagenase digest, but enzymatic tissue disintegration may lead to damage and loss of certain surface proteins [402], which are of relevance for a successful FACS staining. For repetitions of this experiment, other isolation methods should be taken into consideration to maintain the integrity of surface proteins.

Ocular GvHD is a common complication in humans during cGvHD and we detected ocular disturbances in allo-HSCT BDF recipients as well. In a preliminary study, we detected higher frequencies of CD4+ and CD8+ T cells in the eye and adjacent eyelids in cGvHD mice than in controls, while lymphatic (Lyve-1) and vascular (CD31) EC counts were unchanged. Gehlsen et al. described similar results in a chemotherapy-conditioned aGvHD mouse model. The group found higher CD4+ and CD8+ levels in lacrimal glands and in eyelids in aGvHD, as well as increased lymphangiogenesis in the cornea, but no significant change in CD31+ or VEGF+ vessels in cornea or conjunctiva [403], indicating that rather immune cell infiltration and lymphangiogenesis is involved in ocular GvHD progression. To date, it remains unclear if the aGvHD and the cGvHD ocular manifestations differ in their distribution patterns of infiltrating donor immune cells and to which extend lymph- and hemangiogenesis contribute to ocular complications in both of the different disease entities. So far, the estimation of the ocular manifestations of our cGvHD mouse model is of observing nature. In some allo-HSCT recipients we monitored, same as described frequently in patients, blepharitis and swelling of the lacrimal glands as well as dry eye lenses [404], but did not quantify the percentage of affected mice. Regular experimental ophthalmic monitoring in a bigger sample number, as the Schirmer's test or corneal fluorescein staining as performed by Gehlsen et al. [403] could help

to statistically determine the frequency of murine allo-HSCT recipients developing ocular cGvHD manifestations.

4.7. Therapeutic targeting of the endothelium in fibrotic cGvHD after allo-HSCT

The anti-fibrotic and anti-inflammatory substance Pirfenidone, which is an inhibitor of TGF-ß production, respectively TGF-ß associated collagen production in fibroblasts [405, 406] and suppresses the production of pro-inflammatory TNF-α, IL-6 and IL-1ß [407], was shown to be a potential therapeutic agent against e.g. pulmonary, hepatic or cardiac fibrotic diseases as reviewed in various *in vivo* projects by Schaefer et al [408]. After translating those promising results from previous *in vivo* studies to a clinical phase III trial, the drug was approved by the US Food and Drug Administration for the treatment of idiopathic pulmonary fibrosis, where it reduced the progression of the disease and improved the lung function in patients [409]. Administered in an elegant *in vivo* study by Du et al., Pirfenidone showed to effectively ameliorate the cGvHD morbidity in a murine bronchiolitis obliterans BM transplantation model. The authors demonstrated, that Pirfenidone treatment reversed pulmonary fibrosis, TGF-ß production in macrophages as well as allo- and autoreactive B and T cell subsets [301]. In our own investigations, Pirfenidone normalized the endothelial dysfunction, mitigated the transplant-related CD31+ and VECad+ vessel loss occurring in cGvHD target organs colon, liver and lung and alleviated the fibrotic changes as well as the endothelial transformation processes, by decreasing endothelial vWF, αSMA and FSP-1 expression especially in colon and liver. These results indicate, that the endothelium is indeed involved in the fibrotic pathology during cGvHD and that Pirfenidone is a suitable substance to not only regulate fibroblastic or mesenchymal cell types, but also to positively protect the endothelium against damage during cGvHD. Employing the here established murine cGvHD models, which show endothelial damage as well as systemic sclerosis and fibrosis, it should be investigated if Pirfenidone administration is sufficient to alleviate the morbidity and mortality of cGvHD and if Pirfenidone-related normalization of the endothelial function might possibly be beneficial to minimize endothelial damage resulting from pre-transplant conditioning. A combined Pirfenidone treatment together with other cGvHD therapy approaches, e.g. corticosteroid therapy could help to minimize the therapeutic toxicity and improve the overall outcome of the disease.

4.8. EndoMT in cGvHD

To our knowledge, Endothelial-to-mesenchymal transition (EndoMT) has not yet been shown to participate in endothelial dysfunction and multi-organ fibrosis, leading to the exacerbation of cGvHD, but the transitional process has been described to play a role in various diseases, which closely resemble the cGvHD pathophysiology, e.g. systemic sclerosis and pulmonary fibrosis [410, 411], in cancer [412] or in cardiovascular pathologies such as atherosclerosis [413]. During EndoMT, ECs detach from the vessel wall and invade the underlying tissue by gaining migratory and invasive features from acquiring mesenchymal markers, such as αSMA, FSP-1, vimentin or N-cadherin and inversely lose their endothelial markers e.g. CD31, CD146, vWF or VECad as well as their cell- and tight junctions [414].

For the first time, this study managed to elicit a transition of ECs towards a mesenchymal phenotype in cGvHD *in vivo*, hypothesizing that this EndoMT process is partly involved in the propagation of tissue-fibrosis and cGvHD progression.

Next to the loss of vessels and endothelial junctions we found in animals with severe fibrotic cGvHD, we detected a proportion of CD31+ ECs, also carrying the mesenchymal/myofibroblast markers FSP-1 and/or αSMA, which are normally not expressed on ECs. Quantifying co-localized CD31+αSMA+ or CD31+FSP-1+ ECs or respectively triple positive cells, we measured significantly higher proportions of these particular subsets in cGvHD than in controls in the BDF- and in tendency also in the NSG mouse model. Our results indicate that there exists an EC population in cGvHD, which is positive for both endothelial as well as mesenchymal markers, probably caused by EndoMT and that this subset might contribute to the pathology of cGvHD.

During our investigations, we found differently distributed expression patterns of EndoMT-related molecules in different cGvHD target organs. Various *in vitro* studies provided evidence, that an EndoMT does not occur equally in involved tissues, but is depending on the environmental conditions, such as the EndoMT-inducing factor, the tissue origin of the ECs [415] the ambient cytokine milieu [416], and the activated downstream signaling-pathway [417]. Furthermore, the stability of the induced EndoMT-phenotype in ECs is affected by the duration of EndoMT-stimuli [418, 208] or the quality of the EC-surrounding extracellular matrix [419]. Concluding, unevenly distributed EndoMT in various cGvHD target organs can be explained by the magnitude of regulatory factors, but becomes manifested lately as a non-

reversible, permanent alteration of the endothelial towards a mesenchymal phenotype in a setup of chronic tissue injury.

FSP-1, which we used to quantify converted ECs, is a widely accepted marker for specifically targeting fibroblasts. However, it is also expressed in myeloid cells and inflammatory macrophages, especially in the liver [420]. For that reason, it is important to co-localize the triade of signals composed of CD31, FSP-1 and αSMA in order to prevent co-localization artifacts from only two markers, resulting e.g. from superimposition of endothelial tissue and immune cells, which can happen during slicing the cryo-conserved organs. Furthermore, FSP-1 is not expressed on myofibroblasts, which are positive for αSMA and commonly referred to as the pro-fibrotic subtype [420]. Both makers, αSMA as well as FSP-1 are upregulated post-injury and a subset of double positive fibroblasts has been reported to be associated with various diseases [421–423]. Next to the bigger population of αSMA+/FSP1+/CD31+ ECs in immunehistology as well as in FACS analysis, we found higher frequencies of αSMA+/FSP1+/(CD31-) myofibroblasts in cGvHD hepatic and pulmonary tissues that in control tissues, which is a clear sign that the fibrotic cell types are activated upon tissue injury post-transplantation, leading to the massive grade of fibrosis we detected in the Masson-staining in cGvHD. FSP-1 is not only a marker of EndoMT, but could also be a trigger for EC dysfunction and increased vascular leakiness. Luo et al. treated cultured murine primary ECs and HUVECs with FSP-1, which resulted in endothelial leakage due to increased expression of adhesion molecules and decreased expression of the tight junction molecules VE-cadherin, ZO-1, and Occludin [424], which is exactly the same expression pattern we found on dysfunctional ECs during cGvHD.
Aiming to prevent EndoMT and endothelial damage in cGvHD by therapeutic FSP-1 intervention, the specific FSP-1 inhibitor Pirfenidone was successfully used in a cGvHD mouse model. Pirfenidone administration did not only ameliorate cGvHD signs in mice [301], but reliably prevented endothelial damage by normalizing the vessel loss or the overexpression of fibrotic / EndoMT markers as αSMA or FSP-1 in our study. Thus, Pirfenidone could be a potent therapeutic agent not only against cGvHD, but also be utilized for the treatment of endothelium-related complications after allo-HSCT, such as VOD/SOS or TAM.

One major potent EndoMT-trigger is TGF-ß [414]. In ECs, as described in the previous chapter 1.3.6, TGF-ß signals through two canonical TGF-ß receptors, of which ALK1 expression is mainly restricted to ECs and leads to EC proliferation and activation, while

ALK5 signaling quiesces ECs [425]. ALK5 expression was diminished on ECs from murine cGvHD target organs, indicating an increased ALK1-promoted signaling, which might most likely result in aberrant TGF-ß binding, bolstered fibrosis and enhanced EC activation, which in turn promotes elevated immune cell recruitment and long-term EC inflammation and dysfunction. Indeed, when we stimulated MCECs and MuMECs with TGF-ß *in vitro*, the ECs lost their angiogenic properties and did not built tubes in matrigel assays. The migration was enhanced in scratch assays 3 hours after wounding, implicating that the cells rapidly gain contractory and migratory properties of fibroblasts. TGF-ß stimulation for 24 to 48 hours resulted in enhanced metabolism and viability, while both were decreased in contrast to non-stimulated cells after 72 hours. This observation may result from the fact, that TGF-ß has stimulatory as well as inhibitory effects on ECs, depending on the duration, context and microcellular environment of its release [414, 426]. Furthermore, the cellular shape of TGF-ß stimulated EC lines was significantly altered towards a long, spindle-like phenotype typical for fibroblasts. When stimulating *ex vivo* isolated ECs from cGvHD mice with TGF-ß, the cells lose their remaining endothelial receptors and upregulate mesenchymal markers and modify the expression of EndoMT-related transcription factors, such as SMAD2 or Snail. These results suggest that ECs from cGvHD animals are more vulnerable to EndoMT upon *in vitro* TGF-ß stimulation and that the EndoMT process might be participating in endothelial apoptosis and damage, causing vascular loss in cGvHD.

When analyzing both the *in vitro* transformed EC lines and the *ex vivo* isolated and TGF-ß stimulated murine hepatic and pulmonary ECs by FACS, we measured higher frequencies of CD44+, CD105+ and CD133+ cells among the TGF-ß treated ECs lines and also in the primary murine ECs. In cGvHD recipients, expression levels of all three markers was fundamentally increased in lung and liver ECs compared to non-GvHD recipients and TGF-ß stimulation did further increase the expression of the respective cell markers in cGvHD.
The cell surface adhesion receptor CD44 was associated to contribute to EndoMT [427] and moreover described to participate in angiogenesis in various pathologies by regulating diverse ECs functions, such as proliferation, migration, adhesion, invasion, and communication with the surrounding microenvironment [428]. Endoglin (CD105) was not only associated with angiogenesis, but also with inflammatory conditions. Torsney et al. reported a low endoglin expression in quiescent endothelium, which spatially and temporally changed to increased levels during endothelial activation and persistently high amounts correlative with persistent T cell infiltration [429]. Since endoglin is an accessory TGF-ß receptor, it is highly likely that it

also plays a role in the establishment of EndoMT and should be a target to further investigations, especially when deciphering the EndoMT mechanisms during cGvHD.

The progenitor marker CD133, which we found upregulated on ECs during murine cGvHD, is limited to a subset of BM-derived endothelial colony-forming cells (ECFCs) that display a high angiogenic capacity, contribute to vessel regeneration and modulate postnatal vascularization. Upon endothelial damage, CD133+ EPCs are activated to proliferate and differentiate into damaged tissue in order to repair it [430]. However, in patients with diabetes mellitus or systemic sclerosis, high levels of dysfunctional ECFCs have been observed, which do not effectively reduce endothelial co-morbidities [431, 432]. As a hypothesis, dysfunctional ECFCs promote a variety of inflammatory and profibrotic features, such as EndoMT during cGvHD and moreover cause the formation of vascular lesions and the loss of capillaries. It should be further elucidated, to which extend the ECFCs execute colony-forming actions and have the ability to maintain tissue repair in damaged endothelium in cGvHD.

Above from TGF-ß, the initial mechanistic causes for EndoMT have not yet been fully elucidated, but as reviewed by Piera-Velazquez et al., studies suggest that certain factors, can trigger the transition, such as Notch- and Hedgehog signaling pathways, Wnt-signaling, Caveolin-1, Endothelin-1, irradiation or Hypoxia [213]. Particularly with regard to an endothelial protection, intervention against EndoMT triggers, which also play a role in physiologic endothelial regulation or pathology, e.g. Endothelin-1 or Hypoxia with specific inhibitors could be beneficial for preventing endothelial damage in cGvHD. As example, the agent 2-methoxyestradiol was able to prevent EndoMT in irradiation induced pulmonary fibrosis by inhibition of the transcription factor HIF-1α, a key regulator responsible for cellular responses to hypoxia [433]. Other research groups successfully blocked EndoMT in ECs from systemic sclerosis patients by administration of Macitentan, an ET-1 receptor antagonist [434] or by using Bosentan as inhibitor in murine EndoMT [435]. Application of these substances in cGvHD patients might help to prevent not only EndoMT, but to normalize the endothelial function and improve treatment responses, the GvHD disease progression as well as the overall severity of cGvHD in patients.

Another promising approach for targeting EndoMT in GvHD poses the therapeutic manipulation of the endothelial metabolism. During acute GvHD, Riesner et al. identified a variety of endothelial candidate genes, which were differentially regulated in diseased mice, among others carnitine palmitoyltransferase II (CPT2), an enzyme catalyzing the oxidation of

long chain fatty acids. Xiong et al. showed that the induction of EndoMT is accompanied by reduced FAO. By conditional deletion of endothelial CPT2 in mice, they detected augmented embryonic EndoMT concomitant with cardiac valve thickening and increased vascular permeability, thus demonstrating that FAO is indispensible for maintaining normal EC functions [219]. In the first part of this study, endothelial functions, such as angiogenesis, migration or proliferation were successfully influenced by genetic deletion or pharmacologic inhibition of genes regulating the endothelial metabolism, among others *G6pdx* (PPP) or *Eno3* (glycolysis). It would be of special interest, if a genetic or pharmacologic disruption of the candidate genes *G6pdx* or *Eno3* is also sufficient to ameliorate EndoMT in GvHD. In general, results demonstrate that a therapeutic intervention of the endothelial metabolism could be a game changer in treating not only pathological angiogenesis, but also EndoMT-linked pathologies.

Once established, the newly EndoMT-converted mesenchymal cells might further amplify the deposition of extracellular matrix components, finally leading to severe fibrosis in cGvHD. As reviewed by Wynn et al. the immunologic mechanisms underlying cGvHD fibrosis are complex and not fully understood. Acute inflammatory responses e.g. due to recipient conditioning, the allo-HSCT itself or subsequent immunosuppressive medication consequently lead to a persistent immune and EC activation and to early endothelial damage. Injured endothelium releases chemo-attractant molecules to mobilize immune cells to sites of tissue injury, culminating in chronic inflammation and further tissue damage, which initiates the fibrotic cascade. Ultimately, fibroblasts are activated (i.e. by TGF-ß) to become collagen-producing myofibroblasts [93]. TGF-ß, which engages pleiotropic functions in many physiological and pathological processes in the immune system, is the central mediator to initiate tissue fibrosis [218], but is not sufficient to sustain it. During our investigations on the endothelial condition in cGvHD, additional mediators exerting functions in the TGF-ß pathway, such as TGF-ß itself, endoglin, ALK5 or CTGF repetitively came into focus and might be potential molecules for therapeutic targeting against EndoMT in cGvHD. Additionally, other dysregulated factors such as an aberrant B cell tolerance with uncontrolled autoantibody production [91] or pro-inflammatory cytokines e.g. TNF-α or IL-1ß [93, 436] may support the excessive deposition of extracellular matrix in myofibroblasts during cGvHD. Indeed, in our murine cGvHD mouse models, a massive B cell infiltration as well as a tendency of higher TNF-α or INF-γ cytokine levels encourage this theory. Drawing appropriate conclusions, endothelial damage, possibly resulting at least in part from EndoMT

and fibrosis, a hallmark manifestation of cGvHD, might be intricately linked to each other and should not be considered independently.

For cGvHD we propose a temporal disease progression as the following: similar to aGvHD, there might be initial endothelial activation and proceeding angiogenesis, elicited by several yet partly unknown factors, as pre-transplant conditioning, inflammation due to the alloreactive donor-immune cells or e.g. the use of G-CSF. In *in vitro* and *in vivo* studies Bussolino et al. observed an EC activation resulting in enhanced migration and proliferation provoked through G-SCF. Moreover, they described changes in the cellular shape and a reorganization of the cytoskeleton, by which ECs attain a migratory phenotype [437]. Cytoskeleton remodeling is also an elementary hallmark of ECs in EndoMT [438], thus G-CSF could be one potent stimulator of the endothelial transition. Together with the propagating chronic inflammation and the developing fibrotic depositions in the cGvHD target organs, ECs might systemically undergo a switch in their pheno- and genotype towards a mesenchymal signature, further contributing to fibrosis and aggravating the effectiveness of therapeutic intervention of EndoMT against cGvHD.

4.9. Establishment of novel endothelial biomarkers for cGvHD prediction and diagnosis

The fact that the multitude of clinical cGvHD subtypes have not been fully characterized until the present day and that conditioning and clinical practice in treating cGvHD differ between study centers, complicates a search for reliable diagnostic biomarkers for cGvHD patients after allo-HSCT [439]. Unless considerable progress in the identification and validation of novel biomarkers has been achieved [440], there is still no consensus on most markers. One of the few verified candidates for cGvHD prognosis is the B-cell activating factor (BAFF) [441]. In 2016, Yu et al. published a 4-protein panel (ST2, CXCL9, matrix metalloproteinase 3 and osteopontin) for diagnosis and prognosis of cGvHD, which was validated in two independent cohort studies on cGvHD patients [88]. In multicentre analyses, CXCL9 as well as CXCL10 have both been shown to be elevated in serum of patients during cGvHD [86]. Of all aforementioned markers, only BAFF and CXCL10 could be evaluated in two independent, replicated cohort studies as valuable biomarkers in cGvHD diagnostics [270].
In the course of this project, we were able to characterize and describe a profound endothelial damage and dysfunction during established cGvHD, giving rise to the probability of

endothelial biomarkers being sensible tools for the diagnosis of cGvHD. Based on our previous data, evidence indicates an imbalance between angiogenic factors, which foster tissue repair and endothelial factors, which cause inflammation and promote tissue damage. On that purpose, serum levels of nine angiogenic or endothelium-related markers were screened after allo-HSCT. We found significantly elevated levels of Endostatin, CTGF, Endoglin, Follistatin, Endocan and TGF-ß1 in serum of cGvHD diagnosed patients compared to patients, which received an allo-HSCT but did not develop signs of GvHD post transplant. Each of the markers plays a role in EC regulation, vascular development or in endothelial pathology during disease.

As a first potential endothelial biomarker, Endocan is synthesized by vascular ECs and can be detected in serum, where levels are elevated during inflammatory diseases with involvement of endothelial dysfunction and damage. Especially triggered by the proinflammatory cytokines TNF-α or IL1-β, Endocan mediates the recruitment of circulatory lymphocytes and promotes leukocyte adhesion at inflammation sites [442]. Recent studies also indicate, that the protein can be utilized as a marker for the assessment of cancer [443], chronic inflammatory or autoimmune [444, 445] and cardiovascular diseases [446], in which serum concentrations are upregulated in patients. We suggest that Endocan might be jointly responsible for the promotion of the systemic inflammation during cGvHD and can be used as potential biomarker for the evaluation of the endothelial injury after allo-HSCT.

Endostatin, the C-terminal fragment of fibroblast-derived collagen XVIII, which is cleaved and released into serum, was characterized to express potent anti-angiogenic activities by interference of VEGF-receptor binding and to inhibit EC proliferation, migration and tubeformation *in vitro* and *in vivo* [447]. In addition, it induces EC apoptosis [448]. Endostatin serum levels are increased in patients suffering from systemic sclerosis, pulmonary arterial hypertension [288] and renal carcinoma [449]. In experimentally-induced lung fibrosis in rats, early administration of Endostatin ameliorated the fibrosis and decreased the number of infiltrating immune cells as well as the pulmonary microvascular density through VEGF-blocking [289]. Since cGvHD is accompanied by severe fibroblast accumulation in various tissues, the high Endostatin levels can be correlated to the circumstance, that fibroblasts are the main source of collagen XVIII. It should be correlated, if cGvHD patients suffering from severe sclerodermatous manifestations show higher Endostatin levels than patients with other major symptoms. However, linking these results to an endothelial pathology in cGvHD, we hypothesize that an enhancement of serum endostatin might be an emergency reaction to dampen either a pathological angiogenesis, which occurs in early GvHD phases [154] or to

reduce a possible EndoMT during cGvHD, where ECs perpetuate the fibrotic reaction. Alternatively, Endostatin release could be a reaction to circulating endothelial cells, which were found frequently during cGvHD [263] and also contribute to vascular pathologies [450].

As a second potential biomarker predominantly expressed in ECs, CTGF was reported to exhibit not only regulatory functions towards EC adhesion, migration and survival but also mediates vascular assembly, maturation and remodeling processes by association and adherence of pericytes to ECs [451]. CTGF exerts both, pro- [451] as well as anti-angiogenic functions [452]. Apart from regulation of ECs, CTGF is secreted by fibroblast and acts as a major stimulant for excessive extracellular matrix deposition, respectively collagen I production in the context of fibrotic pathologies [453]. To name two examples, upregulated CTGF protein and mRNA levels were detected in fibrotic pulmonary and sclerodermatous GvHD [292, 293]. Consistent with the high CTGF levels in serum of cGvHD patients, we also found higher concentrations of serum TGF-ß1, which goes in line with the observation of the CTGF gene being rapidly induced by TGF-ß and both proteins are often found coexpressed during wound healing and in fibrotic lesions with newly formed connective tissue [454]. Concluding, TGF-ß1 levels should be measured accordingly, when applying CTGF as biomarker for cGvHD. Additionally, in histological analyses of our BDF cGvHD mouse model, we found newly formed CD31+ vascular-like structures within fibrotic connective tissue areas, especially in the lung. These results, together with the human data, lead us to the hypothesis that CTGF might work as an autocrine factor in ECs in response to heal the cGvHD-caused endothelial damage and at the same time acts as a paracrine factor for fibroblasts in fibrotic and inflammatory conditions in cGvHD. This association is bolstered by various published studies, which assume that CTGF levels are regulated in ECs themselves when located within fibrotic areas [455, 456]. It should be investigated, if higher CTGF signals can also be detected in murine immunohistofluorescent samples of cGvHD target organs.

As an auxiliary TGF-ß receptor, endoglin is distinctly upregulated on activated ECs at sites of angiogenesis and vasculogenesis [457], of inflamed tissues and during wound repair [429] and binds TGF-ß1/ß3 with high affinity [458]. Vice versa, an endoglin expression is further stimulated via TGF-ß signaling. The soluble form of endoglin is cleaved from the EC membrane in various pathologic conditions, e.g. endothelial injury, inflammation or activation [459] and serves as a TGF-ß antagonist, as it sequesters TGF-ß ligands before receptor binding [460]. High serum levels of soluble endoglin in cGvHD could be interpreted as answer to increased TGF-ß levels or vice versa to regulate excess angiogenesis and/or

fibrosis, mediated by both factors. In a comparative study, Chen et al. observed endoglin as a marker expressed in adult, long-term repopulating HSCs [461]. Since transplanted patients lack such long-term repopulating HSCs, the measured Endoglin levels could be related to origin from ECs or vascular smooth muscle cells with a high probability. Another player being expressed in ECs and involved in angiogenesis is Follistatin [462]. The protein binds and antagonizes the TGF-ß family member activin-beta A, which in turn is an inhibitor of EC proliferation [463]. In *in vitro* studies, Follistatin enhanced neovascularization, tubeformation and sprouting in ECs and promoted the migratory effect of ECs and mesenchymal stem cells [464]. Circulating Endoglin and Follistatin levels were described to be elevated in patients at the onset of aGvHD by Newell et al., suggesting that high Endoglin/Follistatin levels early after allo-HSCT might be caused by conditioning-related toxicity. Additionally, allo-HSCT patients with high serum concentrations had a nearly 15-fold increased hazard ratio of 1-year non-relapse mortality [465]. Moreover, patients with higher Follistatin serum concentrations post haploidentical transplant were associated with more severe aGvHD, poorer overall survival and the occurrence of VOD [466]. Concluding from the published data on aGvHD and our newly gained results in cGvHD, we hypothesize, that Endoglin in combination with Follistatin, CTGF and TGF-ß can be utilized as biomarker panel determining a patient-specific vulnerability to conditioning toxicity early after allo-HSCT and defining the grade of endothelial damage in patients with established cGvHD. Those markers may not only be seen as angiogenic factors in aGvHD, but also as markers for endothelial damage during manifested cGvHD later after allo-HSCT.

Increased serum TGF-ß1 levels have been already described to be associated with the occurrence of cGvHD in clinics [467]. TGF-ß1 is a key player in immune regulation: it exerts immunosuppressive and anti-inflammatory as well as stimulatory effects on cellular activation or proliferation [468]. Furthermore, it enhances the synthesis of extracellular matrix filaments, such as fibronectin and promotes fibrosis and tissue scarring under pathologic conditions, so, by association, might be responsible for the fibrotic alterations and sclerodermatic changes which can be found frequently during allo-HSCT [467] and cGvHD [469]. Interestingly, although the TGF-ß1 serum concentration was measured to be elevated during cGvHD, the fibronectin concentration did not differ between our two patient groups. As our results indicate, the pleiotropic effects of TGF-ß1 might be causative, but not solely responsible for the sclerodermatic and fibrotic tissue alterations in cGvHD and collateral mechanisms as endothelial transformations and endothelial injury might provoke additional pathological matrix depositions. Concluding, TGF-ß1 and Fibronectin alone are not sufficient as

biomarkers to determine a possible (fibrotic) cGvHD predisposition in patients, but TGF-ß1 in combination with other endothelial markers, could be reliable predictors of cGvHD-related fibrosis and EndoMT. So far, we used the analysed targets as diagnostic tools for cGvHD. It has to be further elucidated, if the newly discovered markers can also be consulted for the prediction of e.g. response to treatments and prognosis of overall cGvHD outcome after allo-HSCT or as biomarkers for clinical diagnosis of aGvHD. Beyond, the sample size of cGvHD and control patients have to be enlarged in prospective preclinical trials to confirm and reliably replicate the here gained results. To summarize, endothelial damage and dysfunction are common features of chronic inflammatory and fibrotic diseases and can be directly related to the host response after allo-HSCT, respectively might be associated with the complex pathophysiology of cGvHD. For that reason, it could be highly beneficial to include endothelial biomarkers into the clinical routine when predicting and diagnosing cGvHD.

4.10. Outlook

In the first part of the present thesis, we identified Eno3 and in particular G6pdx as possible candidate proteins for the inhibition of the pathologic angiogenesis during GvHD. The mechanisms of *G6pdx* downstream signaling under allogeneic conditions should be elicited in *in vitro* or *in vivo* studies (e.g. using CRISPR/Cas9, endothelial assays, metabolomics and an endothelial-*G6pdx*-knockout mouse), to analyse the connection of the endothelium-specific target gene deletion on angiogenesis, GvHD and anti-tumor activity and to find further molecular targets for anti-angiogenic GvHD therapy. Especially the treatment of GvHD mice by use of the G6pdx-inhibitor Polydatin had a positive influence on the aGvHD morbidity and the endothelial function, when administered early, but not on late cGvHD. The results should be verified in additional preclinical experiments to find the most potent treatment schedule before transferring them to the clinical setup. Furthermore, patient samples, such as blood serum or tissue biopsies could help to examine the *G6pdx*-expression during human GvHD, proposing the protein to serve as diagnostic marker after allo-HSCT.

In the second project section, we examined that cGVHD is associated with endothelial damage and dysfunction in murine models and as biomarker analyses revealed, that endothelial participation also plays a role in cGvHD patients. Especially the finding of EndoMT during cGvHD in the murine models should be further investigated. To gain full knowledge of how EndoMT is working, molecules from downstream pathways causing

EndoMT should be further elucidated, e.g. with the help of GvHD mouse models. In this context, the spatial and temporal regulation of EndoMT in the GvHD progression could be examined. Next to the analysed markers αSMA or FSP-1, other EndoMT-related molecules, such as Collagen IV, Fibronectin or Vimentin should be evaluated as therapeutic targets after allo-HSCT. It is of clinical relevance, if EndoMT is also occurring in patients, which could be examined by the use of human biopsies

TGF-ß was characterized as important EndoMT-trigger, but therapeutic intervention of TGF-ß remains challenging because of its pleiotropic immune regulating functions. Since EndoMT can be induced by other mediators, which are also important to an endothelial regulation, as hypoxia or Endothelin-1, the specific therapeutic targeting of such factors might be beneficial to reduce EndoMT without interfering with immune regulating functions. Lately, the antifibrotic drug Pirfenidone applied in this study, ameliorated murine cGvHD and restored the endothelial function. The suitability and safety of Pirfenidone as a treatment against Bronchiolitis after allo-HSCT in patients was recently published by Matthaiou et al. [470], hence the drug might be valuable for normalizing the endothelial dysfunction during GvHD.

As an overall objective, we aim at a translational development of anti-angiogenic or endothelium-specific therapeutic treatments to prevent pathologic angiogenesis or endothelial damage, dysfunction and EndoMT in GvHD without blocking the anti-tumor effect of the graft. We sought to gain deeper knowledge about initiating events and risk factors for severe GVHD, which will help to understand the underlying pathophysiology and allow to treat or even avoid GvHD after allo-HSCT.

5. References

1. Giralt S, Bishop MR (2009) Principles and overview of allogeneic hematopoietic stem cell transplantation. Cancer treatment and research 144:1–21. doi: 10.1007/978-0-387-78580-6_1
2. CLARK ML, LYNCH FX (1952) Clinical symptoms of radiation sickness, time to onset and duration of symptoms among Hiroshima survivors in the lethal and median lethal ranges of radiation. Military surgeon 111(5):360–368
3. JACOBSON LO, MARKS EK, GASTON EO (1953) Effets de la protection de la rate pendant l'irradiation totale sur la formule sanguine du lapin (Effect of protection of the spleen during total body irradiation on the blood in rabbit). Revue d'hematologie 8(4):515–532
4. LORENZ E, UPHOFF D, REID TR et al. (1951) Modification of irradiation injury in mice and guinea pigs by bone marrow injections. Journal of the National Cancer Institute 12(1):197–201
5. Thomas ED, LOCHTE HL, LU WC et al. (1957) Intravenous infusion of bone marrow in patients receiving radiation and chemotherapy. The New England journal of medicine 257(11):491–496. doi: 10.1056/NEJM195709122571102
6. WILSON RE, HENRY L, MERRILL JP (1963) A MODEL SYSTEM FOR DETERMINING HISTOCOMPATIBILITY IN MAN. The Journal of clinical investigation 42:1497–1503. doi: 10.1172/JCI104834
7. DAUSSET J (1958) Iso-leuco-anticorps (Iso-leuko-antibodies). Acta haematologica 20(1-4):156–166. doi: 10.1159/000205478
8. van ROOD JJ, EERNISSE JG, van LEEUWEN A (1958) Leucocyte antibodies in sera from pregnant women. Nature 181(4625):1735–1736. doi: 10.1038/1811735a0
9. MATHE G, AMIEL JL, SCHWARZENBERG L et al. (1965) SUCCESSFUL ALLOGENIC BONE MARROW TRANSPLANTATION IN MAN. CHIMERISM, INDUCED SPECIFIC TOLERANCE AND POSSIBLE ANTI-LEUKEMIC EFFECTS. Blood 25:179–196
10. Gatti RA, Meuwissen HJ, Allen HD et al. (1968) Immunological reconstitution of sex-linked lymphopenic immunological deficiency. Lancet (London, England) 2(7583):1366–1369. doi: 10.1016/s0140-6736(68)92673-1
11. Buckner CD, Clift RA, Fefer A et al. (1973) Aplastic anemia treated by marrow transplantation. Transplantation proceedings 5(1):913–916
12. Thomas ED, Buckner CD, Banaji M et al. (1977) One hundred patients with acute leukemia treated by chemotherapy, total body irradiation, and allogeneic marrow transplantation. Blood 49(4):511–533
13. Passweg JR, Baldomero H, Chabannon C et al. (2022) Impact of the SARS-CoV-2 pandemic on hematopoietic cell transplantation and cellular therapies in Europe 2020. A report from the EBMT activity survey. Bone marrow transplantation 57(5):742–752. doi: 10.1038/s41409-022-01604-x
14. Auletta J.J., Kou J., Chen M., Shaw B.E. (2021) Current use and outcome of hematopoietic stem cell transplantation: CIBMTR US summary slides.
15. Passweg JR, Baldomero H, Chabannon C et al. (2020) The EBMT activity survey on hematopoietic-cell transplantation and cellular therapy 2018. CAR-T's come into focus. Bone marrow transplantation 55(8):1604–1613. doi: 10.1038/s41409-020-0826-4
16. Butturini A, Bortin MM, Seeger RC et al. (1987) Graft-vs-leukemia following bone marrow transplantation. A model of immunotherapy in man. Progress in clinical and biological research 244:371–390
17. Kolb HJ, Mittermüller J, Clemm C et al. (1990) Donor leukocyte transfusions for treatment of recurrent chronic myelogenous leukemia in marrow transplant patients. Blood 76(12):2462–2465
18. Copelan EA (2006) Hematopoietic stem-cell transplantation. The New England journal of medicine 354(17):1813–1826. doi: 10.1056/NEJMra052638

19. Evseeva I, Foeken L, Madrigal A (2019) The EBMT Handbook: Hematopoietic Stem Cell Transplantation and Cellular Therapies. The Role of Unrelated Donor Registries in HSCT, 7th, Cham (CH)
20. Cornelissen JJ, Carston M, Kollman C et al. (2001) Unrelated marrow transplantation for adult patients with poor-risk acute lymphoblastic leukemia. Strong graft-versus-leukemia effect and risk factors determining outcome. Blood 97(6):1572–1577. doi: 10.1182/blood.v97.6.1572
21. McGlave PB, Shu XO, Wen W et al. (2000) Unrelated donor marrow transplantation for chronic myelogenous leukemia. 9 years' experience of the national marrow donor program. Blood 95(7):2219–2225
22. Giralt S, Estey E, Albitar M et al. (1997) Engraftment of allogeneic hematopoietic progenitor cells with purine analog-containing chemotherapy. Harnessing graft-versus-leukemia without myeloablative therapy. Blood 89(12):4531–4536
23. Janeway C, Travers P (2005) Immunobiology. The immune system in health and disease ; [CD-ROM inside ; animations, videos and figures from the book], 6. ed. Garland Science, New York
24. Horton R, Wilming L, Rand V et al. (2004) Gene map of the extended human MHC. Nature reviews. Genetics 5(12):889–899. doi: 10.1038/nrg1489
25. Wieczorek M, Abualrous ET, Sticht J et al. (2017) Major Histocompatibility Complex (MHC) Class I and MHC Class II Proteins. Conformational Plasticity in Antigen Presentation. Frontiers in immunology 8:292. doi: 10.3389/fimmu.2017.00292
26. Bertaina A, Andreani M (2018) Major Histocompatibility Complex and Hematopoietic Stem Cell Transplantation. Beyond the Classical HLA Polymorphism. International journal of molecular sciences 19(2). doi: 10.3390/ijms19020621
27. Rolstad B (2014) The early days of NK cells. An example of how a phenomenon led to detection of a novel immune receptor system - lessons from a rat model. Frontiers in immunology 5:283. doi: 10.3389/fimmu.2014.00283
28. Anthony DeFranco, Richard M. Locksley, Miranda Robertson (2007) Immunity: The Immune Response in Infectious and Inflammatory Disease. New Science Press
29. Armitage JO (1984) Bone marrow transplantation. The Nebraska medical journal 69(3):64–67
30. Robinson J, Barker DJ, Georgiou X et al. (2020) IPD-IMGT/HLA Database. Nucleic acids research 48(D1):D948-D955. doi: 10.1093/nar/gkz950
31. Tiercy J-M (2016) How to select the best available related or unrelated donor of hematopoietic stem cells? Haematologica 101(6):680–687. doi: 10.3324/haematol.2015.141119
32. Fürst D, Neuchel C, Tsamadou C et al. HLA Matching in Unrelated Stem Cell Transplantation up to Date
33. Nowak J (2008) Role of HLA in hematopoietic SCT. Bone marrow transplantation 42 Suppl 2:S71-6. doi: 10.1038/bmt.2008.288
34. Shlomchik WD (2007) Graft-versus-host disease. Nature reviews. Immunology 7(5):340–352. doi: 10.1038/nri2000
35. Kernan NA, Bartsch G, Ash RC et al. (1993) Analysis of 462 transplantations from unrelated donors facilitated by the National Marrow Donor Program. The New England journal of medicine 328(9):593–602. doi: 10.1056/NEJM199303043280901
36. Anasetti C, Petersdorf EW, Martin PJ et al. (2001) Trends in transplantation of hematopoietic stem cells from unrelated donors. Current opinion in hematology 8(6):337–341. doi: 10.1097/00062752-200111000-00004
37. Henslee-Downey PJ, Abhyankar SH, Parrish RS et al. (1997) Use of partially mismatched related donors extends access to allogeneic marrow transplant. Blood 89(10):3864–3872

38. Beatty PG, Clift RA, Mickelson EM et al. (1985) Marrow transplantation from related donors other than HLA-identical siblings. The New England journal of medicine 313(13):765–771. doi: 10.1056/NEJM198509263131301
39. Petersdorf EW, Anasetti C, Martin PJ et al. (2004) Limits of HLA mismatching in unrelated hematopoietic cell transplantation. Blood 104(9):2976–2980. doi: 10.1182/blood-2004-04-1674
40. National Marrow Donor Program (NMDP)/Be The Match (2018) 24th Edition NMDP Standards
41. Buckner CD, Clift RA, Sanders JE et al. (1984) Marrow harvesting from normal donors. Blood 64(3):630–634
42. Bensinger WI, Weaver CH, Appelbaum FR et al. (1995) Transplantation of allogeneic peripheral blood stem cells mobilized by recombinant human granulocyte colony-stimulating factor. Blood 85(6):1655–1658
43. Rowley SD, Feng Z, Chen L et al. (2003) A randomized phase III clinical trial of autologous blood stem cell transplantation comparing cryopreservation using dimethylsulfoxide vs dimethylsulfoxide with hydroxyethylstarch. Bone marrow transplantation 31(11):1043–1051. doi: 10.1038/sj.bmt.1704030
44. Narayanan DL, Phadke SR (2019) Concepts, Utility and Limitations of Cord Blood Banking: What Clinicians Need to Know. Indian journal of pediatrics 86(1):44–48. doi: 10.1007/s12098-018-2651-y
45. Thomas E, Storb R, Clift RA et al. (1975) Bone-marrow transplantation (first of two parts). The New England journal of medicine 292(16):832–843. doi: 10.1056/NEJM197504172921605
46. Kröger N, Zabelina T, Krüger W et al. (2001) Comparison of total body irradiation vs busulfan in combination with cyclophosphamide as conditioning for unrelated stem cell transplantation in CML patients. Bone marrow transplantation 27(4):349–354. doi: 10.1038/sj.bmt.1702802
47. Santos GW, Sensenbrenner LL, Anderson PN et al. (1976) HL-A-identical marrow transplants in aplastic anemia, acute leukemia, and lymphosarcoma employing cyclophosphamide. Transplantation proceedings 8(4):607–610
48. Tutschka PJ, Copelan EA, Klein JP (1987) Bone marrow transplantation for leukemia following a new busulfan and cyclophosphamide regimen. Blood 70(5):1382–1388
49. Shouval R, Fein JA, Cho C et al. (2022) The Simplified Comorbidity Index: a new tool for prediction of nonrelapse mortality in allo-HCT. Blood advances 6(5):1525–1535. doi: 10.1182/bloodadvances.2021004319
50. Rimkus C (2009) Acute complications of stem cell transplant. Seminars in oncology nursing 25(2):129–138. doi: 10.1016/j.soncn.2009.03.007
51. Carreras E (2000) Veno-occlusive disease of the liver after hemopoietic cell transplantation. European journal of haematology 64(5):281–291. doi: 10.1034/j.1600-0609.2000.9r200.x
52. Arnaout K, Patel N, Jain M et al. (2014) Complications of allogeneic hematopoietic stem cell transplantation. Cancer investigation 32(7):349–362. doi: 10.3109/07357907.2014.919301
53. Champlin RE, Horowitz MM, van Bekkum DW et al. (1989) Graft failure following bone marrow transplantation for severe aplastic anemia: risk factors and treatment results. Blood 73(2):606–613
54. Sahin U, Toprak SK, Atilla PA et al. (2016) An overview of infectious complications after allogeneic hematopoietic stem cell transplantation. Journal of infection and chemotherapy : official journal of the Japan Society of Chemotherapy 22(8):505–514. doi: 10.1016/j.jiac.2016.05.006
55. Wolff SN (2002) Second hematopoietic stem cell transplantation for the treatment of graft failure, graft rejection or relapse after allogeneic transplantation. Bone marrow transplantation 29(7):545–552. doi: 10.1038/sj.bmt.1703389

56. Spellman S, Bray R, Rosen-Bronson S et al. (2010) The detection of donor-directed, HLA-specific alloantibodies in recipients of unrelated hematopoietic cell transplantation is predictive of graft failure. Blood 115(13):2704–2708. doi: 10.1182/blood-2009-09-244525
57. Young J-AH (2008) Infectious complications of acute and chronic GVHD. Best practice & research. Clinical haematology 21(2):343–356. doi: 10.1016/j.beha.2008.02.017
58. Mackall C, Fry T, Gress R et al. (2009) Background to hematopoietic cell transplantation, including post transplant immune recovery. Bone marrow transplantation 44(8):457–462. doi: 10.1038/bmt.2009.255
59. Ruutu T, Barosi G, Benjamin RJ et al. (2007) Diagnostic criteria for hematopoietic stem cell transplant-associated microangiopathy: results of a consensus process by an International Working Group. Haematologica 92(1):95–100. doi: 10.3324/haematol.10699
60. Srinivasan R, Balow JE, Sabnis S et al. (2005) Nephrotic syndrome: an under-recognised immune-mediated complication of non-myeloablative allogeneic haematopoietic cell transplantation. British journal of haematology 131(1):74–79. doi: 10.1111/j.1365-2141.2005.05728.x
61. Bearman SI, Anderson GL, Mori M et al. (1993) Venoocclusive disease of the liver: development of a model for predicting fatal outcome after marrow transplantation. Journal of clinical oncology : official journal of the American Society of Clinical Oncology 11(9):1729–1736. doi: 10.1200/JCO.1993.11.9.1729
62. DeLeve LD, Shulman HM, McDonald GB (2002) Toxic injury to hepatic sinusoids: sinusoidal obstruction syndrome (veno-occlusive disease). Seminars in liver disease 22(1):27–42. doi: 10.1055/s-2002-23204
63. Lum LG (1990) Immune recovery after bone marrow transplantation. Hematology/oncology clinics of North America 4(3):659–675
64. Zaia JA (1990) Viral infections associated with bone marrow transplantation. Hematology/oncology clinics of North America 4(3):603–623
65. Ferrara JL, Deeg HJ (1991) Graft-versus-host disease. The New England journal of medicine 324(10):667–674. doi: 10.1056/NEJM199103073241005
66. BILLINGHAM RE, BRENT L, MEDAWAR PB (1954) Quantitative studies on tissue transplantation immunity. II. The origin, strength and duration of actively and adoptively acquired immunity. Proceedings of the Royal Society of London. Series B, Biological sciences 143(910):58–80. doi: 10.1098/rspb.1954.0054
67. Ramdial JL, Mehta RS, Saliba RM et al. (2021) Acute graft-versus-host disease is the foremost cause of late nonrelapse mortality. Bone marrow transplantation 56(8):2005–2012. doi: 10.1038/s41409-021-01274-1
68. Wolff D, Lawitschka A (2019) The EBMT handbook. Hematopoietic stem cell transplantation and cellular therapies, 7th. Springer Open, Leiden, Munich, Cham
69. Filipovich AH, Weisdorf D, Pavletic S et al. (2005) National Institutes of Health consensus development project on criteria for clinical trials in chronic graft-versus-host disease: I. Diagnosis and staging working group report. Biology of blood and marrow transplantation : journal of the American Society for Blood and Marrow Transplantation 11(12):945–956. doi: 10.1016/j.bbmt.2005.09.004
70. Saito T, Shinagawa K, Takenaka K et al. (2002) Ocular manifestation of acute graft-versus-host disease after allogeneic peripheral blood stem cell transplantation. International journal of hematology 75(3):332–334. doi: 10.1007/BF02982052
71. Zeiser R, Teshima T (2021) Nonclassical manifestations of acute GVHD. Blood 138(22):2165–2172. doi: 10.1182/blood.2021012431

72. Pulanic D, Lozier JN, Pavletic SZ (2009) Thrombocytopenia and hemostatic disorders in chronic graft versus host disease. Bone marrow transplantation 44(7):393–403. doi: 10.1038/bmt.2009.196
73. Glucksberg H, Storb R, Fefer A et al. (1974) Clinical manifestations of graft-versus-host disease in human recipients of marrow from HL-A-matched sibling donors. Transplantation 18(4):295–304. doi: 10.1097/00007890-197410000-00001
74. Holler E, Greinix H, Zeiser R (2019) The EBMT Handbook: Hematopoietic Stem Cell Transplantation and Cellular Therapies. Acute Graft-Versus-Host Disease, 7th, Cham (CH)
75. Hill GR, Crawford JM, Cooke KR et al. (1997) Total body irradiation and acute graft-versus-host disease: the role of gastrointestinal damage and inflammatory cytokines. Blood 90(8):3204–3213
76. Ghimire S, Weber D, Mavin E et al. (2017) Pathophysiology of GvHD and Other HSCT-Related Major Complications. Frontiers in immunology 8:79. doi: 10.3389/fimmu.2017.00079
77. Markey KA, Banovic T, Kuns RD et al. (2009) Conventional dendritic cells are the critical donor APC presenting alloantigen after experimental bone marrow transplantation. Blood 113(22):5644–5649. doi: 10.1182/blood-2008-12-191833
78. Ferrara JLM, Levine JE, Reddy P et al. (2009) Graft-versus-host disease. Lancet (London, England) 373(9674):1550–1561. doi: 10.1016/S0140-6736(09)60237-3
79. Goulmy E, Schipper R, Pool J et al. (1996) Mismatches of minor histocompatibility antigens between HLA-identical donors and recipients and the development of graft-versus-host disease after bone marrow transplantation. The New England journal of medicine 334(5):281–285. doi: 10.1056/NEJM199602013340501
80. Wang X-N, Haniffa MA, Holtick U et al. (2009) Regulatory T-cell suppression of CD8+ T-cell-mediated graft-versus-host reaction requires their presence during priming. Transplantation 88(2):188–197. doi: 10.1097/TP.0b013e3181ac14ce
81. Grube M, Holler E, Weber D et al. (2016) Risk Factors and Outcome of Chronic Graft-versus-Host Disease after Allogeneic Stem Cell Transplantation-Results from a Single-Center Observational Study. Biology of blood and marrow transplantation : journal of the American Society for Blood and Marrow Transplantation 22(10):1781–1791. doi: 10.1016/j.bbmt.2016.06.020
82. Arai S, Arora M, Wang T et al. (2015) Increasing incidence of chronic graft-versus-host disease in allogeneic transplantation: a report from the Center for International Blood and Marrow Transplant Research. Biology of blood and marrow transplantation : journal of the American Society for Blood and Marrow Transplantation 21(2):266–274. doi: 10.1016/j.bbmt.2014.10.021
83. Carlens S, Ringdén O, Remberger M et al. (1998) Risk factors for chronic graft-versus-host disease after bone marrow transplantation: a retrospective single centre analysis. Bone marrow transplantation 22(8):755–761. doi: 10.1038/sj.bmt.1701423
84. Jagasia MH, Greinix HT, Arora M et al. (2015) National Institutes of Health Consensus Development Project on Criteria for Clinical Trials in Chronic Graft-versus-Host Disease: I. The 2014 Diagnosis and Staging Working Group report. Biology of blood and marrow transplantation : journal of the American Society for Blood and Marrow Transplantation 21(3):389-401.e1. doi: 10.1016/j.bbmt.2014.12.001
85. Cooke KR, Luznik L, Sarantopoulos S et al. (2017) The Biology of Chronic Graft-versus-Host Disease: A Task Force Report from the National Institutes of Health Consensus Development Project on Criteria for Clinical Trials in Chronic Graft-versus-Host Disease. Biology of blood and marrow transplantation : journal of the American Society for Blood and Marrow Transplantation 23(2):211–234. doi: 10.1016/j.bbmt.2016.09.023

86. Hakim FT, Memon S, Jin P et al. (2016) Upregulation of IFN-Inducible and Damage-Response Pathways in Chronic Graft-versus-Host Disease. Journal of immunology (Baltimore, Md. : 1950) 197(9):3490–3503. doi: 10.4049/jimmunol.1601054
87. Zhao D, Young JS, Chen Y-H et al. (2011) Alloimmune response results in expansion of autoreactive donor CD4+ T cells in transplants that can mediate chronic graft-versus-host disease. Journal of immunology (Baltimore, Md. : 1950) 186(2):856–868. doi: 10.4049/jimmunol.1002195
88. Yu J, Storer BE, Kushekhar K et al. (2016) Biomarker Panel for Chronic Graft-Versus-Host Disease. Journal of Clinical Oncology 34(22):2583–2590. doi: 10.1200/JCO.2015.65.9615
89. Chen X, Vodanovic-Jankovic S, Johnson B et al. (2007) Absence of regulatory T-cell control of TH1 and TH17 cells is responsible for the autoimmune-mediated pathology in chronic graft-versus-host disease. Blood 110(10):3804–3813. doi: 10.1182/blood-2007-05-091074
90. van der Waart AB, van der Velden WJFM, Blijlevens NM et al. (2014) Targeting the IL17 pathway for the prevention of graft-versus-host disease. Biology of blood and marrow transplantation : journal of the American Society for Blood and Marrow Transplantation 20(6):752–759. doi: 10.1016/j.bbmt.2014.02.007
91. Flynn R, Du J, Veenstra RG et al. (2014) Increased T follicular helper cells and germinal center B cells are required for cGVHD and bronchiolitis obliterans. Blood 123(25):3988–3998. doi: 10.1182/blood-2014-03-562231
92. Wynn TA, Barron L (2010) Macrophages: master regulators of inflammation and fibrosis. Seminars in liver disease 30(3):245–257. doi: 10.1055/s-0030-1255354
93. Wynn TA, Ramalingam TR (2012) Mechanisms of fibrosis: therapeutic translation for fibrotic disease. Nature medicine 18(7):1028–1040. doi: 10.1038/nm.2807
94. Zeiser R, Blazar BR (2017) Pathophysiology of Chronic Graft-versus-Host Disease and Therapeutic Targets. The New England journal of medicine 377(26):2565–2579. doi: 10.1056/NEJMra1703472
95. Korngold R, Sprent J (1978) Lethal graft-versus-host disease after bone marrow transplantation across minor histocompatibility barriers in mice. Prevention by removing mature T cells from marrow. The Journal of experimental medicine 148(6):1687–1698. doi: 10.1084/jem.148.6.1687
96. Chu Y-W, Gress RE (2008) Murine models of chronic graft-versus-host disease: insights and unresolved issues. Biology of blood and marrow transplantation : journal of the American Society for Blood and Marrow Transplantation 14(4):365–378. doi: 10.1016/j.bbmt.2007.12.002
97. Snell GD (1992) The Nobel Lectures in Immunology. Lecture for the Nobel Prize for Physiology or Medicine, 1980: Studies in histocompatibility. Scandinavian Journal of Immunology 36(4):513–526. doi: 10.1111/j.1365-3083.1992.tb03218.x
98. Kolb HJ, Holler E (1997) Adoptive immunotherapy with donor lymphocyte transfusions. Current opinion in oncology 9(2):139–145. doi: 10.1097/00001622-199703000-00006
99. Storb R, Rudolph RH, Thomas ED (1971) Marrow grafts between canine siblings matched by serotyping and mixed leukocyte culture. The Journal of clinical investigation 50(6):1272–1275. doi: 10.1172/JCI106605
100. Teshima T, Ordemann R, Reddy P et al. (2002) Acute graft-versus-host disease does not require alloantigen expression on host epithelium. Nat Med 8(6):575–581. doi: 10.1038/nm0602-575
101. Anderson BE, McNiff JM, Jain D et al. (2005) Distinct roles for donor- and host-derived antigen-presenting cells and costimulatory molecules in murine chronic graft-versus-host disease: requirements depend on target organ. Blood 105(5):2227–2234. doi: 10.1182/blood-2004-08-3032
102. Shlomchik WD, Couzens MS, Tang CB et al. (1999) Prevention of graft versus host disease by inactivation of host antigen-presenting cells. Science 285(5426):412–415. doi: 10.1126/science.285.5426.412

103. Schroeder MA, DiPersio JF (2011) Mouse models of graft-versus-host disease: advances and limitations. Disease models & mechanisms 4(3):318–333. doi: 10.1242/dmm.006668
104. Hill GR, Ferrara JLM (2000) The primacy of the gastrointestinal tract as a target organ of acute graft-versus-host disease: rationale for the use of cytokine shields in allogeneic bone marrow transplantation. Blood 95(9):2754–2759. doi: 10.1182/blood.V95.9.2754.009k25_2754_2759
105. Reddy P, Negrin R, Hill GR (2008) Mouse models of bone marrow transplantation. Biology of blood and marrow transplantation : journal of the American Society for Blood and Marrow Transplantation 14(1 Suppl 1):129–135. doi: 10.1016/j.bbmt.2007.10.021
106. Pickel K, Hoffmann MK (1977) Suppressor T cells arising in mice undergoing a graft-vs-host response. Journal of immunology (Baltimore, Md. : 1950) 118(2):653–656
107. Hildebrandt GC, Olkiewicz KM, Corrion LA et al. (2004) Donor-derived TNF-alpha regulates pulmonary chemokine expression and the development of idiopathic pneumonia syndrome after allogeneic bone marrow transplantation. Blood 104(2):586–593. doi: 10.1182/blood-2003-12-4259
108. van Leeuwen L, Guiffre A, Atkinson K et al. (2002) A two-phase pathogenesis of graft-versus-host disease in mice. Bone marrow transplantation 29(2):151–158. doi: 10.1038/sj.bmt.1703328
109. Korngold R (1992) Lethal graft-versus-host disease in mice directed to multiple minor histocompatibility antigens: features of CD8+ and CD4+ T cell responses. Bone marrow transplantation 9(5):355–364
110. Cooke KR, Kobzik L, Martin TR et al. (1996) An experimental model of idiopathic pneumonia syndrome after bone marrow transplantation. I. The roles of minor H antigens and endotoxin. Blood 88(8):3230–3239
111. Ito R, Katano I, Kawai K et al. (2009) Highly sensitive model for xenogenic GVHD using severe immunodeficient NOG mice. Transplantation 87(11):1654–1658. doi: 10.1097/TP.0b013e3181a5cb07
112. King MA, Covassin L, Brehm MA et al. (2009) Human peripheral blood leucocyte non-obese diabetic-severe combined immunodeficiency interleukin-2 receptor gamma chain gene mouse model of xenogeneic graft-versus-host-like disease and the role of host major histocompatibility complex. Clinical and experimental immunology 157(1):104–118. doi: 10.1111/j.1365-2249.2009.03933.x
113. Riesner K, Kalupa M, Shi Y et al. (2016) A preclinical acute GVHD mouse model based on chemotherapy conditioning and MHC-matched transplantation. Bone marrow transplantation 51(3):410–417. doi: 10.1038/bmt.2015.279
114. Sadeghi B, Aghdami N, Hassan Z et al. (2008) GVHD after chemotherapy conditioning in allogeneic transplanted mice. Bone marrow transplantation 42(12):807–818. doi: 10.1038/bmt.2008.261
115. Hoffmann-Fezer G, Gall C, Zengerle U et al. (1993) Immunohistology and immunocytology of human T-cell chimerism and graft-versus-host disease in SCID mice. Blood 81(12):3440–3448
116. Shultz LD, Lyons BL, Burzenski LM et al. (2005) Human lymphoid and myeloid cell development in NOD/LtSz-scid IL2R gamma null mice engrafted with mobilized human hemopoietic stem cells. Journal of immunology (Baltimore, Md. : 1950) 174(10):6477–6489. doi: 10.4049/jimmunol.174.10.6477
117. Zeiser R, Blazar BR (2016) Preclinical models of acute and chronic graft-versus-host disease: how predictive are they for a successful clinical translation? Blood 127(25):3117–3126. doi: 10.1182/blood-2016-02-699082
118. Sakoda Y, Hashimoto D, Asakura S et al. (2007) Donor-derived thymic-dependent T cells cause chronic graft-versus-host disease. Blood 109(4):1756–1764. doi: 10.1182/blood-2006-08-042853

119. Jaffee BD, Claman HN (1983) Chronic graft-versus-host disease (GVHD) as a model for scleroderma. Cellular immunology 77(1):1–12. doi: 10.1016/0008-8749(83)90001-1
120. McCormick LL, Zhang Y, Tootell E et al. (1999) Anti-TGF-beta treatment prevents skin and lung fibrosis in murine sclerodermatous graft-versus-host disease: a model for human scleroderma. Journal of immunology (Baltimore, Md. : 1950) 163(10):5693–5699
121. Hamilton BL, Parkman R (1983) Acute and chronic graft-versus-host disease induced by minor histocompatibility antigens in mice. Transplantation 36(2):150–155. doi: 10.1097/00007890-198308000-00008
122. Via CS, Sharrow SO, Shearer GM (1987) Role of cytotoxic T lymphocytes in the prevention of lupus-like disease occurring in a murine model of graft-vs-host disease. Journal of immunology (Baltimore, Md. : 1950) 139(6):1840–1849
123. Slayback DL, Dobkins JA, Harper JM et al. (2000) Genetic factors influencing the development of chronic graft-versus-host disease in a murine model. Bone marrow transplantation 26(9):931–938. doi: 10.1038/sj.bmt.1702661
124. Wit D de, van Mechelen M, Zanin C et al. (1993) Preferential activation of Th2 cells in chronic graft-versus-host reaction. Journal of immunology (Baltimore, Md. : 1950) 150(2):361–366
125. Tschetter JR, Mozes E, Shearer GM (2000) Progression from acute to chronic disease in a murine parent-into-F1 model of graft-versus-host disease. Journal of immunology (Baltimore, Md. : 1950) 165(10):5987–5994. doi: 10.4049/jimmunol.165.10.5987
126. Zhang C, Todorov I, Zhang Z et al. (2006) Donor CD4+ T and B cells in transplants induce chronic graft-versus-host disease with autoimmune manifestations. Blood 107(7):2993–3001. doi: 10.1182/blood-2005-09-3623
127. Pals ST, Radaszkiewicz T, Roozendaal L et al. (1985) Chronic progressive polyarthritis and other symptoms of collagen vascular disease induced by graft-vs-host reaction. Journal of immunology (Baltimore, Md. : 1950) 134(3):1475–1482
128. Vidal S, Labrador M, Rodríguez-Sánchez JL et al. (1996) The role of BALB/c donor CD8+ lymphocytes in graft-versus-host disease in (BALB/c x A/J)F1 (CAF1) mice. Journal of immunology (Baltimore, Md. : 1950) 156(3):997–1005
129. (1989) Methotrexate and cyclosporine versus cyclosporine alone for prophylaxis of graft-versus-host disease in patients given HLA-identical marrow grafts for …
130. Ratanatharathorn V, Nash RA, Przepiorka D et al. (1998) Phase III Study Comparing Methotrexate and Tacrolimus (Prograf, FK506) With Methotrexate and Cyclosporine for Graft-Versus-Host Disease Prophylaxis After HLA-Identical Sibling Bone Marrow Transplantation. Blood 92(7):2303–2314. doi: 10.1182/blood.V92.7.2303
131. Chao NJ, Schmidt GM, Niland JC et al. (1993) Cyclosporine, methotrexate, and prednisone compared with cyclosporine and prednisone for prophylaxis of acute graft-versus-host disease. The New England journal of medicine 329(17):1225–1230. doi: 10.1056/NEJM199310213291703
132. Martin PJ, Schoch G, Fisher L et al. (1990) A retrospective analysis of therapy for acute graft-versus-host disease: initial treatment. Blood 76(8):1464–1472
133. Atkinson K, Horowitz MM, Gale RP et al. (1990) Risk factors for chronic graft-versus-host disease after HLA-identical sibling bone marrow transplantation. Blood 75(12):2459–2464. doi: 10.1182/blood.V75.12.2459.2459
134. Przepiorka D, Anderlini P, Saliba R et al. (2001) Chronic graft-versus-host disease after allogeneic blood stem cell transplantation. Blood 98(6):1695–1700. doi: 10.1182/blood.v98.6.1695
135. Lee SJ, Vogelsang G, Flowers MED (2003) Chronic graft-versus-host disease. Biology of Blood and Marrow Transplantation 9(4):215–233. doi: 10.1053/bbmt.2003.50026

136. Fowler DH, Pavletic SZ (2015) Syk and tired of current chronic GVHD therapies. Blood 125(26):3974–3975. doi: 10.1182/blood-2015-05-640672
137. Garnett C, Apperley JF, Pavlů J (2013) Treatment and management of graft-versus-host disease: improving response and survival. Therapeutic advances in hematology 4(6):366–378. doi: 10.1177/2040620713489842
138. Martin PJ, Schoch G, Fisher L et al. (1991) A retrospective analysis of therapy for acute graft-versus-host disease: secondary treatment. Blood 77(8):1821–1828. doi: 10.1182/blood.V77.8.1821.1821
139. Grkovic L, Baird K, Steinberg SM et al. (2012) Clinical laboratory markers of inflammation as determinants of chronic graft-versus-host disease activity and NIH global severity. Leukemia 26(4):633–643. doi: 10.1038/leu.2011.254
140. Wolff D, Fatobene G, Rocha V et al. (2021) Steroid-refractory chronic graft-versus-host disease: treatment options and patient management. Bone marrow transplantation 56(9):2079–2087. doi: 10.1038/s41409-021-01389-5
141. Wolff D, Schleuning M, Harsdorf S von et al. (2011) Consensus Conference on Clinical Practice in Chronic GVHD: Second-Line Treatment of Chronic Graft-versus-Host Disease. Biology of blood and marrow transplantation : journal of the American Society for Blood and Marrow Transplantation 17(1):1–17. doi: 10.1016/j.bbmt.2010.05.011
142. Finke J, Bethge WA, Schmoor C et al. (2009) Standard graft-versus-host disease prophylaxis with or without anti-T-cell globulin in haematopoietic cell transplantation from matched unrelated donors: a randomised, open-label, multicentre phase 3 trial. The Lancet. Oncology 10(9):855–864. doi: 10.1016/S1470-2045(09)70225-6
143. Jacobsohn DA, Vogelsang GB (2002) Novel pharmacotherapeutic approaches to prevention and treatment of GVHD. Drugs 62(6):879–889. doi: 10.2165/00003495-200262060-00002
144. Luznik L, Fuchs EJ (2010) High-dose, post-transplantation cyclophosphamide to promote graft-host tolerance after allogeneic hematopoietic stem cell transplantation. Immunologic research 47(1-3):65–77. doi: 10.1007/s12026-009-8139-0
145. Penack O, Marchetti M, Ruutu T et al. (2020) Prophylaxis and management of graft versus host disease after stem-cell transplantation for haematological malignancies: updated consensus recommendations of the European Society for Blood and Marrow Transplantation. The Lancet. Haematology 7(2):e157-e167. doi: 10.1016/S2352-3026(19)30256-X
146. Mielke S, Lutz M, Schmidhuber J et al. (2014) Salvage therapy with everolimus reduces the severity of treatment-refractory chronic GVHD without impairing disease control: a dual center retrospective analysis. Bone marrow transplantation 49(11):1412–1418. doi: 10.1038/bmt.2014.170
147. Ratanatharathorn V, Ayash L, Reynolds C et al. (2003) Treatment of chronic graft-versus-host disease with anti-CD20 chimeric monoclonal antibody. Biology of blood and marrow transplantation : journal of the American Society for Blood and Marrow Transplantation 9(8):505–511. doi: 10.1016/s1083-8791(03)00216-7
148. Pidala J, Kim J, Roman-Diaz J et al. (2010) Pentostatin as rescue therapy for glucocorticoid-refractory acute and chronic graft-versus-host disease. Annals of transplantation 15(4):21–29
149. Olivieri A, Locatelli F, Zecca M et al. (2009) Imatinib for refractory chronic graft-versus-host disease with fibrotic features. Blood 114(3):709–718. doi: 10.1182/blood-2009-02-204156
150. Ruutu T, Gratwohl A, Witte T de et al. (2014) Prophylaxis and treatment of GVHD: EBMT-ELN working group recommendations for a standardized practice. Bone marrow transplantation 49(2):168–173. doi: 10.1038/bmt.2013.107
151. Mohty M, Malard F, Abecassis M et al. (2015) Sinusoidal obstruction syndrome/veno-occlusive disease: current situation and perspectives-a position statement from the European Society for

Blood and Marrow Transplantation (EBMT). Bone marrow transplantation 50(6):781–789. doi: 10.1038/bmt.2015.52
152. Xie Z, Ghosh CC, Patel R et al. (2012) Vascular endothelial hyperpermeability induces the clinical symptoms of Clarkson disease (the systemic capillary leak syndrome). Blood 119(18):4321–4332. doi: 10.1182/blood-2011-08-375816
153. Jodele S, Laskin BL, Dandoy CE et al. (2015) A new paradigm: Diagnosis and management of HSCT-associated thrombotic microangiopathy as multi-system endothelial injury. Blood reviews 29(3):191–204. doi: 10.1016/j.blre.2014.11.001
154. Riesner K, Shi Y, Jacobi A et al. (2017) Initiation of acute graft-versus-host disease by angiogenesis. Blood 129(14):2021–2032. doi: 10.1182/blood-2016-08-736314
155. Cordes S, Mokhtari Z, Bartosova M et al. (2021) Endothelial damage and dysfunction in acute graft-versus-host disease. Haematologica 106(8):2147–2160. doi: 10.3324/haematol.2020.253716
156. Mir E, Palomo M, Rovira M et al. (2017) Endothelial damage is aggravated in acute GvHD and could predict its development. Bone marrow transplantation 52(9):1317–1325. doi: 10.1038/bmt.2017.121
157. Dietrich S, Falk CS, Benner A et al. (2013) Endothelial vulnerability and endothelial damage are associated with risk of graft-versus-host disease and response to steroid treatment. Biology of blood and marrow transplantation : journal of the American Society for Blood and Marrow Transplantation 19(1):22–27. doi: 10.1016/j.bbmt.2012.09.018
158. Andrulis M, Dietrich S, Longerich T et al. (2012) Loss of endothelial thrombomodulin predicts response to steroid therapy and survival in acute intestinal graft-versus-host disease. Haematologica 97(11):1674–1677. doi: 10.3324/haematol.2011.061051
159. Aird WC (2013) Endothelium. In: Konkle BA, Kitchens CS, Kessler CM (eds) Consultative hemostasis and thrombosis, 3rd ed. Elsevier/Saunders, Philadelphia, Pa, pp 33–41
160. Smyth LCD, Rustenhoven J, Scotter EL et al. (2018) Markers for human brain pericytes and smooth muscle cells. Journal of chemical neuroanatomy 92:48–60. doi: 10.1016/j.jchemneu.2018.06.001
161. Bernard I, Limonta D, Mahal LK et al. (2020) Endothelium Infection and Dysregulation by SARS-CoV-2: Evidence and Caveats in COVID-19. Viruses 13(1). doi: 10.3390/v13010029
162. Aird WC (2007) Phenotypic heterogeneity of the endothelium: I. Structure, function, and mechanisms. Circulation research 100(2):158–173. doi: 10.1161/01.RES.0000255691.76142.4a
163. Dejana E (2004) Endothelial cell-cell junctions: happy together. Nature reviews. Molecular cell biology 5(4):261–270. doi: 10.1038/nrm1357
164. Wallez Y, Huber P (2008) Endothelial adherens and tight junctions in vascular homeostasis, inflammation and angiogenesis. Biochimica et biophysica acta 1778(3):794–809. doi: 10.1016/j.bbamem.2007.09.003
165. Lemichez E, Lecuit M, Nassif X et al. (2010) Breaking the wall: targeting of the endothelium by pathogenic bacteria. Nat Rev Microbiol 8(2):93–104. doi: 10.1038/nrmicro2269
166. Patan S (2004) Vasculogenesis and angiogenesis. Cancer treatment and research 117:3–32. doi: 10.1007/978-1-4419-8871-3_1
167. Starke K, Born GVR, Duckles SP et al. (2006) The vascular endothelium. Handbook of experimental pharmacology, vol 176,2. Springer, Berlin
168. Kobayashi H, Lin PC (2009) Angiogenesis links chronic inflammation with cancer. Methods in molecular biology (Clifton, N.J.) 511:185–191. doi: 10.1007/978-1-59745-447-6_8
169. Cheng R, Ma J (2015) Angiogenesis in diabetes and obesity. Reviews in endocrine & metabolic disorders 16(1):67–75. doi: 10.1007/s11154-015-9310-7
170. Carmeliet P (2003) Angiogenesis in health and disease. Nat Med 9(6):653–660. doi: 10.1038/nm0603-653

171. Gale NW, Yancopoulos GD (1999) Growth factors acting via endothelial cell-specific receptor tyrosine kinases: VEGFs, angiopoietins, and ephrins in vascular development. Genes & development 13(9):1055–1066. doi: 10.1101/gad.13.9.1055
172. Carmeliet P, Jain RK (2011) Molecular mechanisms and clinical applications of angiogenesis. Nature 473(7347):298–307. doi: 10.1038/nature10144
173. Nyberg P, Xie L, Kalluri R (2005) Endogenous inhibitors of angiogenesis. Cancer research 65(10):3967–3979. doi: 10.1158/0008-5472.CAN-04-2427
174. Carmeliet P (2000) Mechanisms of angiogenesis and arteriogenesis. Nat Med 6(4):389–395. doi: 10.1038/74651
175. Bock K de, Georgiadou M, Carmeliet P (2013) Role of endothelial cell metabolism in vessel sprouting. Cell metabolism 18(5):634–647. doi: 10.1016/j.cmet.2013.08.001
176. Bock K de, Georgiadou M, Schoors S et al. (2013) Role of PFKFB3-driven glycolysis in vessel sprouting. Cell 154(3):651–663. doi: 10.1016/j.cell.2013.06.037
177. Vander Heiden MG, Cantley LC, Thompson CB (2009) Understanding the Warburg effect: the metabolic requirements of cell proliferation. Science (New York, N.Y.) 324(5930):1029–1033. doi: 10.1126/science.1160809
178. Potente M, Carmeliet P (2017) The Link Between Angiogenesis and Endothelial Metabolism. Annual review of physiology 79:43–66. doi: 10.1146/annurev-physiol-021115-105134
179. Schoors S, Bruning U, Missiaen R et al. (2015) Fatty acid carbon is essential for dNTP synthesis in endothelial cells. Nature 520(7546):192–197. doi: 10.1038/nature14362
180. Eelen G, Zeeuw P de, Treps L et al. (2018) Endothelial Cell Metabolism. Physiological reviews 98(1):3–58. doi: 10.1152/physrev.00001.2017
181. Cantelmo AR, Conradi L-C, Brajic A et al. (2016) Inhibition of the Glycolytic Activator PFKFB3 in Endothelium Induces Tumor Vessel Normalization, Impairs Metastasis, and Improves Chemotherapy. Cancer cell 30(6):968–985. doi: 10.1016/j.ccell.2016.10.006
182. Zhang R, Li R, Liu Y et al. (2019) The Glycolytic Enzyme PFKFB3 Controls TNF-α-Induced Endothelial Proinflammatory Responses. Inflammation 42(1):146–155. doi: 10.1007/s10753-018-0880-x
183. Schoors S, Bock K de, Cantelmo AR et al. (2014) Partial and transient reduction of glycolysis by PFKFB3 blockade reduces pathological angiogenesis. Cell metabolism 19(1):37–48. doi: 10.1016/j.cmet.2013.11.008
184. Ricard N, Bailly S, Guignabert C et al. (2021) The quiescent endothelium: signalling pathways regulating organ-specific endothelial normalcy. Nature reviews. Cardiology 18(8):565–580. doi: 10.1038/s41569-021-00517-4
185. Pober JS, Sessa WC (2007) Evolving functions of endothelial cells in inflammation. Nature reviews. Immunology 7(10):803–815. doi: 10.1038/nri2171
186. Pober JS, Cotran RS (1990) The role of endothelial cells in inflammation. Transplantation 50(4):537–544. doi: 10.1097/00007890-199010000-00001
187. Vestweber D (2015) How leukocytes cross the vascular endothelium. Nature reviews. Immunology 15(11):692–704. doi: 10.1038/nri3908
188. Félétou M (2011) The Endothelium: Part 1: Multiple Functions of the Endothelial Cells—Focus on Endothelium-Derived Vasoactive Mediators, San Rafael (CA)
189. Daar AS, Fuggle SV, Fabre JW et al. (1984) The detailed distribution of HLA-A, B, C antigens in normal human organs. Transplantation 38(3):287–292. doi: 10.1097/00007890-198409000-00018
190. Daar AS, Fuggle SV, Fabre JW et al. (1984) The detailed distribution of MHC Class II antigens in normal human organs. Transplantation 38(3):293–298. doi: 10.1097/00007890-198409000-00019
191. Choi J, Enis DR, Koh KP et al. (2004) T lymphocyte-endothelial cell interactions. Annual review of immunology 22:683–709. doi: 10.1146/annurev.immunol.22.012703.104639

192. Shiao SL, McNiff JM, Pober JS (2005) Memory T cells and their costimulators in human allograft injury. Journal of immunology (Baltimore, Md. : 1950) 175(8):4886–4896. doi: 10.4049/jimmunol.175.8.4886
193. Asahara T, Murohara T, Sullivan A et al. (1997) Isolation of putative progenitor endothelial cells for angiogenesis. Science (New York, N.Y.) 275(5302):964–967. doi: 10.1126/science.275.5302.964
194. Hou L, Kim JJ, Woo YJ et al. (2016) Stem cell-based therapies to promote angiogenesis in ischemic cardiovascular disease. American Journal of Physiology - Heart and Circulatory Physiology 310(4):H455-65. doi: 10.1152/ajpheart.00726.2015
195. Liu P, Zhou B, Gu D et al. (2009) Endothelial progenitor cell therapy in atherosclerosis: a double-edged sword? Ageing research reviews 8(2):83–93. doi: 10.1016/j.arr.2008.11.002
196. Devaraj S, Jialal I (2012) Dysfunctional endothelial progenitor cells in metabolic syndrome. Experimental diabetes research 2012:585018. doi: 10.1155/2012/585018
197. Loomans CJM, Wan H, Crom R de et al. (2006) Angiogenic murine endothelial progenitor cells are derived from a myeloid bone marrow fraction and can be identified by endothelial NO synthase expression. Arteriosclerosis, thrombosis, and vascular biology 26(8):1760–1767. doi: 10.1161/01.ATV.0000229243.49320.c9
198. Woywodt A, Bahlmann FH, Groot K de et al. (2002) Circulating endothelial cells: life, death, detachment and repair of the endothelial cell layer. Nephrol Dial Transplant 17(10):1728–1730. doi: 10.1093/ndt/17.10.1728
199. Goon PKY, Lip GYH, Boos CJ et al. (2006) Circulating endothelial cells, endothelial progenitor cells, and endothelial microparticles in cancer. Neoplasia (New York, N.Y.) 8(2):79–88. doi: 10.1593/neo.05592
200. Mancuso P, Antoniotti P, Quarna J et al. (2009) Validation of a standardized method for enumerating circulating endothelial cells and progenitors: flow cytometry and molecular and ultrastructural analyses. Clinical cancer research : an official journal of the American Association for Cancer Research 15(1):267–273. doi: 10.1158/1078-0432.CCR-08-0432
201. Foster W, Shantsila E, Carruthers D et al. (2009) Circulating endothelial cells and rheumatoid arthritis: relationship with plasma markers of endothelial damage/dysfunction. Rheumatology (Oxford, England) 48(3):285–288. doi: 10.1093/rheumatology/ken486
202. Rajagopalan S, Somers EC, Brook RD et al. (2004) Endothelial cell apoptosis in systemic lupus erythematosus: a common pathway for abnormal vascular function and thrombosis propensity. Blood 103(10):3677–3683. doi: 10.1182/blood-2003-09-3198
203. Welch-Reardon KM, Wu N, Hughes CCW (2015) A role for partial endothelial-mesenchymal transitions in angiogenesis? Arteriosclerosis, thrombosis, and vascular biology 35(2):303–308. doi: 10.1161/ATVBAHA.114.303220
204. Madar S, Goldstein I, Rotter V (2013) 'Cancer associated fibroblasts'--more than meets the eye. Trends in molecular medicine 19(8):447–453. doi: 10.1016/j.molmed.2013.05.004
205. Gasparics Á, Rosivall L, Krizbai IA et al. (2016) When the endothelium scores an own goal: endothelial cells actively augment metastatic extravasation through endothelial-mesenchymal transition. American Journal of Physiology - Heart and Circulatory Physiology 310(9):H1055-63. doi: 10.1152/ajpheart.00042.2016
206. Li J, Qu X, Bertram JF (2009) Endothelial-myofibroblast transition contributes to the early development of diabetic renal interstitial fibrosis in streptozotocin-induced diabetic mice. The American journal of pathology 175(4):1380–1388. doi: 10.2353/ajpath.2009.090096
207. Mendoza FA, Piera-Velazquez S, Farber JL et al. (2016) Endothelial Cells Expressing Endothelial and Mesenchymal Cell Gene Products in Lung Tissue From Patients With Systemic Sclerosis-

Associated Interstitial Lung Disease. Arthritis & rheumatology (Hoboken, N.J.) 68(1):210–217. doi: 10.1002/art.39421
208. Rieder F, Kessler SP, West GA et al. (2011) Inflammation-induced endothelial-to-mesenchymal transition: a novel mechanism of intestinal fibrosis. The American journal of pathology 179(5):2660–2673. doi: 10.1016/j.ajpath.2011.07.042
209. Xu X, Tan X, Hulshoff MS et al. (2016) Hypoxia-induced endothelial-mesenchymal transition is associated with RASAL1 promoter hypermethylation in human coronary endothelial cells. FEBS letters 590(8):1222–1233. doi: 10.1002/1873-3468.12158
210. Ranchoux B, Antigny F, Rucker-Martin C et al. (2015) Endothelial-to-mesenchymal transition in pulmonary hypertension. Circulation 131(11):1006–1018. doi: 10.1161/CIRCULATIONAHA.114.008750
211. Mintet E, Rannou E, Buard V et al. (2015) Identification of Endothelial-to-Mesenchymal Transition as a Potential Participant in Radiation Proctitis. The American journal of pathology 185(9):2550–2562. doi: 10.1016/j.ajpath.2015.04.028
212. Piera-Velazquez S, Jimenez SA (2012) Molecular mechanisms of endothelial to mesenchymal cell transition (EndoMT) in experimentally induced fibrotic diseases. Fibrogenesis & Tissue Repair 5(Suppl 1):S7. doi: 10.1186/1755-1536-5-S1-S7
213. Piera-Velazquez S, Mendoza FA, Jimenez SA (2016) Endothelial to Mesenchymal Transition (EndoMT) in the Pathogenesis of Human Fibrotic Diseases. Journal of Clinical Medicine 5(4). doi: 10.3390/jcm5040045
214. Sabbineni H, Verma A, Somanath PR (2018) Isoform-specific effects of transforming growth factor β on endothelial-to-mesenchymal transition. Journal of cellular physiology 233(11):8418–8428. doi: 10.1002/jcp.26801
215. Arciniegas E, Sutton AB, Allen TD et al. (1992) Transforming growth factor beta 1 promotes the differentiation of endothelial cells into smooth muscle-like cells in vitro. Journal of cell science 103 (Pt 2):521–529. doi: 10.1242/jcs.103.2.521
216. Medici D, Potenta S, Kalluri R (2011) Transforming growth factor-β2 promotes Snail-mediated endothelial-mesenchymal transition through convergence of Smad-dependent and Smad-independent signalling. The Biochemical journal 437(3):515–520. doi: 10.1042/BJ20101500
217. Mammoto T, Muyleart M, Konduri GG et al. (2018) Twist1 in Hypoxia-induced Pulmonary Hypertension through Transforming Growth Factor-β-Smad Signaling. American journal of respiratory cell and molecular biology 58(2):194–207. doi: 10.1165/rcmb.2016-0323OC
218. Goumans M-J, Liu Z, Dijke P ten (2009) TGF-beta signaling in vascular biology and dysfunction. Cell research 19(1):116–127. doi: 10.1038/cr.2008.326
219. Xiong J, Kawagishi H, Yan Y et al. (2018) A Metabolic Basis for Endothelial-to-Mesenchymal Transition. Molecular cell 69(4):689-698.e7. doi: 10.1016/j.molcel.2018.01.010
220. Totoson P, Maguin-Gaté K, Nappey M et al. (2016) Endothelial Dysfunction in Rheumatoid Arthritis: Mechanistic Insights and Correlation with Circulating Markers of Systemic Inflammation. PLoS ONE 11(1):e0146744. doi: 10.1371/journal.pone.0146744
221. Piper MK, Raza K, Nuttall SL et al. (2007) Impaired endothelial function in systemic lupus erythematosus. Lupus 16(2):84–88. doi: 10.1177/0961203306074842
222. Kocaman O, Sahin T, Aygun C et al. (2006) Endothelial dysfunction in patients with ulcerative colitis. Inflammatory bowel diseases 12(3):166–171. doi: 10.1097/01.MIB.0000217764.88980.74
223. Anyfanti P, Margouta A, Goulas K et al. (2022) Endothelial Dysfunction in Psoriasis: An Updated Review. Frontiers in medicine 9:864185. doi: 10.3389/fmed.2022.864185
224. Eissner G, Lindner H, Behrends U et al. (1996) Influence of bacterial endotoxin on radiation-induced activation of human endothelial cells in vitro and in vivo: protective role of IL-10. Transplantation 62(6):819–827. doi: 10.1097/00007890-199609270-00020

225. Robaye B, Mosselmans R, Fiers W et al. (1991) Tumor necrosis factor induces apoptosis (programmed cell death) in normal endothelial cells in vitro. The American journal of pathology 138(2):447–453
226. Biedermann BC (2008) Vascular endothelium and graft-versus-host disease. Best practice & research. Clinical haematology 21(2):129–138. doi: 10.1016/j.beha.2008.02.003
227. Cooke KR, Jannin A, Ho V (2008) The contribution of endothelial activation and injury to end-organ toxicity following allogeneic hematopoietic stem cell transplantation. Biology of blood and marrow transplantation : journal of the American Society for Blood and Marrow Transplantation 14(1 Suppl 1):23–32. doi: 10.1016/j.bbmt.2007.10.008
228. Luft T, Dreger P, Radujkovic A (2021) Endothelial cell dysfunction: a key determinant for the outcome of allogeneic stem cell transplantation. Bone marrow transplantation 56(10):2326–2335. doi: 10.1038/s41409-021-01390-y
229. Talekar MK, Freedman JL (2017) Engraftment Syndrome and Associated Cytokine Storm and Capillary Leak Syndrome. In: Brown VI (ed) Hematopoietic Stem Cell Transplantation for the Pediatric Hematologist/Oncologist. Springer, Cham, pp 195–199
230. Pagliuca S, Michonneau D, Sicre de Fontbrune F et al. (2019) Allogeneic reactivity-mediated endothelial cell complications after HSCT: a plea for consensual definitions. Blood advances 3(15):2424–2435. doi: 10.1182/bloodadvances.2019000143
231. Lesterhuis WJ, Rennings AJ, Leenders WP et al. (2009) Vascular endothelial growth factor in systemic capillary leak syndrome. The American journal of medicine 122(6):e5-7. doi: 10.1016/j.amjmed.2009.01.020
232. Abboud R, Wan F, Mariotti J et al. (2021) Cytokine release syndrome after haploidentical hematopoietic cell transplantation: an international multicenter analysis. Bone marrow transplantation 56(11):2763–2770. doi: 10.1038/s41409-021-01403-w
233. Shimabukuro-Vornhagen A, Gödel P, Subklewe M et al. (2018) Cytokine release syndrome. Journal for immunotherapy of cancer 6(1):56. doi: 10.1186/s40425-018-0343-9
234. Catani L, Gugliotta L, Vianelli N et al. (1996) Endothelium and bone marrow transplantation. Bone marrow transplantation 17(2):277–280
235. Akil A, Zhang Q, Mumaw CL et al. (2015) Biomarkers for Diagnosis and Prognosis of Sinusoidal Obstruction Syndrome after Hematopoietic Cell Transplantation. Biology of blood and marrow transplantation : journal of the American Society for Blood and Marrow Transplantation 21(10):1739–1745. doi: 10.1016/j.bbmt.2015.07.004
236. Stavrou E, Lazarus HM (2010) Thrombotic microangiopathy in haematopoietic cell transplantation: an update. Mediterranean journal of hematology and infectious diseases 2(3):e2010033. doi: 10.4084/MJHID.2010.033
237. Zeigler ZR, Rosenfeld CS, Andrews DF et al. (1996) Plasma von Willebrand factor antigen (vWF:AG) and thrombomodulin (TM) levels in adult thrombotic thrombocytopenic purpura/hemolytic uremic syndromes (TTP/HUS) and bone marrow transplant-associated thrombotic microangiopathy (BMT-TM). Am. J. Hematol. 53(4):213–220. doi: 10.1002/(SICI)1096-8652(199612)53:4<213:AID-AJH1>3.0.CO;2-0
238. Laurence J, Mitra D (1997) Apoptosis of microvascular endothelial cells in the pathophysiology of thrombotic thrombocytopenic purpura/sporadic hemolytic uremic syndrome. Seminars in hematology 34(2):98–105
239. Palomo M, Diaz-Ricart M, Carbo C et al. (2009) The release of soluble factors contributing to endothelial activation and damage after hematopoietic stem cell transplantation is not limited to the allogeneic setting and involves several pathogenic mechanisms. Biology of blood and marrow transplantation : journal of the American Society for Blood and Marrow Transplantation 15(5):537–546. doi: 10.1016/j.bbmt.2009.01.013

240. Penack O, Henke E, Suh D et al. (2010) Inhibition of neovascularization to simultaneously ameliorate graft-vs-host disease and decrease tumor growth. Journal of the National Cancer Institute 102(12):894–908. doi: 10.1093/jnci/djq172
241. Penack O, Socié G, van den Brink MRM (2011) The importance of neovascularization and its inhibition for allogeneic hematopoietic stem cell transplantation. Blood 117(16):4181–4189. doi: 10.1182/blood-2010-10-312934
242. Penack O, Holtan S (2019) The Endothelium During Allogeneic Stem Cell Transplantation. In: Socié G, Zeiser R, Blazar BR (eds) Immune biology of allogeneic hematopoietic stem cell transplantation. Models in discovery and translation, Second edition, Chapter 21. Academic Press, London, San Diego, CA, pp 401–414
243. Ge T, Yang J, Zhou S et al. (2020) The Role of the Pentose Phosphate Pathway in Diabetes and Cancer. Frontiers in endocrinology 11:365. doi: 10.3389/fendo.2020.00365
244. Leopold JA, Walker J, Scribner AW et al. (2003) Glucose-6-phosphate dehydrogenase modulates vascular endothelial growth factor-mediated angiogenesis. Journal of Biological Chemistry 278(34):32100–32106. doi: 10.1074/jbc.M301293200
245. Vizán P, Sánchez-Tena S, Alcarraz-Vizán G et al. (2009) Characterization of the metabolic changes underlying growth factor angiogenic activation: identification of new potential therapeutic targets. Carcinogenesis 30(6):946–952. doi: 10.1093/carcin/bgp083
246. Leopold JA, Cap A, Scribner AW et al. (2001) Glucose-6-phosphate dehydrogenase deficiency promotes endothelial oxidant stress and decreases endothelial nitric oxide bioavailability. FASEB journal : official publication of the Federation of American Societies for Experimental Biology 15(10):1771–1773. doi: 10.1096/fj.00-0893fje
247. Mele L, Paino F, Papaccio F et al. (2018) A new inhibitor of glucose-6-phosphate dehydrogenase blocks pentose phosphate pathway and suppresses malignant proliferation and metastasis in vivo. Cell death & disease 9(5):572. doi: 10.1038/s41419-018-0635-5
248. Koutcher JA, Alfieri AA, Matei C et al. (1996) Effect of 6-aminonicotinamide on the pentose phosphate pathway: 31P NMR and tumor growth delay studies. Magnetic resonance in medicine 36(6):887–892. doi: 10.1002/mrm.1910360611
249. Du Q-H, Peng C, Zhang H (2013) Polydatin: a review of pharmacology and pharmacokinetics. Pharmaceutical biology 51(11):1347–1354. doi: 10.3109/13880209.2013.792849
250. Hu W-H, Wang H-Y, Kong X-P et al. (2019) Polydatin suppresses VEGF-induced angiogenesis through binding with VEGF and inhibiting its receptor signaling. FASEB journal : official publication of the Federation of American Societies for Experimental Biology 33(1):532–544. doi: 10.1096/fj.201800750R
251. Yao H, Gong J, Feng Z et al. (052020) Pentose Phosphate Pathway Controls Endothelial Cell Proliferation During Hyperoxic Lung Injury in Neonates. In: C27. BRONCHOPULMONARY DYSPLASIA AND CONGENITAL LUNG LESIONS I. American Thoracic Society, A4663-A4663
252. Gao J, Zhao R, Xue Y et al. (2013) Role of enolase-1 in response to hypoxia in breast cancer: exploring the mechanisms of action. Oncology reports 29(4):1322–1332. doi: 10.3892/or.2013.2269
253. Jung D-W, Kim W-H, Park S-H et al. (2013) A unique small molecule inhibitor of enolase clarifies its role in fundamental biological processes. ACS chemical biology 8(6):1271–1282. doi: 10.1021/cb300687k
254. Cho H, Um J, Lee J-H et al. (2017) ENOblock, a unique small molecule inhibitor of the non-glycolytic functions of enolase, alleviates the symptoms of type 2 diabetes. Sci Rep 7(1):44186. doi: 10.1038/srep44186

255. Strydom DJ (1998) The angiogenins. Cellular and molecular life sciences : CMLS 54(8):811–824. doi: 10.1007/s000180050210
256. Crabtree B, Holloway DE, Baker MD et al. (2007) Biological and structural features of murine angiogenin-4, an angiogenic protein. Biochemistry 46(9):2431–2443. doi: 10.1021/bi062158n
257. Hooper LV, Stappenbeck TS, Hong CV et al. (2003) Angiogenins: a new class of microbicidal proteins involved in innate immunity. Nat Immunol 4(3):269–273. doi: 10.1038/ni888
258. Yan L, He Z, Li W et al. (2021) The Overexpression of Acyl-CoA Medium-Chain Synthetase-3 (ACSM3) Suppresses the Ovarian Cancer Progression via the Inhibition of Integrin β1/AKT Signaling Pathway. Frontiers in oncology 11:644840. doi: 10.3389/fonc.2021.644840
259. Shen N, Ffrench P, Guyotat D et al. (1994) Expression of adhesion molecules in endothelial cells during allogeneic bone marrow transplantation. European journal of haematology 52(5):296–301. doi: 10.1111/j.1600-0609.1994.tb00099.x
260. Roy J, Platt JL, Weisdorf DJ (1993) The immunopathology of upper gastrointestinal acute graft-versus-host disease. Lymphoid cells and endothelial adhesion molecules. Transplantation 55(3):572–578. doi: 10.1097/00007890-199303000-00022
261. Matsuda Y, Hara J, Osugi Y et al. (2001) Serum levels of soluble adhesion molecules in stem cell transplantation-related complications. Bone marrow transplantation 27(9):977–982. doi: 10.1038/sj.bmt.1703026
262. Luft T, Dietrich S, Falk C et al. (2011) Steroid-refractory GVHD: T-cell attack within a vulnerable endothelial system. Blood 118(6):1685–1692. doi: 10.1182/blood-2011-02-334821
263. Almici C, Skert C, Bruno B et al. (2017) Circulating endothelial cell count: a reliable marker of endothelial damage in patients undergoing hematopoietic stem cell transplantation. Bone marrow transplantation 52(12):1637–1642. doi: 10.1038/bmt.2017.194
264. Medinger M, Tichelli A, Bucher C et al. (2013) GVHD after allogeneic haematopoietic SCT for AML: angiogenesis, vascular endothelial growth factor and VEGF receptor expression in the BM. Bone marrow transplantation 48(5):715–721. doi: 10.1038/bmt.2012.200
265. Leonhardt F, Grundmann S, Behe M et al. (2013) Inflammatory neovascularization during graft-versus-host disease is regulated by αv integrin and miR-100. Blood 121(17):3307–3318. doi: 10.1182/blood-2012-07-442665
266. Shulman HM, Sullivan KM, Weiden PL et al. (1980) Chronic graft-versus-host syndrome in man. The American journal of medicine 69(2):204–217. doi: 10.1016/0002-9343(80)90380-0
267. Biedermann BC, Sahner S, Gregor M et al. (2002) Endothelial injury mediated by cytotoxic T lymphocytes and loss of microvessels in chronic graft versus host disease. Lancet (London, England) 359(9323):2078–2083. doi: 10.1016/S0140-6736(02)08907-9
268. Deschaumes C, Verneuil L, Ertault-Daneshpouy M et al. (2007) CD95 ligand-dependant endothelial cell death initiates oral mucosa damage in a murine model of acute graft versus host disease. Laboratory investigation; a journal of technical methods and pathology 87(5):417–429. doi: 10.1038/labinvest.3700541
269. Kitko CL, Levine JE, Storer BE et al. (2014) Plasma CXCL9 elevations correlate with chronic GVHD diagnosis. Blood 123(5):786–793. doi: 10.1182/blood-2013-08-520072
270. Kariminia A, Holtan SG, Ivison S et al. (2016) Heterogeneity of chronic graft-versus-host disease biomarkers: association with CXCL10 and CXCR3+ NK cells. Blood 127(24):3082–3091. doi: 10.1182/blood-2015-09-668251
271. Ribatti D, Nico B, Crivellato E et al. (2005) Endothelial progenitor cells in health and disease. Histology and histopathology 20(4):1351–1358. doi: 10.14670/HH-20.1351
272. Endemann DH, Schiffrin EL (2004) Endothelial dysfunction. Journal of the American Society of Nephrology : JASN 15(8):1983–1992. doi: 10.1097/01.ASN.0000132474.50966.DA

273. Dessein PH, Joffe BI, Singh S (2005) Biomarkers of endothelial dysfunction, cardiovascular risk factors and atherosclerosis in rheumatoid arthritis. Arthritis research & therapy 7(3):R634-43. doi: 10.1186/ar1717
274. Riccieri V, Stefanantoni K, Vasile M et al. (2011) Abnormal plasma levels of different angiogenic molecules are associated with different clinical manifestations in patients with systemic sclerosis. Clinical and experimental rheumatology 29(2 Suppl 65):S46-52
275. Zhou Y, Huang H, Yuan L-J et al. (2015) CD146 as an adverse prognostic factor in uterine sarcoma. European Journal of Medical Research 20(1):67. doi: 10.1186/s40001-015-0160-2
276. Luft T, Benner A, Terzer T et al. (2020) EASIX and mortality after allogeneic stem cell transplantation. Bone marrow transplantation 55(3):553–561. doi: 10.1038/s41409-019-0703-1
277. Nishinarita S, Yamamoto M, Takizawa T et al. (1990) Increased plasma fibronectin in patients with systemic lupus erythematosus. Clinical Rheumatology 9(2):214–219. doi: 10.1007/BF02031971
278. Przybysz M, Borysewicz K, Kątnik-Prastowska I (2013) Fibronectin molecular status determination useful to differentiate between rheumatoid arthritis and systemic lupus erythematosus patients. Rheumatology International 33(1):37–43. doi: 10.1007/s00296-011-2269-0
279. Bhattacharyya S, Tamaki Z, Wang W et al. (2014) FibronectinEDA promotes chronic cutaneous fibrosis through Toll-like receptor signaling. Science translational medicine 6(232):232ra50. doi: 10.1126/scitranslmed.3008264
280. van der Straaten HM, Canninga-van Dijk MR, Verdonck LF et al. (2004) Extra-domain-A fibronectin: a new marker of fibrosis in cutaneous graft-versus-host disease. The Journal of investigative dermatology 123(6):1057–1062. doi: 10.1111/j.0022-202X.2004.23474.x
281. Holtan SG, Verneris MR, Schultz KR et al. (2015) Circulating angiogenic factors associated with response and survival in patients with acute graft-versus-host disease: results from Blood and Marrow Transplant Clinical Trials Network 0302 and 0802. Biology of blood and marrow transplantation : journal of the American Society for Blood and Marrow Transplantation 21(6):1029–1036. doi: 10.1016/j.bbmt.2015.02.018
282. Yoshio T, Masuyama J, Mimori A et al. (1995) Endothelin-1 release from cultured endothelial cells induced by sera from patients with systemic lupus erythematosus. Annals of the rheumatic diseases 54(5):361–365. doi: 10.1136/ard.54.5.361
283. Aghaei M, Gharibdost F, Zayeni H et al. (2012) Endothelin-1 in systemic sclerosis. Indian dermatology online journal 3(1):14–16. doi: 10.4103/2229-5178.93484
284. Hiroyasu S, Shiraishi M, Kusano T et al. (1997) Involvement of endothelin in graft-versus-host disease after rat small bowel transplantation. Transplant international : official journal of the European Society for Organ Transplantation 10(2):121–124. doi: 10.1007/s001470050024
285. Newell LF, Defor TE, Cutler CS et al. (2017) Follistatin and Endoglin: Potential Biomarkers of Endothelial Damage and Non-Relapse Mortality after Myeloablative Allogeneic Hematopoietic Cell Transplantation in Blood and Marrow Transplant Clinical Trials Network (BMT CTN) 0402. Biology of Blood and Marrow Transplantation 23(3):S73-S74. doi: 10.1016/j.bbmt.2017.01.030
286. Wipff J, Avouac J, Borderie D et al. (2008) Disturbed angiogenesis in systemic sclerosis: high levels of soluble endoglin. Rheumatology (Oxford, England) 47(7):972–975. doi: 10.1093/rheumatology/ken100
287. Li D, Wang Y, Xu N et al. (2011) Follistatin-like protein 1 is elevated in systemic autoimmune diseases and correlated with disease activity in patients with rheumatoid arthritis. Arthritis research & therapy 13(1):R17. doi: 10.1186/ar3241

288. Reiseter S, Molberg Ø, Gunnarsson R et al. (2015) Associations between circulating endostatin levels and vascular organ damage in systemic sclerosis and mixed connective tissue disease: an observational study. Arthritis research & therapy 17:231. doi: 10.1186/s13075-015-0756-5
289. Wan Y-Y, Tian G-Y, Guo H-S et al. (2013) Endostatin, an angiogenesis inhibitor, ameliorates bleomycin-induced pulmonary fibrosis in rats. Respiratory research 14(1):56. doi: 10.1186/1465-9921-14-56
290. Yang X, Lin K, Ni S et al. (2017) Serum connective tissue growth factor is a highly discriminatory biomarker for the diagnosis of rheumatoid arthritis. Arthritis research & therapy 19(1):257. doi: 10.1186/s13075-017-1463-1
291. Liu S-C, Chuang S-M, Hsu C-J et al. (2014) CTGF increases vascular endothelial growth factor-dependent angiogenesis in human synovial fibroblasts by increasing miR-210 expression. Cell death & disease 5:e1485. doi: 10.1038/cddis.2014.453
292. Vanstapel A, Goldschmeding R, Broekhuizen R et al. (2021) Connective Tissue Growth Factor in Chronic Lung Allograft Dysfunction: An Explorative Study. The Journal of Heart and Lung Transplantation 40(4):S151-S152. doi: 10.1016/j.healun.2021.01.461
293. Zhou L, Askew D, Wu C et al. (2007) Cutaneous gene expression by DNA microarray in murine sclerodermatous graft-versus-host disease, a model for human scleroderma. The Journal of investigative dermatology 127(2):281–292. doi: 10.1038/sj.jid.5700517
294. Krishnan S, Kiang JG, Fisher CU et al. (2005) Increased caspase-3 expression and activity contribute to reduced CD3zeta expression in systemic lupus erythematosus T cells. Journal of immunology (Baltimore, Md. : 1950) 175(5):3417–3423. doi: 10.4049/jimmunol.175.5.3417
295. Yang B, Lan S, Dieudé M et al. (2018) Caspase-3 Is a Pivotal Regulator of Microvascular Rarefaction and Renal Fibrosis after Ischemia-Reperfusion Injury. Journal of the American Society of Nephrology : JASN 29(7):1900–1916. doi: 10.1681/ASN.2017050581
296. Laplante P, Sirois I, Raymond M-A et al. (2010) Caspase-3-mediated secretion of connective tissue growth factor by apoptotic endothelial cells promotes fibrosis. Cell death and differentiation 17(2):291–303. doi: 10.1038/cdd.2009.124
297. Aciksari G, Kavas M, Atici A et al. (2018) Endocan Levels and Endothelial Dysfunction in Patients With Sarcoidosis. Angiology 69(10):878–883. doi: 10.1177/0003319718775283
298. Balta S, Mikhailidis DP, Demirkol S et al. (2015) Endocan: A novel inflammatory indicator in cardiovascular disease? Atherosclerosis 243(1):339–343. doi: 10.1016/j.atherosclerosis.2015.09.030
299. Lindås R, Tvedt THA, Hatfield KJ et al. (2014) Preconditioning serum levels of endothelial cell-derived molecules and the risk of posttransplant complications in patients treated with allogeneic stem cell transplantation. Journal of transplantation 2014:404096. doi: 10.1155/2014/404096
300. Ullman-Culleré MH, Foltz CJ (1999) Body condition scoring. A rapid and accurate method for assessing health status in mice. Laboratory animal science 49(3):319–323
301. Du J, Paz K, Flynn R et al. (2017) Pirfenidone ameliorates murine chronic GVHD through inhibition of macrophage infiltration and TGF-β production. Blood 129(18):2570–2580. doi: 10.1182/blood-2017-01-758854
302. Fehrenbacher JC, Vasko MR, Duarte DB (2012) Models of inflammation. Carrageenan- or complete Freund's Adjuvant (CFA)-induced edema and hypersensitivity in the rat. Current protocols in pharmacology Chapter 5:Unit5.4. doi: 10.1002/0471141755.ph0504s56
303. Lerner KG, Kao GF, Storb R et al. (1974) Histopathology of graft-vs.-host reaction (GvHR) in human recipients of marrow from HL-A-matched sibling donors. Transplantation proceedings 6(4):367–371

304. Cooke KR, Kobzik L, Martin TR et al. (1996) An experimental model of idiopathic pneumonia syndrome after bone marrow transplantation. I. The roles of minor H antigens and endotoxin. Blood 88(8):3230–3239
305. Shulman HM, Kleiner D, Lee SJ et al. (2006) Histopathologic diagnosis of chronic graft-versus-host disease. National Institutes of Health Consensus Development Project on Criteria for Clinical Trials in Chronic Graft-versus-Host Disease: II. Pathology Working Group Report. Biology of blood and marrow transplantation : journal of the American Society for Blood and Marrow Transplantation 12(1):31–47. doi: 10.1016/j.bbmt.2005.10.023
306. Schindelin J, Arganda-Carreras I, Frise E et al. (2012) Fiji. An open-source platform for biological-image analysis. Nature methods 9(7):676–682. doi: 10.1038/nmeth.2019
307. Bolte S, Cordelières FP (2006) A guided tour into subcellular colocalization analysis in light microscopy. Journal of microscopy 224(Pt 3):213–232. doi: 10.1111/j.1365-2818.2006.01706.x
308. Livak KJ, Schmittgen TD (2001) Analysis of relative gene expression data using real-time quantitative PCR and the 2(-Delta Delta C(T)) Method. Methods (San Diego, Calif.) 25(4):402–408. doi: 10.1006/meth.2001.1262
309. Concordet J-P, Haeussler M (2018) CRISPOR. Intuitive guide selection for CRISPR/Cas9 genome editing experiments and screens. Nucleic acids research 46(W1):W242-W245. doi: 10.1093/nar/gky354
310. Ran FA, Hsu PD, Wright J et al. (2013) Genome engineering using the CRISPR-Cas9 system. Nature protocols 8(11):2281–2308. doi: 10.1038/nprot.2013.143
311. M. Wayne Davis, M. Jorgensen (2022) ApE, A Plasmid Editor: A Freely Available DNA Manipulation and Visualization Program. TECHNOLOGY AND CODE article. Frontiers Bioinformatics(Section Data Visualization)
312. Jat PS, Noble MD, Ataliotis P et al. (1991) Direct derivation of conditionally immortal cell lines from an H-2Kb-tsA58 transgenic mouse. Proceedings of the National Academy of Sciences of the United States of America 88(12):5096–5100. doi: 10.1073/pnas.88.12.5096
313. Lidington EA, Rao RM, Marelli-Berg FM et al. (2002) Conditional immortalization of growth factor-responsive cardiac endothelial cells from H-2K(b)-tsA58 mice. American journal of physiology. Cell physiology 282(1):C67-74. doi: 10.1152/ajpcell.2002.282.1.C67
314. Lipps C, Klein F, Wahlicht T et al. (2018) Expansion of functional personalized cells with specific transgene combinations. Nature communications 9(1):994. doi: 10.1038/s41467-018-03408-4
315. Matsumura T, Takesue M, Westerman KA et al. (2004) Establishment of an immortalized human-liver endothelial cell line with SV40T and hTERT. Transplantation 77(9):1357–1365. doi: 10.1097/01.tp.0000124286.82961.7e
316. Mosmann T (1983) Rapid colorimetric assay for cellular growth and survival. Application to proliferation and cytotoxicity assays. Journal of immunological methods 65(1-2):55–63. doi: 10.1016/0022-1759(83)90303-4
317. Gilles Carpentier (2012) Contribution: Angiogenesis Analyzer.
318. (1988) Nervous System. Springer, Berlin, Heidelberg
319. Torti VR, Heath JE, Fulton R et al. (2004) Toxicity study of 6-aminonicotinamide (6-AN), 6-MMPR, and PALA in mice. Cancer Res 64(7_Supplement):485
320. Sari I, Cetin A, Kaynar L et al. (2008) Disturbance of pro-oxidative/antioxidative balance in allogeneic peripheral blood stem cell transplantation. Annals of clinical and laboratory science 38(2):120–125
321. Yi T, Li X, Wang E et al. (2018) Activation of the Nuclear Erythroid 2-Related Factor 2 Antioxidant Responsive Element (Nrf2-ARE) Signaling Pathway Alleviates Acute Graft-Versus-Host Disease by Reducing Oxidative Stress and Inhibiting Infiltration of Inflammatory Cells in an

Allogeneic Stem Cell Transplantation Mouse Model. Medical Science Monitor : International Medical Journal of Experimental and Clinical Research 24:5973–5979. doi: 10.12659/MSM.908130

322. Sun Y, Wang Y, Toubai T et al. (2015) BET bromodomain inhibition suppresses graft-versus-host disease after allogeneic bone marrow transplantation in mice. Blood 125(17):2724–2728. doi: 10.1182/blood-2014-08-598037
323. Hecker PA, Leopold JA, Gupte SA et al. (2013) Impact of glucose-6-phosphate dehydrogenase deficiency on the pathophysiology of cardiovascular disease. American Journal of Physiology - Heart and Circulatory Physiology 304(4):H491-500. doi: 10.1152/ajpheart.00721.2012
324. Leopold JA, Zhang Y-Y, Scribner AW et al. (2003) Glucose-6-phosphate dehydrogenase overexpression decreases endothelial cell oxidant stress and increases bioavailable nitric oxide. Arteriosclerosis, thrombosis, and vascular biology 23(3):411–417. doi: 10.1161/01.ATV.0000056744.26901.BA
325. Kalucka J, Bierhansl L, Conchinha NV et al. (2018) Quiescent Endothelial Cells Upregulate Fatty Acid β-Oxidation for Vasculoprotection via Redox Homeostasis. Cell metabolism 28(6):881-894.e13. doi: 10.1016/j.cmet.2018.07.016
326. Park C, Lee Y, Je S et al. (2019) Overexpression and Selective Anticancer Efficacy of ENO3 in STK11 Mutant Lung Cancers. Molecules and Cells 42(11):804–809. doi: 10.14348/molcells.2019.0099
327. Pancholi V (2001) Multifunctional alpha-enolase: its role in diseases. Cellular and molecular life sciences : CMLS 58(7):902–920. doi: 10.1007/pl00000910
328. Discher DJ, Bishopric NH, Wu X et al. (1998) Hypoxia regulates beta-enolase and pyruvate kinase-M promoters by modulating Sp1/Sp3 binding to a conserved GC element. Journal of Biological Chemistry 273(40):26087–26093. doi: 10.1074/jbc.273.40.26087
329. Shi Y, Liu J, Zhang R et al. (2023) Targeting Endothelial ENO1 (Alpha-Enolase) -PI3K-Akt-mTOR Axis Alleviates Hypoxic Pulmonary Hypertension. Hypertension 80(5):1035–1047. doi: 10.1161/HYPERTENSIONAHA.122.19857
330. Stappenbeck TS, Hooper LV, Gordon JI (2002) Developmental regulation of intestinal angiogenesis by indigenous microbes via Paneth cells. Proceedings of the National Academy of Sciences of the United States of America 99(24):15451–15455. doi: 10.1073/pnas.202604299
331. Haraldsen G, Rugtveit J, Kvale D et al. (1995) Isolation and longterm culture of human intestinal microvascular endothelial cells. Gut 37(2):225–234. doi: 10.1136/gut.37.2.225
332. Bevilacqua MP, Nelson RM, Mannori G et al. (1994) Endothelial-leukocyte adhesion molecules in human disease. Annual review of medicine 45:361–378. doi: 10.1146/annurev.med.45.1.361
333. Nguyen HD, Kuril S, Bastian D et al. (2018) T-Cell Metabolism in Hematopoietic Cell Transplantation. Frontiers in immunology 9:176. doi: 10.3389/fimmu.2018.00176
334. Tijaro-Ovalle NM, Karantanos T, Wang H-T et al. (2019) Metabolic Targets for Improvement of Allogeneic Hematopoietic Stem Cell Transplantation and Graft-vs.-Host Disease. Frontiers in immunology 10:295. doi: 10.3389/fimmu.2019.00295
335. Mhandire K, Saggu K, Buxbaum NP (2021) Immunometabolic Therapeutic Targets of Graft-versus-Host Disease (GvHD). Metabolites 11(11). doi: 10.3390/metabo11110736
336. Li X, Sun X, Carmeliet P (2019) Hallmarks of Endothelial Cell Metabolism in Health and Disease. Cell metabolism 30(3):414–433. doi: 10.1016/j.cmet.2019.08.011
337. Walker DL, Reid JM, Svingen PA et al. (1999) Murine pharmacokinetics of 6-aminonicotinamide (NSC 21206), a novel biochemical modulating agent. Biochemical pharmacology 58(6):1057–1066. doi: 10.1016/s0006-2952(99)00179-3

338. Karami A, Fakhri S, Kooshki L et al. (2022) Polydatin: Pharmacological Mechanisms, Therapeutic Targets, Biological Activities, and Health Benefits. Molecules (Basel, Switzerland) 27(19). doi: 10.3390/molecules27196474
339. Xie X, Peng J, Huang K et al. (2012) Polydatin ameliorates experimental diabetes-induced fibronectin through inhibiting the activation of NF-κB signaling pathway in rat glomerular mesangial cells. Molecular and Cellular Endocrinology 362(1-2):183–193. doi: 10.1016/j.mce.2012.06.008
340. Yao J, Wang J-Y, Liu L et al. (2011) Polydatin ameliorates DSS-induced colitis in mice through inhibition of nuclear factor-kappaB activation. Planta medica 77(5):421–427. doi: 10.1055/s-0030-1250462
341. Liao P, He Y, Yang F et al. (2018) Polydatin effectively attenuates disease activity in lupus-prone mouse models by blocking ROS-mediated NET formation. Arthritis research & therapy 20(1):254. doi: 10.1186/s13075-018-1749-y
342. Salhotra A, Tsai W, Yang D et al. (2020) Assessment of Anti-Oxidant Markers of Inflammation in Patients with Chronic Graft-Versus-Host Disease. Biology of Blood and Marrow Transplantation 26(3):S191-S192. doi: 10.1016/j.bbmt.2019.12.758
343. Zhao K-S, Jin C, Huang X et al. (2003) The mechanism of Polydatin in shock treatment. Clinical hemorheology and microcirculation 29(3-4):211–217
344. Deng Y-H, Alex D, Huang H-Q et al. (2011) Inhibition of TNF-α-mediated endothelial cell-monocyte cell adhesion and adhesion molecules expression by the resveratrol derivative, trans-3,5,4'-trimethoxystilbene. Phytotherapy research : PTR 25(3):451–457. doi: 10.1002/ptr.3279
345. Jain RK, Duda DG, Clark JW et al. (2006) Lessons from phase III clinical trials on anti-VEGF therapy for cancer. Nature clinical practice. Oncology 3(1):24–40. doi: 10.1038/ncponc0403
346. Quagliariello V, Berretta M, Buccolo S et al. (2021) Polydatin Reduces Cardiotoxicity and Enhances the Anticancer Effects of Sunitinib by Decreasing Pro-Oxidative Stress, Pro-Inflammatory Cytokines, and NLRP3 Inflammasome Expression. Frontiers in oncology 11:680758. doi: 10.3389/fonc.2021.680758
347. Bouïs D, Hospers GA, Meijer C et al. (2001) Endothelium in vitro: a review of human vascular endothelial cell lines for blood vessel-related research. Angiogenesis 4(2):91–102. doi: 10.1023/a:1012259529167
348. Bachetti T, Morbidelli L (2000) Endothelial cells in culture: a model for studying vascular functions. Pharmacological research 42(1):9–19. doi: 10.1006/phrs.1999.0655
349. Durr E, Yu J, Krasinska KM et al. (2004) Direct proteomic mapping of the lung microvascular endothelial cell surface in vivo and in cell culture. Nature biotechnology 22(8):985–992. doi: 10.1038/nbt993
350. Fallon ME, Mathews R, Hinds MT (2022) In Vitro Flow Chamber Design for the Study of Endothelial Cell (Patho)Physiology. Journal of Biomechanical Engineering 144(2). doi: 10.1115/1.4051765
351. Verlaat L, Riesner K, Kalupa M et al. (2022) Novel pre-clinical mouse models for chronic Graft-versus-Host Disease. Frontiers in immunology 13:1079921. doi: 10.3389/fimmu.2022.1079921
352. Majolino I, Saglio G, Scimè R et al. (1996) High incidence of chronic GVHD after primary allogeneic peripheral blood stem cell transplantation in patients with hematologic malignancies. Bone marrow transplantation 17(4):555–560
353. Storek J, Gooley T, Siadak M et al. (1997) Allogeneic peripheral blood stem cell transplantation may be associated with a high risk of chronic graft-versus-host disease. Blood 90(12):4705–4709
354. Chen H-R, Ji S-Q, Wang H-X et al. (2002) Allogeneic bone marrow transplantation for chronic myeloid leukemia using HLA identical sibling donors primed with G-CSF. Zhongguo shi yan xue ye xue za zhi 10(4):340–346

355. Ochs LA, Blazar BR, Roy J et al. (1996) Cytokine expression in human cutaneous chronic graft-versus-host disease. Bone marrow transplantation 17(6):1085–1092
356. Inamoto Y, Flowers MED, Sandmaier BM et al. (2014) Failure-free survival after initial systemic treatment of chronic graft-versus-host disease. Blood 124(8):1363–1371. doi: 10.1182/blood-2014-03-563544
357. Strasser SI, Shulman HM, Flowers ME et al. (2000) Chronic graft-versus-host disease of the liver: presentation as an acute hepatitis. Hepatology (Baltimore, Md.) 32(6):1265–1271. doi: 10.1053/jhep.2000.20067
358. Maung K, Ramalingam S, Chaudhry M et al. (2020) Pre-transplant hepatic steatosis (fatty liver) is associated with chronic graft-vs-host disease but not mortality. PLoS ONE 15(9):e0238824. doi: 10.1371/journal.pone.0238824
359. Dudek AZ, Mahaseth H, Defor TE et al. (2003) Bronchiolitis obliterans in chronic graft-versus-host disease: analysis of risk factors and treatment outcomes. Biology of Blood and Marrow Transplantation 9(10):657–666. doi: 10.1016/s1083-8791(03)00242-8
360. Chien JW, Duncan S, Williams KM et al. (2010) Bronchiolitis obliterans syndrome after allogeneic hematopoietic stem cell transplantation-an increasingly recognized manifestation of chronic graft-versus-host disease. Biology of blood and marrow transplantation : journal of the American Society for Blood and Marrow Transplantation 16(1 Suppl):S106-14. doi: 10.1016/j.bbmt.2009.11.002
361. Shulman HM, Cardona DM, Greenson JK et al. (2015) NIH Consensus development project on criteria for clinical trials in chronic graft-versus-host disease: II. The 2014 Pathology Working Group Report. Biology of blood and marrow transplantation : journal of the American Society for Blood and Marrow Transplantation 21(4):589–603. doi: 10.1016/j.bbmt.2014.12.031
362. Wynn TA (2004) Fibrotic disease and the T(H)1/T(H)2 paradigm. Nature reviews. Immunology 4(8):583–594. doi: 10.1038/nri1412
363. Levi-Schaffer F, Weg VB (1997) Mast cells, eosinophiles and fibrosis. Clinical and experimental allergy : journal of the British Society for Allergy and Clinical Immunology 27 Suppl 1:64–70. doi: 10.1111/j.1365-2222.1997.tb01829.x
364. Ding L, Yang J, Zhang C et al. (2021) Neutrophils Modulate Fibrogenesis in Chronic Pulmonary Diseases. Frontiers in medicine 8:616200. doi: 10.3389/fmed.2021.616200
365. Choi KL, Giorno R, Claman HN (1987) Cutaneous mast cell depletion and recovery in murine graft-vs-host disease. Journal of immunology (Baltimore, Md. : 1950) 138(12):4093–4101
366. Nonomura A, Kono N, Mizukami Y et al. (1996) Histological changes of the liver in experimental graft-versus-host disease across minor histocompatibility barriers. VIII. Role of eosinophil infiltration. Liver 16(1):42–47. doi: 10.1111/j.1600-0676.1996.tb00702.x
367. Mensen A, Jöhrens K, Anagnostopoulos I et al. (2014) Bone marrow T-cell infiltration during acute GVHD is associated with delayed B-cell recovery and function after HSCT. Blood 124(6):963–972. doi: 10.1182/blood-2013-11-539031
368. Jacobson CA, Sun L, Kim HT et al. (2014) Post-transplantation B cell activating factor and B cell recovery before onset of chronic graft-versus-host disease. Biology of blood and marrow transplantation : journal of the American Society for Blood and Marrow Transplantation 20(5):668–675. doi: 10.1016/j.bbmt.2014.01.021
369. Sarantopoulos S, Blazar BR, Cutler C et al. (2015) B cells in chronic graft-versus-host disease. Biology of blood and marrow transplantation : journal of the American Society for Blood and Marrow Transplantation 21(1):16–23. doi: 10.1016/j.bbmt.2014.10.029
370. Sarantopoulos S, Stevenson KE, Kim HT et al. (2009) Altered B-cell homeostasis and excess BAFF in human chronic graft-versus-host disease. Blood 113(16):3865–3874. doi: 10.1182/blood-2008-09-177840

371. Reddy V, Iturraspe JA, Tzolas AC et al. (2004) Low dendritic cell count after allogeneic hematopoietic stem cell transplantation predicts relapse, death, and acute graft-versus-host disease. Blood 103(11):4330–4335. doi: 10.1182/blood-2003-09-3325
372. Leveque-El Mouttie L, Koyama M, Le Texier L et al. (2016) Corruption of dendritic cell antigen presentation during acute GVHD leads to regulatory T-cell failure and chronic GVHD. Blood 128(6):794–804. doi: 10.1182/blood-2015-11-680876
373. Widmer MB, Bach FH (1972) Allogeneic and xenogeneic response in mixed leukocyte cultures. The Journal of experimental medicine 135(5):1204–1208. doi: 10.1084/jem.135.5.1204
374. Freeman GJ, Borriello F, Hodes RJ et al. (1993) Murine B7-2, an alternative CTLA4 counter-receptor that costimulates T cell proliferation and interleukin 2 production. The Journal of experimental medicine 178(6):2185–2192. doi: 10.1084/jem.178.6.2185
375. Hülsdünker J, Zeiser R (2015) Insights into the pathogenesis of GvHD: what mice can teach us about man. Tissue antigens 85(1):2–9. doi: 10.1111/tan.12497
376. Kollman C, Howe CW, Anasetti C et al. (2001) Donor characteristics as risk factors in recipients after transplantation of bone marrow from unrelated donors: the effect of donor age. Blood 98(7):2043–2051. doi: 10.1182/blood.V98.7.2043
377. Hurst JL, West RS (2010) Taming anxiety in laboratory mice. Nature methods 7(10):825–826. doi: 10.1038/nmeth.1500
378. Santos GW, Tutschka PJ, Brookmeyer R et al. (1983) Marrow transplantation for acute nonlymphocytic leukemia after treatment with busulfan and cyclophosphamide. The New England journal of medicine 309(22):1347–1353. doi: 10.1056/NEJM198312013092202
379. Schulte D, Küppers V, Dartsch N et al. (2011) Stabilizing the VE-cadherin-catenin complex blocks leukocyte extravasation and vascular permeability. The EMBO journal 30(20):4157–4170. doi: 10.1038/emboj.2011.304
380. Hackman RC, Madtes DK, Petersen FB et al. (1989) Pulmonary venoocclusive disease following bone marrow transplantation. Transplantation 47(6):989–992. doi: 10.1097/00007890-198906000-00014
381. Seguchi M, Hirabayashi N, Fujii Y et al. (2000) Pulmonary hypertension associated with pulmonary occlusive vasculopathy after allogeneic bone marrow transplantation. Transplantation 69(1):177–179. doi: 10.1097/00007890-200001150-00030
382. Wingard JR, Mellits ED, Jones RJ et al. (1989) Association of hepatic veno-occlusive disease with interstitial pneumonitis in bone marrow transplant recipients. Bone marrow transplantation 4(6):685–689
383. Grigg A, Buchanan M, Whitford H (2005) Late-onset pulmonary arterial hypertension in association with graft-versus-host disease after allogeneic stem-cell transplantation. Am. J. Hematol. 80(1):38–42. doi: 10.1002/ajh.20373
384. Thenappan T, Ormiston ML, Ryan JJ et al. (2018) Pulmonary arterial hypertension: pathogenesis and clinical management. BMJ (Clinical research ed.) 360:j5492. doi: 10.1136/bmj.j5492
385. Skalli O, Pelte MF, Peclet MC et al. (1989) Alpha-smooth muscle actin, a differentiation marker of smooth muscle cells, is present in microfilamentous bundles of pericytes. The journal of histochemistry and cytochemistry : official journal of the Histochemistry Society 37(3):315–321. doi: 10.1177/37.3.2918221
386. Sun K-H, Chang Y, Reed NI et al. (2016) α-Smooth muscle actin is an inconsistent marker of fibroblasts responsible for force-dependent TGFβ activation or collagen production across multiple models of organ fibrosis. American Journal of Physiology - Lung Cellular and Molecular Physiology 310(9):L824-36. doi: 10.1152/ajplung.00350.2015

387. Ando H, Kubin T, Schaper W et al. (1999) Cardiac microvascular endothelial cells express alpha-smooth muscle actin and show low NOS III activity. The American journal of physiology 276(5):H1755-68. doi: 10.1152/ajpheart.1999.276.5.H1755
388. Wang Y, Liang A, Luo J et al. (2014) Blocking Notch in endothelial cells prevents arteriovenous fistula failure despite CKD. Journal of the American Society of Nephrology : JASN 25(4):773–783. doi: 10.1681/ASN.2013050490
389. Lee K-H, Lee J-H, Choi S-J et al. (2004) Failure of trilineage blood cell reconstitution after initial neutrophil engraftment in patients undergoing allogeneic hematopoietic cell transplantation - frequency and outcomes. Bone marrow transplantation 33(7):729–734. doi: 10.1038/sj.bmt.1704428
390. Richardson MR, Yoder MC (2011) Endothelial progenitor cells: quo vadis? Journal of molecular and cellular cardiology 50(2):266–272. doi: 10.1016/j.yjmcc.2010.07.009
391. Asosingh K, Aldred MA, Vasanji A et al. (2008) Circulating angiogenic precursors in idiopathic pulmonary arterial hypertension. The American journal of pathology 172(3):615–627. doi: 10.2353/ajpath.2008.070705
392. Hill JM, Zalos G, Halcox JPJ et al. (2003) Circulating endothelial progenitor cells, vascular function, and cardiovascular risk. The New England journal of medicine 348(7):593–600. doi: 10.1056/NEJMoa022287
393. Wara AK, Foo S, Croce K et al. (2011) TGF-β1 signaling and Krüppel-like factor 10 regulate bone marrow-derived proangiogenic cell differentiation, function, and neovascularization. Blood 118(24):6450–6460. doi: 10.1182/blood-2011-06-363713
394. Rose JA, Erzurum S, Asosingh K (2015) Biology and flow cytometry of proangiogenic hematopoietic progenitors cells. Cytometry. Part A : the journal of the International Society for Analytical Cytology 87(1):5–19. doi: 10.1002/cyto.a.22596
395. Wang W, Ye Y, Du Y et al. (2022) EPC infusion ameliorates acute graft-versus-host disease-related endothelial injury after allogeneic bone marrow transplantation. Frontiers in immunology 13:1019657. doi: 10.3389/fimmu.2022.1019657
396. Cao X-N, Kong Y, Song Y et al. (2018) Impairment of bone marrow endothelial progenitor cells in acute graft-versus-host disease patients after allotransplant. British journal of haematology 182(6):870–886. doi: 10.1111/bjh.15456
397. Takamatsu A, Nakashima Y, Haji S et al. (2022) Circulating endothelial cells and endothelial progenitor cells as potential predictors of acute GVHD after allogeneic hematopoietic stem cell transplantation. European journal of haematology 109(2):146–153. doi: 10.1111/ejh.13781
398. Medinger M, Heim D, Gerull S et al. (2016) Increase of endothelial progenitor cells in acute graft-versus-host disease after allogeneic haematopoietic stem cell transplantation for acute myeloid leukaemia. Leukemia research 47:22–25. doi: 10.1016/j.leukres.2016.05.011
399. Heldin CH, Miyazono K, Dijke P ten (1997) TGF-beta signalling from cell membrane to nucleus through SMAD proteins. Nature 390(6659):465–471. doi: 10.1038/37284
400. Lebrin F, Goumans M-J, Jonker L et al. (2004) Endoglin promotes endothelial cell proliferation and TGF-beta/ALK1 signal transduction. The EMBO journal 23(20):4018–4028. doi: 10.1038/sj.emboj.7600386
401. Andrae J, Gallini R, Betsholtz C (2008) Role of platelet-derived growth factors in physiology and medicine. Genes & development 22(10):1276–1312. doi: 10.1101/gad.1653708
402. Kvietys PR, Granger DN (1997) Endothelial cell monolayers as a tool for studying microvascular pathophysiology. The American journal of physiology 273(6):G1189-99. doi: 10.1152/ajpgi.1997.273.6.G1189

403. Gehlsen U, Stary D, Maass M et al. (2021) Ocular Graft-versus-Host Disease in a Chemotherapy-Based Minor-Mismatch Mouse Model Features Corneal (Lymph-) Angiogenesis. International journal of molecular sciences 22(12). doi: 10.3390/ijms22126191
404. Riemens A, te Boome L, Imhof S et al. (2010) Current insights into ocular graft-versus-host disease. Current opinion in ophthalmology 21(6):485–494. doi: 10.1097/ICU.0b013e32833eab64
405. Li Z, Liu X, Wang B et al. (2017) Pirfenidone suppresses MAPK signalling pathway to reverse epithelial-mesenchymal transition and renal fibrosis. Nephrology (Carlton, Vic.) 22(8):589–597. doi: 10.1111/nep.12831
406. Hisatomi K, Mukae H, Sakamoto N et al. (2012) Pirfenidone inhibits TGF-β1-induced over-expression of collagen type I and heat shock protein 47 in A549 cells. BMC pulmonary medicine 12:24. doi: 10.1186/1471-2466-12-24
407. Oku H, Shimizu T, Kawabata T et al. (2008) Antifibrotic action of pirfenidone and prednisolone: different effects on pulmonary cytokines and growth factors in bleomycin-induced murine pulmonary fibrosis. European journal of pharmacology 590(1-3):400–408. doi: 10.1016/j.ejphar.2008.06.046
408. Schaefer CJ, Ruhrmund DW, Pan L et al. (2011) Antifibrotic activities of pirfenidone in animal models. European Respiratory Review 20(120):85–97. doi: 10.1183/09059180.00001111
409. King TE, Bradford WZ, Castro-Bernardini S et al. (2014) A phase 3 trial of pirfenidone in patients with idiopathic pulmonary fibrosis. The New England journal of medicine 370(22):2083–2092. doi: 10.1056/NEJMoa1402582
410. Manetti M, Romano E, Rosa I et al. (2017) Endothelial-to-mesenchymal transition contributes to endothelial dysfunction and dermal fibrosis in systemic sclerosis. Annals of the rheumatic diseases 76(5):924–934. doi: 10.1136/annrheumdis-2016-210229
411. Di Benedetto P, Ruscitti P, Berardicurti O et al. (2021) Endothelial-to-mesenchymal transition in systemic sclerosis. Clinical and experimental immunology 205(1):12–27. doi: 10.1111/cei.13599
412. Clere N, Renault S, Corre I (2020) Endothelial-to-Mesenchymal Transition in Cancer. Frontiers in cell and developmental biology 8:747. doi: 10.3389/fcell.2020.00747
413. Souilhol C, Harmsen MC, Evans PC et al. (2018) Endothelial-mesenchymal transition in atherosclerosis. Cardiovascular research 114(4):565–577. doi: 10.1093/cvr/cvx253
414. van Meeteren LA, Dijke P ten (2012) Regulation of endothelial cell plasticity by TGF-β. Cell Tissue Res 347(1):177–186. doi: 10.1007/s00441-011-1222-6
415. Ursoli Ferreira F, Eduardo Botelho Souza L, Hassibe Thomé C et al. (2019) Endothelial Cells Tissue-Specific Origins Affects Their Responsiveness to TGF-β2 during Endothelial-to-Mesenchymal Transition. International journal of molecular sciences 20(3). doi: 10.3390/ijms20030458
416. Pérez L, Muñoz-Durango N, Riedel CA et al. (2017) Endothelial-to-mesenchymal transition: Cytokine-mediated pathways that determine endothelial fibrosis under inflammatory conditions. Cytokine & growth factor reviews 33:41–54. doi: 10.1016/j.cytogfr.2016.09.002
417. Song S, Zhang M, Yi Z et al. (2016) The role of PDGF-B/TGF-β1/neprilysin network in regulating endothelial-to-mesenchymal transition in pulmonary artery remodeling. Cellular signalling 28(10):1489–1501. doi: 10.1016/j.cellsig.2016.06.022
418. Sniegon I, Prieß M, Heger J et al. (2017) Endothelial Mesenchymal Transition in Hypoxic Microvascular Endothelial Cells and Paracrine Induction of Cardiomyocyte Apoptosis Are Mediated via TGFβ1/SMAD Signaling. International journal of molecular sciences 18(11). doi: 10.3390/ijms18112290
419. Thannickal VJ, Henke CA, Horowitz JC et al. (2014) Matrix biology of idiopathic pulmonary fibrosis: a workshop report of the national heart, lung, and blood institute. The American journal of pathology 184(6):1643–1651. doi: 10.1016/j.ajpath.2014.02.003

420. Österreicher CH, Penz-Österreicher M, Grivennikov SI et al. (2011) Fibroblast-specific protein 1 identifies an inflammatory subpopulation of macrophages in the liver. Proceedings of the National Academy of Sciences of the United States of America 108(1):308–313. doi: 10.1073/pnas.1017547108
421. Zeisberg EM, Potenta SE, Sugimoto H et al. (2008) Fibroblasts in kidney fibrosis emerge via endothelial-to-mesenchymal transition. Journal of the American Society of Nephrology : JASN 19(12):2282–2287. doi: 10.1681/ASN.2008050513
422. Zeisberg EM, Tarnavski O, Zeisberg M et al. (2007) Endothelial-to-mesenchymal transition contributes to cardiac fibrosis. Nat Med 13(8):952–961. doi: 10.1038/nm1613
423. Boor P, Floege J (2012) The renal (myo-)fibroblast: a heterogeneous group of cells. Nephrology, dialysis, transplantation : official publication of the European Dialysis and Transplant Association - European Renal Association 27(8):3027–3036. doi: 10.1093/ndt/gfs296
424. Luo J, Liang M, Mitch WE et al. (2015) FSP-1 Impairs the Function of Endothelium Leading to Failure of Arteriovenous Grafts in Diabetic Mice. Endocrinology 156(6):2200–2210. doi: 10.1210/en.2014-1841
425. Goumans M-J, Valdimarsdottir G, Itoh S et al. (2002) Balancing the activation state of the endothelium via two distinct TGF-beta type I receptors. The EMBO journal 21(7):1743–1753. doi: 10.1093/emboj/21.7.1743
426. Pollman MJ, Naumovski L, Gibbons GH (1999) Vascular cell apoptosis: cell type-specific modulation by transforming growth factor-beta1 in endothelial cells versus smooth muscle cells. Circulation 99(15):2019–2026. doi: 10.1161/01.cir.99.15.2019
427. Isobe S, Kataoka M, Endo J et al. (2019) Endothelial-Mesenchymal Transition Drives Expression of CD44 Variant and xCT in Pulmonary Hypertension. American journal of respiratory cell and molecular biology 61(3):367–379. doi: 10.1165/rcmb.2018-0231OC
428. Chen L, Fu C, Zhang Q et al. (2020) The role of CD44 in pathological angiogenesis. FASEB journal : official publication of the Federation of American Societies for Experimental Biology 34(10):13125–13139. doi: 10.1096/fj.202000380RR
429. Torsney E, Charlton R, Parums D et al. (2002) Inducible expression of human endoglin during inflammation and wound healing in vivo. Inflammation research : official journal of the European Histamine Research Society … [et al.] 51(9):464–470. doi: 10.1007/pl00012413
430. Handgretinger R, Gordon PR, Leimig T et al. (2003) Biology and plasticity of CD133+ hematopoietic stem cells. Annals of the New York Academy of Sciences 996:141–151. doi: 10.1111/j.1749-6632.2003.tb03242.x
431. Lyons CJ, O'Brien T (2020) The Functionality of Endothelial-Colony-Forming Cells from Patients with Diabetes Mellitus. Cells 9(7). doi: 10.3390/cells9071731
432. Ota Y, Kuwana M (2020) Endothelial cells and endothelial progenitor cells in the pathogenesis of systemic sclerosis. European journal of rheumatology 7(Suppl 3):S139-S146. doi: 10.5152/eurjrheum.2019.19158
433. Choi S-H, Hong Z-Y, Nam J-K et al. (2015) A Hypoxia-Induced Vascular Endothelial-to-Mesenchymal Transition in Development of Radiation-Induced Pulmonary Fibrosis. Clinical cancer research : an official journal of the American Association for Cancer Research 21(16):3716–3726. doi: 10.1158/1078-0432.CCR-14-3193
434. Cipriani P, Di Benedetto P, Ruscitti P et al. (2015) The Endothelial-mesenchymal Transition in Systemic Sclerosis Is Induced by Endothelin-1 and Transforming Growth Factor-β and May Be Blocked by Macitentan, a Dual Endothelin-1 Receptor Antagonist. The Journal of rheumatology 42(10):1808–1816. doi: 10.3899/jrheum.150088

435. Wermuth PJ, Li Z, Mendoza FA et al. (2016) Stimulation of Transforming Growth Factor-β1-Induced Endothelial-To-Mesenchymal Transition and Tissue Fibrosis by Endothelin-1 (ET-1): A Novel Profibrotic Effect of ET-1. PLoS ONE 11(9):e0161988. doi: 10.1371/journal.pone.0161988
436. Yanik G, Cooke KR (2006) The lung as a target organ of graft-versus-host disease. Seminars in hematology 43(1):42–52. doi: 10.1053/j.seminhematol.2005.09.004
437. Bussolino F, Ziche M, Wang JM et al. (1991) In vitro and in vivo activation of endothelial cells by colony-stimulating factors. The Journal of clinical investigation 87(3):986–995. doi: 10.1172/JCI115107
438. Ciszewski WM, Wawro ME, Sacewicz-Hofman I et al. (2021) Cytoskeleton Reorganization in EndMT-The Role in Cancer and Fibrotic Diseases. International journal of molecular sciences 22(21). doi: 10.3390/ijms222111607
439. Flowers MED, Martin PJ (2015) How we treat chronic graft-versus-host disease. Blood 125(4):606–615. doi: 10.1182/blood-2014-08-551994
440. Paczesny S (2018) Biomarkers for posttransplantation outcomes. Blood 131(20):2193–2204. doi: 10.1182/blood-2018-02-791509
441. Ahmed SS, Wang XN, Norden J et al. (2015) Identification and validation of biomarkers associated with acute and chronic graft versus host disease. Bone marrow transplantation 50(12):1563–1571. doi: 10.1038/bmt.2015.191
442. Béchard D, Scherpereel A, Hammad H et al. (2001) Human endothelial-cell specific molecule-1 binds directly to the integrin CD11a/CD18 (LFA-1) and blocks binding to intercellular adhesion molecule-1. Journal of immunology (Baltimore, Md. : 1950) 167(6):3099–3106. doi: 10.4049/jimmunol.167.6.3099
443. Sarrazin S, Adam E, Lyon M et al. (2006) Endocan or endothelial cell specific molecule-1 (ESM-1): a potential novel endothelial cell marker and a new target for cancer therapy. Biochimica et biophysica acta 1765(1):25–37. doi: 10.1016/j.bbcan.2005.08.004
444. Scherpereel A, Depontieu F, Grigoriu B et al. (2006) Endocan, a new endothelial marker in human sepsis. Critical care medicine 34(2):532–537. doi: 10.1097/01.ccm.0000198525.82124.74
445. Bălănescu P, Lădaru A, Bălănescu E et al. (2016) Endocan, Novel Potential Biomarker for Systemic Sclerosis: Results of a Pilot Study. Journal of Clinical Laboratory Analysis 30(5):368–373. doi: 10.1002/jcla.21864
446. Zhao T, Kecheng Y, Zhao X et al. (2018) The higher serum endocan levels may be a risk factor for the onset of cardiovascular disease: A meta-analysis. Medicine 97(49):e13407. doi: 10.1097/MD.0000000000013407
447. Wickström SA, Veikkola T, Rehn M et al. (2001) Endostatin-induced modulation of plasminogen activation with concomitant loss of focal adhesions and actin stress fibers in cultured human endothelial cells. Cancer Res 61(17):6511–6516
448. Dhanabal M, Ramchandran R, Waterman MJ et al. (1999) Endostatin induces endothelial cell apoptosis. Journal of Biological Chemistry 274(17):11721–11726. doi: 10.1074/jbc.274.17.11721
449. Feldman AL, Tamarkin L, Paciotti GF et al. (2000) Serum Endostatin Levels Are Elevated and Correlate with Serum Vascular Endothelial Growth Factor Levels in Patients with Stage IV Clear Cell Renal Cancer. Clin Cancer Res 6(12):4628–4634
450. Schuch G, Heymach JV, Nomi M et al. (2003) Endostatin inhibits the vascular endothelial growth factor-induced mobilization of endothelial progenitor cells. Cancer Res 63(23):8345–8350
451. Babic AM, Chen CC, Lau LF (1999) Fisp12/mouse connective tissue growth factor mediates endothelial cell adhesion and migration through integrin alphavbeta3, promotes endothelial cell survival, and induces angiogenesis in vivo. Molecular and cellular biology 19(4):2958–2966. doi: 10.1128/MCB.19.4.2958

452. Inoki I, Shiomi T, Hashimoto G et al. (2002) Connective tissue growth factor binds vascular endothelial growth factor (VEGF) and inhibits VEGF-induced angiogenesis. FASEB journal : official publication of the Federation of American Societies for Experimental Biology 16(2):219–221. doi: 10.1096/fj.01-0332fje
453. Brigstock DR (2010) Connective tissue growth factor (CCN2, CTGF) and organ fibrosis: lessons from transgenic animals. Journal of cell communication and signaling 4(1):1–4. doi: 10.1007/s12079-009-0071-5
454. Grotendorst GR (1997) Connective tissue growth factor: a mediator of TGF-beta action on fibroblasts. Cytokine & growth factor reviews 8(3):171–179. doi: 10.1016/s1359-6101(97)00010-5
455. Uzel MI, Kantarci A, Hong HH et al. (2001) Connective tissue growth factor in drug-induced gingival overgrowth. Journal of periodontology 72(7):921–931. doi: 10.1902/jop.2001.72.7.921
456. Dammeier J, Brauchle M, Falk W et al. (1998) Connective tissue growth factor: a novel regulator of mucosal repair and fibrosis in inflammatory bowel disease? The international journal of biochemistry & cell biology 30(8):909–922. doi: 10.1016/s1357-2725(98)00046-6
457. Jonker L, Arthur HM (2002) Endoglin expression in early development is associated with vasculogenesis and angiogenesis. Mechanisms of development 110(1-2):193–196. doi: 10.1016/s0925-4773(01)00562-7
458. Cheifetz S, Bellón T, Calés C et al. (1992) Endoglin is a component of the transforming growth factor-beta receptor system in human endothelial cells. Journal of Biological Chemistry 267(27):19027–19030
459. López-Novoa JM, Bernabeu C (2010) The physiological role of endoglin in the cardiovascular system. American Journal of Physiology - Heart and Circulatory Physiology 299(4):H959-74. doi: 10.1152/ajpheart.01251.2009
460. Venkatesha S, Toporsian M, Lam C et al. (2006) Soluble endoglin contributes to the pathogenesis of preeclampsia. Nat Med 12(6):642–649. doi: 10.1038/nm1429
461. Chen C-Z, Li M, Graaf D de et al. (2002) Identification of endoglin as a functional marker that defines long-term repopulating hematopoietic stem cells. Proceedings of the National Academy of Sciences of the United States of America 99(24):15468–15473. doi: 10.1073/pnas.202614899
462. Kozian DH, Ziche M, Augustin HG (1997) The activin-binding protein follistatin regulates autocrine endothelial cell activity and induces angiogenesis. Laboratory investigation; a journal of technical methods and pathology 76(2):267–276
463. Kretser DM de, O'Hehir RE, Hardy CL et al. (2012) The roles of activin A and its binding protein, follistatin, in inflammation and tissue repair. Molecular and Cellular Endocrinology 359(1-2):101–106. doi: 10.1016/j.mce.2011.10.009
464. Fahmy-Garcia S, Farrell E, Witte-Bouma J et al. (2019) Follistatin Effects in Migration, Vascularization, and Osteogenesis in vitro and Bone Repair in vivo. Front. Bioeng. Biotechnol. 7:38. doi: 10.3389/fbioe.2019.00038
465. Newell LF, Defor TE, Cutler C et al. (2020) Follistatin and Soluble Endoglin Predict 1-Year Nonrelapse Mortality after Allogeneic Hematopoietic Cell Transplantation. Biology of blood and marrow transplantation : journal of the American Society for Blood and Marrow Transplantation 26(3):606–611. doi: 10.1016/j.bbmt.2019.11.006
466. Azzazi MO, El Salakawy WA, Mohamed HS (2022) Serum follistatin level as a prognostic marker in Haploidentical stem cell transplantation. Transplant immunology 71:101542. doi: 10.1016/j.trim.2022.101542
467. Liem LM, Fibbe WE, van Houwelingen HC et al. (1999) Serum transforming growth factor-beta1 levels in bone marrow transplant recipients correlate with blood cell counts and chronic graft-versus-host disease. Transplantation 67(1):59–65. doi: 10.1097/00007890-199901150-00009

468. Ruscetti F, Varesio L, Ochoa A et al. (1993) Pleiotropic effects of transforming growth factor-beta on cells of the immune system. Annals of the New York Academy of Sciences 685:488–500. doi: 10.1111/j.1749-6632.1993.tb35911.x
469. Anscher MS, Peters WP, Reisenbichler H et al. (1993) Transforming growth factor beta as a predictor of liver and lung fibrosis after autologous bone marrow transplantation for advanced breast cancer. The New England journal of medicine 328(22):1592–1598. doi: 10.1056/NEJM199306033282203
470. Matthaiou EI, Sharifi H, O'Donnell C et al. (2022) The safety and tolerability of pirfenidone for bronchiolitis obliterans syndrome after hematopoietic cell transplant (STOP-BOS) trial. Bone marrow transplantation 57(8):1319–1326. doi: 10.1038/s41409-022-01716-4

6. Supplements

List of figures

Supplemental Figure 1: Plasmid vector pSpCas9(BB)-2A-GFP (PX458). Vector designed by Ran et al. [310], graphics taken from https://www.addgene.org/48138/.

Supplemental Table 1: Tubeformation parameters measured by 'Angio Analyser' Plugin for Fiji ImageJ. From [317].

1.	number of extremities in the analysed area
2.	number of nodes in the analysed area
3.	number of junctions in the analysed area
4.	number of master junctions in the analysed area
5.	number of master segments in the analysed area
6.	sum of the length of the detected master segments in the analysed area
7.	number of meshes in the analysed area
8.	sum of mesh areas detected in the analysed area
9.	sum of number of segments, isolated elements and branches in the analysed area
10.	number of segments in the analysed area
11.	number of branches in the analysed area
12.	number of isolated elements in the analysed area
13.	sum of length of segments, isolated elements and branches in the analysed area
14.	sum of length of the trees composed from segments and branches in the analysed area
15.	sum of length of the segments in the analysed area
16.	sum of length of the branches in the analysed area
17.	sum of length of the isolated elements in the analysed area
18.	mean distance separating two branches in the trees in the analysed area. (Tot. segments length / Nb branches)
19.	mean distance separating two master junctions in the trees in the analysed area. (Tot. master segments length / Nb master segments)
20.	mean mesh size in the analysed area

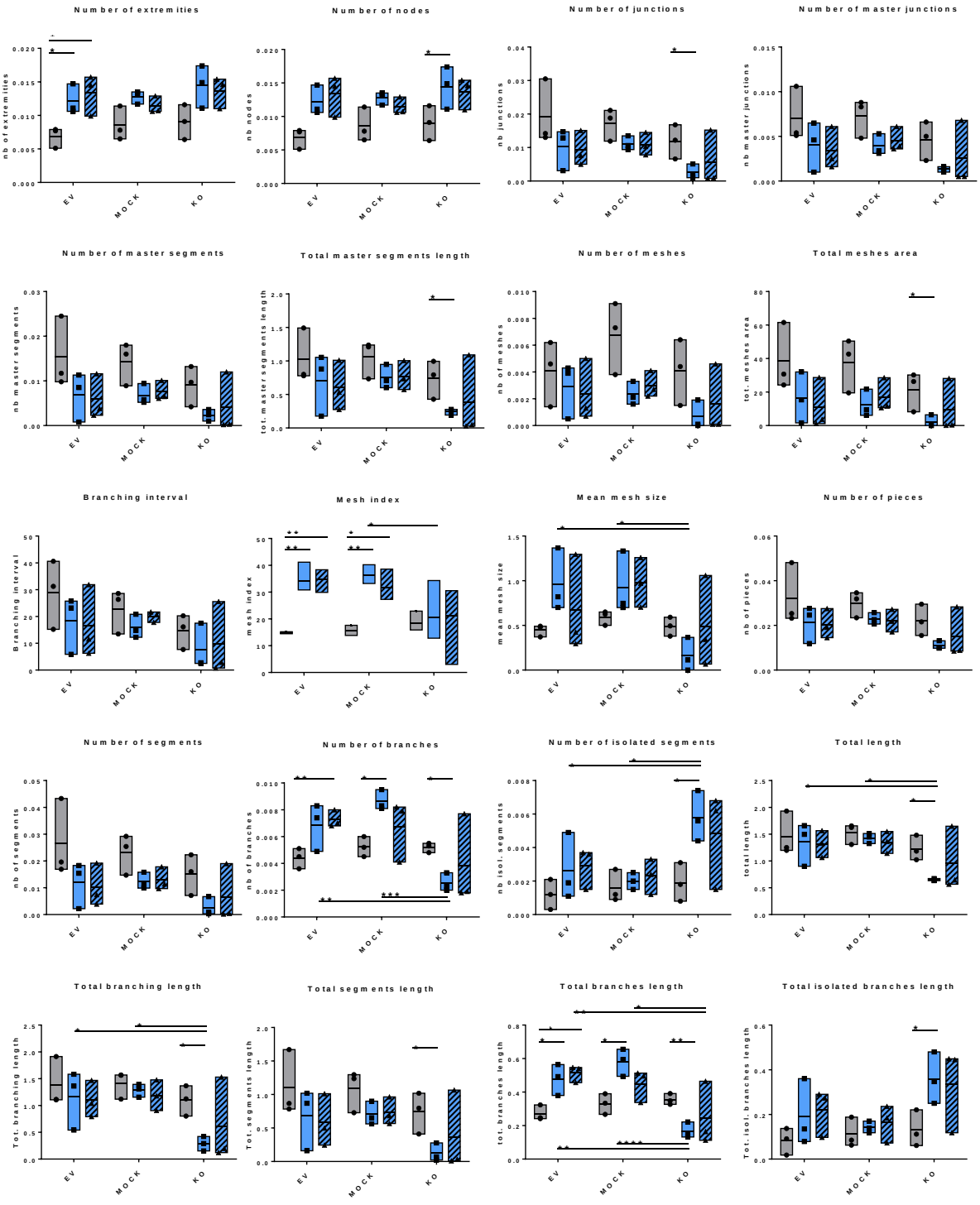

Supplemental Figure 2: Angiogenic behaviour of *Eno3*-KO in tubeformation assay.

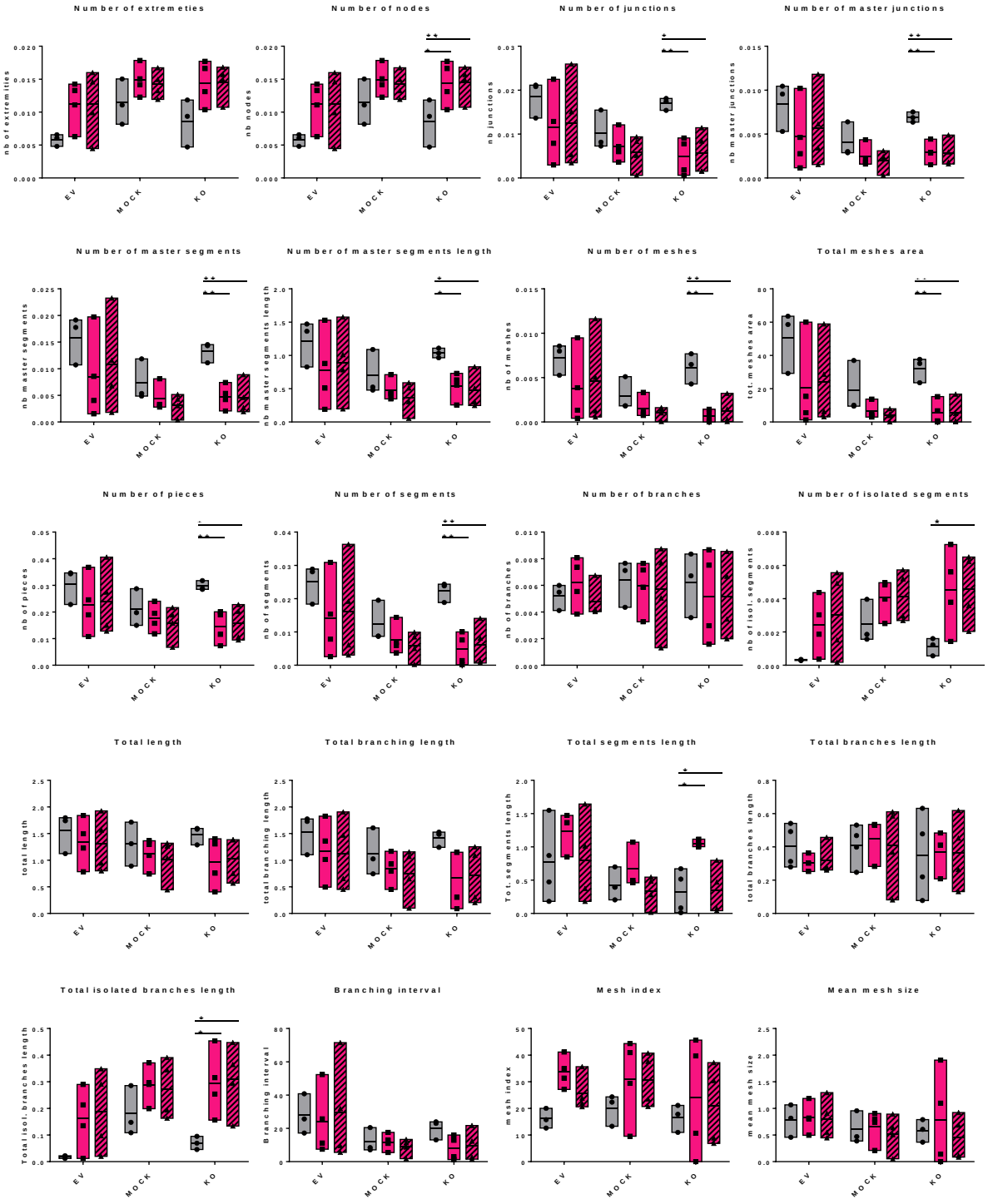

Supplemental Figure 3: Angiogenic behaviour of *G6pdx*-KO in tubeformation assay.

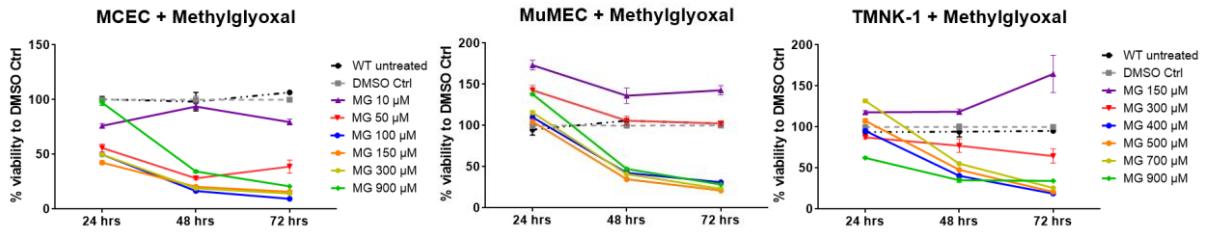

Supplemental Figure 4: Influence of pharmacologic inhibitor Methylglyoxal (MG) on endothelial viability and metabolic activity of MCEC, MuMEC and TMNK-1 in MTT-assays over 72 hrs. WT=Wild type, MCEC= Murine cardiac endothelial cells, MuMEC=murine microvascular endothelial cells, TMNK-1= immortalized human liver sinusoidal EC line. Data pooled from 2 independent experiments with 3 replicates per inhibitor-concentration. Error bars indicate mean ± SEM.

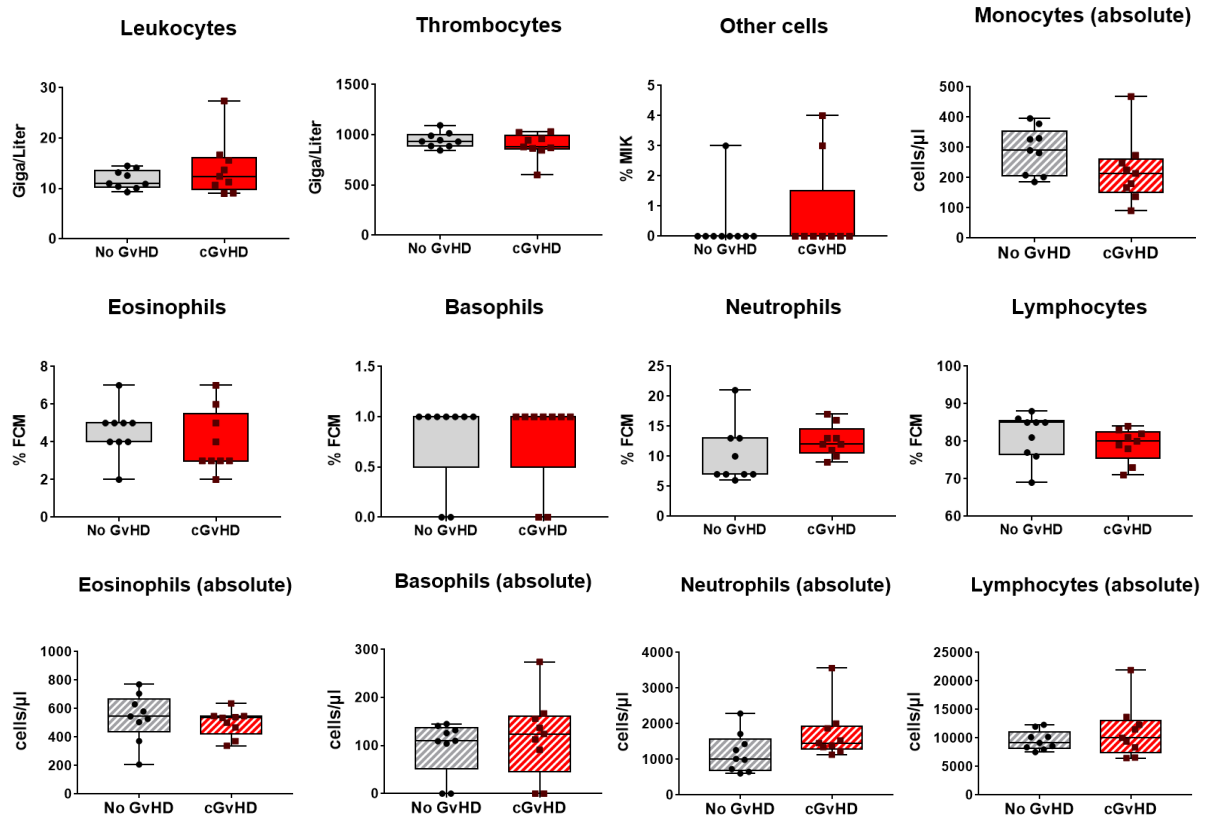

Supplemental Figure 5: Differential blood count in cGvHD at d+90 after transplantation in C57BL/6→BDF. Blood was sampled from mice and differential blood count was performed by Synlab, Berlin. Data pooled from 2 independent experiments. n=9 per gropu. Error bars represent mean±SEM. *P<0.05, **P<0.01, ***P<0.001, ****P<0.0001 by unpaired students *t*-test.

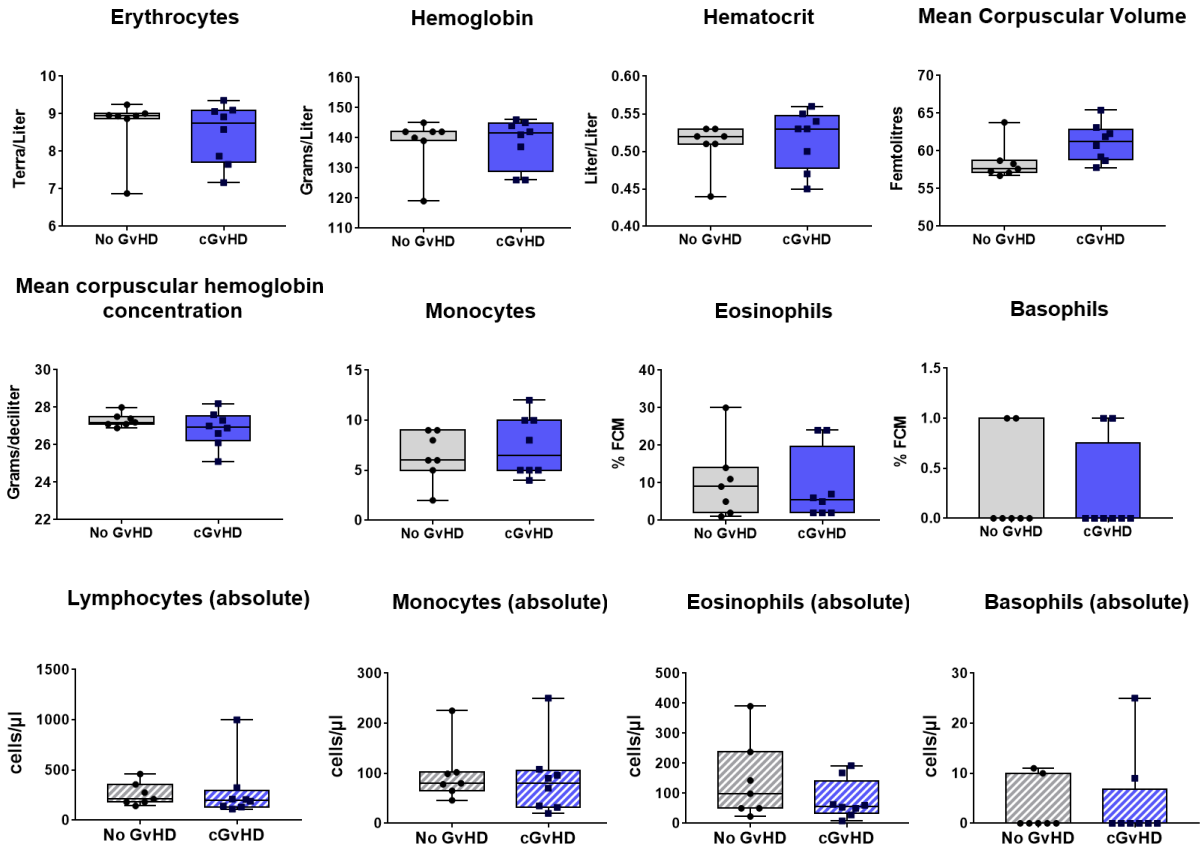

Supplemental Figure 6: Differential blood count in cGvHD at d+90 after xeno-transplantation in huPBMCs→NSG. Blood was sampled from mice and differential blood count was performed by Synlab, Berlin. Representative data from one out of two experiments. n=8 per group. *P<0.05, **P<0.01, ***P<0.001, ****P<0.0001 by unpaired students *t*-test.

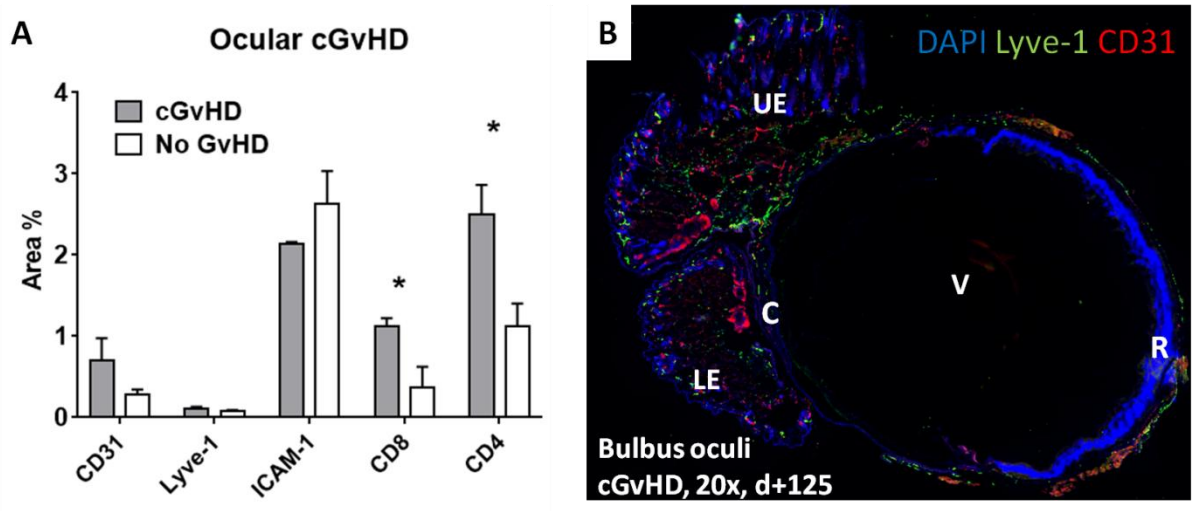

Supplemental Figure 7: Characterization of ocular cGvHD in the C57BL/6 → B6D2F1 mouse model. (A) Immunofluorescence quantification of EC markers CD31, Lyve-1 and ICAM-1 and of

CD8 and CD4 T cell subsets in eyeball and eyelids of cGvHD mice. Data from one representative experiment. Error bars indicate mean +SEM. n=3 per group. *P<0.05. (B) Representative fluorescence image of an ocular staining for EC markers Lyve-1 and CD31. UE=upper eyelid, LE=lower eyelid, C=cornea, V= vitreous, R=retina.

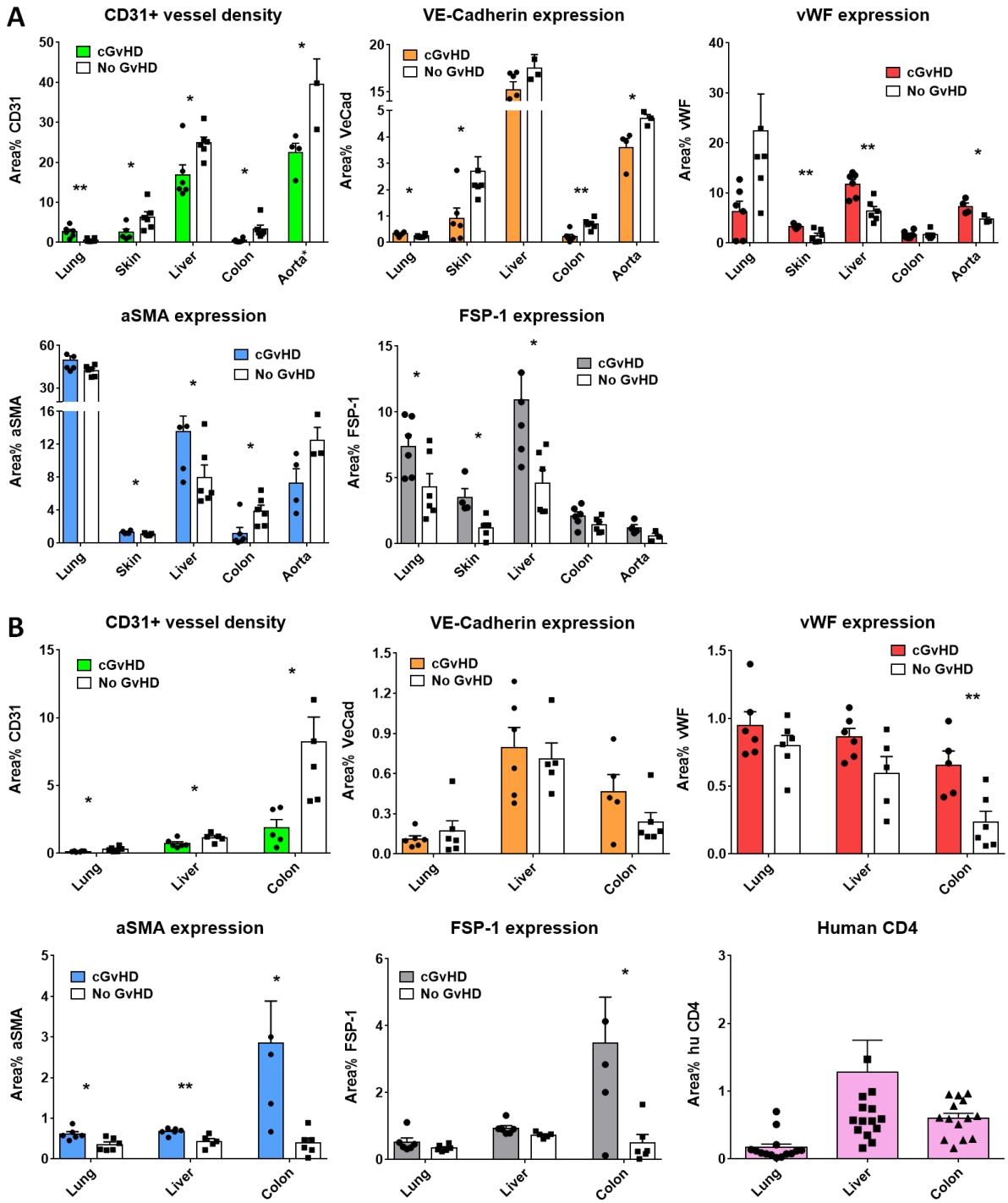

Supplemental Figure 8: Immunohistofluorescence quantification of the single-marker expression of whole-tissue CD31, VECad, vWF, αSMA and FSP-1 in cGvHD target organs of (A) B6D2F1- and (B) NSG-recipients. Representative data from one out of two experiments. n=6 per group,

(huCD4 n=13 per group). *P<0.05, **P<0.01, ***P<0.001, ****P<0.0001 by unpaired students *t*-test. Error bars indicate mean +SEM.

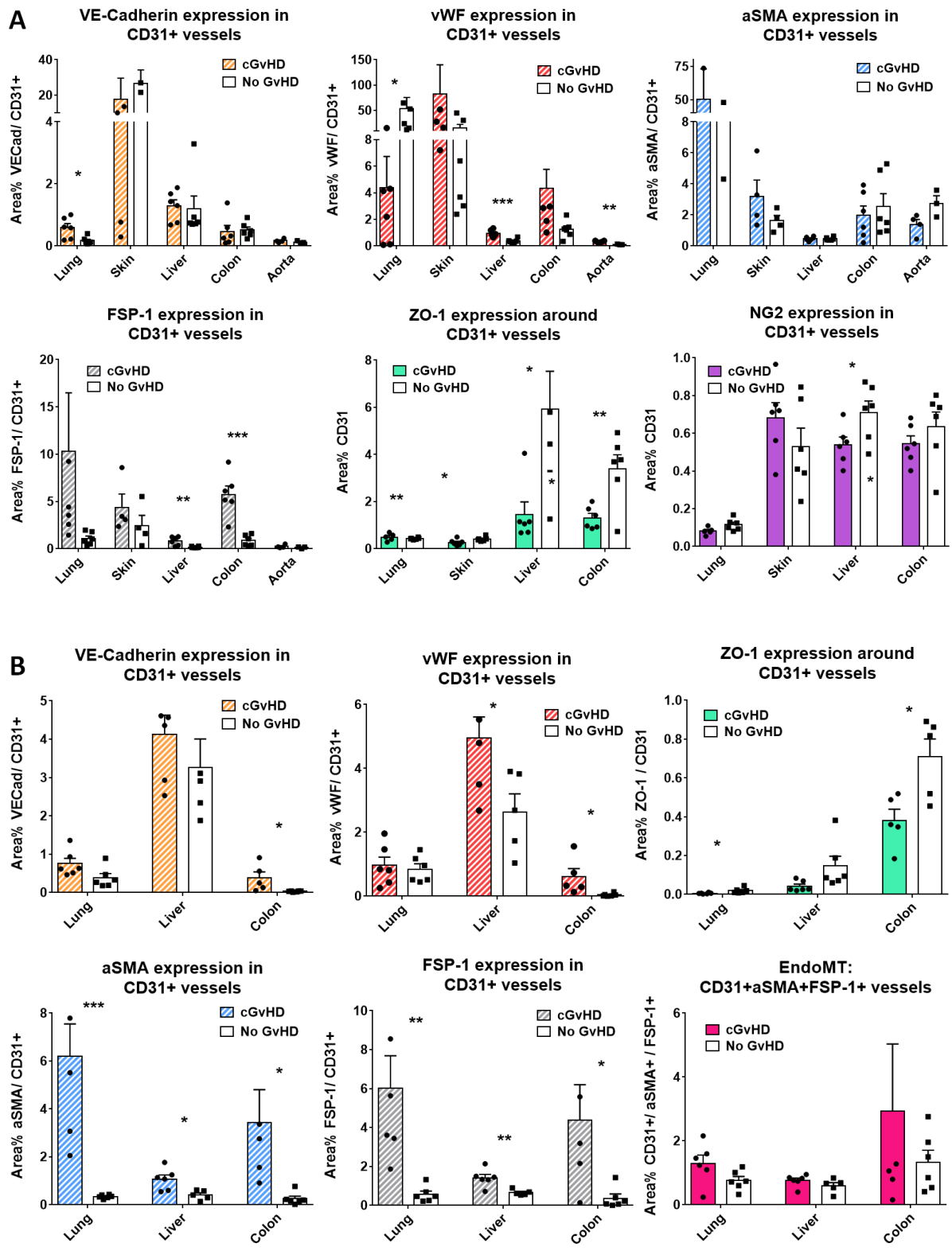

Supplemental Figure 9: Immunohistofluorescence quantification of the expression of VECad, vWF, αSMA, FSP-1 and NG2 co-localized with CD31+ vessels in cGvHD target organs of B6D2F1- and (B) NSG-recipients. Representative data from one out of two experiments. n=6 per

group. *P<0.05, **P<0.01, ***P<0.001, ****P<0.0001 by unpaired students *t*-test. Error bars indicate mean +SEM.

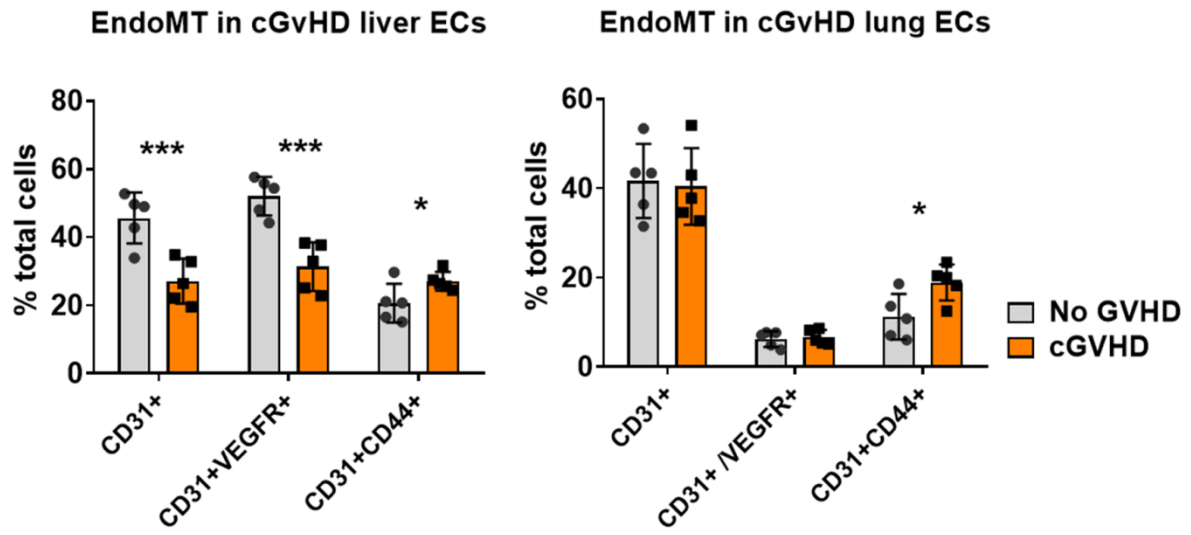

Supplemental Figure 10: EndoMT markers in FACS analysis from isolated liver and lung ECs from C57BL/6 → B6D2F1 mice at day+90 after transplantation. No GvHD n=5; cGvHD n=5. Data from one representative experiment. Error bars indicate mean ± SEM, *P<0.05, **P<0.01, ***P<0.001 by unpaired students t-test.

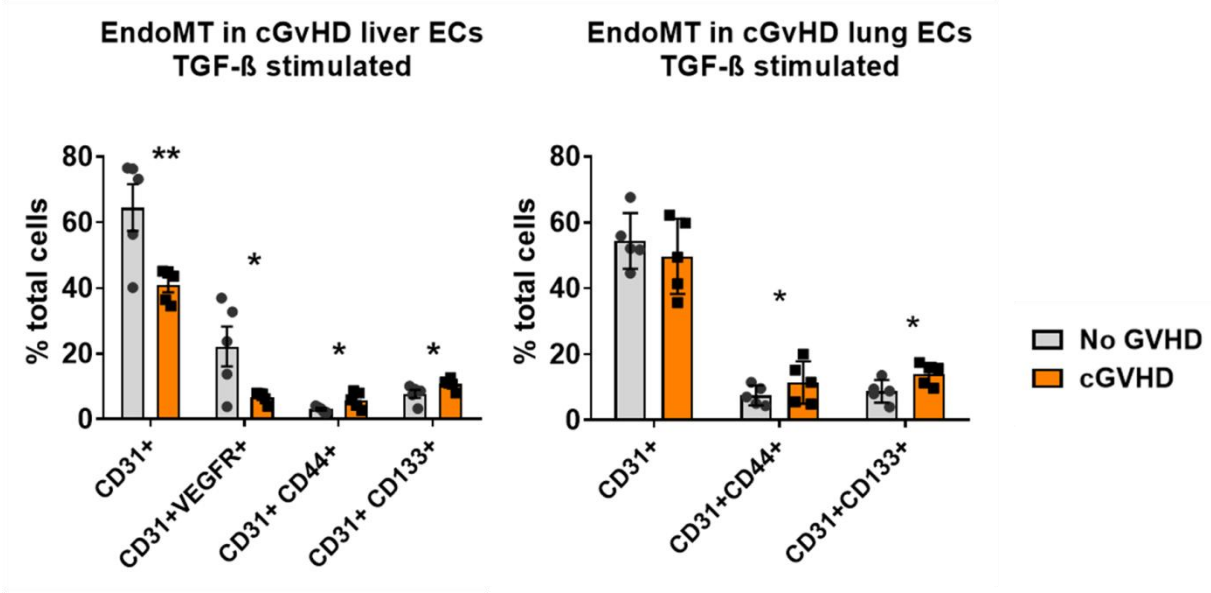

Supplemental Figure 11: EndoMT markers in FACS analysis from TGF-ß stimulated liver and lung ECs from C57BL/6 → B6D2F1 at day+90 after transplantation. No GvHD n=5; cGvHD n=5. Data from one representative experiment. Error bars indicate mean ± SEM, *P<0.05, **P<0.01, ***P<0.001 by unpaired students t-test.

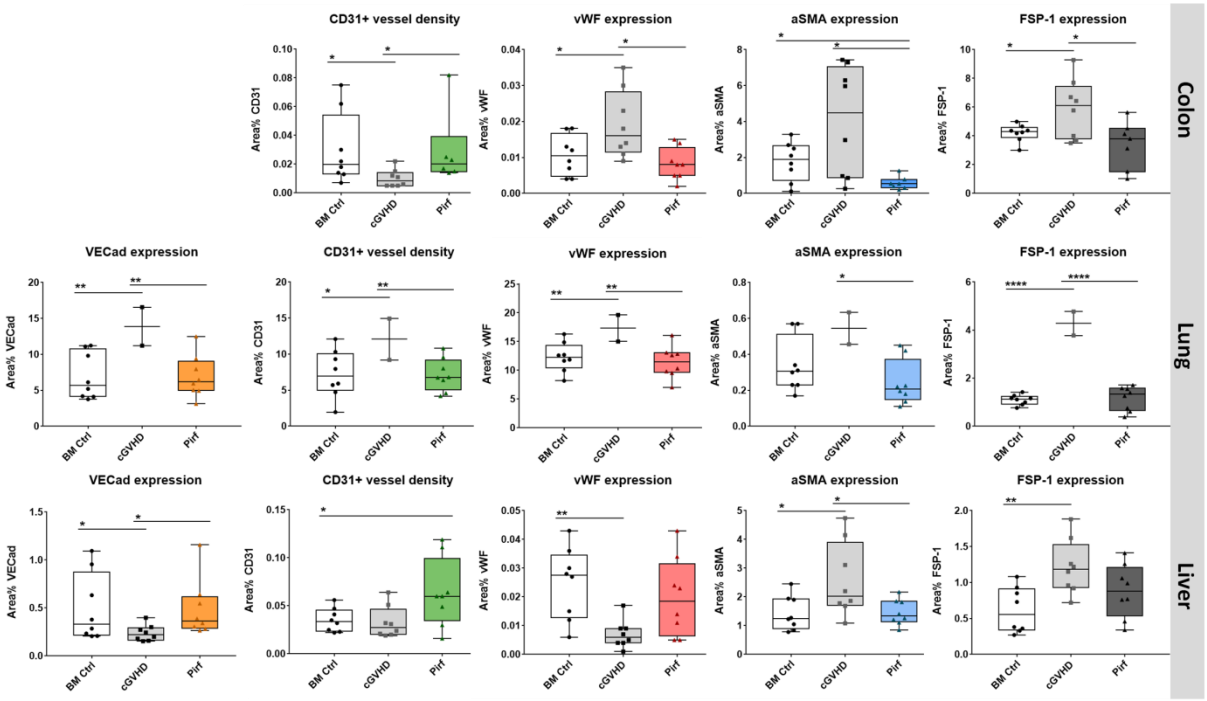

Supplemental Figure 12: Expression of total tissue CD31, VECad, vWF, αSMA and FSP-1 in C57BL/6 → B6D2F1 cGvHD target organs colon, lung and liver of pirfenidone treated mice. n=8 per group, (except n=2 for cGvHD lung). *P<0.05, **P<0.01, ***P<0.001, ****P<0.0001 by unpaired students *t*-test. Error bars indicate mean +SEM. BM Ctrl = Bone marrow control (No GvHD); Pirf = Pirfenidone treated cGvHD.